

**PALLADIUM-CATALYZED AEROBIC α,β -DEHYDROGENATION
OF CARBONYL COMPOUNDS:
METHOD DEVELOPMENT AND MECHANISTIC STUDY**

by

Tianning Diao

A dissertation submitted in partial fulfillment of the requirements for the degree of

Doctor of Philosophy

(Chemistry)

at the

UNIVERSITY OF WISCONSIN-MADISON

2012

Date of final oral examination: 09/18/12

The dissertation is approved by the following members of the Final Oral Committee:

Shannon S. Stahl, Professor, Chemistry

Clark R. Landis, Professor, Chemistry

Tehshik P. Yoon, Associate Professor, Chemistry

Hans J. Reich, Professor, Chemistry

Weiping Tang, Assistant Professor, Pharmacy

**Palladium-Catalyzed Aerobic α,β -Dehydrogenation of Carbonyl Compounds:
Method Development and Mechanistic Study**

Tianning Diao

Under the supervision of Professor Shannon S. Stahl
at the University of Wisconsin-Madison

ABSTRACT: α,β -Unsaturated carbonyl compounds are versatile intermediates in the synthesis of pharmaceuticals and biologically active molecules. The research described herein focuses on the development and mechanistic study of Palladium catalysts for direct aerobic dehydrogenation of ketones and aldehydes to afford the corresponding α,β -unsaturated carbonyl compounds. The discovery and application of a novel aerobic dehydrogenation catalyst, $\text{Pd}(\text{DMSO})_2(\text{TFA})_2$, led to selective dehydrogenation of various cyclohexanone derivatives to afford cyclohexenone products that are of synthetic interest. A complementary $\text{Pd}(\text{TFA})_2/4,5$ -diazafuorenone catalyst was developed for α,β -dehydrogenation of acyclic ketones and aldehydes, with useful applications in preparing unsaturated heterocyclic carbonyl compounds. Characterization of the solution-phase structure of the $\text{Pd}(\text{DMSO})_2(\text{TFA})_2$ catalyst by NMR spectroscopy suggested that the bis-DMSO ligation to Pd^{II} was favorable under the catalytic conditions. Further kinetic studies of $\text{Pd}(\text{DMSO})_2(\text{TFA})_2$ -catalyzed dehydrogenation of cyclohexenone revealed that the DMSO ligands kinetically control the selectivity of dehydrogenation.

A fundamental study of the influence of O₂ on the acetoxylation of (π -allyl)Pd complexes is also detailed. The fact that O₂ is capable of promoting reductive C–O bond formation of (π -allyl)Pd complexes has important implications in understanding the interaction between Pd and O₂ and provides a basis for development of Pd-catalyzed aerobic allylic acetoxylation of alkenes.

ACKNOWLEDGMENTS

I would like to express my deepest gratitude to my advisor, Prof. Shannon Stahl, for his expertise, enthusiasm and for sparking my passion for chemistry and scientific research. I knew that Shannon was the advisor I wanted for graduate school while listening to his presentation at Fudan University in 2006. For the past five years, I have been soaking up Shannon's critical and logical ways of thinking and performing science. My efforts to reach Shannon's standards have led to the research described in this thesis. I am deeply grateful to the time and patience that Shannon has devoted to mentor me. I am excited about continuing my career with everything I have learnt from him.

My chemistry insights and my research has been greatly benefited from the classes taught by Prof. Clark Landis, Prof. Tehshik Yoon and Prof. Hans Reich. The Wednesday night "super group" discussions with Clark and Tehshik are always inspiring and entertaining. I also thank Prof. Weiping Tang for being one of my committee members and for taking the time to read my thesis.

I am grateful to Richard McDonald, who successfully prevented me from getting lost in graduate school when I first started. Rick's diligence and passion for chemistry has set a good example for me to look up to. Doris Pun's invaluable friendship has helped me survive graduate school. Her help in lab also led to my very first crystal of a Pd complex. I also thank former and current Stahl group members, who have contributed to an amazing working environment, been supportive in lab and enriched my personal life in Madison. I will miss our "girls' night outs".

I wouldn't have been able to accomplish any of the research described here without the chemistry department staff. The state-of-the-art NMR facilities run by Charlie Fry, Monika Ivancic and Bob Shanks have enabled my mechanistic studies. I am grateful to the time that

Charlie has devoted to answer my questions and help me with my NMR experiments. I also thank Martha Vestling for maintaining the GC-MS spectrometer, and Ilia Guzei and Lara Spencer for solving crystal structures.

My five years in graduate school would not be fun without my fantastic friends. I especially want to thank my wonderful roommate, Daria Fedyukina.

This thesis is dedicated to my parents, my grandparents and Hong. My family is my inspiration and the source of motivation and support for my career. My mom's unconditional love encourages me to take challenges, as I know she always has my back. Dad's wisdom, inherited from grandpa, guides my every step in life and helps me to find my inner peace during challenging times. Hong has enriched my life and become one of my major sources of laughter.

TABLE OF CONTENTS

Abstract	i
Acknowledgements	iii
Table of Contents	v
List of Tables	x
List of Figures	xii
List of Schemes	xviii
Abbreviations and Acronyms	xxi
Chapter 1. Oxidation Adjacent to C=O bonds by Dehydrogenation	1
1.1 Introduction to α,β -Dehydrogenation of Carbonyl Compounds	2
1.2 Summary of Non-Transition Metal Based Methods	4
1.3 Pd-Mediated/Catalyzed Dehydrogenation	8
1.3.1 Stoichiometric Pd Salts	8
1.3.2 Pd Catalysts Coupled with Stoichiometric Oxidants	11
1.3.3 Pd-Mediated/Catalyzed Dehydrogenation of Silyl Enol Ethers	17
1.4 Transition Metals other than Pd	23
1.5 Transfer Dehydrogenation	28
1.6 Transition Metal-Based Heterogeneous Catalysts	29
1.7 Summary and Outlook	31
1.8 References	32
Chapter 2. Pd(DMSO)₂(TFA)₂-Catalyzed Aerobic α,β-Dehydrogenation of Cyclic Ketones	43
2.1 Introduction to Dehydrogenation of Cyclic Carbonyl Compounds	44
2.2 Results and Discussions	46
2.2.1 Optimization of Catalyst and Reaction Conditions for Aerobic α,β -Oxidation of Cyclic Ketones	46
2.2.2 Investigation of the Chemoselectivity of Pd(DMSO) ₂ (TFA) ₂ -Catalyzed Dehydrogenation	49
2.2.3 Substrate Scope	52
2.2.4 Unsuccessful Substrates	55
2.2.5 Conclusion	57
2.3. Experimental	57
2.3.1 General Procedure for Catalyst Optimization	57
2.3.2 General Procedure for Dehydrogenation of Cyclohexanones and Product Isolation	60
2.3.3 Procedure for Aerobic Dehydrogenation of Cyclohexanone 2-1 in a Flow Reactor	63
2.3.4 Acquisition of Time Course Data	64

2.3.5 Characterization Data of Enone Products	64
2.4 References	72
Chapter 3. Palladium/4,5-Diazafluorenone-Catalyzed Aerobic α,β-Dehydrogenation of Carbonyl Compounds	81
3.1 Introduction to Dehydrogenation of Carbonyl Compounds	82
3.2 Results and Discussions	85
3.2.1 Optimization of Catalyst and Reaction Conditions for Aerobic α,β -Oxidation of Cyclopentanone 3-1	85
3.2.2 Applications of the Pd(TFA) ₂ /4,5-Diazafluorenone Catalyst in the Dehydrogenation of Carbonyl Molecules	87
3.2.3 Limitations of the Pd(TFA) ₂ /4,5-Diazafluorenone Catalyst System	90
3.2.4 Mechanistic Investigation of Pd(TFA) ₂ /4,5-diazafluorenone catalyzed Dehydrogenation Reaction	91
3.2.5 Conclusion	94
3.3 Experimental	94
3.3.1 General Considerations	94
3.3.2 General Procedure for Catalyst Optimization	95
3.3.3 Procedure for Dehydrogenation of 3-1 in a Parr Pressure Vessel and Product Isolation	96
3.3.4 Procedure for Dehydrogenation of Benzylacetone 3-3	96
3.3.5 Synthesis of the Deuterated Substrates 3-3-<i>d</i>₅ and 3-3-<i>d</i>₂	98
3.3.6 Reaction Profiles and Kinetic Fittings of Oxidizing 4- <i>tert</i> -Butylcyclohexanone with Different Catalysts	102
3.3.7 Investigation of Kinetic Isotope Effects	104
3.3.8 ¹ H NMR Spectroscopic Data	105
3.4 Contributions	125
3.5 References	125
Chapter 4. Characterization of DMSO Coordination to Palladium(II) in Solution	117
4.1 Introduction	118
4.2 Results and Discussions	121
4.2.1 Solid-Phase Structures of DMSO-Ligated Pd(TFA) ₂ Complexes	121
4.2.2 The Solution-Phase Structure of Pd(TFA) ₂ /DMSO in EtOAc	124
4.2.3 Effect of the Anionic Ligand: Coordination Chemistry of DMSO to Pd(OAc) ₂ in EtOAc	133
4.2.4 The Solution Phase Structure of Pd(TFA) ₂ /DMSO in THF- <i>d</i> ₈	135
4.2.5 Comparison of the Kinetics of DMSO Ligand Exchange in EtOAc and THF- <i>d</i> ₈	140
4.2.6 Solution Structures of Pd(TFA) ₂ /DMSO in AcOH- <i>d</i> ₄ and Toluene- <i>d</i> ₈	142
4.2.7 Summary and Analysis	146

4.3 Experimental	148
4.3.1 General Considerations and Procedures	148
4.3.2 Investigation of the DMSO Ligand Exchange in EtOAc and THF- d_8	150
4.4 Contributions	154
4.5 References	154
Chapter 5. Mechanistic Investigation of Pd(DMSO)$_2$(TFA)$_2$-Catalyzed Aerobic Dehydrogenation of Cyclohexanones	159
5.1 Introduction	160
5.2 Results	162
5.2.1 Kinetic Data of Pd(DMSO) $_2$ (TFA) $_2$ -Catalyzed Oxidation of Cyclohexanone	162
5.2.2 Kinetic Study of Pd(DMSO) $_2$ (TFA) $_2$ -Catalyzed Oxidation of Cyclohexanone to Phenol	167
5.3 Discussion	172
5.3.1 Mechanism of Pd(DMSO) $_2$ (TFA) $_2$ -Catalyzed Oxidation of Cyclohexanone to Cyclohexenone	172
5.3.2 Mechanism of Pd(DMSO) $_2$ (TFA) $_2$ -Catalyzed Oxidation of Cyclohexenone to Phenol and the Origin of the Chemoselectivity	175
5.3.4 Conclusions	177
5.4 Experimental	177
5.4.1 General Considerations	177
5.4.2 General Procedure for Acquiring Kinetic Data	178
5.4.3 Raw Kinetic Data	178
5.4.4 Methods for Determining the Length of Induction Period	181
5.4.5 O $_2$ Dependence for Pd(DMSO) $_2$ (TFA) $_2$ -Catalyzed Oxidation of 4- <i>tert</i> -Butylcyclohexanone	182
5.5 References	183
Chapter 6. Additional Results for Mechanistic Study of Pd(DMSO)$_2$(TFA)$_2$-Catalyzed Aerobic Oxidation of Cyclohexanone	188
6.1. Introduction	191
6.2. Results	191
6.2.1 Variable Temperature Studies of Three Catalyst Systems for Dehydrogenation of Cyclohexanone	191
6.2.2 Additional Kinetic Data for Pd(DMSO) $_2$ (TFA) $_2$ -Catalyzed Dehydrogenation of Cyclohexanone	193
6.2.3 Additional Kinetic Data for Pd(DMSO) $_2$ (TFA) $_2$ -Catalyzed Dehydrogenation of Cyclohexenone	195
6.2.4 Kinetic Studies of Dehydrogenation of Cyclohexenone Catalyzed by Unligated Pd(TFA) $_2$	201
6.2.5 Assessment of the Homogeneity of Pd(DMSO) $_2$ (TFA) $_2$ -Catalyzed Dehydrogenation	203

6.2.6 Pd-Catalyzed Disproportionation of Cyclohexenone to Cyclohexanone and Phenol	205
6.3 Discussions	206
6.3.1 Additional Insights into Pd(DMSO) ₂ (TFA) ₂ -Catalyzed Dehydrogenation of Cyclohexanone	206
6.3.2 The Homogeneous/Heterogeneous Characterization of Pd-Catalyzed Dehydrogenation of Cyclohexenone	208
6.3.3 Proposed Mechanism for Pd(DMSO) ₂ (TFA) ₂ -Catalyzed Dehydrogenation of Cyclohexenone	210
6.3.4 Conclusion	213
6.4 Experimental	213
6.4.1 General Procedures and Considerations	213
6.4.2 Procedures for Dynamic Light Scattering (DLS) Measurements	215
6.5 Contributions	215
6.6 References	215
Chapter 7. O₂-Promoted Allylic Acetoxylation of (π-Allyl)Pd Complexes	219
7.1 Introduction	220
7.2 Results	223
7.2.1 O ₂ -Promoted Acetoxylation of the (π-allyl)PdCl Complexes	223
7.2.2 “Unligated” Pd Catalyzed Aerobic Allylic Acetoxylation of Terminal Alkenes	225
7.2.3 Characterization of the (π-allyl)PdCl Complexes in the AcOH/CH ₃ CN Solvent Mixture	226
7.2.4 Kinetics Studies of BQ- and O ₂ -Promoted Acetoxylation of the (π-allyl)PdCl Complex 7-1c	229
7.2.5 Acetate Exchange Experiments	231
7.3 Discussions	232
7.3.1 The Identity of 7-1c under the Reaction Conditions	232
7.3.2 Mechanism of O ₂ -Promoted Acetoxylation of 7-1c and the Comparison with BQ	233
7.3.3 Conclusion	238
7.4 Experimental	238
7.4.1 General Procedures and Considerations	238
7.4.2 ¹ H NMR Spectra and Timecourse of O ₂ -Promoted Acetoxylation of 7-1c	239
7.4.3 Procedure for the Acetate Exchange Experiments	242
7.4.4 Derivation of the Equilibrium Constant Between 7-1c' and 7-1c	241
7.4.5 Rate Laws Derivations	245
7.5 References	246
Appendix 1. Efforts Towards Enantioselective Formal Synthesis of (+) Infectocaryone and (+) Cryptocaryone via Aerobic Dehydrogenation	251

Appendix 2. <i>Additional NMR Experiments and Spectroscopic Data for Chapter 4</i>	259
Appendix 3. <i>NMR Spectra of Compounds</i>	273
Appendix 4. <i>X-Ray Crystal Structure Determination</i>	297

LIST OF TABLES

- Table 1-1. Pd^{II}-Mediated α,β -Dehydrogenation of Carbonyl Compounds
- Table 1-2. Early Examples of Pd-Catalyzed Aerobic Dehydrogenation of Cyclohexanone
- Table 1-3. Cu, Ni and Mn-Promoted Dehydrogenation of Heterocycles
- Table 1-4. Pd/C-Catalyzed Dehydrogenation of Ketones and Lactones
- Table 1-5. Heterogeneous Dehydrogenation of Simple Cyclohexanones
- Table 2-1. Catalyst Optimization of Aerobic Oxidative Dehydrogenation of 4-*tert*-Butylcyclohexanone
- Table 2-2. Pd-Catalyzed Aerobic Dehydrogenation of Diverse Cycloketones
- Table 2-3. Unsuccessful Substrates for Pd(DMSO)₂(TFA)₂-Catalyzed Aerobic Dehydrogenation Reactions
- Table 3-1. Catalyst Optimization for the Aerobic Dehydrogenation of **3-1**
- Table 3-2. Pd-Catalyzed Aerobic Dehydrogenation of Aldehydes and Ketones
- Table 3-3. Unsuccessful Substrates for Pd(TFA)₂/4,5-Diazafluorenone-Catalyzed Aerobic Dehydrogenation Reactions
- Table 3-4. Comparison of Pd Catalysts in the Oxidation of 4-*tert*-Butylcyclohexanone
- Table 4-1. IR and ¹H NMR Spectroscopic Data of DMSO and Transition Metal-coordinated DMSO Reported in the Literature
- Table 4-2. Estimated Rate Constants for the Equilibrium Between **4-2a** and **4-3a** Derived from the Peak Line Broadening
- Table 6-1. Disproportionation of Cyclohexenone to Cyclohexanone and Phenol
- Table 7-1. Acetoxylation of (π -allyl)Pd Complexes in the Presence of BQ or O₂

Table 7-2. Pd(OAc)₂-Catalyzed Aerobic Allylic Acetoxylation Reactions

LIST OF FIGURES

- Figure 2-1. Comparison of kinetic profiles of $\text{Pd}(\text{DMSO})_2(\text{TFA})_2$ - and $\text{Pd}(\text{TFA})_2/2\text{-Me}_2\text{Npy}$ -catalyzed dehydrogenation of **2-1**.
- Figure 2-2. Dependence of the oxidation of cyclohexanone on the O_2 pressure.
- Figure 3-1. Timecourses and fittings of Pd-catalyzed aerobic dehydrogenation of 4-*tert*-butylcyclohexanone.
- Figure 3-2. Initial rates of dehydrogenation of proteo- and deuterated benzylacetone.
- Figure 4-1. Molecular structure of $\text{Pd}(\text{S-DMSO})(\text{O-DMSO})(\text{TFA})_2$ **4-3a(s)**, with 50% probability ellipsoids.
- Figure 4-2. IR spectrum of $\text{Pd}(\text{S-DMSO})(\text{O-DMSO})(\text{TFA})_2$ **4-3a(s)**.
- Figure 4-3. Molecular structure of $\text{Pd}(\text{S-DMSO})(\text{OH}_2)(\text{TFA})_2$ **4-2a(s)**, with 50% probability ellipsoids.
- Figure 4-4. IR spectrum of $\text{Pd}(\text{S-DMSO})(\text{OH}_2)(\text{TFA})_2$ **4-2a(s)**.
- Figure 4-5. ^1H NMR spectra of $\text{Pd}(\text{TFA})_2$ in EtOAc in the presence of various quantities of DMSO at $-60\text{ }^\circ\text{C}$.
- Figure 4-6. ^{19}F NMR spectra of $\text{Pd}(\text{TFA})_2$ in EtOAc in the presence of various quantities of DMSO at $-60\text{ }^\circ\text{C}$.
- Figure 4-7. NMR spectra of $\text{Pd}(\text{TFA})_2/\text{DMSO}$ (1:1.6) in EtOAc at various temperatures.
- Figure 4-8. Plots of $\text{Pd}(\text{TFA})_2/\text{DMSO}$ complexes present in solution as a function of added [DMSO] on the basis of ^1H and ^{19}F NMR data, (A) and (B), respectively.
- Figure 4-9. Concentrations of **4-3a** and **4-3b** at different temperatures, based on analysis of the ^{19}F NMR spectra.
- Figure 4-10. van't Hoff plot of the equilibrium between **4-3a** and **4-3b**.

- Figure 4-11. ^1H NMR spectra of $\text{Pd}(\text{OAc})_2$ in EtOAc with various quantities of DMSO at 24 °C.
- Figure 4-12. Titration curves of DMSO into the solution of $\text{Pd}(\text{OAc})_2$ in EtOAc at 24 °C.
- Figure 4-13. ^1H NMR spectra of $\text{Pd}(\text{TFA})_2$ in $\text{THF-}d_8$ with various quantities of DMSO at -60 °C.
- Figure 4-14. ^{19}F NMR spectra of $\text{Pd}(\text{TFA})_2$ in $\text{THF-}d_8$ with various quantities of DMSO at -60 °C.
- Figure 4-15. ^1H NMR spectra of $\text{Pd}(\text{TFA})_2$ in $\text{THF-}d_8$ with various quantities of DMSO at 24 °C.
- Figure 4-16. Titration curve of DMSO into the solution of $\text{Pd}(\text{TFA})_2$ in $\text{THF-}d_8$.
- Figure 4-17. ^1H NMR spectra of $\text{Pd}(\text{TFA})_2$ in $\text{AcOH-}d_4$ with various quantities of DMSO at 24 °C.
- Figure 4-18. ^{19}F NMR spectra of $\text{Pd}(\text{TFA})_2$ in $\text{AcOH-}d_4$ with various quantities of DMSO at 24 °C.
- Figure 4-19. Titration curves of DMSO into the solution of $\text{Pd}(\text{TFA})_2$ in $\text{AcOH-}d_4$ at 24 °C.
- Figure 4-20. NMR spectra of $\text{Pd}(\text{TFA})_2/\text{DMSO}$ in toluene- d_8 at 24 °C.
- Figure 4-21. 1D EXSY NMR spectra of $\text{Pd}(\text{TFA})_2$ with 3 equiv. of DMSO in EtOAc (mix time = 0.28 sec).
- Figure 4-22. 1D EXSY NMR spectra of $\text{Pd}(\text{TFA})_2/\text{DMSO}$ in $\text{THF-}d_8$ (mix time = 0.25 sec).
- Figure 5-1. Reaction time course of $\text{Pd}(\text{DMSO})_2(\text{TFA})_2$ -catalyzed aerobic oxidation of cyclohexanone.
- Figure 5-2. Kinetic orders for $\text{Pd}(\text{DMSO})_2(\text{TFA})_2$ -catalyzed oxidation of cyclohexanone to cyclohexenone: dependence of the initial rate on substrate concentration (A);

dependence of the initial rate on catalyst concentration, where the “catalyst” is a 1:2 mixture of Pd(TFA)₂ and DMSO (B).

Figure 5-3. (A) Effect of the DMSO ligand on Pd-catalyzed oxidation of cyclohexanone to cyclohexenone evident from the dependence of the initial rate on the DMSO/Pd ratio. (B) Comparison of time courses for the dehydrogenation of cyclohexanone in the absence and presence of DMSO.

Figure 5-4. Dependence of the initial rate of Pd-catalyzed oxidation of cyclohexanone on different anionic ligands of Pd.

Figure 5-5. Time-courses of Pd(TFA)₂-catalyzed oxidation of cyclohexenone to phenol in the presence (blue) and absence (black) of DMSO.

Figure 5-6. Effect of products on the induction period in Pd(DMSO)₂(TFA)₂-catalyzed oxidation of cyclohexenone to phenol.

Figure 5-7. Dependence of the length of induction period on the Pd-catalyzed oxidation of cyclohexenone to phenol on [DMSO].

Figure 5-8. Dependence of the initial rate of Pd-catalyzed oxidation of cyclohexenone to phenol on the DMSO/Pd ratio.

Figure 5-9. Time courses for the oxidation of cyclohexanone with varying concentrations in the presence of a fixed catalyst concentration.

Figure 5-10. Time courses for oxidation of cyclohexanone in the presence of different catalyst loadings, where the “catalyst” is a 1:2 mixture of Pd(TFA)₂ and DMSO.

Figure 5-11. Time courses for oxidation of cyclohexanone in the presence of different quantities of DMSO with fixed Pd(TFA)₂ concentration.

- Figure 5-12. Time courses of Pd-catalyzed oxidation of cyclohexanone on different anionic ligands of Pd.
- Figure 5-13. Dependence of the initial rate of Pd-catalyzed oxidation of cyclohexenone to phenol on the DMSO/Pd ratio.
- Figure 5-14. Time course of Pd(DMSO)₂(TFA)₂-catalyzed oxidation of cyclohexenone to phenol.
- Figure 5-15. Dependence of the initial rate of Pd(DMSO)₂(TFA)₂-catalyzed aerobic oxidation of 4-*tert*-butylcyclohexanone on O₂ pressure.
- Figure 6-1. Reaction time courses for the dehydrogenation of cyclohexanone with different catalyst systems.
- Figure 6-2. Eyring plot for Pd(DMSO)₂(TFA)₂-catalyzed dehydrogenation of cyclohexanone.
- Figure 6-3. Reaction time course of Pd(DMSO)₂(TFA)₂-catalyzed aerobic oxidation of cyclohexanone in AcOH.
- Figure 6-4. Dependence of Pd(TFA)₂-catalyzed oxidation of cyclohexanone on sulfoxide ligands.
- Figure 6-5. Dependence of Pd(DMSO)₂(TFA)₂-catalyzed oxidation of cyclohexanone on acid and base additives.
- Figure 6-6. Dependence of the initial rate on [cyclohexenone] for Pd(DMSO)₂(TFA)₂-catalyzed oxidation of cyclohexenone to phenol.
- Figure 6-7. Dependence of the initial rate on the [catalyst], where the “catalyst” is an 1:2 mixture of Pd(TFA)₂ and DMSO, for Pd(DMSO)₂(TFA)₂-catalyzed oxidation of cyclohexenone to phenol.

- Figure 6-8. Dependence of the initial rate on the $[\text{Pd}(\text{TFA})_2]$ in the presence of excess DMSO ligand for $\text{Pd}(\text{DMSO})_2(\text{TFA})_2$ -catalyzed oxidation of cyclohexenone to phenol.
- Figure 6-9. Dependence of the initial rate of $\text{Pd}(\text{DMSO})_2(\text{TFA})_2$ -catalyzed oxidation of cyclohexenone to phenol on the ratio of DMSO/Pd.
- Figure 6-10. Dependence of the length of induction period on the Pd-catalyzed oxidation of cyclohexenone to phenol on $[\text{DMSO}]$.
- Figure 6-11. Dependence of the length of induction period on $[\text{cyclohexenone}]$ for $\text{Pd}(\text{DMSO})_2(\text{TFA})_2$ -catalyzed oxidation of cyclohexenone to phenol.
- Figure 6-12. Dependence of the length of induction period on catalyst concentration, where $[\text{Pd}(\text{TFA})_2]$ is varied at fixed $[\text{DMSO}]$ in excess (A) and the “catalyst” is an 1:2 mixture of $\text{Pd}(\text{TFA})_2$ and DMSO (B).
- Figure 6-13. Reaction time courses of Pd-catalyzed oxidation of cyclohexenone to phenol.
- Figure 6-14. Kinetic orders for unligated- $\text{Pd}(\text{TFA})_2$ catalyzed dehydrogenation of cyclohexenone to phenol, dependence of initial rate on $[\text{cyclohexenone}]$ (A) and on $[\text{Pd}(\text{TFA})_2]$ (B).
- Figure 6-15. Hg test for $\text{Pd}(\text{DMSO})_2(\text{TFA})_2$ -catalyzed aerobic dehydrogenation of cyclohexanone to cyclohexenone.
- Figure 6-16. Mercury test for $\text{Pd}(\text{TFA})_2$ -catalyzed aerobic oxidation of cyclohexenone to phenol in the presence of DMSO ligands (A) and the absence of DMSO ligands (B).
- Figure 7-1. Hammett plot of the acetoxylation of *p*-substituted $(\pi\text{-Allyl})\text{PdCl}$ complexes in the presence of BQ (A) and O_2 (B).

- Figure 7-2. Titration of CH_3CN into a solution of **7-1c** in AcOH determined by UV-Visible spectroscopy, UV-Visible spectra (A) and the absorption of the peak at 270 nm as a function of $[\text{CH}_3\text{CN}]$ (B).
- Figure 7-3. Titration of CD_3CN into a solution of **7-1c** in $\text{AcOH-}d_4$ determined by ^1H NMR spectroscopy: ^1H NMR spectra (A) and the integration of the peak at 4.65 ppm ($[\text{C}_6\text{H}_5\text{CH}_2\text{CHCH}_2\text{PdCl}]_2$) as a function of $[\text{CH}_3\text{CN}]$ (B).
- Figure 7-4. Dependence of the ^1H chemical shift of the benzylic proton of **7-1c** on $[\text{LiOAc}]$.
- Figure 7-5. Kinetic orders of O_2 -promoted acetoxylation of **7-1c**: dependence of the initial rate on **[7-1c]** (A) and $[\text{O}_2]$ (B).
- Figure 7-6. Rate dependence of the acetoxylation of **7-1c** on $[\text{LiOAc}]$.
- Figure 7-7. Kinetic orders of BQ-promoted acetoxylation of **7-1c**: dependence of the initial rate on **[7-1c]** (A) and $[\text{BQ}]$ (B).
- Figure 7-8. The ^1H NMR spectrum of **7-1c** under the reaction conditions (A) and crude spectrum of the same sample after 24 h (B).
- Figure 7-9. The initial time course of O_2 -promoted acetoxylation of **7-1c**.
- Figure 7-10. The acetate exchange experiment of allylbenzene **7-2c** in the presence of **7-1c** at $t = 0$ (A) and $t = 12$ h (B).

LIST OF SCHEMES

- Scheme 1-1. α,β -Unsaturated Carbonyl Compounds in Organic Reactions
- Scheme 1-2. Summary of pK_a s of the α -C–H of Carbonyl Compounds
- Scheme 1-3. α,β -Dehydrogenation of 2-Phenylcyclohexanone via Halogenation-Dehydrohalogenation
- Scheme 1-4. Pathways for Sulfur/Selenium-Based Dehydrogenation of Carbonyl Compounds
- Scheme 1-5. Proposed Mechanism for Pd^{II}-Mediated Dehydrogenation of Cyclohexanones
- Scheme 1-6. Proposed Pathways for Regioselective PdCl₂-Mediated Dehydrogenation of β -Amino Ketones
- Scheme 1-7. Proposed Catalytic Cycle for Pd-Catalyzed Dehydrogenation of Ketones
- Scheme 1-8. Pd(OAc)₂/Amine-Catalyzed Dehydrogenation of Hydrocinnamaldehyde Derivatives
- Scheme 1-9. Preparation of a Bicyclic Cyclohexenone Compound via Saegusa Reaction
- Scheme 1-10. Synthesis of a Cyclopentenone Intermediate by Saegusa Reaction
- Scheme 1-11. Comparison of Saegusa with Larock Conditions for Dehydrosilylation of a Triethylsilyloxy Alkene
- Scheme 1-12. Preparation of the Chiral 4-ⁱPr-cyclohexenone via Tandem Asymmetric Deprotonation-Saegusa Oxidation
- Scheme 1-13. Proposed Mechanism for Cu^IBr-Catalyzed Dehydrogenation of a 4-Oxazoline
- Scheme 2-1. Hydrogenation/Dehydrogenation of C–C Bonds (A) and Pd-Catalyzed Dehydrogenation of Cyclohexanones (B)
- Scheme 2-2. Proposed Mechanism for Pd^{II}-Catalyzed Dehydrogenation of Cyclic Ketones

- Scheme 3-1. Palladium-catalyzed Dehydrogenation of Cyclohexanones
- Scheme 3-2. Attempted Dehydrogenation of a Pharmaceutically Important Cyclopentanone derivative
- Scheme 3-3. Dehydrogenation of β -Aryl Carbonyl Compounds
- Scheme 3-4. Aerobic Dehydrogenation of Naringenin with the Pd(TFA)₂/4,5-Diazafluorenone Catalyst System
- Scheme 3-5. Deuterium Kinetic Isotope Effects Based on Independent Initial-rate Measurements
- Scheme 3-6. Proposed Catalytic Cycle for Pd-catalyzed α,β -Dehydrogenation of Carbonyl Compounds
- Scheme 4-1. Dimeric Carboxylate-Bridged Pd^{II} Complexes Reported in the Literature
- Scheme 4-2. Summary of Solution Structures of Pd(TFA)₂/DMSO in Various Solvents
- Scheme 4-3. Equations for Calculation of Ligand Exchange Rates Based on Line Broadening
- Scheme 4-4. Representative Equations for DMSO Ligand Exchange Rates
- Scheme 5-1. Comparison of Rate Constants of the Oxidation of 4-*tert*-Butylcyclohexanone
- Scheme 5-2. Proposed Mechanism for Pd-catalyzed Dehydrogenation of Cyclohexanones
- Scheme 5-3. Deuterium Kinetic Isotope Effects (KIE) Derived from Independent Measurement of Initial Rates of Dehydrogenation of Cyclohexanone to Cyclohexenone
- Scheme 5-4. Deuterium Kinetic Isotope Effects of Dehydrogenation of Cyclohexenone to Phenol Derived from Independent Measurement of Initial Rates
- Scheme 5-5. Proposed Mechanism for Pd(DMSO)₂(TFA)₂-Catalyzed Dehydrogenation of Cyclohexanone

- Scheme 6-1. The Generic Catalytic Cycle of Pd-Catalyzed Aerobic Oxidation Reactions
- Scheme 6-2. Deuterium Kinetic Isotope Effects (KIE) Derived from Independent Measurement of Initial Rates of Pd(TFA)₂-Catalyzed Dehydrogenation of Cyclohexenone to Phenol
- Scheme 6-3. Possible Pathways for Acid-Accelerated Dehydrogenation of Cyclohexanone
- Scheme 6-4. Proposed Mechanism for Pd(DMSO)₂(TFA)₂-Catalyzed Oxidation of Cyclohexenone to Phenol
- Scheme 7-1. Pd-Catalyzed Oxidative Allylic Functionalization Reactions
- Scheme 7-2. BQ-Promoted Oxidative Allylic C-H Acetoxylation
- Scheme 7-3. Acetoxylation of **7-1c** via the Pd^{II} Associative Pathway and Derived Rate Laws
- Scheme 7-4. Acetoxylation of **7-1c** via the Pd⁰ Trapping Pathway and Derived Rate Laws
- Scheme 7-5. Reversible Pathways for Formation of **7-2c-d₃** from **7-2c**
- Scheme 7-6. Equations for Calculation of the Equilibrium Constant Between **7-1c'** and **7-1c**
- Scheme 7-7. Equations for Derivation of the Saturation Dependence of [**7-1c''**] on [LiOAc]
- Scheme 7-8. Equations for Derivation of the Rate Laws

ABBREVIATIONS AND ACRONYMS

atm	atmosphere
DMSO	dimethyl sulfoxide
KIE	deuterium kinetic isotope effect
4 Å MS	4 Å molecular sieves
NMR	nuclear magnetic resonance
py	pyridine
TMS	trimethylsiloxyl
TBS	<i>tert</i> -butyldimethylsiloxyl
DMF	dimethylformamide
IR	Infrared
LDA	lithium Diisopropylamide
Pd	palladium
Ph	phenyl
Bn	benzyl
TFA	trifluoroacetate

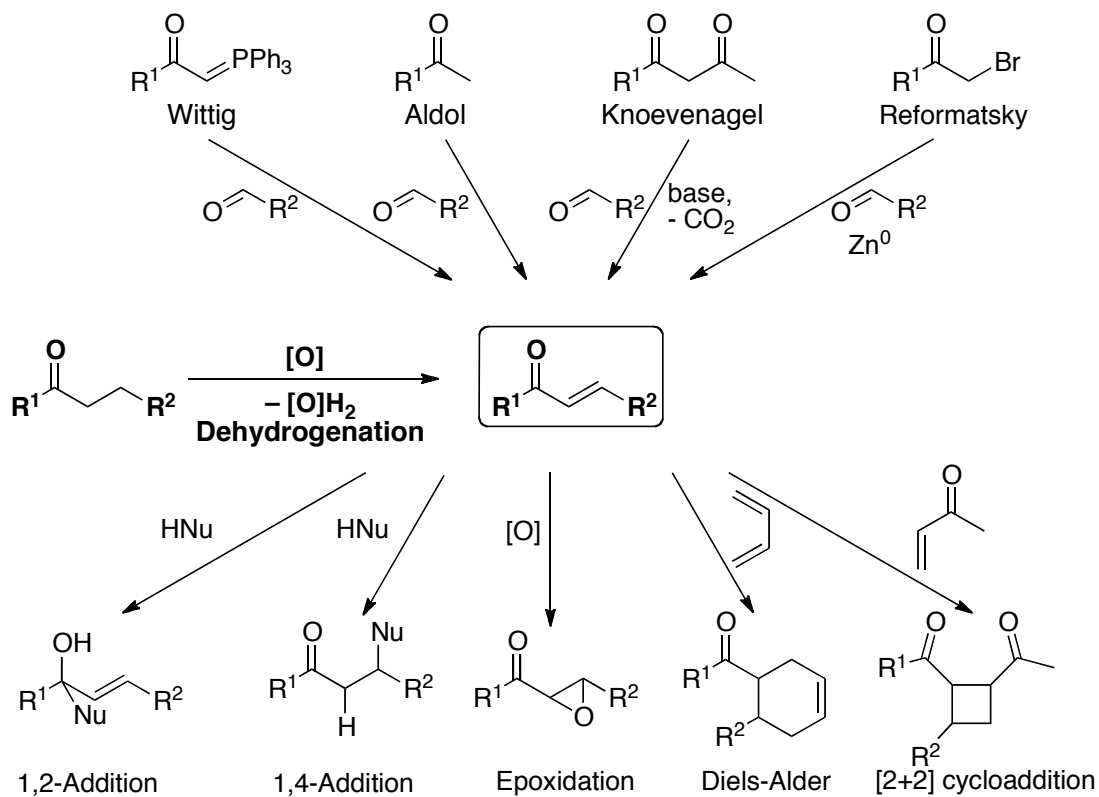
CHAPTER 1

Oxidation Adjacent to C=O bonds by Dehydrogenation

1.1 Introduction to α,β -Dehydrogenation of Carbonyl Compounds

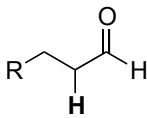
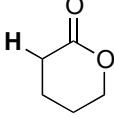
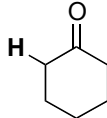
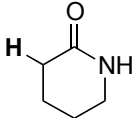
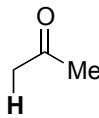
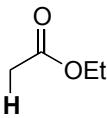
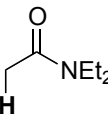
α,β -Unsaturated carbonyl compounds are featured in a variety of natural products and pharmaceutical compounds, and they are versatile intermediates in the synthesis of pharmaceuticals and biologically active compounds. Many of the synthetic methods that lead to such structures rely on condensation reactions that construct the C=C bonds from simpler molecular fragments (Scheme 1-1). An oxidative strategy that introduces unsaturation functionality into a pre-established molecular skeletons provides an appealing alternative method to accessing α,β -unsaturated carbonyl compounds.¹ The field of α,β -dehydrogenation of carbonyl compounds has been dominated by several stoichiometric methods, including halogenation/ dehydrohalogenation reactions, the use of selenium reagents and the recently developed hypervalent iodine reagents. Catalytic dehydrogenation reactions employing cheap and environmentally benign oxidants would provide an appealing alternative to these stoichiometric reagents. This introduction chapter focuses on transition metal-based stoichiometric and catalytic methods for the oxidation of saturated C–C bonds adjacent to C=O bonds. These reactions have provided important insights into the development of synthetically useful transition metal-catalyzed dehydrogenation reactions.

Scheme 1-1. α,β -Unsaturated Carbonyl Compounds in Organic Reactions



While various oxidative methods proceed with different mechanisms, the pK_a of the $\alpha\text{-C-H}$ of a carbonyl compound is often highly related to the reactivity of the substrate under various dehydrogenation conditions. The $\alpha\text{-}pK_a$ values of different carbonyl compounds are summarized in Scheme 1-2.² Aldehydes have the most acidic $\alpha\text{-C-H}$ and are often the most reactive. In contrast, esters and amides have the least acidic $\alpha\text{-C-H}$ s and exhibit low reactivities with many dehydrogenation reagents.

Scheme 1-2. Summary of pK_a Values of the α -C-H of Carbonyl Compounds

Substrates							
α - pK_a in DMSO	~ 17	25.2	26.4	26.6	26.5	29.5	34

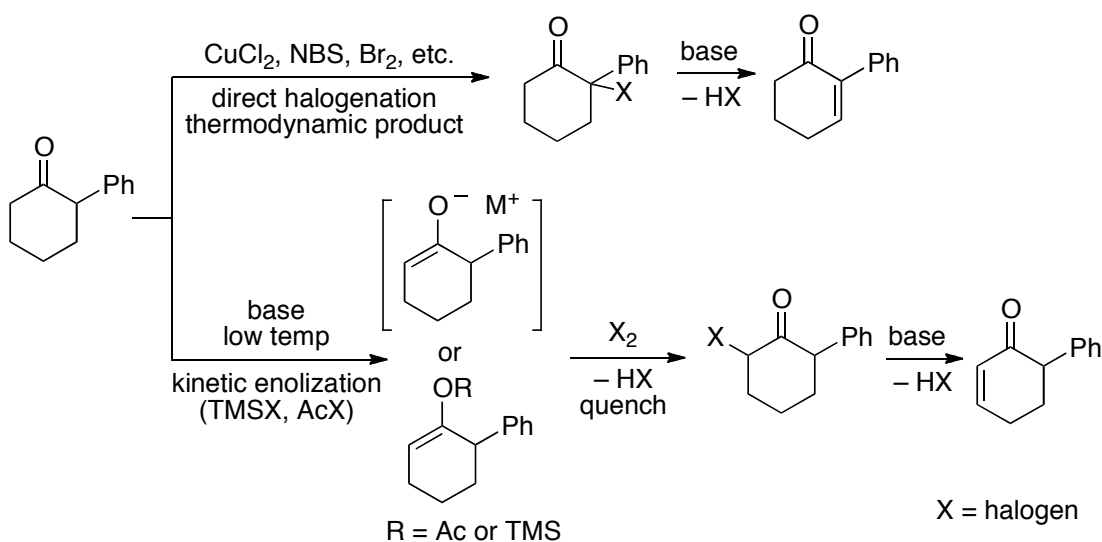
The selectivity as well as reactivity of various transition metal-based reagents will be discussed and compared in this chapter, with a focus on Pd-based complexes. Chemoselectivity issues that must be addressed include the relative rate of α,β -dehydrogenation adjacent to a carbonyl compounds versus oxidation of other functional groups, such as alcohols and other carbonyl groups in the molecule. For cases in which the resulting α,β -unsaturated compounds are susceptible to further reaction, the selectivity between mono-dehydrogenation and multiple dehydrogenation steps is also of interest. For example, oxidation of a cyclohexanone could afford the corresponding cyclohexenone or phenol, both of which are synthetic precursors to complicated organic molecules. Oxidation of an unsymmetric ketone could lead to two regioisomers. Oxidative reactions that can selectively afford one regioisomer relative to the other are exceptionally valuable.

1.2 Summary of Non-Transition Metal Based Methods

The stepwise α -halogenation followed by dehydrohalogenation in the presence of a base represents an early classical method for preparing α,β -unsaturated carbonyl compounds.¹ Direct halogenation with a halogenation reagent, such as *N*-bromosuccinamide (NBS),³ CuBr_2 ⁴ or Br_2 ⁵ usually requires high temperatures or exposure to light and favors the thermodynamic regioisomer, whereas base-mediated enolization^{6,7} followed by halogenation can lead to both

thermodynamic and kinetic products with good regioselectivity (Scheme 1-3).⁸ Elimination of the α -halo carbonyl compounds is often induced by a base to afford the corresponding α,β -unsaturated carbonyl compounds and hydrogen halides as the by-product. Various readily available enolization methods for ketones, aldehydes, esters and amides provide the basis for a broad substrate scope for the halogenation-dehydrohalogenation method. The basic conditions for the elimination step, however, limit the tolerance with base sensitive functional groups.

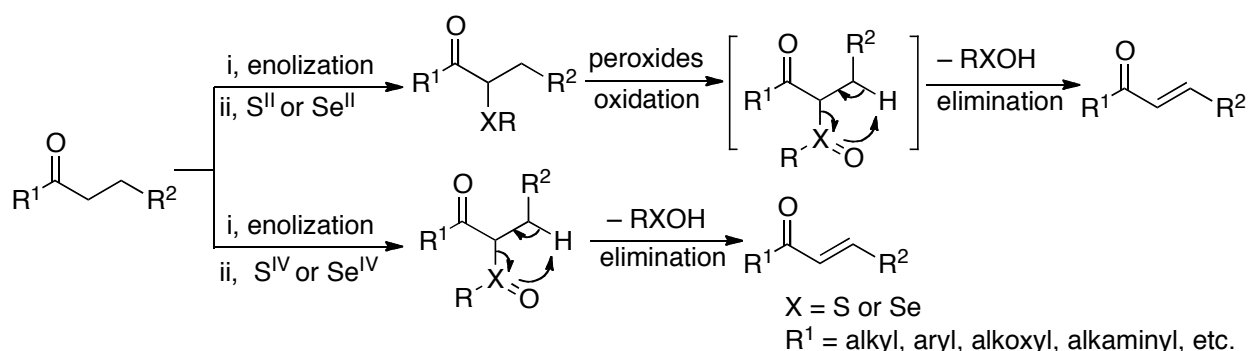
Scheme 1-3. α,β -Dehydrogenation of 2-Phenylcyclohexanone via Halogenation-Dehydrohalogenation



Organosulfur⁹ and organoselenium-mediated dehydrogenation reactions represent useful alternative methods relative to the halogenation/dehydrohalogenation reaction.^{10,11} A typical protocol consists of formation of α -C-S/C-Se bonds and subsequent oxidative elimination (Scheme 1-4). Similar to halogenation reactions, regioselective generation of α -sulfides or selenides from carbonyl compounds is facilitated by enolate/enol ether formation with various bases.^{6,7} Organo-S(II) and S(IV) reagents include biaryl and bialkyl disulfides, alkylsulfinyl

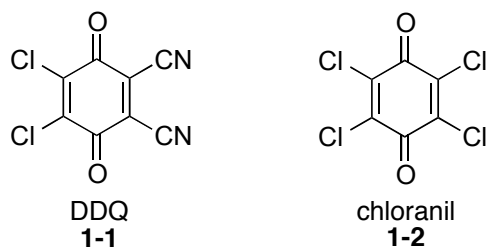
chlorides, thiosulfonates^{12,13} and sulfones,¹⁴ whereas reagents for forming α -selenides include phenylselenium halides, diselenides and selenic anhydrides.^{15,16} The subsequent elimination of the sulfoxide/selenium oxide intermediates is the key step of the overall reaction. Compared to the base-mediated elimination of hydrogen halides, the 5-membered concerted pathway requires lower energy, resulting in mild reaction conditions. The substrate scope of sulfur and selenium-based methods includes a broad range of carbonyl compounds, including ketones, aldehydes, lactones, lactams, esters and amides. The broad substrate scope, in addition to the excellent functional group tolerance resulting from mild reaction conditions, contributes to the widespread utility of organoselenium reagents, as well as sulfur-based reagents, in organic syntheses.

Scheme 1-4. Pathways for Sulfur/Selenium-Based Dehydrogenation of Carbonyl Compounds

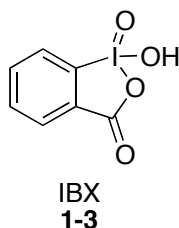


Methods discussed above require multiple-step processes and the use of toxic and expensive stoichiometric reagents. Quinone-based stoichiometric oxidants, 2,3-dichloro-5,6-dicyano-1,4-benzo-quinone (DDQ) **1-1** and chloranil **1-2** in particular,^{17,18} have high oxidation potentials and are shown to conduct efficient one-pot oxidation of carbonyl compounds.¹⁹ These reagents are especially useful in the oxidation of steroid derivatives and challenging substrates, such as esters and amides.²⁰ The powerful oxidation ability of quinones, however, leads to the lack of

chemoselectivity of quinone-mediated dehydrogenations. Substrates that are susceptible to overoxidation can undergo multi-step dehydrogenation in the presence of excess quinone oxidants.



2-Iodoxybenzoic acid (IBX) **1-3**^{21,22} has been recognized as an oxidant for organic reactions since 1893,²³ but it was not until 2000 that Nicolaou and coworkers demonstrated its full potential in α,β -dehydrogenation of ketones and aldehydes.^{24,25} Compared to the aforementioned stepwise strategies, IBX-mediated dehydrogenation lacks a mechanism to control the regioselectivity when oxidizing an unsymmetrical ketone.²⁶ IBX-mediated oxidation of silyl enol ethers, however, provides an opportunity to generate regioselective products.²⁷ Substrates bearing high α -p*K*_as, such as lactones, lactams, esters and amides,²⁸ however, pose a challenge for the IBX conditions. Nevertheless, the reliable reactivity and user-friendly protocol of IBX^{24,25} and its variants^{29,30} have led to the extensive utility of this method in natural product syntheses.³¹ The high molecular weight of IBX and equivalent oxidants, in addition to the production of by-products, restricts the synthetic utility on large-scale. Recently, a catalytic hypervalent iodine reagent, 2-iodoxybenzenesulfonic acid has been enabled, using Oxone® (2KHSO₅·KHSO₄·K₂SO₄) as the stoichiometric oxidant.³²

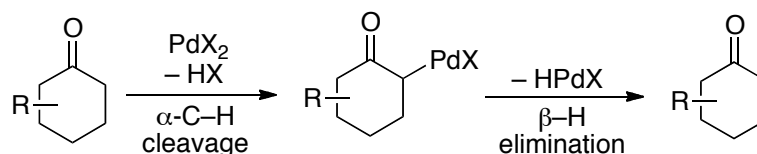


1.3 Pd-Mediated/Catalyzed Dehydrogenation

1.3.1 Stoichiometric Pd Salts

Modern organic syntheses increasingly require catalytic methods that employ cheap and green stoichiometric reagents in the context of atom economy and environmental sustainability. This goal becomes possible with the use of transition metal catalysts. Formation of organometallic intermediates is also expected to lower the transition state energy of the oxidation process, potentially resulting in mild reaction conditions and good functional group tolerance. Numerous studies of C–H activation by Pd as well as β -hydride elimination^{33,34} have provided the mechanistic basis for Pd-mediated dehydrogenation of carbonyl compounds. The general mechanism for Pd^{II}-mediated dehydrogenation of a cyclohexanone is expected to be initiated with Pd^{II}-mediated C–H cleavage to generate a Pd-enolate intermediate,³⁵ followed by β -H elimination to form the Pd-hydride and the cyclohexenone product (Scheme 1-5). Studies of the stoichiometric Pd-mediated dehydrogenation reactions provide important insights and foundations for the catalytic reactions.

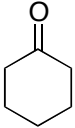
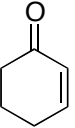
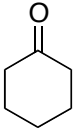
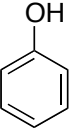
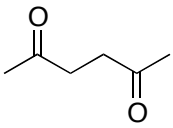
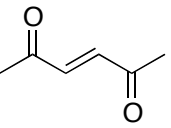
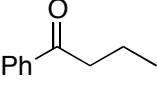
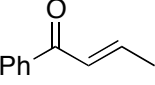
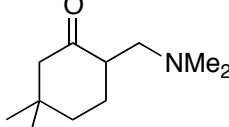
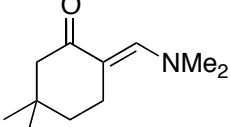
Scheme 1-5. Proposed Mechanism for Pd^{II}-Mediated Dehydrogenation of Cyclohexanones



Early exploration of Pd-mediated dehydrogenation reactions has focused on cyclic ketones or

substrates that lead to stable conjugated compounds upon dehydrogenation.³⁶ Bierling and coworkers first identified PdCl₂ for dehydrogenation of cyclohexanone in *tert*-BuOH and water to selectively afford cyclohexenone or phenol, respectively (Table 1-1, entries 1 and 2).^{37,38} PdCl₂ in *tert*-BuOH is also shown to aromatize 3,5-dimethylcyclohexenone to 3,5-dimethylphenol³⁹ and convert 2,2-dimethylcyclopentadione to the corresponding cyclopentendione as a synthetic intermediate for fredericamycin.⁴⁰

Table 1-1. Pd^{II}-Mediated α,β -Dehydrogenation of Carbonyl Compounds

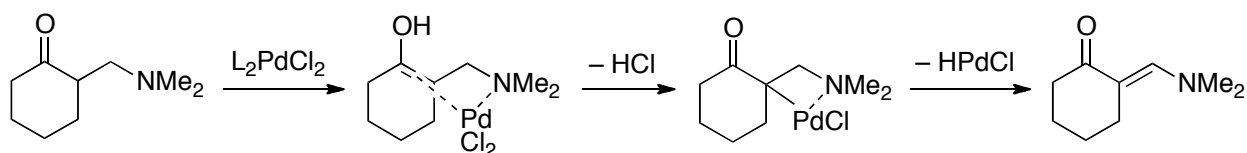
Entry	Substrate	Product	Conditions	Yield (%)
1			PdCl ₂ (0.02 equiv.) Solvent: <i>t</i> -BuOH	82/Pd
2			PdCl ₂ (0.06 equiv.) Solvent: H ₂ O	95/Pd
3			PdCl ₂ (PhCN) ₂ (0.34 equiv.) Solvent: <i>t</i> -BuOH 80 °C, 3 h	90/Pd
4			PdCl ₂ (PhCN) ₂ (1 equiv.) Ag(OTf) or Sn(OTf) ₂	78
5			PdCl ₂ (PhCN) ₂ (1 equiv.) Et ₃ N (2 equiv.) Solvent: CH ₃ CN reflux, 0.25 h	95

PdCl₂(PhCN)₂ exhibits good reactivity in dehydrogenating 2,5-hexanedione (Table 1-1, entry 3),⁴¹ and the combination of Pd with Ag(OTf) or Sn(OTf)₂ leads to improved yields with general

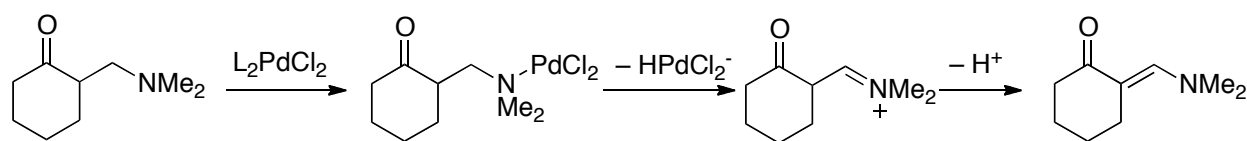
aldehydes and ketones (entry 4).⁴² The beneficial effect of metal additives may arise from their ability to form metal enolates with carbonyl compounds, followed by transmetalation to Pd^{II}. Dehydrogenation of a β -amino ketone with PdCl₂(PhCN)₂ selectively generates enaminone relative to the cyclohexen-1-one isomer (entry 5).⁴³ The authors attribute this selectivity to amine-directed formation of the Pd-enolate intermediate (Scheme 1-6). Alternatively, Pd can first oxidize the amine to afford an iminium intermediate, followed by tautomerization to generate the β -enaminone product.

Scheme 1-6. Proposed Pathways for Regioselective PdCl₂-Mediated Dehydrogenation of β -Amino Ketones

Directed Dehydrogenation

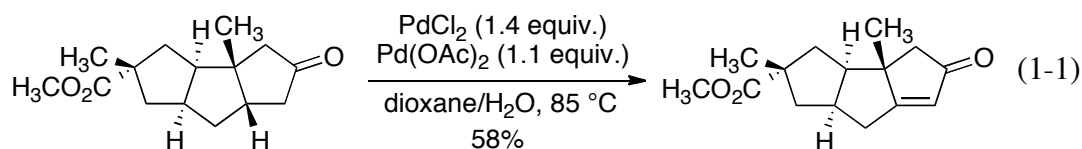


Amine Dehydrogenation

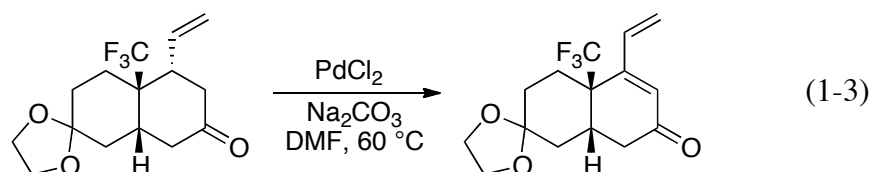
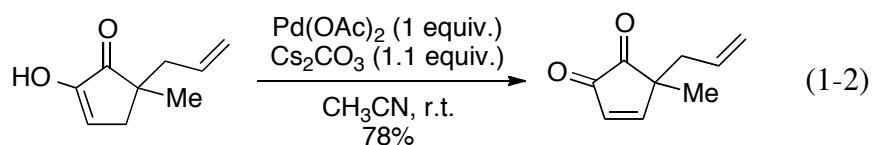


The use of stoichiometric Pd^{II} complexes as the oxidant for dehydrogenation reactions has found applications in natural product syntheses on the laboratory scale, especially with substrates that are challenging with other dehydrogenation methods. For example, a cyclopentenone compound is prepared, as a key intermediate to (\pm)-hirsutic acid C, in 58% yield by using a combination of stoichiometric PdCl₂ and Pd(OAc)₂ (eq 1-1).^{44,45} In comparison, step-wise selenium-based reagents and Saegusa-type dehydrosilylation methods (cf. section 1.3.3) lead to

unsatisfactory overall yields.



The mild conditions for Pd^{II}-mediated dehydrogenation allow for good functional group tolerance. A cyclopentane- α -dione intermediate to (–)-terpestacin decomposes under oxidative conditions, but undergoes facile dehydrogenation in the presence of stoichiometric Pd(OAc)₂ at room temperature (eq 1-2).⁴⁶ Regioselectivity has proved to be possible in synthetic examples. For instance, dehydrogenation of a trifluoromethylated perhydronaphthalene derivative favors formation of the conjugated cyclohexenone product (eq 1-3).⁴⁷ However, the origins of regioselectivity in Pd-mediated dehydrogenation are not clear without thorough understanding of the precise mechanism.

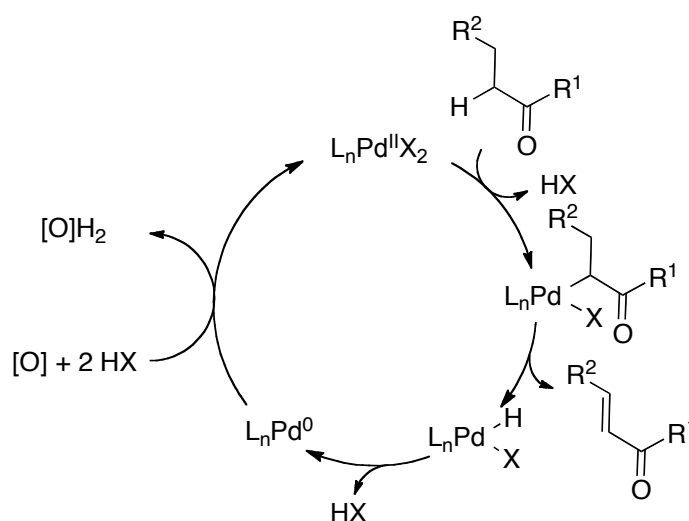


1.3.2 Pd Catalysts Coupled with Stoichiometric Oxidants

In light of the availability of various cheap oxidants capable of oxidizing Pd⁰ to Pd^{II}, such as peroxides, phosphates, benzoquinone (BQ) and O₂, considerable efforts have been made to use

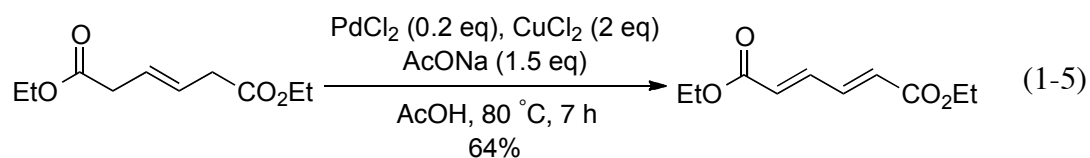
catalytic Pd coupled with a variety of oxidants for the dehydrogenation of ketones. Scheme 1-7 shows a generic catalytic cycle for these reactions. The half-reaction for substrate oxidation is consistent with the Pd-mediated reactions initiated with formation of a Pd^{II}-enolate intermediate, followed by β -hydride elimination to afford the enone product. The resulting Pd⁰ intermediate can be oxidized by an external oxidant to regenerate the Pd^{II} catalyst.

Scheme 1-7. Proposed Catalytic Cycle for Pd-Catalyzed Dehydrogenation of Ketones

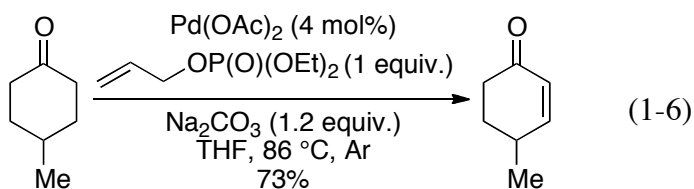


The PdCl₂ catalyst, identified for dehydrogenating ketones (cf. section 1.3.2), is used in catalytic quantities in combination with *tert*-BuOOH (eq 1-4)⁴⁸ or CuCl₂ (eq 1-5)⁴⁹ as the stoichiometric oxidant. Dehydrogenation of unsubstituted cyclohexanone and the 1,6-diester under these conditions, respectively, proceed to the desired unsaturated product in modest yields. However, dehydrogenation of more general substrates are not enabled with these conditions.

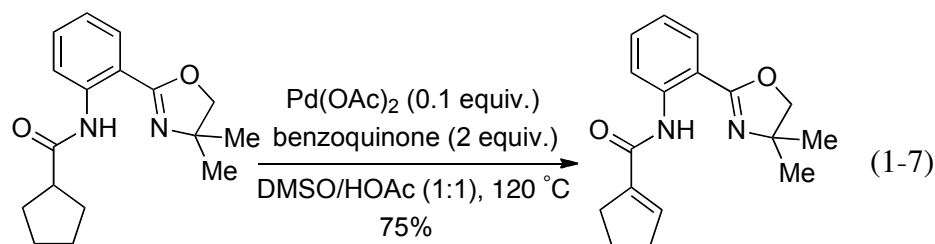




Oxidative addition of Pd^0 to allyl esters to generate $(\pi\text{-allyl})\text{Pd}^{\text{II}}$ allow the use of allyl esters as oxidants for Pd^0 . $\text{Pd}(\text{OAc})_2$ -catalyzed dehydrogenation reactions are enabled by Shvo and coworkers, using diethyl allyl phosphate as the oxidant (eq 1-6).⁵⁰ This method showed an improved substrate scope relative to previous methods, including cyclic ketones and acyclic aldehydes. The diethyl allyl phosphate is readily accessible from condensation of the commercially available diethyl chlorophosphate and allyl alcohol, which enhances the utility of this method in organic syntheses.⁵¹



The substrate scope of Pd -catalyzed dehydrogenation reactions reflects the acidity of $\alpha\text{-C-H}$ of carbonyl compounds. The high $\text{p}K_a$ of $\alpha\text{-C-Hs}$ of esters and amides results in the lack of reactivities of these substrates in Pd -catalyzed dehydrogenation reactions. $\text{Pd}(\text{OAc})_2$ -catalyzed dehydrogenation of amides has been achieved by Yu and coworkers by employing a tethered oxazoline substituent as the directing group to facilitate the reaction (eq 1-7).⁵² The reaction utilizes BQ to reoxidize Pd . However, the requirement of a contrived substrate results in the lack synthetic utility.



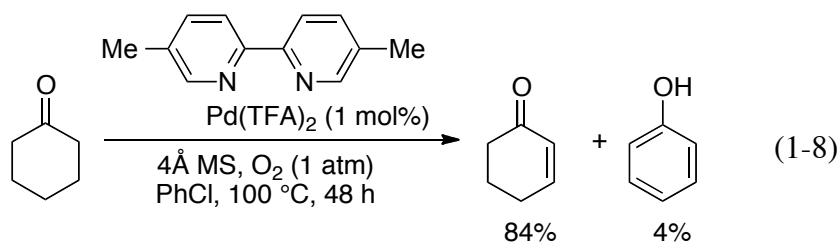
Molecular oxygen represents an ideal oxidant in the context of green chemistry, and is capable of oxidizing Pd^0 to Pd^{II} .⁵³ On laboratory scales, 1 atm O_2 can be achieved by using O_2 balloons, and > 1 atm O_2 requires Parr vessel reactors behind a blast shield. In large-scale processes, the low cost of O_2 makes it an optimal oxidant. Safety concerns associated with mixing of O_2 with flammable organic components can be addressed by utilizing dilute O_2 in N_2 .⁵⁴

Early efforts of aerobic Pd-catalyzed dehydrogenation reactions focus on simple unsubstituted cyclohexanones under 1 atm O_2 .⁵⁵ Cyclohexenone and phenol are both observed as the product under various conditions (Table 1-2). Co-catalysts, including $\text{Cu}(\text{acac})_2$, BQ and $\text{Ag}(\text{OTf})$, are used to facilitate the reoxidation of Pd^0 by O_2 , but $< 30\%$ yields are generally obtained (entries 1-2).^{36, 56} $\text{Pd}(\text{TFA})_2$ is demonstrated to be superior than other Pd sources and the use of unligated $\text{Pd}(\text{TFA})_2$ affords cyclohexenone in 51% yield with 13% phenol as the by-product (entry 3).⁵⁷ Addition of phosphine ligands did not result in a higher yield (entry 4).⁵⁸

Table 1-2. Early Examples of Pd-Catalyzed Aerobic Dehydrogenation of Cyclohexanone

Entry	Catalyst	Yield (%)	
1	0.2% Pd(acac) ₂ , 20% Cu(acac) ₂ or benzoquinone	19	11
2	2% PdCl(NO ₂)(MeCN) ₂ , 2% Ag(OTf)	27	1
3	2% Pd(TFA) ₂ , r.t., 5 days	51	13
4	5% Pd(TFA) ₂ , P(<i>p</i> -Tol) ₃	6	0

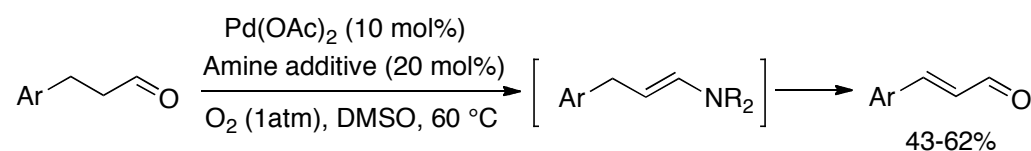
A remarkable improvement of the yield for dehydrogenation of cyclohexenone is achieved by Tsuji and coworkers in 2007, using a 5,5'-Me₂bpy-ligated Pd(TFA)₂ catalyst (eq 1-8).⁵⁹ However, these conditions are limited to unsubstituted cyclohexanone substrates, as the dehydrogenation of 2-*tert*-butylcyclohexanone and 3,5-dimethylcyclohexanone affords the corresponding cyclohexenone in only 19% and 9% yields, respectively. Dehydrogenation of acyclic ketones, such as 4-phenyl-2-butanone, also results in low yield (<20%).



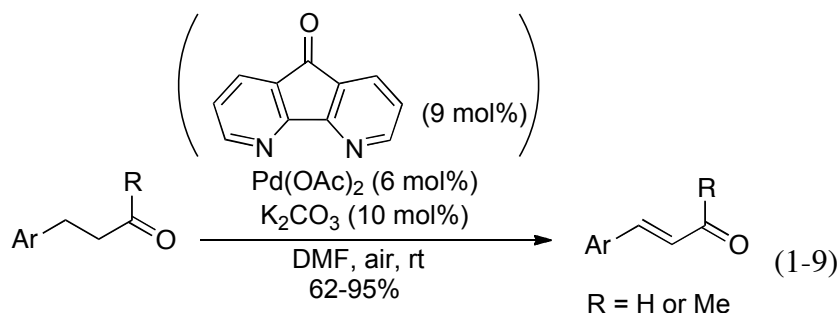
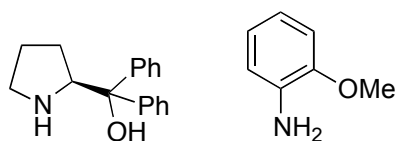
Aerobic dehydrogenation of acyclic carbonyl compounds appears to be more challenging relative to cyclic ketones. Hydrocinnamaldehyde derivatives bear more acidic α-C-Hs than other carbonyl compounds, and are shown to undergo dehydrogenation in the presence of Pd(OAc)₂

and amine co-catalysts in modest yields (Scheme 1-8).^{60,61} The amine additives are proposed to be crucial for promoting the reaction by forming an enamine intermediate from the reaction of hydrocinnamaldehydes with the amine additive. Analogous ketones, for example benzylactone, are unreactive under these conditions. Improved yields for dehydrogenating hydrocinnamaldehyde derivatives are achieved with a 4,5-diazafluorenone-ligated Pd(OAc)₂ catalyst (eq 1-9).⁶² In the same report, a number of β-arylbutanones are shown to undergo dehydrogenation to the corresponding β-arylbutenones in the absence of the 4,5-diazafluorenone ligand.

Scheme 1-8. Pd(OAc)₂/Amine-Catalyzed Dehydrogenation of Hydrocinnamaldehyde Derivatives

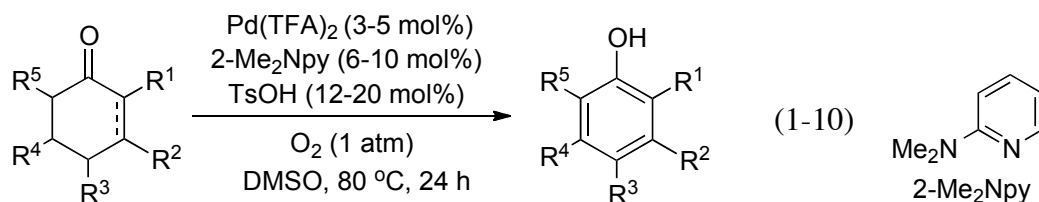


Amine additives



Pd-catalyzed aromatization reactions that convert cyclohexanones and cyclohexenones to phenol derivatives are also explored recently and provided an appealing method for synthesis of

substituted phenols.⁶³ Pd(TFA)₂ in combination with 2-Me₂Npy and TsOH displays good reactivity for this transformation with a number of alkyl and aryl-substituted substrates (eq 1-10). The capability of accessing substituted phenol derivatives with this reaction complements traditional cross-coupling reactions, and has great potential in organic synthesis.



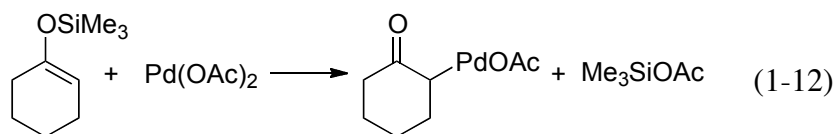
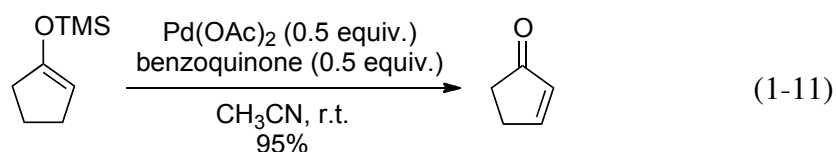
The scope and utility of Pd-catalyzed α,β -dehydrogenations are expanded by tandem dehydrogenation followed by condensation reactions. The in-situ trapping of the resulting β -keto- α,β -unsaturated ester from dehydrogenation with a nucleophile provides a unique way to access β' -aryl β -keto esters.⁶⁴ Pd(TFA)₂ in combination of *tert*-butyl perbenzoate is used as the catalyst system. In another example, condensation of the carbonyl of a cyclohexenone with amines affords diarylamine derivatives.⁶⁵ The anaerobic conditions with nitrobenzene as the oxidant and a coupling partner allow phosphine ligands being used.

Methods presented above demonstrated that Pd-catalyzed dehydrogenation reactions are plausible with a cheap oxidant, such as O₂, and clearly identified challenges and opportunities exist in this field. In order for Pd-catalyzed dehydrogenation reactions to be synthetically useful, catalysts that enable a broad substrate scope with high yields need to be identified. Substrates that are susceptible to further dehydrogenation at the γ,δ -position often result in a mixture of products with various degree of oxidation. Catalysts that perform selective oxidation to afford one product relative to others would be particularly valuable. Substrates with less acidic α -C-H bonds, including esters and amides, are essentially unreactive with current Pd catalysts. In

addition, decomposition of the Pd catalyst is observed in many reactions with insufficient O₂ pressure. Future development of catalysts that allow the use of air rather than O₂ with an expanded substrate scope would enable extensive application of the aerobic oxidation methods in organic syntheses.

1.3.3 Pd-Mediated/Catalyzed Dehydrogenation of Silyl Enol Ethers

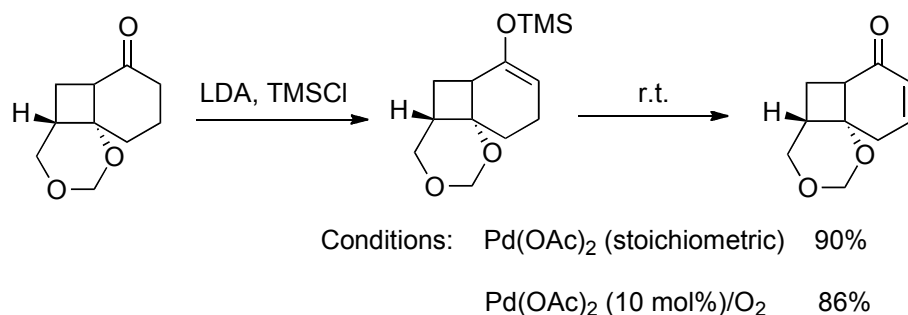
Silyl enol ethers are masked ketones that are readily accessible and of higher reactivity relative to ketones. Saegusa and coworkers first reported dehydrosilylation of trimethylsilyloxyalkene derivatives to generate α,β -unsaturated enones, using sub-stoichiometric Pd(OAc)₂ (0.5 equiv.) in combination with BQ as the oxidant (eq 1-11).⁶⁶ The Saegusa reaction is expected to proceed via a similar Pd-enolate intermediate to that of direct Pd-mediated dehydrogenation of ketones, despite the use of silyl enol ether (eq 1-12). Subsequent β -H elimination affords the corresponding enone product and Pd-H.



Larock and coworkers' development of a Pd(OAc)₂-catalyzed aerobic Saegusa reaction is inspired by the synthesis of a tricyclic enone fragment for Taxane.⁶⁷ Catalytic Pd(OAc)₂ in DMSO under 1 atm O₂ led to comparable yields relative to stoichiometric Pd(OAc)₂ in oxidation of the trimethylsilyloxycyclohexene derivative (Scheme 1-9).⁶⁸ Replacement of CH₃CN with DMSO as the solvent in the Saegusa conditions provides a beneficial effect on stabilizing the Pd

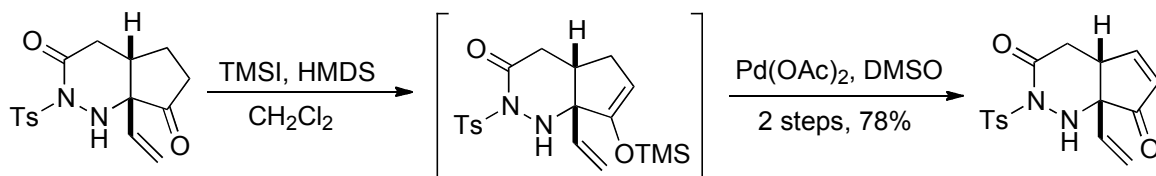
catalyst under aerobic conditions. The intrinsic high reactivity of silyl enol ethers with Pd^{II} enables good conversion of challenging substrates under the Saegusa/Larock conditions relative to the direct dehydrogenation, and the mild conditions are beneficial for compounds with sensitive functional groups. These features result in extensive utility of the dehydrosilylation method in natural product and pharmaceutical compound syntheses.⁶⁹

Scheme 1-9. Preparation of a Bicyclic Cyclohexenone Compound via Saegusa Reaction

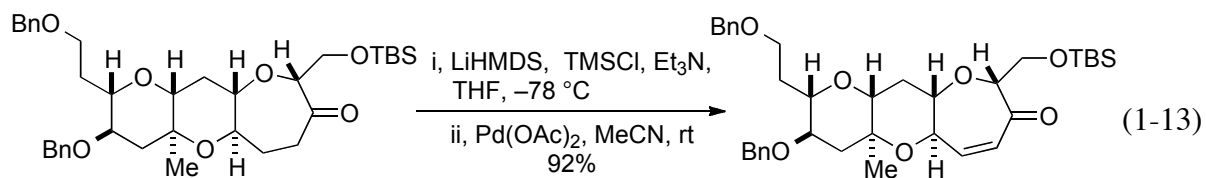


A large number of methods available for preparing silyl enol ethers provides further leverage for the Saegusa reaction.⁸ Common bases include triethylamine, lithium diisopropylamine (LDA) and lithium bis(trimethylsilylamine) (LiHMDS). TMSCl and TMS(OTf) are the prevailing choices of trimethylsilylation reagents. Particular substrates, however, require optimization of the conditions for forming silyl enol ethers. The bicyclic cyclopentenone intermediate is a precursor to Palau'amine, and has been synthesized by the Saegusa reaction in 78% yield (Scheme 1-10). The preparation of the trimethylsilyloxycyclopentenone requires TMSI in combination with the bis(trimethylsilyl)amine (HMDS). Meanwhile, the halogenation-dehydrohalogenation, selenium reagents and IBX proved to be unsuccessful with this substrate.⁷⁰

Scheme 1-10. Synthesis of a Cyclopentenone Intermediate by Saegusa Reaction



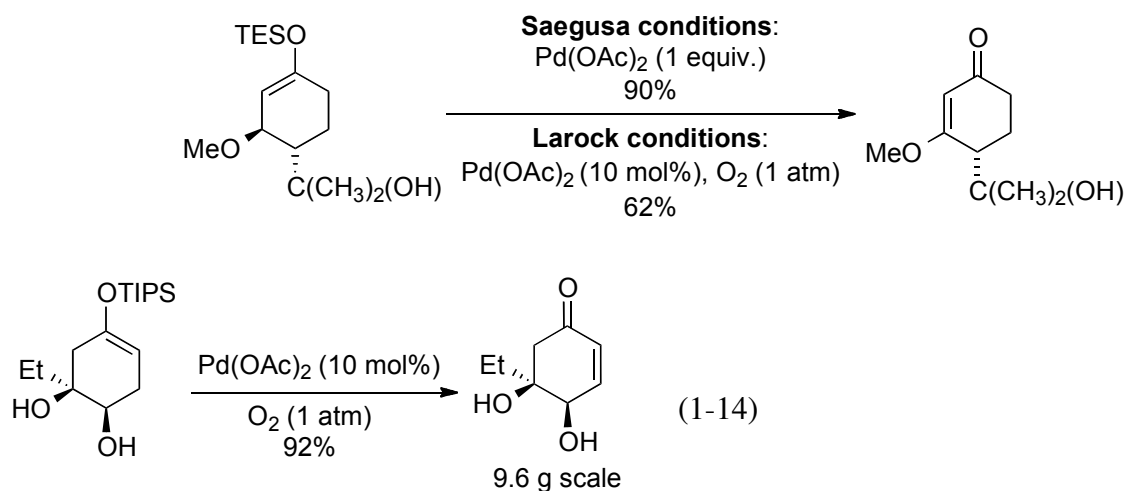
Most sequential trimethylsilylation-dehydrogenation reactions require isolation and purification of the silyl enol ether intermediate, which leads to loss of materials and waste of solvents. In some cases, however, only solvent removal after the silylation step is required and the resulting mixture can be directly reacted with Pd^{II}. For instance, dehydrogenative synthesis of the 3-oxepinone derivative, as a synthetic intermediate for (-)-gambierol, proved to be unsuccessful with selenium reagents and IBX (eq 1-13).⁷¹ One-pot silyl enol ether formation followed by Pd(OAc)₂-mediated dehydrosilylation affords the 3-oxepinone in good yield. Similar pseudo-one-pot Saegusa procedures have also been used in the synthesis of enone intermediates to palau'amine⁷⁰ and (+)-aspidospermidine.⁷²



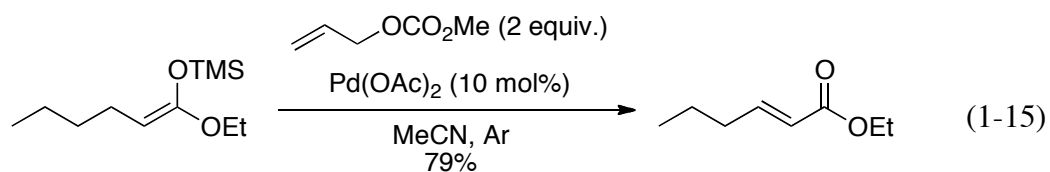
Saegusa and Larock's original method development focuses on the dehydrogenation of the trimethylsilyloxy alkenes. The identity of the silyl group exhibits a significant influence on the reactivity. In the dehydrosilylation of a 3-methoxyl triethylsilyloxy cyclohexene substrate, Saegusa conditions with stoichiometric Pd(OAc)₂ lead to the corresponding 3-methoxylcyclohexenone in good yield, whereas Larock's catalytic conditions results in modest yield (Scheme 1-11).⁷³ Subsequent conversion of this cyclohexenone leads to the total synthesis

of (-)-platyphyllide. During the synthesis of (-)-lomaiviticin aglycon, however, the catalytic conditions proved to be successful in the dehydrosilylation of a triisopropylsilyloxy cyclohexene intermediate on a 9.6 g scale (eq 1-14).⁷⁴ Remarkably, although Pd(OAc)₂ is known to be capable of oxidizing alcohols to ketones, the primary and secondary alcohol substituents in the above two examples survive the dehydrosilylation conditions.

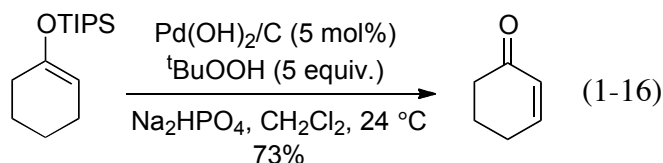
Scheme 1-11. Comparison of Saegusa with Larock Conditions for Dehydrosilylation of a Triethylsilyloxy Alkene



While the Saegusa/Larock dehydrosilylation conditions are versatile for a variety of cyclic and acyclic ketones and aldehydes derived from trimethylsilyloxyalkenes, attempts to oxidize silyl ketene acetals result in low yields, due to the hydrolysis of the substrate to the corresponding esters.⁶⁷ Tsuji and coworkers achieved catalytic dehydrosilylation of silyl ketene acetals with Pd(OAc)₂ under Ar, using allyl methyl carbonate as the stoichiometric oxidant (eq 1-15).⁷⁵ Several unsaturated esters and lactones are prepared via this reaction.⁷⁶



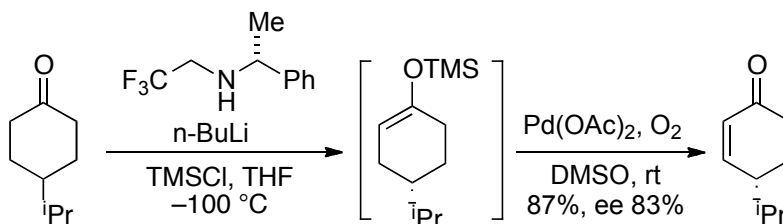
A heterogeneous catalyst, $\text{Pd(OH)}_2/\text{C}$, is reported by Corey and coworkers for dehydrosilylation of the triisopropylsilyloxy cyclic alkene derivatives, using *t*-BuOOH as the oxidant (eq 1-16).⁷⁷ Compared to O_2 , *t*-BuOOH is easier to handle on a laboratory scale and is a complement to O_2 . Analogous to the Saegusa and Larock conditions, the $\text{Pd(OH)}_2/\text{C}$ -catalyzed dehydrosilylation proceeds at room temperature. The substrate scope includes both 5- and 6-membered cyclic ketones



The regioselectivity of silyl enol ether formation can be easily controlled by base-mediated enolization methods. In addition, the sequential silyl enol ether formation-dehydrogenation method provides a way to control the stereochemistry of the product. Chiral bases have been developed for enantioselective deprotonation of 4-substituted cyclohexanones to generate the corresponding chiral silyl enol ethers (Scheme 1-12).⁷⁸⁻⁸⁰ Dehydrosilylation of the resulting chiral silyl enol ethers are shown to afford the corresponding chiral 4-substituted cyclohexenone.⁸¹ This strategy has found applications in the enantioselective synthesis of a fragment of Labiatin⁸² and a fumagillin analogue, as a potential MetAP-2 Reversible Inhibitor.⁸³ Despite great potential in synthesis, this strategy is limited by the lack of chiral bases leading to high enantioselective

deprotonation under practical conditions. The best reported ee obtained with chiral bases is < 95%, and requires temperatures below $-100\text{ }^{\circ}\text{C}$.

Scheme 1-12. Preparation of the Chiral 4-*i*-Pr-cyclohexenone via Tandem Asymmetric Deprotonation-Sagusa Oxidation⁸²

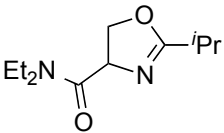
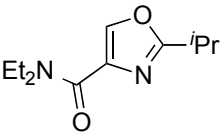
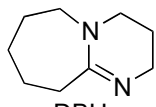
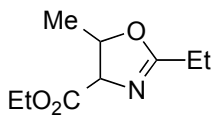
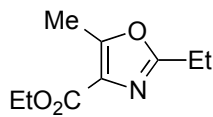
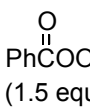
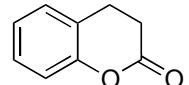
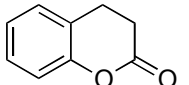
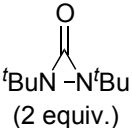
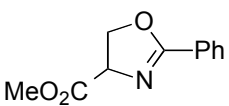
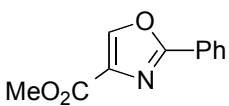
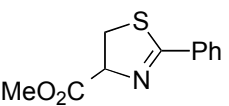
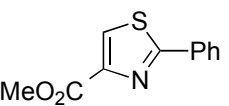
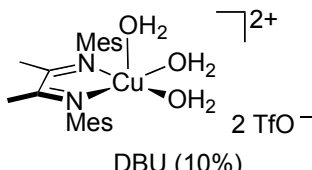
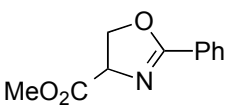
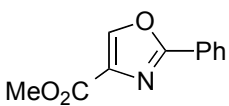
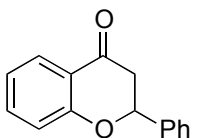
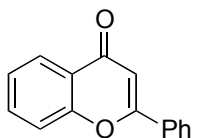
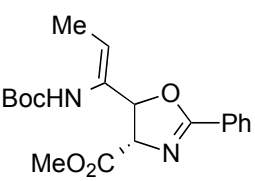
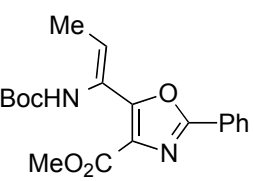


1.4 Transition Metals other than Pd

A number of transition metals other than Pd, including Cu, Ni and Mn, are shown to promote dehydrogenation reactions via different mechanisms relative to Pd, thus resulting in a distinct but valuable substrate scope. In particular, heterocycles could undergo competing oxidative degradation or poison Pd catalysts as a result of strong coordination to the electrophilic palladium center. Such an interaction between heterocycles and first-row metals are much weaker relative to Pd. Barrish and coworkers first discovered that in the presence of 2 equiv. of $\text{Cu}^{\text{II}}\text{Br}_2$ and DBU (1,8-diazabicyclo[5.4.0]undec-7-ene), the reaction has been applied to prepare a 4-carbamoyloxazole compound as the precursor to calyculin C.⁸⁴ Meyers and coworkers reported a similar reaction with 4-carboxyl oxazoline derivatives, using a stoichiometric Cu^{I} salt in combination with *tert*-butyl perbenzoate as the oxidant (entry 2).^{85,86} A catalytic method for the oxidation of dihydrocoumarin and a few other oxazoline and thiazoline derivatives is achieved by Shi and coworkers with the Cu^{I} loading reduced to 10% in the presence of the *N,N*-di-*tert*-butyldiaziridinone oxidant (entry 3).⁸⁷ Aerobic oxidation of 4-carboxylthiazolines to the

corresponding thiazoles are achieved with $\text{Cu}(\text{OAc})_2$ ⁸⁸ and a diimine-ligated Cu^{II} cation catalyst (entries 4 and 5).⁸⁹ The $\text{Cu}(\text{OAc})_2$ catalyst is also effective with 4-carboxyl and carbamyl oxazolines, while oxidation of 4-carboxyloxazoline with the diimine-ligated Cu^{II} proceeds with dramatically decreased yields. Nickel peroxides also promoted the stoichiometric dehydrogenation of 4-carbamyloxazolines and flavanone in moderate yields (entries 6-7).⁹⁰ Manganese dioxide, as another prominent inorganic oxidant, has also demonstrated activity with oxazolines⁹¹ (entry 8) and thiazolines.⁹²

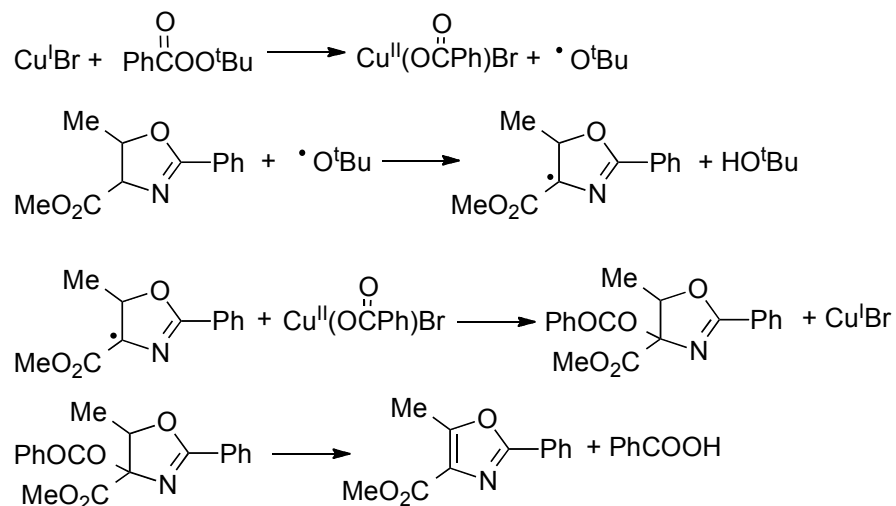
Table 1-3. Cu, Ni and Mn-Promoted Dehydrogenation of Heterocycles

Entry	Substrate	Product	Catalyst/Additive	Oxidant	Yield (%)
1			 DBU (2 equiv.)	Cu ^{II} Br ₂ (2 equiv.)	65
2			Cu ^I Br (1.1 equiv.)	 PhCOOtBu (1.5 equiv.)	63
3			(PPh ₃)CuCl (10 mol%)	 tBuN-C(=O)-NtBu (2 equiv.)	60
4			Cu(OAc) ₂ (10 mol%)	O ₂ (1 atm)	82
5			 DBU (10%)	air	88
6				Ni ^{II} O ₂ (1.5 equiv.)	69
7				Ni ^{II} O ₂ (1.6 equiv.)	71
8				Mn ^{IV} O ₂	42

Despite the lack of thorough mechanistic studies, the reactions presented above are speculated to proceed through single electron transfer. Scheme 1-13 illustrates a representative

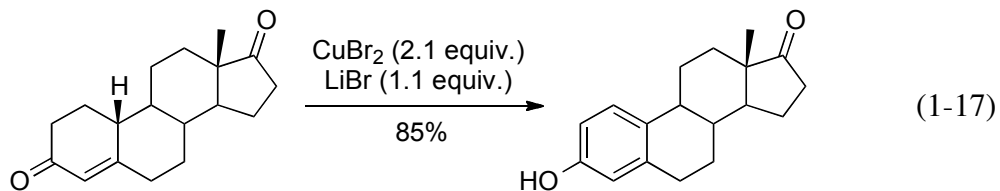
mechanism for Cu^IBr-catalyzed dehydrogenation of a 4-carbomethoxy oxazoline.⁸⁶ The reaction is initiated with oxidation of Cu^I to Cu^{II} by *tert*-butyl perbenzoate with concomitant formation of the *tert*-butoxyl radical, known as the Kharasch-Sosnovsky reaction.⁹³ The *tert*-butoxyl radical abstracts a hydrogen atom from the oxazoline to form a radical intermediate, which is stabilized by the adjacent carboxylate and the imine groups. One electron oxidation of the radical intermediate by Cu^{II} affords an acyloxy oxazoline, followed by fast elimination to afford the corresponding oxazole. These base metal-mediated/catalyzed dehydrogenations of heterocycles serve as a complement to Pd-catalyzed dehydrogenation methods. However, current conditions lack a general substrate scope. Understanding of the mechanism could lead to the development of synthetically useful methods with good functional group compatibility, and have major impact in organic synthesis.

Scheme 1-13. Proposed Mechanism for Cu^IBr-Catalyzed Dehydrogenation of a 4-Oxazoline

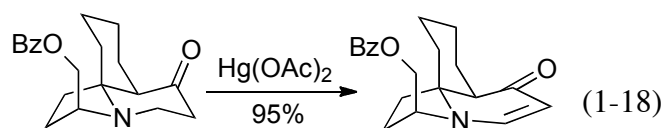


Besides heterocycles, Cu catalysts are also effective for converting cyclohexenone derivatives to phenols. Stoichiometric quantity of CuBr₂ oxidizes the cyclohexenone fragment of

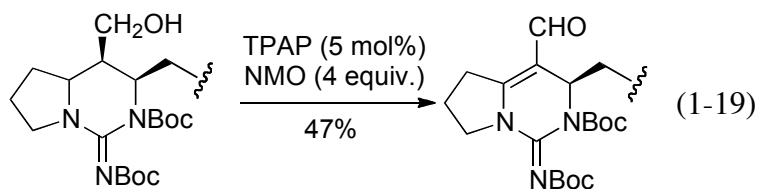
estr-4-ene-3,17-dione to the corresponding phenol derivative (eq 1-17),⁹⁴ while the cyclopentanone fragment remained intact under the reaction conditions. A recent $\text{Cu}(\text{OTf})_2$ catalyzed aerobic dehydrogenation of cyclohexenone is coupled with in-situ condensation with alcohols to generate aromatic ethers.⁹⁵



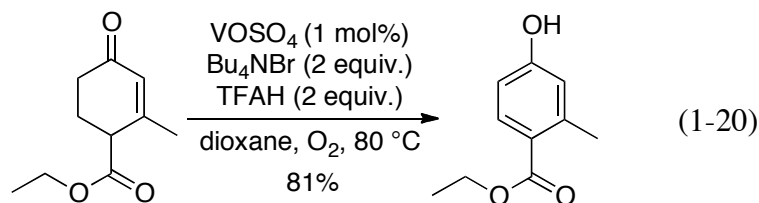
Transition metals with high oxidation states can serve as stoichiometric oxidants for the α,β -dehydrogenation of challenging substrates. Padwa and coworkers presented the use of $\text{Hg}(\text{OAc})_2$ to oxidize an azadecaline ring into the corresponding $2H$ -piperidonyl enone, in the total synthesis of (\pm)-cylindricine C (eq 1-18).⁹⁶ A variety of the aforementioned oxidative methods and reagents, including α -halogenation-elimination, PhSeCl , IBX and dehydrosilylation failed to produce any synthetically useful quantity of cyclohexenone product.⁹⁷



Tetrapropylammonium perruthenate (TPAP) is often used as an oxidant to convert alcohols to aldehydes and ketones.⁹⁸ The synthesis of (+)-Batzellatin A employs catalytic TPAP in combination with NMO (4-methylmorpholine *N*-oxide) to perform a one-pot oxidation of the guanidine derived primary alcohol to the corresponding β -amino enal in modest yield (eq 1-19).⁹⁹ While two regioisomers are expected, only the desired one is observed.



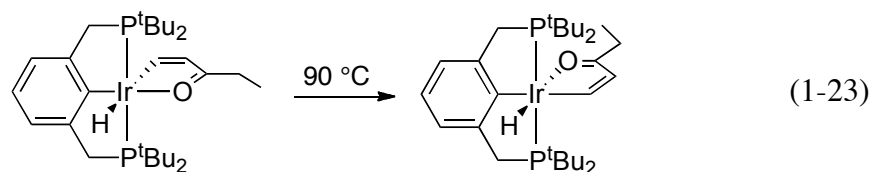
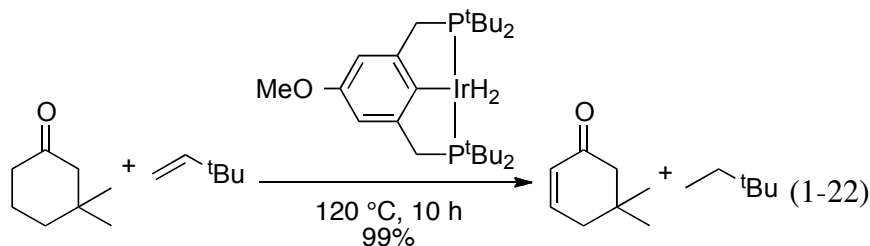
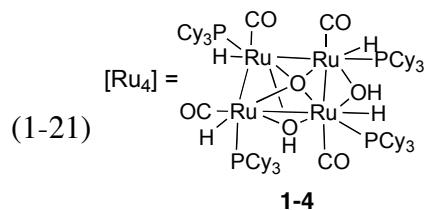
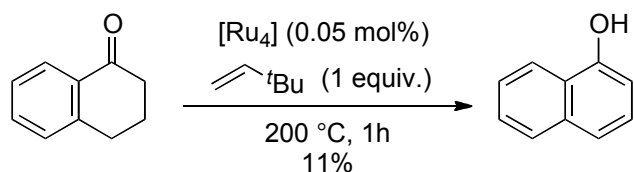
A vanadium catalyst, VO_2SO_4 , is shown to catalyze the aerobic oxidation of 3-methyl-4-ethylcarboxylcyclohexenone to the corresponding phenol (eq 1-20).¹⁰⁰ Although the substrate scope is very limited, due to the abundance of vanadium, this vanadium-based catalyst has a great potential for dehydrogenation reactions on the large scale. Development of new generations of catalysts with improved reactivity and expanded substrate scope will benefit from valuable mechanistic understandings and insights.



1.5 Transfer Dehydrogenation

Transfer dehydrogenation utilizes cheap alkenes as the hydrogen acceptor to provide the driving force for converting a saturated ketone into the corresponding α,β -unsaturated ketone. This strategy represents an appealing alternative to dehydrogenation reactions. A tetra-nuclear ruthenium catalyst **1-14** carries out the dehydrogenation of α -tetralone into 1-naphthol with limited success (eq 1-21).¹⁰¹ Pincer-ligated complexes are common catalysts for transfer dehydrogenation of alkanes. Transfer dehydrogenation of 3,3-dimethylcyclohexanone with a pincer-Ir catalyst and *tert*-butylethylene affords the corresponding cyclohexenone in good yield (eq 1-22).¹⁰² However, when it comes to a general substrate, such as the acyclic pentanone,

formation of a stable metallacycle between the pentenone product and the Ir catalyst stops catalytic turnover (eq 1-23). This side reaction represents a general problem that limits the substrate scope of transfer dehydrogenation reactions. New catalysts that avoid this catalyst poisoning process can find useful utility in organic synthesis.



1.6 Transition Metal-Based Heterogeneous Catalysts

While heterogeneous catalytic hydrogenations of alkenes are commonplace in organic synthesis,¹⁰³ the reverse reaction, formation of C=C bonds from saturated C–C bonds upon release of molecular H₂ has received much less attention. These reactions require harsh conditions and constant removal of H₂ to ensure driving forces for the forward reaction. The conversion of cyclohexanone derivatives into the corresponding phenols has a thermodynamic driving force from aromatization, and reactions of this type are the primary focus of

heterogeneous catalytic dehydrogenation. Several examples of Pd/C-catalyzed dehydrogenation reactions have been developed with limited success (Table 1-4). Aromatization of cyclohexenones and benzo-fused cyclohexanones take place at high temperatures in the presence of catalytic Pd/C (entries 1 and 2).^{104, 105} Mono-oxidation is achieved with the α -piperidylcyclopentanone (entry 3);¹⁰⁶ and an γ,δ -unsaturated lactone derivative (entry 4).¹⁰⁷

Table 1-4. Pd/C-Catalyzed Dehydrogenation of Ketones and Lactones

Entry	Substrate	Product	Conditions ^a	Yield (%)
1			Ph ₂ O, reflux	84
2			<i>p</i> -cymene 230–300 °C	71
3			350–370 °C	85
4			<i>p</i> -cymene reflux	60 ^b

^aReactions carried out with 5% Pd/C. ^bReaction carried out with 10% Pd/C.

A few Ni and Re-based heterogeneous catalysts can also catalyze the aromatization of cyclohexanone derivatives (Table 1-5). These reactions are carried out in continuous-flow reactors with a carrier gas, such N₂, H₂ and air, in order to constantly remove H₂.¹⁰⁸⁻¹¹⁰ The high

temperature and the lack of a general substrate scope limit the utility of these heterogeneous catalytic reactions for bench chemists. However, development of heterogeneous catalysts that enable highly efficient dehydrogenation of this type could find significant application in large-scale processes. The use of a heterogeneous catalyst would also be advantageous when combined with an external oxidant, including green oxidants such as O_2 , to enhance the thermodynamic driving force by accepting H_2 .

Table 1-5. Heterogeneous Dehydrogenation of Simple Cyclohexanones^a

Entry	Substrate	Catalyst	Major Product	Yield (%)
1		Ni^0 catalyst		36
2		Sn-Ni-SiO ₂		60
3		Cs ₄ [Re ₆ S ₈]SS _{2/2} (S ₂) _{3/2}		82

^aReaction conditions: T = 320–400 °C.

1.7 Summary and Outlook

Various oxidative methods are effective at α,β -dehydrogenating carbonyl compounds. The past century has witnessed the success of sulfur and selenium-based reagents in organic syntheses. By taking advantage of versatile enolate formation methods and the facile syn-elimination of β -Hs with sulfur-oxides and selenium-oxides, these reagents exhibit admirable

regioselectivity and a broad substrate scope. In particular, otherwise unreactive substrates, including esters and amides, undergo facile oxidation with sulfur and selenium reagents. The drawbacks of these reagents, however, are evident, including high expense, toxicity, unpleasant odors and requirement of multi-step procedures. Hypervalent iodine reagents, particularly IBX, are becoming the most prominent oxidation reagents for α,β -dehydrogenation since the beginning of 21st century. Compared to the previous reagents, IBX is cheap, relatively safe and capable of performing selective oxidations in a single step. However, regioselective dehydrogenation of unsymmetrical substrates represents a challenge for IBX and related reagents.

Catalytic dehydrogenation methods that apply green and sustainable oxidants remain a highly desirable goal for modern organic syntheses. Pd and other transition metal complexes coupled with environmentally benign oxidants, such as O₂, provide an appealing strategy for atom economic dehydrogenation reactions. While examples over the past decades have shed light on potentially plausible solutions to this issue, development of more robust catalysts with expanded substrate scope and control of chemo- and regioselectivities will build on thorough understanding of reaction mechanisms to eventually have significant impact in organic syntheses.

1.8 References

-
1. Buckle, D. R.; Pinto, I. L. Oxidation Adjacent to C=X Bonds by Dehydrogenation. In *Comprehensive Organic Synthesis - Selectivity, Strategy and Efficiency in Modern Organic Chemistry*; Trost, B. M., Fleming, I., Eds.; Elsevier 1991; Vol. 7, pp 119-149.

-
2. For a comprehensive summary of pK_a , see: <http://www.chem.wisc.edu/areas/reich/pkatable/>.
 3. Corey, E. J. *J. Am. Chem. Soc.* **1953**, 75, 2301-2304.
 4. Glazier, E. R. *J. Org. Chem.* **1962**, 27, 2937-2938.
 5. Jones, G. *J. Chem. Soc. C* **1970**, 1230-1232.
 6. Stotter, P. L.; Hill, K. A. *J. Org. Chem.* **1973**, 38, 2576-2578.
 7. Rathke, M. W.; Lindert, A. *Tetrahedron Lett.* **1971**, 12, 3995-3998.
 8. d'Angelo, J. *Tetrahedron* **1976**, 32, 2979-2990.
 9. Trost, B. M. *Chem. Rev.* **1978**, 78, 363-382.
 10. Sharpless, K. B.; Young, M. W.; Lauer, R. F. *Tetrahedron Lett.* **1973**, 14, 1979-1982.
 11. For recent books, see: (a) Bach, T. G. In *Organoselenium Chemistry*; Liotta, D., Ed.; Wiley: New York, 1987. (b) Back, T. G. *Organoselenium Chemistry: A Practical Approach* Oxford University Press: Oxford, 1999. (c) Wirth, T. *Organoselenium Chemistry: Modern Developments in Organic Synthesis*; Springer: Berlin, 2000, Vol. 208.
 12. Seebach, D.; Teschner, M. *Chem. Ber.* **1976**, 109, 1601-1616.
 13. Trost, B. M.; Salzmann, T. N.; Hiroi, K. *J. Am. Chem. Soc.* **1976**, 98, 4887-4902.
 14. Monteiro, H. J.; de Souza, J. P. *Tetrahedron Lett.* **1975**, 16, 921-924.
 15. Reich, H. J. *Acc. Chem. Res.* **1979**, 12, 22-30.

-
16. Sharpless, K. B.; Gordon, K. M.; Lauer, R. F.; Patrick, D. W.; Singer, S. P.; Young, M. W. *Chem. Scr.* **1975**, A 8, 9-13.
17. Buckle, D. R.; Collier, S. J.; McLaws, M. D. 2,3-Dichloro-5,6-dicyano-1,4-benzo-quinone. In *Encyclopedia of Reagents for Organic Synthesis*; John Wiley & Sons, Inc.: New York, 2005.
18. Buckle, D. R. Chloranil. In *Encyclopedia of Reagents for Organic Synthesis*; John Wiley & Sons, Inc.: New York, 2001.
19. Di Filippo, M.; Izzo, I.; Raimondi, S.; De Riccardis, F.; Sodano, G. *Tetrahedron Lett.* **2001**, 42, 1575-1577.
20. Bhattacharya, A.; DiMichele, L. M.; Dolling, U. H.; Douglas, A. W.; Grabowski, E. J. J. *J. Am. Chem. Soc.* **1988**, 110, 3318-3319.
21. IBX is readily accessible by oxidation of 2-iodobenzoic acid with oxone (2KHSO₅·KHSO₄·K₂SO₄) or potassium bromide: (a) Frigerio, M. Santagostino and S. Sputore, *J. Org. Chem.*, 1999, **64**, 4537-4538. (b) Robert K. Boeckman, J.; Shao, P.; Mullins, J. J. *organic syntheses* **2000**, 77, 141-147.
22. IBX has been considered explosive under impact or heated to >200 °C, for detail discussions, see: ref. 24 and (a) J. B. Plumb and D. J. Harper, *Chem. Eng. News*, 1990, **68**, 3-3. (b) Duschek, A.; Kirsch, S. F. *Angew. Chem. Int. Ed.* **2011**, 50, 1524-1552. (c) D. B. Dess and J. C. Martin, *J. Am. Chem. Soc.*, 1991, **113**, 7277-7287. (d) Fallis, A. G.; Tessier, P. E. "2-Iodoxybenzoic acid (IBX)." In *Encyclopedia of Reagents for Organic Synthesis*; John Wiley & Sons, Inc.: New York, 2003.

-
23. Hartman, C.; Meyer, V. *Chem. Ber.* **1893**, *26*, 1727.
24. Nicolaou, K. C.; Zhong, Y. L.; Baran, P. S. *J. Am. Chem. Soc.* **2000**, *122*, 7596-7597.
25. Nicolaou, K. C.; Montagnon, T.; Baran, P. S.; Zhong, Y. L. *J. Am. Chem. Soc.* **2002**, *124*, 2245-2258.
26. IBX-mediated dehydrogenation reaction is expected to proceed via a single electron transfer (SET) mechanism: K. C. Nicolaou, P. S. Baran, R. Kranich, Y.-L. Zhong, K. Sugita and N. Zou, *Angew. Chem. Int. Ed.*, 2001, **40**, 202-206. See also: ref. 25.
27. Nicolaou, K. C.; Gray, D. L. F.; Montagnon, T.; Harrison, S. T. *Angew. Chem. Int. Ed.* **2002**, *41*, 996-999.
28. For a Dess-Martin periodinane (DMP)-mediated oxidation of *N*-b-carbonyl amides, see: Nicolaou, K. C.; Mathison, C. J. N. *Angew. Chem. Int. Ed.* **2005**, *44*, 5992-5997.
29. Nicolaou, K. C.; Montagnon, T.; Baran, P. S. *Angew. Chem. Int. Ed.* **2002**, *41*, 993-996.
30. K. C. Nicolaou, T. Montagnon and P. S. Baran, *Angew. Chem. Int. Ed.*, 2002, **41**, 1386-1389.
31. For a review, see: Silva, J. L. F.; Olofsson, B. *Natural Product Reports* **2011**, *28*, 1722-1754.
32. Uyanik, M.; Akakura, M.; Ishihara, K. *J. Am. Chem. Soc.* **2009**, *131*, 251-262.

-
33. (a) Hartwig, J. In *Organotransition Metal Chemistry: From Bonding to Catalysis*; Hartwig, J., Ed.; University Science Books: Sausalito, 2010. pp. 825-870. (b) Hartwig, J. In *Organotransition Metal Chemistry: From Bonding to Catalysis*; Hartwig, J., Ed.; University Science Books: Sausalito, 2010, pp. 398-405.
34. For the formation of Pd enolates, see the following review and references cited therein: Culkin, D. A.; Hartwig, J. F. *Acc. Chem. Res.* **2003**, *36*, 234-245.
35. Fuchita, Y.; Harada, Y. *Inorg. Chim. Acta* **1993**, *208*, 43-47.
36. Theissen, R. J. *J. Org. Chem.* **1971**, *36*, 752-757.
37. Baltz, H.; Bierling, B.; Kirschke, K.; Oberender, H.; Schulz, M.; office, E. p., Ed. 1971; Vol. DE2050566 (A1)
38. Bierling, B.; Kirschke, K.; Oberender, H.; Schulz, M. *J. Prakt. Chem.* **1972**, *314*, 170-180.
39. Shan, S. *Jingxi Shiyong Huagong Jinzhan* **2005**, *6*, 24-25; *Chem. Abstr.* **146**, 401642.
40. Parker, K. A.; Koziski, K. A.; Breault, G. *Tetrahedron Lett.* **1985**, *26*, 2181-2182.
41. Kirschke, K.; Muller, H.; Timm, D. *J. Prakt. Chem.* **1975**, *317*, 807-811.
42. Mukaiyama, T.; Ohshima, M.; Nakatsuka, T. *Chem. Lett.* **1983**, *12*, 1207-1210.
43. Murahashi, S. I.; Mitsue, Y.; Tsumiyama, T. *Bull. Chem. Soc. Jpn.* **1987**, *60*, 3285-3290.
44. Greene, A. E.; Luche, M. J.; Depres, J. P. *J. Am. Chem. Soc.* **1983**, *105*, 2435-2439.

-
45. Greene, A. E.; Luche, M. J.; Serra, A. A. *J. Org. Chem.* **1985**, *50*, 3957-3962.
46. Trost, B. M.; Dong, G.; Vance, J. A. *Chem. Eur. J.* **2010**, *16*, 6265-6277.
47. Hanzawa, Y.; Ito, H.; Kohara, N.; Sasaki, H.; Fukuda, H.; Morikawa, T.; Taguchi, T.; Iitaka, Y. *Tetrahedron Lett.* **1991**, *32*, 4143-4146.
48. Baltz, H.; Bierling, B.; Kirschke, K.; Oberender, H.; Schulz, M. UK, 1973; Vol. GB 1340612.
49. Susuki, T.; Tsuji, J. *Bull. Chem. Soc. Jpn.* **1973**, *46*, 655-656.
50. Shvo, Y.; Arisha, A. H. I. *J. Org. Chem.* **1998**, *63*, 5640-5642.
51. Guijarro, D.; Mancheño, B.; Yus, M. *Tetrahedron* **1994**, *50*, 8551-8558.
52. Giri, R.; Mangel, N.; Foxman, B. M.; Yu, J.-Q. *Organometallics* **2008**, *27*, 1667-1670.
53. (a) Stahl, S. S. *Science* **2005**, *309*, 1824-1826. (b) Konnick, M. M.; Stahl, S. S. *J. Am. Chem. Soc.* **2008**, *130*, 5753-5762. (c) Popp, B. V.; Stahl, S. S. *Chem. Eur. J.* **2009**, *15*, 2915-2922. (d) Decharin, N.; Popp, B. V.; Stahl, S. S. *J. Am. Chem. Soc.* **2011**, *133*, 13268-13271.
54. Ye, X. A.; Johnson, M. D.; Diao, T. N.; Yates, M. H.; Stahl, S. S. *Green Chemistry* **2010**, *12*, 1180-1186.
55. For a review, see: Muzart, J. *Eur. J. Org. Chem.* **2010**, 3779-3790.
56. Wenzel, T. T. *J. Chem. Soc. Chem. Comm.* **1989**, 932-933.

-
57. Muzart, J.; Pete, J. P. *J. Mol. Catal.* **1982**, *15*, 373-376.
58. Park, Y. W.; Oh, H. H. *Bull. Korean Chem. Soc.* **1997**, *18*, 1123-1124.
59. Tokunaga, M.; Harada, S.; Iwasawa, T.; Obora, Y.; Tsuji, Y. *Tetrahedron Lett.* **2007**, *48*, 6860-6862.
60. Zhu, J.; Liu, J.; Ma, R. Q.; Xie, H. X.; Li, J.; Jiang, H. L.; Wang, W. *Adv. Synth. Catal.* **2009**, *351*, 1229-1232.
61. Liu, J.; Zhu, J.; Jiang, H. L.; Wang, W.; Li, J. *Chem. Asian J.* **2009**, *4*, 1712-1716
62. Gao, W.; He, Z.; Qian, Y.; Zhao, J.; Huang, Y. *Chem. Sci.* **2012**, *3*, 883-886.
63. Izawa, Y.; Pun, D.; Stahl, S. S. *Science* **2011**, *333*, 209-213.
64. (a) Leskinen, M. V.; Yip, K.-T.; Valkonen, A.; Pihko, P. M. *J. Am. Chem. Soc.* **2012**, *134*, 5750-5753. (b) Yip, K.-T.; Nimje, R. Y.; Leskinen, M. V.; Pihko, P. M. *Chem. Eur. J.* **2012**, *10.1002/chem.201201988*.
65. Xie, Y.; Liu, S.; Liu, Y.; Wen, Y.; Deng, G.-J. *Org. Lett.* **2012**, *14*, 1692-1695.
66. Ito, Y.; Hirao, T.; Saegusa, T. *J. Org. Chem.* **1978**, *43*, 1011-1013
67. Larock, R. C.; Hightower, T. R.; Kraus, G. A.; Hahn, P.; Zheng, D. *Tetrahedron Lett.* **1995**, *36*, 2423-2426.
68. Kraus, G. A.; Zheng, D. *Synlett* **1993**, *1993*, 71-72.

-
69. For a synthetic example, see: Trost, B. M.; Zhang, T. *Chem. Eur. J.* **2011**, *17*, 3630-3643.
70. Namba, K.; Kaihara, Y.; Yamamoto, H.; Imagawa, H.; Tanino, K.; Williams, R. M.; Nishizawa, M. *Chem. Eur. J.* **2009**, *15*, 6560-6563.
71. Fuwa, H.; Kainuma, N.; Tachibana, K.; Sasaki, M. *J. Am. Chem. Soc.* **2002**, *124*, 14983-14992.
72. Marino, J. P.; Rubio, M. B.; Cao, G.; de Dios, A. *J. Am. Chem. Soc.* **2002**, *124*, 13398-13399.
73. Hiraoka, S.; Harada, S.; Nishida, A. *J. Org. Chem.* **2010**, *75*, 3871-3874.
74. Herzon, S. B.; Lu, L.; Woo, C. M.; Gholap, S. L. *J. Am. Chem. Soc.* **2011**, *133*, 7260-7263.
75. Tsuji, J.; Takahashi, K.; Minami, I.; Shimizu, I. *Tetrahedron Lett.* **1984**, *25*, 4783-4786.
76. Minami, I.; Takahashi, K.; Shimizu, I.; Kimura, T.; Tsuji, J. *Tetrahedron* **1986**, *42*, 2971-2977.
77. Yu, J. Q.; Wu, H. C.; Corey, E. J. *Org. Lett.* **2005**, *7*, 1415-1417.
78. Aoki, K.; Tomioka, K.; Noguchi, H.; Koga, K. *Tetrahedron* **1997**, *53*, 13641-13656.
79. Anderson, J. D.; García García, P.; Hayes, D.; Henderson, K. W.; Kerr, W. J.; Moir, J. H.; Fondekar, K. P. *Tetrahedron Lett.* **2001**, *42*, 7111-7114.
80. Graf, C.-D.; Malan, C.; Knochel, P. *Angew. Chem. Int. Ed.* **1998**, *37*, 3014-3016.

-
81. Shirai, R.; Tanaka, M.; Koga, K. *J. Am. Chem. Soc.* **1986**, *108*, 543-545.
82. Clark, J. S.; Vignard, D.; Parkin, A. *Org. Lett.* **2011**, *13*, 3980-3983.
83. Rodeschini, V.; Van de Weghe, P.; Salomon, E.; Tarnus, C.; Eustache, J. *J. Org. Chem.* **2005**, *70*, 2409-2412.
84. Pihko, P. M.; Koskinen, A. M. P. *J. Org. Chem.* **1998**, *63*, 92-98.
85. Meyers, A. I.; Tavares, F. *Tetrahedron Lett.* **1994**, *35*, 2481-2484.
86. Meyers, A. I.; Tavares, F. X. *J. Org. Chem.* **1996**, *61*, 8207-8215.
87. Ramirez, T. A.; Zhao, B.; Shi, Y. *Tetrahedron Lett.* **2010**, *51*, 1822-1825.
88. Huang, Y.; Gan, H.; Li, S.; Xu, J.; Wu, X.; Yao, H. *Tetrahedron Lett.* **2010**, *51*, 1751-1753.
89. Dawsey, A. C.; Li, V.; Hamilton, K. C.; Wang, J.; Williams, T. J. *Dalton Trans.* **2012**, *41*, 7994-8002.
90. Evans, D. L.; Minster, D. K.; Jordis, U.; Hecht, S. M.; Mazzu, A. L.; Meyers, A. I. *J. Org. Chem.* **1979**, *44*, 497-501.
91. Shin, C.-g.; Nakamura, Y.; Okumura, K. *Chem. Lett.* **1993**, *22*, 1405-1408.
92. Hamada, Y.; Shibata, M.; Sugiura, T.; Kato, S.; Shioiri, T. *J. Org. Chem.* **1987**, *52*, 1252-1255.
93. Andrus, M. B.; Lashley, J. C. *Tetrahedron* **2002**, *58*, 845-866.

-
94. Rao, P. N.; Cessac, J. W.; Kim, H. K. *Steroids* **1994**, *59*, 621-627.
95. Simon, M.-O.; Girard, S. A.; Li, C.-J. *Angew. Chem. Int. Ed.* **2012**, *51*, 7537-7540.
96. A. C. Flick and A. Padwa, *Arkivoc*, 2011, 137-161.
97. A. C. Flick and A. Padwa, *Tetrahedron Lett.*, 2008, **49**, 5739-5741.
98. Ley, S. V.; Norman, J.; Griffith, W. P.; Marsden, S. P. *Synthesis* **1994**, *1994*, 639-666.
99. Shimokawa, J.; Ishiwata, T.; Shirai, K.; Koshino, H.; Tanatani, A.; Nakata, T.; Hashimoto, Y.; Nagasawa, K. *Chem. Eur. J.* **2005**, *11*, 6878-6888.
100. T. Moriuchi, K. Kikushima, T. Kajikawa and T. Hirao, *Tetrahedron Lett.*, 2009, **50**, 7385-7387.
101. C. S. Yi and D. W. Lee, *Organometallics*, 2009, **28**, 947-949.
102. X. Zhang, D. Y. Wang, T. J. Emge and A. S. Goldman, *Inorg. Chim. Acta*, 2011, **369**, 253-259.
103. Nishimura, S. *Handbook of Heterogeneous Catalytic Hydrogenation for Organic Synthesis*; John Wiley & Sons, 2001.
104. Horning, E. C.; Horning, M. G. *J. Am. Chem. Soc.* **1947**, *69*, 1359-1361.
105. Newman, M. S.; Blum, J. *J. Am. Chem. Soc.* **1964**, 503-507.

-
106. Karakhanov, R. A.; Vartanyan, M. M.; Apandiev, R. B.; Karzhavina, N. P. *Izv. Akad. Nauk SSSR, Ser. Khim.* **1982**, 1905.
107. Jones, T. H.; Fales, H. M. *Tetrahedron Lett.* **1983**, 24, 5439-5440.
108. Williams, E. A.; Meikle, R. W.; Redemann, C. T. *J. Agric. Food. Chem.* **1965**, 13, 210-213.
109. Hales, N. J.; Heaney, H.; Hollinshead, J. H.; Ley, S. V. *Tetrahedron* **1995**, 51, 7741-7754.
110. Kamiguchi, S.; Nagashima, S.; Chihara, T. *Chem. Lett.* **2007**, 36, 1340-1341.

CHAPTER 2

Pd(DMSO)₂(TFA)₂-Catalyzed Aerobic α,β -Dehydrogenation of Cyclic Ketones

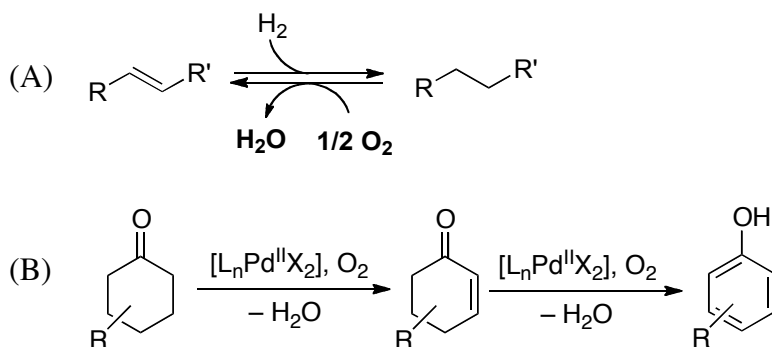
This work has been published under the following:

Diao, T.; Stahl, S. S. *J. Am. Chem. Soc.* **2011**, *133*, 14566-14569.

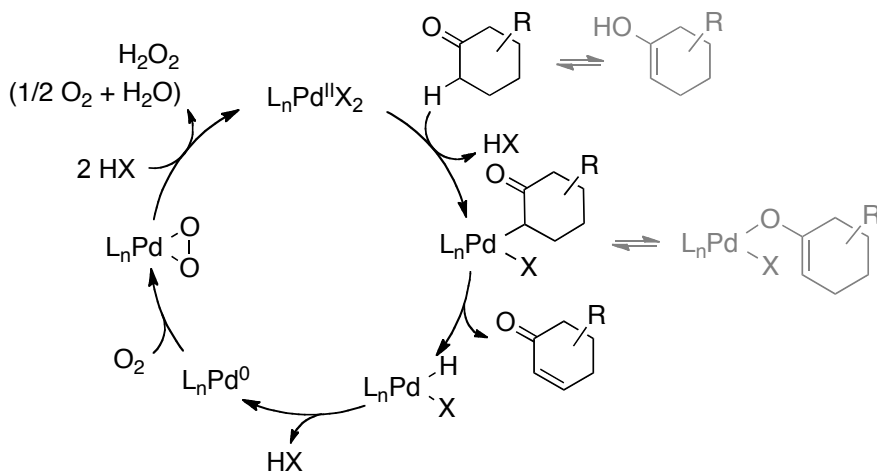
2.1 Introduction to Dehydrogenation of Cyclic Carbonyl Compounds

Molecular hydrogen and oxygen are the quintessential reducing and oxidizing agents, respectively. While hydrogenation reactions are commonplace in multistep organic synthesis, aerobic oxidation reactions are seldom used. For example, numerous highly selective methods and sophisticated catalysts exist for the hydrogenation of alkenes;¹ however, complementary aerobic dehydrogenation methods for alkene synthesis are unavailable² (Scheme 2-1(A)). We recently reported a method for Pd^{II}-catalyzed aerobic dehydrogenation of cyclohexanones to phenols.³ These reactions proceed via a cyclohexenone intermediate that undergoes further dehydrogenation to the phenol under the reaction conditions (Scheme 2-1(B)). Here, we report the identification of a different Pd catalyst system that enables selective dehydrogenation of cycloketones to afford enones rather than phenols. Cyclohexenones and related α,β -unsaturated carbonyl compounds are key intermediates in the synthesis of pharmaceuticals and other biologically active compounds.⁴ Their preparation typically requires two or more steps⁵⁻⁷ and/or the use of stoichiometric reagents, such as 2-iodoxybenzoic acid (IBX)^{8,9} or 2,3-dichloro-5,6-dicyano-1,4-benzoquinone (DDQ).¹⁰ Catalytic methods for aerobic dehydrogenation of ketones to enones would provide appealing, atom-economical alternatives to these stoichiometric methods.

Scheme 2-1. Hydrogenation/Dehydrogenation of C–C Bonds (A) and Pd-Catalyzed Dehydrogenation of Cyclohexanones (B)



The synthesis of enones via Pd^{II}-mediated dehydrosilylation of silyl enol ethers was reported by Ito and Saegusa in 1978.^{6a} In some cases, these reactions have been achieved with catalytic Pd^{II},^{6b,c} but the use of ≥ 0.5 equiv of Pd^{II} is commonly required to obtain good yields of products.^{4b,c,11} Methods for direct Pd^{II}-catalyzed dehydrogenation of ketones have been pursued as an alternative to Saegusa reactions; however, previous examples exhibit quite limited substrate scope.¹²⁻¹⁵ Both Saegusa-type dehydrosilylation and direct dehydrogenation reactions are expected to be initiated by formation of a Pd^{II}-enolate, followed by β -hydride elimination to afford the enone product (Scheme 2-2).¹⁶ The resulting Pd^{II}-hydride intermediate can be oxidized by O₂ to regenerate the Pd^{II} catalyst.^{17,18} Recent advances in Pd^{II}-catalyzed aerobic oxidation and C–H functionalization reactions¹⁹ provided useful starting points for our investigation of dehydrogenation catalysts.

Scheme 2-2. Proposed Mechanism for Pd^{II}-Catalyzed Dehydrogenation of Cyclic Ketones

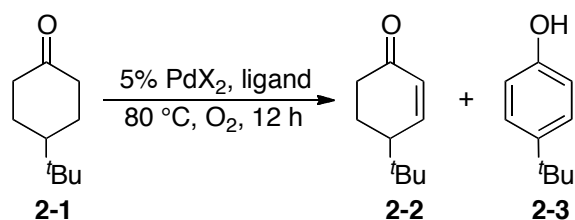
2.2. Results and Discussions

2.2.1 Optimization of Catalyst and Reaction Conditions for Aerobic α,β -Oxidation of Cyclic Ketones

Initial catalyst screening efforts focused on the dehydrogenation of 4-*tert*-butylcyclohexanone **2-1** under relatively mild conditions: 1 atm O₂, 80 °C, 12 h (Table 2-1). Use of the recently reported Pd^{II} catalyst for conversion of cyclohexanones to phenols³ resulted in incomplete conversion and, as expected, favored formation of phenol **2-3** over the enone **2-2** (entry 1). The best previous catalyst for the conversion of cyclohexanone to cyclohexenone, reported by Tsuji and coworkers,^{12e} forms enone **2-2** selectively, but only in 19% yield under these conditions (entry 2). Improved results were obtained by using catalytic Pd(OAc)₂ in DMSO,^{20,21} affording a mixture of enone and phenol products in 63% and 14% yield, respectively (entry 3). The best results were obtained by using DMSO as a ligand (10 mol %) with Pd(TFA)₂ (5 mol %; TFA = trifluoroacetate) in acetic acid (entry 7). This catalyst system led to a 91% yield of the desired enone **2-2**. Replacing DMSO with other monodentate and

bidentate ligands led to inferior results (entries 13–19).²² The benefit of using DMSO as a catalytic ligand, rather than a solvent, has been observed recently in two other Pd-catalyzed aerobic oxidation reactions, including chelate-directed C–H arylation of anilides²³ and oxidative amination of alkenes.²⁴

Table 2-1. Catalyst Optimization of Aerobic Oxidative Dehydrogenation of 4-*tert*-Butylcyclohexanone **2-1**^a



Entry	PdX ₂	Ligand (mol%)	Solvent	2-2 (%) ^b	2-3 (%) ^b
1	Pd(TFA) ₂	2-Me ₂ N-pyridine (10)/TsOH(20)	DMSO	23	33
2	Pd(TFA) ₂	5,5'-Me ₂ bpy (5)/4Å MS	PhCl	19	0
3	Pd(OAc) ₂		DMSO	63	14
4	Pd(TFA) ₂		DMSO	34	56
5	Pd(TFA) ₂		HOAc	24	1
6	Pd(OAc) ₂	DMSO (10)	HOAc	86	8
7	Pd(TFA)₂	DMSO (10)	HOAc	91	8
8	Pd(TFA) ₂	DMSO (10)	Toluene	67	3
9	Pd(TFA) ₂	DMSO (10)	THF	66	8
10	Pd(TFA) ₂	DMSO (10)	Dioxane	84	10
11	Pd(TFA) ₂	DMSO (10)	EtOAc	30	6
12	Pd(TFA) ₂	DMSO (10)	PhCl	11	0
13	Pd(TFA) ₂	pyridine (10)	HOAc	55	2
14	Pd(TFA) ₂	2-Me ₂ N-pyridine (10)	HOAc	3	1
15	Pd(TFA) ₂	2-F-pyridine (10)	HOAc	37	2
16	Pd(TFA) ₂	bipyridine (5)	HOAc	0	0
17	Pd(TFA) ₂	5,5'-Me ₂ bpy (5)	HOAc	0	0
18	Pd(TFA) ₂	phenanthroline (5)	HOAc	0	0
19	Pd(TFA) ₂	1,2-bis(phenyl-sulfinyl)ethane (5)	HOAc	9	4

^a Conditions: [**1**] = 0.2 M (15.4 mg, 0.1 mmol), 5% PdX₂ (0.005 mmol), 10% ligand (0.01 mmol), Solvent (0.5 mL), 1 atm O₂, 80 °C, 12 h. ^b Determined by GC, external standard = tetradecane.

2.2.2 Investigation of the Chemoselectivity of Pd(DMSO)₂(TFA)₂-Catalyzed Dehydrogenation

The high selectivity for formation of the enone with the Pd(DMSO)₂(TFA)₂ catalyst system is noteworthy in light of the preferential formation of phenols with a Pd(TFA)₂/2-*N,N*-dimethylaminopyridine (2-Me₂Npy) catalyst system.³ A comparison of time courses for reactions with the two catalyst systems (Figure 2-1) highlights the significant differences between the relative rates of the corresponding dehydrogenation steps (cf. Scheme 2-1(B)). Fitting of the time-course data to a simple sequential kinetic model, A → B → C,²⁵ reveals that the first dehydrogenation step is 38-fold *faster* than the second step when Pd(DMSO)₂(TFA)₂ is used as the catalyst. In contrast, the first step is nearly 2-fold *slower* than the second step with the Pd(TFA)₂/2-Me₂Npy catalyst system.²⁶ Further mechanistic studies are ongoing, but the observations have important implications for use of the present catalyst system in the synthesis of enones.

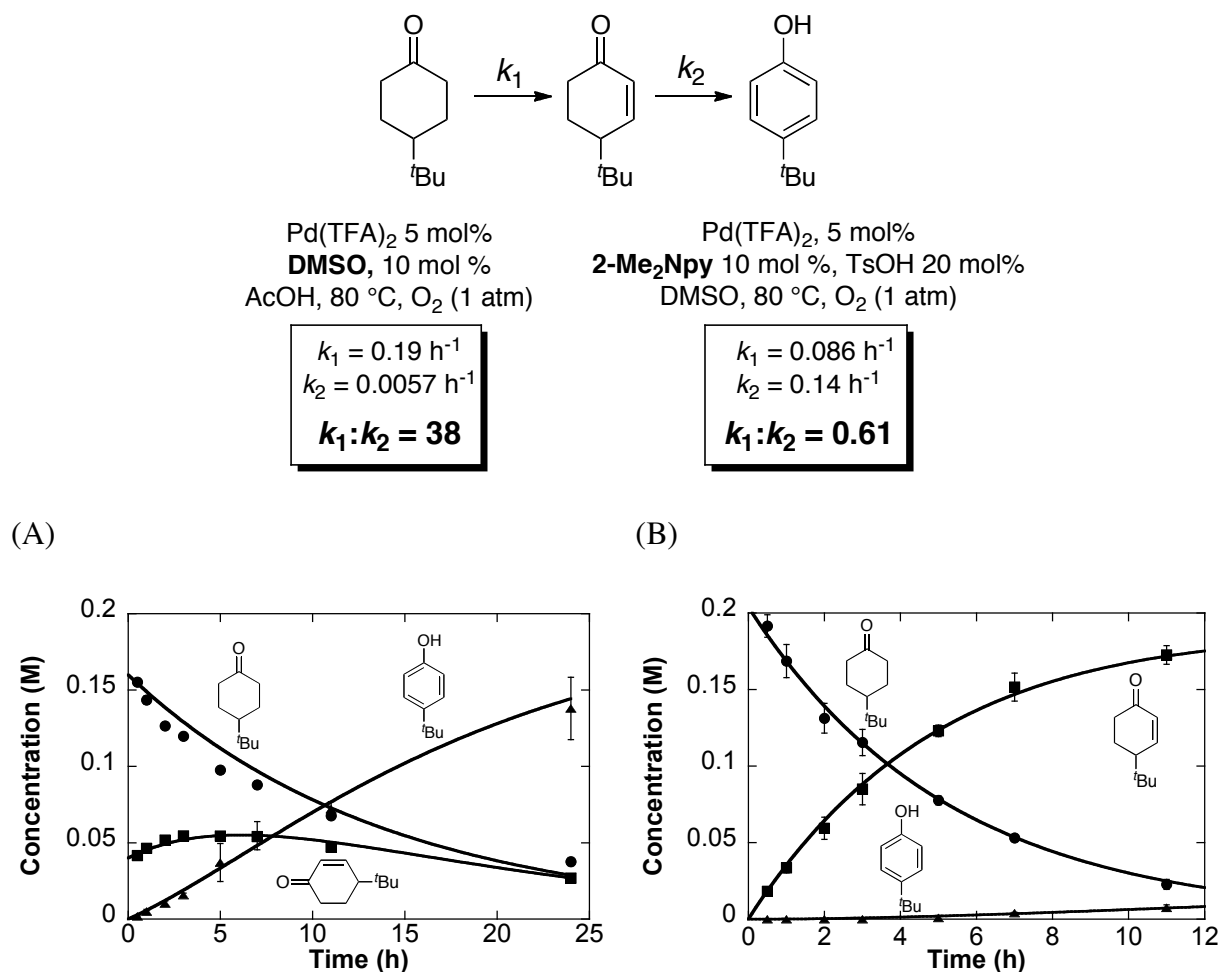
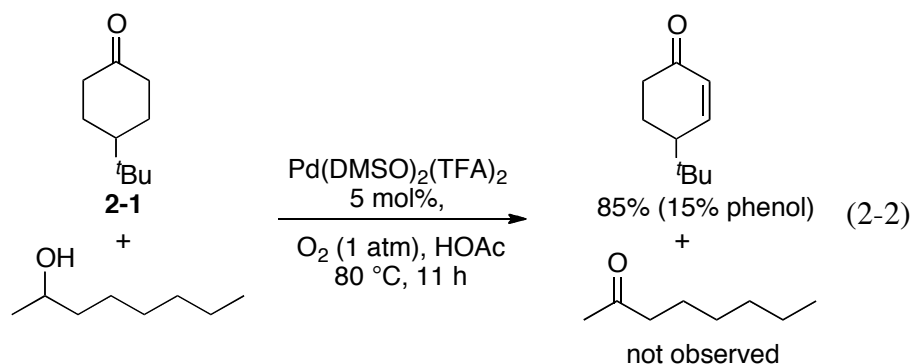
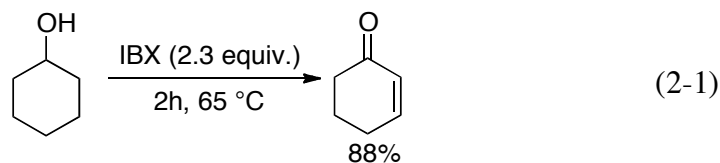


Figure 2-1. Comparison of kinetic profiles of Pd(DMSO)₂(TFA)₂- and Pd(TFA)₂/2-Me₂Npy-catalyzed dehydrogenation of **2-1**. (A) Time course for Pd(DMSO)₂(TFA)₂-catalyzed dehydrogenation of **2-1**. Reaction conditions: [**2-1**] = 0.2 M (0.1 mmol), 5% Pd(DMSO)₂(TFA)₂ (0.005 mmol), AcOH (0.5 mL), 1 atm O₂, 80 °C. (B) Time course for Pd(TFA)₂/2-Me₂Npy-catalyzed dehydrogenation of **2-1**. Reaction conditions: [**2-1**] = 0.2 M (0.1 mmol), Pd(TFA)₂ (0.005 mmol), 2-Me₂Npy (0.01 mmol), TsOH (0.02 mmol), DMSO (0.5 mL), 1 atm O₂, 80 °C. Internal standard = 1,4-dimethoxybenzene. Error bars represent standard deviations from 3 independent measurements.

Besides α,β -dehydrogenation, IBX also serves as an efficient oxidant for converting alcohols into aldehydes and ketones.⁸ For example, in the presence of cyclohexanol, IBX conducted a two-step oxidation to afford the cyclohexenone (eq 2-1). In order to examine the selectivity of Pd(DMSO)₂(TFA)₂-catalyzed dehydrogenation over alcohol oxidation, we performed a competition experiment. An equimolar mixture of **2-1** and 2-octyl alcohol were submitted to the standard Pd(DMSO)₂(TFA)₂ catalyst system conditions. Oxidation of **2-1** proceeded smoothly to afford 85% cyclohexenone, whereas no alcohol oxidation product, 2-octanone, was observed (eq 2-2). The majority of 2-octyl alcohol was recovered with trace quantities of 2-octyl acetate detected by GC-MS spectroscopy. The absence of 2-octanone highlighted the chemo-selectivity of this Pd(DMSO)₂(TFA)₂ catalyst for dehydrogenation with is superior to IBX oxidation.



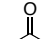

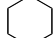
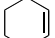
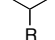
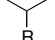

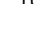


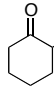
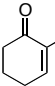
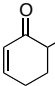
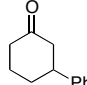
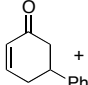
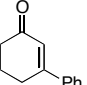
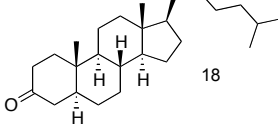
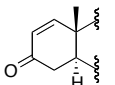
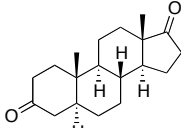
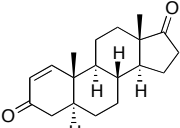
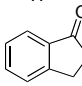
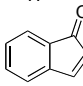
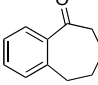
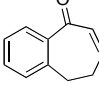
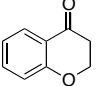
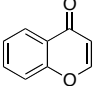
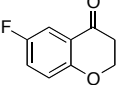
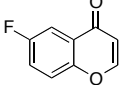
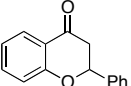
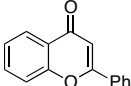
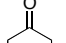
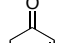
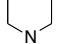
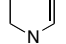
2.2.3 Substrate Scope

A number of 4-substituted cyclohexanone derivatives underwent dehydrogenation in good yields with the Pd(DMSO)₂(TFA)₂ catalyst (Table 2-2, entries 1–5). Substrates with electron-deficient substituents (entries 2 and 3) exhibited somewhat faster rates, and the conditions

tolerated various functional groups, including trifluoromethyl and siloxy groups (entries 2 and 5). The parent cyclohexanone (entry 1) decomposed under the acidic conditions, but a good yield of enone was obtained by performing the reaction in ethyl acetate.²⁷ Dehydrogenation of 2- and 3-substituted cyclohexanones can afford two different enone products, and reactions of 2- and 3-phenylcyclohexanone proceeded with modest (~3:1) regioselectivity (entries 6 and 7). The ability to achieve highly regioselective dehydrogenation was demonstrated in the reactions of two steroid derivatives (entries 8 and 9), each of which afforded one of two possible enones in excellent yield. In both cases, the regioselectivity favored formation of the less substituted alkene. No dehydrogenation of the cyclopentanone fragment was observed in the reaction leading to 5 α -androst-1-ene-3,17-dione (entry 9). The lower reactivity of cyclopentanones was also evident in the dehydrogenation of indanone, which afforded the corresponding enone in 54% yield, with toluene as the optimal solvent (entry 10). In contrast, 1-benzosuberone underwent dehydrogenation in good yield (81%, entry 11).

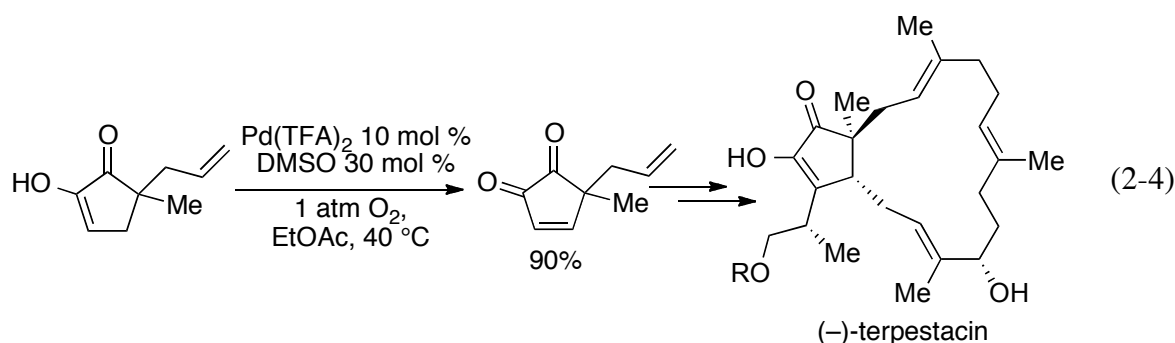
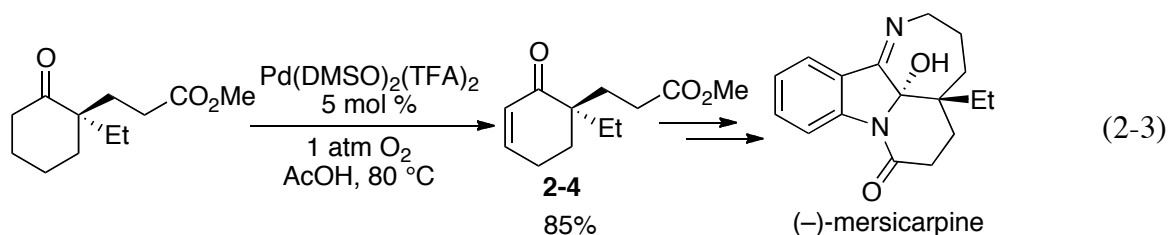
Chromones²⁸ and flavones have important biological activity,²⁹ and the saturated dihydrobenzopyranones are readily prepared via condensation of simple precursors.³⁰ Aerobic dehydrogenation reactions to form chromone, 6-fluorochromone,³¹ and flavone³² proceeded in good yield (entries 12–14). Related *N*-methyl- and *N*-Boc-piperidone derivatives underwent successful dehydrogenation to the corresponding dihydro-4-pyridone derivatives (entries 15 and 16).

Table 2-2. Pd-Catalyzed Aerobic Dehydrogenation of Diverse Cycloketones ^a

Entry	Substrate	Reaction time (h)	Temp. (°C)	Enone	Yield (%) ^b
1	 R = H	24	60		72 ^c
2	 R = CF ₃	5	80		81
3	 R = Ph	6	80		83
4	 R = <i>tert</i> -Bu	12	80		91
5	 R = OTBS	20	80		76
6		24	60	 +  3.0 : 1	84 ^c
7		24	60	 +  2.7 : 1	86 ^c
8		18	80		94
9		12	80		93
10		48	60		54 ^d
11		36	80		81 ^d
12		48	100		80
13		36	80		78
14		32	100		66
15	 R = Me	24	60		74
16	 R = Boc	48	80		72 ^e

^a Reactions conditions: [substrate] = 0.2 M (0.8 mmol), [Pd(TFA)₂] = 0.01 M (0.04 mmol = 5 mol %), [DMSO] = 0.02 M (0.08 mmol), solvent = AcOH (4 ml), 1 atm O₂. ^b Isolated yield. ^c Ethyl acetate was used as solvent to prevent product decomposition in acetic acid, [substrate] = 0.8 M (0.8 mmol), ethyl acetate (1 mL). ^d [substrate] = 0.4 M (0.8 mmol), [Pd(TFA)₂] = 0.02 M, [DMSO] = 0.2 M, solvent = toluene (2 ml). ^e In DMSO; no additional ligand.

Cyclic enones are common intermediates in the synthesis of natural products, and the aerobic dehydrogenation reactions described here could find broad utility in this context. For example, α,α -disubstituted cyclohexenone **2-4** has been used as an intermediate in the synthesis of (–)-mersicarpine. This enone was obtained in 85% yield using the $\text{Pd}(\text{DMSO})_2(\text{TFA})_2$ catalytic method (eq 2-3); the original protocol employed stoichiometric IBX and proceeded in 72% yield.³³ Catalytic Saegusa-type^{6c} and stoichiometric IBX⁸ oxidation methods failed in the synthesis of a cyclopentene- α -dione precursor to the natural product (–)-terpestacin, and stoichiometric $\text{Pd}(\text{OAc})_2$ was used instead.³⁴ Application of the aerobic $\text{Pd}(\text{TFA})_2/\text{DMSO}$ catalyst system to this reaction afforded the enedione in 90% yield (eq 2-4).

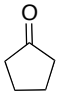
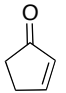
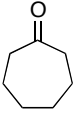
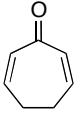
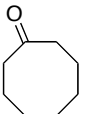
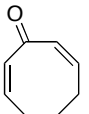
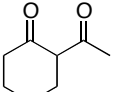
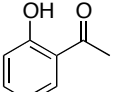
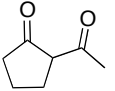
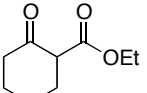
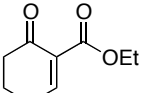
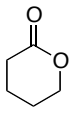
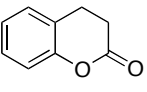
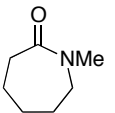


2.2.4 Unsuccessful Substrates

Oxidation of cyclopentanone led to clean formation of cyclopentenone in 25% yield after 8 h. Longer reaction times resulted in poor mass balance, as determined by ¹H NMR spectroscopy. The lost material may arise from over-oxidation of cyclopentenone to the anti-aromatic 1,3-cyclopentadienone, which subsequently undergoes fast decomposition (Table 2-3, entry 1).

Overoxidation was also observed for cyclic ketones with a ring size greater than 6. Cycloheptanone and cyclooctanone led to a mixture of dehydrogenation products, with 2,6-cycloheptadien-1-one and 2,7-cyclooctadien-1-one formed as the major products in 24 and 25% yields, respectively (entries 2-3). 2-Acetylcyclohexanone favors aromatization over mono-dehydrogenation to afford 2-hydroxyacetophenone in high yield (entry 4), whereas no reaction was observed with 2-acetylcyclopentanone (entry 5). The six-membered ketoester afforded the desired product with a fast rate, but the conversion is low due to catalyst decomposition (entry 6). Despite the similar pK_a s compared to ketones,³⁵ lactones and lactams exhibit no reactivity under these conditions (entries 7-9).

Table 2-3. Unsuccessful Substrates for Pd(DMSO)₂(TFA)₂-Catalyzed Aerobic Dehydrogenation Reactions^a

Entry	Substrate	Major Product	Yield (%) ^b
1			25
2			26
3			25
4			95
5		no reaction	
6			14
7		no reaction	
8		no reaction	
9		no reaction	

^a Reactions conditions: [substrate] = 0.2 M (0.1 mmol), [Pd(TFA)₂] = 0.01 M (0.005 mmol = 5 mol %), [DMSO] = 0.01 M (0.02 mmol), solvent = AcOH (0.5 ml), 1 atm O₂.^b determined by GC or ¹H NMR spectroscopy.

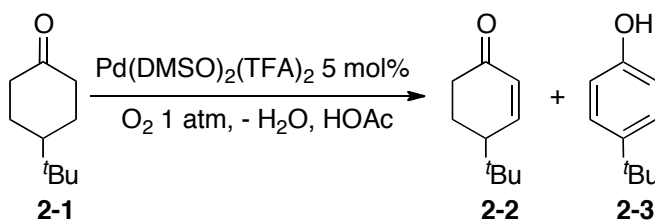
2.2.5 Conclusion

In summary, we have identified a Pd^{II} catalyst system that enables direct dehydrogenation of cyclic ketones to the corresponding enones with a number of important substrates. The high selectivity for enone rather than phenol formation sharply contrasts other Pd^{II}-catalyzed dehydrogenation methods^{3,13} and warrants further mechanistic investigation. The ability to replace stoichiometric reagents (e.g., Br₂, organoselenium reagents, and IBX) with O₂ as an oxidant has important implications for large-scale applications of these methods in pharmaceutical and fine-chemical synthesis.³⁶

2.3 Experimental

2.3.1 General Procedure for Catalyst Optimization

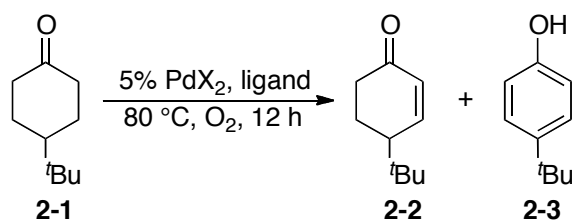
Catalytic aerobic oxidation reactions were performed using a custom reaction apparatus that enabled several reactions to be performed simultaneously under a constant pressure of O₂ (approx 1 atm) with controlled temperature and orbital agitation. Control experiments demonstrated that similar results can be obtained using a standard round-bottom flask equipped with a stir bar and a balloon of O₂ (see below), or using a stainless steel (or Hastelloy) Parr pressure vessel for reactions carried out under elevated pressures of O₂.



To a disposable 13 mm thick-walled culture tube was added Pd(TFA)₂, (1.65 mg, 0.005 mmol, 0.05 equiv), DMSO (0.7 μL, 0.01 mmol, 0.1 equiv), and 0.25 ml acetic acid. The reaction tubes were placed in a 48-well parallel reactor mounted on a Glas-Col large capacity mixer. The

headspace was purged with O₂ for 10 min, after which a solution of 4-*tert*-butylcyclohexanone (15.4 mg, 0.1 mmol, 1 equiv) in acetic acid (0.25 ml) was added via syringe. The solution was agitated vigorously at 80 °C for 12 h. After 12 h, the reaction vessel was vented. External standard (tetradecane, 10 μl, 0.038mmol) was added. The solution was then diluted with CH₂Cl₂ and analyzed by GC.

Table 2-3. Additional Catalyst Optimization Data for the Aerobic Oxidative Dehydrogenation of 4-*tert*-Butylcyclohexanone **2-1**^a



entry	Pd	ligand (mol%)	solvent	additive	2-2 (%) ^b	2-3 (%) ^b
1	Pd(OAc) ₂		DMSO		63	14
2	Pd(TFA) ₂		DMSO		34	56
3	Pd(TFA) ₂	2-Me ₂ Npy (10)	DMSO	TsOH (20%)	23	33
4	Pd(TFA) ₂	5,5-Me ₂ bpy (5)	PhCl	4Å MS, 50 mg	19	0
5	Pd(TFA) ₂	5,5-Me ₂ bpy (5)	PhCl		23	0
6	Pd(OAc) ₂		AcOH		13	0
7	Pd(TFA) ₂		AcOH		24	1
8	Pd(OAc) ₂	DMSO (10)	AcOH		86	8
9	Pd(TFA) ₂	DMSO (10)	AcOH		91	8
10	Pd(TFA) ₂	DMSO (10)	AcOH	4Å MS, 50 mg	6	0
11	Pd(TFA) ₂	DMSO (10)	Toluene		67	3
12	Pd(TFA) ₂	DMSO (10)	Mesitylene		86	6
13	Pd(TFA) ₂	DMSO (10)	THF		66	8
14	Pd(TFA) ₂	DMSO (10)	Dioxane		84	10
15	Pd(TFA) ₂	DMSO (10)	EtOAc		30	6

16	Pd(TFA) ₂	DMSO (10)	DMF		27	2
17	Pd(TFA) ₂	DMSO (10)	DMA		47	5
18	Pd(TFA) ₂	DMSO (10)	PhCN		16	2
19	Pd(TFA) ₂	DMSO (10)	PhCl		11	0
20	Pd(TFA) ₂	DMSO (10)	PhCl	4Å MS, 50 mg	12	0
21	Pd(TFA) ₂	MePhSO (10)	AcOH		22	0
22	Pd(TFA) ₂	tetramethylenesulfoxide (10)	AcOH		65	4
23	Pd(TFA) ₂	trimethylenesulfoxide (10)	AcOH		7	0
24	Pd(TFA) ₂	Pyridine (10)	AcOH		55	2
25	Pd(TFA) ₂	2-MeOpy (10)	AcOH		8	0
26	Pd(TFA) ₂	2-Me ₂ Npy (10)	AcOH		3	1
27	Pd(TFA) ₂	4-NH ₂ py (10)	AcOH		79	4
28	Pd(TFA) ₂	2-NH ₂ py (10)	AcOH		1	0
29	Pd(TFA) ₂	2-F py (10)	AcOH		37	2
30	Pd(TFA) ₂	3-Nitropy (10)	AcOH		4	0
31	Pd(TFA) ₂	bpy (5)	AcOH		0	0
32	Pd(TFA) ₂	6,6'-Me ₂ bpy (5)	AcOH		31	3
33	Pd(TFA) ₂	5,5'-Me ₂ bpy (5)	AcOH		0	0
34	Pd(TFA) ₂	4,4'-Me ₂ bpy (5)	AcOH		0	0
35	Pd(TFA) ₂	4,4'-di <i>tert</i> butyl-bpy (5)	AcOH		11	0
36	Pd(TFA) ₂	phenanthroline (5)	AcOH		0	0
37	Pd(TFA) ₂	6,6'-dimethylphen (5)	AcOH		26	2
38	Pd(TFA) ₂	bipyrimidine (5)	AcOH		6	0
39	Pd(TFA) ₂	Bissulfoxide (5)	HOAc		9	4
40	Pd(TFA) ₂	DMSO (10)	AcOH	NaOAc (10%)	85	6
41	Pd(TFA) ₂	DMSO (10)	AcOH	NaOBn (10%)	82	4
42	Pd(TFA) ₂	DMSO (10)	AcOH	Na ₂ CO ₃ (10%)	83	5
43	Pd(TFA) ₂	DMSO (10)	AcOH	pentamethylpiperidine (10%)	83	6
44	Pd(TFA) ₂	DMSO (10)	AcOH	TsOH (10%)	5	20

^aReaction conditions: see procedures above. ^bGC yield.

2.3.2 General Procedure for Dehydrogenation of Cyclohexanones and Product Isolation

Good gas-liquid mixing is critical for these reactions, and analysis of different reaction format revealed that the best results are obtained with orbital agitation. Nevertheless, the reactions could be carried out in a round-bottom flask equipped with a balloon of O₂, with magnetic stirring, or by using high-pressure diluted O₂ (9% in N₂) in a Parr pressure vessel, with magnetic stirring. Representative procedures employing each of these formats is described below.

Dehydrogenation of 2-1 with orbital agitation. To two disposable 13 mm thick-walled culture tubes were added Pd(TFA)₂ (6.6 mg, 0.02 mmol, 0.05 equiv), DMSO (2.8 μL, 0.01 mmol, 0.1 equiv), and acetic acid (1 ml). The reaction tubes were placed in a 48-well parallel reactor mounted on a Glas-Col large capacity mixer. The headspace was purged with O₂ for 10 min, after which a solution of 4-*tert*-butyl cyclohexanone (61.6 mg, 0.4 mmol, 1 equiv) in acetic acid (1 ml) was added via syringe. The solution was agitated vigorously at 80 °C for 12 h. After 12 h, the reaction was cooled down, and O₂ was vented from the reactor. The two reaction mixtures were combined and acetic acid was removed under vacuum using a rotovap. Silica gel was saturated with 1% triethylamine in hexane, and loaded onto a column. The column was then washed with hexane to remove excess triethylamine. The reaction mixture was loaded onto the column and flushed with 10% ethyl acetate in hexane. The cyclohexenone product **2-2** was obtained in 91% yield as a colorless liquid, and the phenol byproduct **2-3** was obtained as a white solid in 8% yield.

Dehydrogenation of 2-1 in a round-bottom flask. To a 25 ml round-bottom flask equipped with a stir bar was added Pd(TFA)₂ (13 mg, 0.04 mmol, 0.05 equiv) and 4-*tert*-butyl

cyclohexanone (123 mg, 0.8 mmol). A reflux condenser was placed on the flask and sealed with a septum. A balloon was attached via a needle. The flask and balloon were purged and filled with O₂, followed by addition of DMSO (5.6 μL, 0.02 mmol, 0.1 equiv) and acetic acid (4 ml). The flask was stirred at 80 °C for 12 h. After 12 h, O₂ was vented from the flask. Acetic acid was removed under vacuum using a rotovap. Products **2-2** and **2-3** were isolated as described above and obtained in 90% and 6% yield, respectively.

Dehydrogenation of 5α-Cholestan-3-one (Table 2-2, entry 8) in a round-bottom flask. To a 25 ml round-bottom flask equipped with a stir bar was added Pd(TFA)₂ (3.3 mg, 0.01 mmol, 0.05 equiv) and 5α-Cholestan-3-one (78 mg, 0.2 mmol). A reflux condenser was placed on the flask and sealed with a septum. A balloon was attached via a needle. The flask and balloon were purged and filled with O₂, followed by addition of DMSO (1.4 μL, 0.02 mmol, 0.1 equiv) and acetic acid (1 ml). The stock solution of NMR internal standard, 1,3,5-trimethoxybenzene (0.001 mmol, in DMSO-*d*₆), was added. The mixture was then neutralized with saturated NaHCO₃ aqueous solution and extracted with CDCl₃. The organic layer was transferred to an NMR tube via a pipet and analyzed by ¹H NMR spectroscopy, which revealed the enone product was formed in 90% NMR, comparable to the yield obtained from the reaction carried out with orbital agitation.

Dehydrogenation of unsubstituted cyclohexanone in a Parr pressure vessel. The oxidation of cyclohexanone in acetic acid afforded cyclohexenone in only modest yield (~50%) with poor mass balance. Improved mass balance was observed when the reaction was carried out in ethyl acetate. A good yield (72%) could be obtained with 1 atm O₂ when the reaction was mixed via orbital agitation; however, attempts to perform the oxidation in a round-bottom flask with an O₂ balloon failed, due to fast decomposition of the Pd catalyst (the use of AcOH as the solvent

appears to stabilize the catalyst). We speculated that the catalyst would be more stable with elevated pressures of O₂ and the reaction was analyzed under different pressures of O₂ (Figure 2-2). Low O₂ pressure led to low conversion and observation of significant amounts of Pd black. Elevated O₂ pressure resulted in a significant increase in product formation. A typical protocol for this reaction format is as follows:

To a 45 mL Hastelloy Parr pressure vessel equipped with a stir bar was added Pd(TFA)₂ (13.2 mg, 0.04 mmol, 0.05 equiv), DMSO (5.6 μL, 0.02 mmol, 0.1 equiv), ethyl acetate (1 ml) and cyclohexanone (80 μl, 0.8 mmol). The vessel was sealed and 70 atm of 9% O₂ in N₂ (6.3 atm partial pressure of O₂) was supplied to the vessel. The reaction was heated to 60 °C with vigorous stirring for 24 h. After 24 h, the O₂ was vented from the vessel. The product was purified as described above, and afforded a 70% yield of cyclohexenone and 20% phenol.

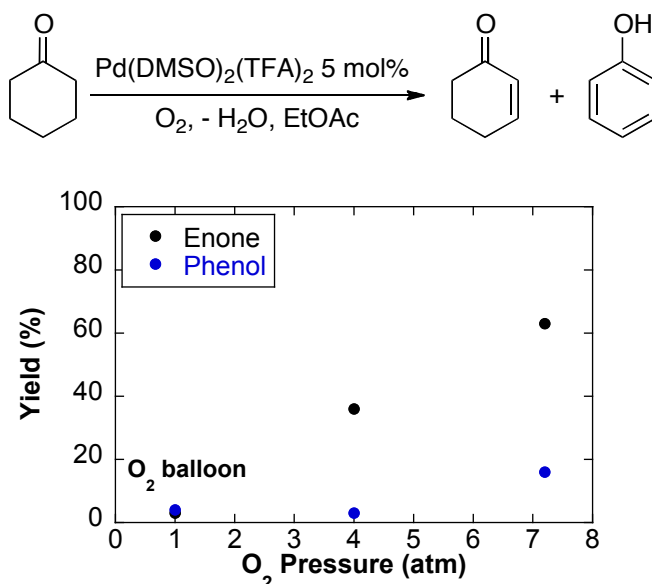


Figure 2-2. Dependence of the oxidation of cyclohexanone on the O₂ pressure. Conditions: [cyclohexanone] = 0.8 M (0.8 mmol), 5% Pd(TFA)₂ (0.04 mmol), 10% DMSO (0.08 mmol), ethyl acetate (1 mL).

2.3.3 Procedure for Aerobic Dehydrogenation of Cyclohexanone 2-1 in a Flow Reactor

The flow reactor used in these studies has been described previously.³⁶ The total volume of the tube reactor is 66 mL. An oil bath set to 100 °C was used to regulate the reaction-zone temperature of the flow reactor. The flow reactor was first rinsed with toluene and dried by passing nitrogen gas through the tubing at 100 °C. The reactor was pressurized with a 500 psig of dilute O₂ gas (8% O₂ in N₂). Four sequential metering valves connected to the O₂ outlet were adjusted to obtain the desired gas flow rate. The total gas flow out of the vapor-outlet valve was maintained around 1.6 sccm. The reactor was then purged with the dilute oxygen gas for 10-15 minutes (8% O₂ in N₂; 500 psig). Two syringe pumps were used for delivery of the reagents and catalyst. The first syringe pump was charged with Pd(DMSO)₂(TFA)₂ stock solution in acetic acid (0.02 M, 180 ml), and the second syringe pump was charged with 4-*tert*-

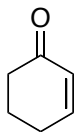
butylcyclohexanone stock solution in acetic acid (0.4 M, 180 ml). The feed rates of both pumps were adjusted to 0.014 ml/min (residence time = 12 h). Both syringe pumps were started to initiate the flow of liquid solution with continuous delivery of dilute oxygen gas through the reactor. After starting the pumps ($t = 0$), the time when liquid started to accumulate in the liquid product tank was recorded as the actual liquid residence time. The product was analyzed by GC and isolated as described above (88% GC yield; 78% isolated yield). The discrepancy between GC and isolated yield was due to loss of material when the acetic acid solvent was removed under vacuum.

2.3.4 Acquisition of Time Course Data

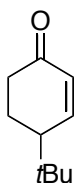
The reactions were performed using orbital shakers under standard conditions, as described above. The catalyst was heated to 80 °C and the temperature was allowed to equilibrate for 5 min. A stock solution of internal standard (1,4-dimethoxybenzene) was injected via syringe. Injection of substrates dissolved in solvent established the $t = 0$ point. After various time intervals, aliquots were withdrawn from the reaction mixture via pipet, diluted with CH_2Cl_2 and analyzed by GC. Time course data were imported into the kinetic simulation software COPASI,³⁷ and a simple sequential first-order kinetic model, $\text{A} \rightarrow \text{B} \rightarrow \text{C}$, was used to fit the data in COPASI using Levenberg-Marquardt numerical methods.

2.3.5 Characterization Data of Enone Products

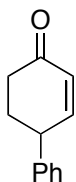
All compounds in Table 2-2 and eqs 1 and 2 have been reported previously. In all cases, the product identities were established by comparison of the ^1H NMR spectra with previously reported data. In one case (Table 2-2, entry 8), full characterization was not previously reported; these data are included below.



(Table 2-2, Entry 1): Prepared as described above. Purified by silica gel column chromatography using a 0-20% EtOAc in hexane gradient elution to give 72% yield of the product as a colorless oil. ^1H NMR data match previously reported data.³⁸ ^1H NMR (CDCl_3): δ 7.000 (dt, 1H, $J = 10.1, 4.1$ Hz), 6.03 (d, 1H, $J = 10.1, 2.0$ Hz), 2.44 (t, 2H, $J = 6.4$ Hz), 2.40-2.30 (m, 2H), 2.09-1.97 (m, 2H).

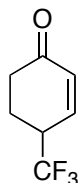


(Table 2-2, Entry 2): Prepared as described above. Purified by silica gel column chromatography that has been saturated with 1% Et_3N using a 0-10% EtOAc in hexane gradient elution to give 91% yield of the product as a colorless liquid. ^1H NMR data match previously reported data.³⁹ ^1H NMR (CDCl_3): 7.02 (dd, 1H, $J = 10.4, 2.0$ Hz), 6.04 (dd, 1H, $J = 10.4, 2.8$ Hz), 2.53 (dt, 1H, $J = 16.6, 3.6$ Hz), 2.34 (ddd, 1H, $J = 16.6, 14.2, 4.8$ Hz), 2.45-2.16 (m, 1H), 2.16-2.03 (m, 1H), 1.82-1.66 (m, 1H), 0.98 (s, 9H).

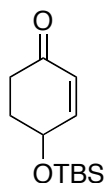


(Table 2-2, Entry 3): Prepared as described above. Purified by silica gel column chromatography that has been saturated with 1% Et_3N using a 0-10% EtOAc in hexane gradient elution to give 83% yield of the product as a white solid. ^1H NMR data match previously

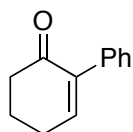
reported data.⁴⁰ ¹H NMR (CDCl₃): δ 7.40-7.32 (m, 2H), 7.32-7.27 (m, 1H), 7.25-7.19 (m, 2H), 7.00 (ddd, 1H, J = 10.2, 2.9, 1.4 Hz), 6.17 (ddd, 1H, J = 10.2, 2.5, 0.6 Hz), 3.78-3.68 (m, 1H), 2.62-2.45 (m, 2H), 2.45-2.30 (m, 1H), 2.13-1.98 (m, 1H).



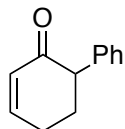
(Table 2-2, Entry 4): Prepared as described above. Purified by silica gel column chromatography using a 0-20% EtOAc in hexane gradient elution to give 81% yield of the product as a colorless oil. ¹H NMR data match previously reported data.⁴¹ ¹H NMR (CDCl₃): δ 6.88 (ddd, 1H, J = 10.3, 2.5, 1.5), 6.22 (dd, 1H, J = 10.3, 2.6 Hz), 3.30-3.11 (m, 1H), 2.65 (dt, 1H, J = 17.4, 4.6 Hz), 2.51-2.40 (m, 1H), 2.36-2.28 (m, 1H), 2.21-2.06 (m, 1H).



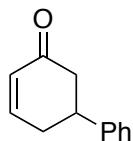
(Table 2-2, Entry 5): Prepared as described above. Purified by silica gel column chromatography using a 0-15% EtOAc in hexane gradient elution to give 76% yield of the product as a slightly yellow oil. ¹H NMR data match previously reported data.⁴² ¹H NMR (CDCl₃): δ 6.84 (dt, 1H, J = 10.3, 2.1 Hz), 5.93 (ddd, 1H, J = 10.3, 1.8, 1.0 Hz), 4.56-4.49 (m, 1H), 2.58 (dt, 1H, J = 17.1, 5.1 Hz), 2.35 (ddd, 1H, J = 17.1, 12.7, 4.4 Hz), 2.21 (dq, J = 14.4, 4.4, 1.8 Hz), 2.00 (tdd, J = 12.7, 9.0, 4.4 Hz), 0.92 (9H, s), 0.13 (3H, s), 0.12 (3H, s).



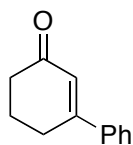
(Table 2-2, Entry 6): Prepared as described above. Purified by silica gel column chromatography using a 0-20% EtOAc in hexane gradient elution to give 63% yield of the product as a colorless oil. ^1H NMR data match previously reported data.⁴³ ^1H NMR (CDCl_3): δ 7.39-7.24 (m, 5H), 7.03 (t, 1H, $J = 4.4$ Hz), 2.64-2.48 (m, 4H), 2.17-2.05 (m, 2H).



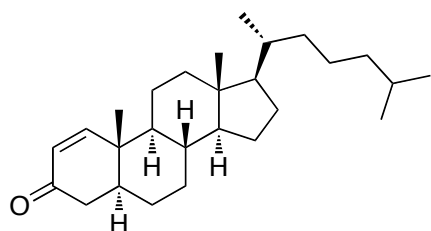
(Table 2-2, Entry 6): Prepared as described above. Purified by silica gel column chromatography using a 0-20% EtOAc in hexane gradient elution to give 21% yield of the product as a colorless oil. ^1H NMR data match previously reported data.⁴⁴ ^1H NMR (CDCl_3): δ 7.38-7.22 (m, 3H), 7.20-7.12 (m, 2H), 7.04 (dt, 1H, $J = 10.1, 4.2$ Hz), 6.17 (dt, 1H, $J = 10.1, 1.8$ Hz), 3.61 (t, 1H, $J = 8.1$ Hz), 2.53-2.43 (m, 2H), 2.34-2.23 (m, 2H).



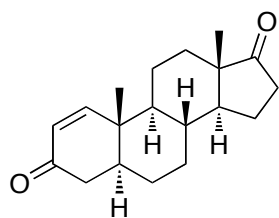
(Table 2-2, Entry 7): Prepared as described above. Purified by silica gel column chromatography using a 0-20% EtOAc in hexane gradient elution to give 63% yield of the product as a colorless oil. ^1H NMR data match previously reported data.⁴⁵ ^1H NMR (CDCl_3): δ 7.41-7.31 (m, 2H), 7.31-7.15 (m, 3H), 7.05 (ddd, 1H, $J = 9.9, 5.5, 2.4$ Hz), 6.13 (ddt, 1H, $J = 9.9, 2.4, 0.6$ Hz), 3.36 (h, 1H, $J = 5.3$ Hz), 2.73-2.65 (m, 2H), 2.65-2.60 (m, 1H), 2.56 (dt, 1H, $J = 10.7, 2.4$ Hz)



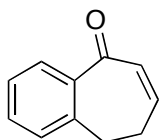
(Table 2-2, Entry 7): Prepared as described above. Purified by silica gel column chromatography using a 0-20% EtOAc in hexane gradient elution to give 23% yield of the product as a colorless oil. ^1H NMR data match previously reported data.⁴⁶ ^1H NMR (CDCl_3): δ 7.57-7.52 (m, 2H), 7.45-7.38 (m, 3H), 6.43 (t, 1H, $J = 1.4$ Hz), 2.78 (td, 2H, $J = 5.8, 1.4$ Hz), 2.53-2.44 (m, 2H), 2.22-2.11 (m, 2H).



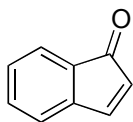
(Table 2-2, Entry 8): Prepared as described above. Purified by silica gel column chromatography using a 0-15% EtOAc in hexane gradient elution to give 94% yield of the product as a white solid. This compound has been reported previously;⁴⁷ however, full characterization data have not been reported. ^1H NMR (CDCl_3): δ 7.14 (d, 1H, $J = 10.0$ Hz), 5.85 (d, 1H, $J = 10.0$ Hz), 2.37 (dd, 1H, $J = 17.4, 13.8$ Hz), 2.21 (dd, 1H, $J = 17.4, 4.2$ Hz), 2.05 (dt, 1H, $J = 12.6, 3.4$ Hz), 1.99-1.77 (m, 2H), 1.77-1.65 (m, 2H), 1.63-0.95 (m, 20H), 1.00 (s, 3H), 0.91 (d, 3H, $J = 6.9$ Hz), 0.87 (d, 3H, $J = 6.5$ Hz), 0.86 (d, 3H, $J = 6.5$ Hz), 0.69 (s, 3H). ^{13}C NMR (CDCl_3): δ 200.5, 158.9, 127.6, 56.6, 56.4, 50.2, 44.5, 42.9, 41.2, 40.0, 39.7, 39.2, 36.3, 36.0, 35.9, 31.5, 28.4, 28.2, 27.9, 24.3, 24.0, 23.0, 22.8, 21.5, 18.9, 13.2, 12.4. HRMS (ESI) [$\text{M} + \text{Na}^+$]/ z calcd. 384.3387, found 384.3376. M.P. = 99–100 °C.



(Table 2-2, Entry 9): Prepared as described above. Purified by silica gel column chromatography using a 20-40% EtOAc in hexane gradient elution to give 93% yield of the product as a white solid. ^1H NMR data match previously reported data.⁴⁸ ^1H NMR (CDCl_3): δ 7.14 (d, 1H, $J = 10.5$ Hz), 5.87 (d, 1H, $J = 10.5$ Hz), 2.53-2.32 (m, 2H), 2.24 (ddd, 1H, $J = 17.7$, 4.3, 0.8 Hz), 2.17-2.06 (m, 1H), 2.02-1.81 (m, 5H), 1.67 (qd, 1H, $J = 10.6$, 4.2 Hz), 1.60-1.27 (m, 6H), 1.15-0.99 (m, 2H), 1.05 (s, 3H), 0.91 (s, 3H).

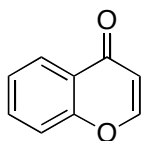


(Table 2-2, Entry 10): Prepared as described above. 50% DMSO was used as ligand and toluene was the solvent. The reaction was heated to 60 °C for 24 h, then 80 °C for another 24 h. Purified by silica gel column chromatography using a 0-10% EtOAc in hexane gradient elution to give 81% yield of the product as a slightly yellow oil. ^1H NMR data match previously reported data.⁴⁹ ^1H NMR (CDCl_3): δ 7.75 (dd, 1H, $J = 7.5$, 1.4 Hz), 7.42 (td, 1H, $J = 7.5$, 1.4 Hz), 7.31 (td, 1H, $J = 8.8$, 1.4 Hz), 7.19 (d, 1H, $J = 7.5$ Hz), 6.75 (dt, 1H, $J = 12.2$, 4.9 Hz), 6.28 (dt, 1H, $J = 12.2$, 2.0 Hz), 3.11-2.98 (m, 2H), 2.65-2.53 (m, 2H).

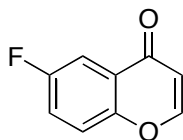


(Table 2-2, Entry 11): Prepared as described above. 50% DMSO was used as ligand and toluene was the solvent. Purified by silica gel column chromatography using a 0-20% EtOAc in hexane gradient elution to give 54% yield of the product as a yellow oil. ^1H NMR data match previously reported data.⁵⁰ ^1H NMR (CDCl_3): δ 7.57 (d, 1H, $J = 6.2$ Hz), 7.43 (d, 1H, $J = 7.0$

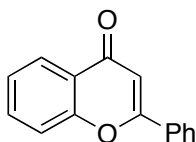
Hz), 7.35 (t, 1H, J = 7.0 Hz), 7.23 (t, 1H, J = 7.0 Hz), 7.06 (d, 1H, J = 7.0 Hz), 5.89 (d, 1H, J = 6.2 Hz).



(Table 2-2, Entry 12): Prepared as described above. Purified by silica gel column chromatography using a 20-40% EtOAc in hexane gradient elution to give 80% yield of the product as a white solid. ^1H NMR data match previously reported data.⁵¹ ^1H NMR (CDCl_3): δ 8.22 (dd, 1H, J = 8.0, 1.4 Hz), 7.87 (d, 1H, J = 6.1 Hz), 7.68 (ddd, 1H, J = 8.6, 8.0, 1.4 Hz), 7.47 (d, 1H, J = 8.6 Hz), 7.42 (t, 1H, J = 8.0 Hz), 6.36 (d, 1H, J = 6.1 Hz).

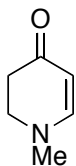


(Table 2-2, Entry 13): Prepared as described above. Purified by silica gel column chromatography using a 30% EtOAc in hexane gradient elution to give 78% yield of the product as a white solid. ^1H NMR data match previously reported data.⁵² ^1H NMR (CDCl_3): δ 7.87 (d, 1H, J = 6.0 Hz), 7.85 (dd, 1H, J = 8.2, 3.2 Hz), 7.48 (dd, 1H, J = 9.0, 4.4 Hz), 7.40 (ddd, 1H, J = 9.0, 7.5, 3.2 Hz), 6.34 (d, 1H, J = 6.0 Hz).

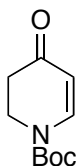


(Table 2, Entry 14): Prepared as described above. The reaction mixture was washed with water and extracted with ethyl acetate. The mixture was purified by silica gel column chromatography using a gradient 0%-30% EtOAc in hexane elution to give 88% yield of the

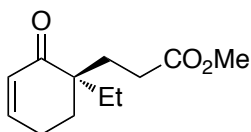
product as a white solid. ^1H NMR data match previously reported data.⁵³ ^1H NMR (CDCl_3): δ 8.25 (dd, 1H, $J = 8.0, 1.6$ Hz), 7.99-7.89 (m, 2H), 7.72 (ddd, 1H, $J = 8.6, 7.1, 1.6$ Hz), 7.59 (dd, 1H, $J = 8.6, 1.0$ Hz), 7.57-7.49 (m, 3H), 7.44 (ddd, 1H, $J = 8.0, 7.1, 1.0$), 6.88 (s, 1H).



(Table 2-2, Entry 15): Prepared as described above. Purified by filtration through a pipette of Al_2O_3 , eluted with pure ethyl acetate to give 74% yield of the product as a colorless oil. ^1H NMR data match previously reported data.⁵⁴ ^1H NMR (CDCl_3): δ 6.98 (d, 1H, $J = 7.4$ Hz), 4.92 (d, 1H, $J = 7.4$ Hz), 3.44 (t, 2H, $J = 7.7$ Hz), 2.48 (t, 2H, $J = 7.7$ Hz).

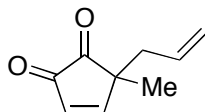


(Table 2-2, Entry 16): $\text{Pd}(\text{TFA})_2$ in DMSO was used for this substrate. No ligand was added. Purified by silica gel column chromatography using a 30-40% EtOAc in hexane gradient elution to give 72% yield of the product as a white solid. ^1H NMR data match previously reported data.⁵⁵ ^1H NMR (CDCl_3): δ 7.82 (br, 1H), 5.31 (d, 1H, $J = 8.3$ Hz), 3.98 (t, 2H, $J = 7.4$ Hz), 2.55 (t, 2H, $J = 7.4$ Hz), 1.54 (s, 9H).



(eq 2-1): Prepared as described above. Purified by silica gel column chromatography using a 10-20% EtOAc in hexane gradient elution to give 85% yield of the product as a pale yellow oil. ^1H NMR data match previously reported data.⁵⁶ ^1H NMR (CDCl_3): δ 6.85 (dt, 1H, $J = 10.0, 4.0$

Hz), 5.90 (dt, 1H, J = 10.0, 2.0 Hz), 3.66 (s, 3H), 2.45-2.35 (m, 2H), 2.35-2.16 (m, 2H), 1.98-1.77 (m, 4H), 1.70-1.46 (m, 2H), 0.84 (t, 3H, J = 7.7 Hz).



(eq 2-2): Prepared as described above. Good gas-liquid mixing is very crucial to this substrate to prevent catalyst decomposition. After catalyst and solvent were mixed and purged with O₂, the substrate was added via syringe while agitating. Reaction conditions: [substrate] = 0.025 M, [Pd(TFA)₂] = 0.0025 M (10%), [DMSO] = 0.0075 M (30%), 1 atm O₂. Purified by silica gel column chromatography using a 0-20% EtOAc in hexane gradient elution to give 90% yield of the product as a yellow oil. ¹H NMR data match previously reported data.³⁴ ¹H NMR (CDCl₃): δ 7.83 (d, 1H, J = 7.3 Hz), 6.88 (d, 1H, J = 7.3 Hz), 5.59 (dddd, 1H, J = 17.5, 10.4, 7.9, 7.3 Hz), 5.16-5.01 (m, 2H), 2.47 (dd, 1H, J = 13.8, 7.9 Hz), 2.36 (ddt, 1H, J = 13.8, 7.1, 1.0 Hz), 1.28 (s, 3H).

2.4 References

1. (a) Nishimura, S. *Handbook of Heterogeneous Catalytic Hydrogenation for Organic Synthesis*; Wiley-Interscience, 2001. (b) *The Handbook of Homogeneous Hydrogenation*; de Vries, J. G.; Elsevier, C. J., Eds.; Wiley-VCH, Weinheim, 2007.

2. Transfer-dehydrogenation methods are currently the most effective methods for dehydrogenation of saturated carbon-carbon bonds; however, the application of these methods in organic synthesis is rare. For leading references to these methods, see the following recent

review articles: (a) Doberiner, G. E.; Crabtree, R. H. *Chem. Rev.* **2010**, *110*, 681-703. (b) Choi, J.; MacArthur, A. H. R.; Brookhart, M.; Goldman, A. S. *Chem. Rev.* **2011**, *111*, 1761-1779.

3. Izawa, Y.; Pun, D.; Stahl, S. S. *Science* **2011**, *333*, 209-213.

4. Numerous examples of cyclohexanone dehydrogenation in natural product synthesis exist. For recent examples, see: (a) Herzon, S. B.; Lu, L.; Woo, C. M.; Gholap, S. L. *J. Am. Chem. Soc.* **2011**, *133*, 7260-7263. (b) Yokoe, H.; Mitsuhashi, C.; Matsuoka, Y.; Yoshimura, T.; Yoshida, M.; Shishido, K. *J. Am. Chem. Soc.* **2011**, *133*, 8854-8857. (c) Petronijevic, F. R.; Wipf, P. *J. Am. Chem. Soc.* **2011**, *133*, 7704-7707.

5. For reviews of methods for α,β -dehydrogenation of carbonyl compounds, see: (a) Buckle, D. R.; Pinto, I. L. In *Comprehensive Organic Synthesis*; Trost, B. M., Fleming, I., Eds.; Oxford **1991**; Vol. 7, pp. 119-149. (b) Larock, R. C. In *Comprehensive Organic Transformations*; John Wiley & Sons: New York, 1999; pp. 251-256.

6. For Pd-catalyzed dehydrogenation of silyl enol ethers ("Saegusa reactions"), see: (a) Ito, Y.; Hirao, T.; Saegusa, T. *J. Org. Chem.* **1978**, *43*, 1011-1013. (b) Larock, R. C.; Hightower, T. R.; Kraus, G. A.; Hahn, P.; Zheng, D. *Tetrahedron Lett.* **1995**, *36*, 2423-2426. (c) Yu, J. Q.; Wu, H. C.; Corey, E. J. *Org. Lett.* **2005**, *7*, 1415-1417.

7. Common methods include bromination/dehydrobromination and selenoxide and sulfoxide elimination reactions. See the following leading references: (a) Miller, B.; Wong, H.-S. *Tetrahedron* **1972**, *28*, 2369-2376. (b) Stotter, P. L.; Hill, K. A. *J. Org. Chem.* **1973**, *38*, 2576-2578. (c) Trost, B. M.; Salzmann, T. N.; Hiroi, K. *J. Am. Chem. Soc.* **1976**, *98*, 4887-4902. (d)

Sharpless, K. B.; Lauer, R. F.; Teranishi, A. Y. *J. Am. Chem. Soc.* **1973**, *95*, 6137-6139. (e)

Reich, H. J. *Acc. Chem. Res.* **1979**, *12*, 22-30.

8. (a) Nicolaou, K. C.; Zhong, Y. L.; Baran, P. S. *J. Am. Chem. Soc.* **2000**, *122*, 7596-7597.
(b) Nicolaou, K. C.; Montagnon, T.; Baran, P. S.; Zhong, Y. L. *J. Am. Chem. Soc.* **2002**, *124*, 2245-2258. (c) Nicolaou, K. C.; Montagnon, T.; Baran, P. S. *Angew. Chem. Int. Ed.* **2002**, *41*, 993-996. (d) Nicolaou, K. C.; Gray, D. L. F.; Montagnon, T.; Harrison, S. T. *Angew. Chem. Int. Ed.* **2002**, *41*, 996-999.

9. For a method employing catalytic 2-iodoxybenzene sulfonate (IBS) in combination stoichiometric Oxone[®], see: Uyanik, M.; Akakura, M.; Ishihara, K. *J. Am. Chem. Soc.* **2009**, *131*, 251-262.

10. (a) Walker, D.; Hiebert, J. D. *Chem. Rev.* **1967**, *67*, 153-195. (b) Buckle, D. R. "2,3-Dichloro-5,6-dicyano-1,4-benzoquinone." In *Encyclopedia of Reagents for Organic Synthesis*. John Wiley & Sons, Inc. New York, 2010. (c) Bhattacharya, A.; DiMichele, L. M.; Dolling, U. H.; Douglas, A. W.; Grabowski, E. J. J. *J. Am. Chem. Soc.* **1988**, *110*, 3318-3319.

11. The requirement for large amounts of Pd^{II} in these reactions may arise from inhibition of catalyst reoxidation, arising from enone coordination to Pd⁰: Porth, S.; Bats, J. W.; Trauner, D.; Giester, G.; Mulzer, J. *Angew. Chem. Int. Ed.* **1999**, *38*, 2015-2016.

12. (a) Theissen, R. J. *J. Org. Chem.* **1971**, *36*, 752-757. (b) Muzart, J.; Pete, J. P. *J. Mol. Catal.* **1982**, *15*, 373-376. (c) Wenzel, T. T. *J. Chem. Soc., Chem. Commun.* **1989**, 932-933. (d)

Park, Y. W.; Oh, H. H. *Bull. Kor. Chem. Soc.* **1997**, *18*, 1123-1124. (e) Tokunaga, M.; Harada, S.; Iwasawa, T.; Obora, Y.; Tsuji, Y. *Tetrahedron Lett.* **2007**, *48*, 6860-6862.

13. For a recent review of reactions of this type, see: Muzart, J. *Eur. J. Org. Chem.* **2010**, 3779-3790.

14. Pd^{II}-catalyzed dehydrogenation of β -aryl aldehydes has been explored recently; however, the current substrate scope is rather limited: (a) Zhu, J.; Liu, J.; Ma, R. Q.; Xie, H. X.; Li, J.; Jiang, H. L.; Wang, W. *Adv. Synth. Catal.* **2009**, *351*, 1229-1232. (b) Liu, J.; Zhu, J.; Jiang, H. L.; Wang, W.; Li, J. *Chem. Asian J.* **2009**, *4*, 1712-1716.

15. Direct dehydrogenation of 3,3-dimethylcyclohexanone was reported recently with 1–5 mol% of an Ir-pincer catalyst and *t*Bu-ethylene as the H₂ acceptor. Other cyclohexanone substrates lacking *gem*-disubstitution undergo stoichiometric dehydrogenation, forming an Ir-phenoxide product. Zhang, X. W.; Wang, D. Y.; Emge, T. J.; Goldman, A. S. *Inorg. Chim. Acta.* **2011**, *369*, 253-259.

16. The mechanism could proceed via *C*- and/or *O*-bound Pd enolates, although β -hydride elimination is expected to occur from the *C*-bound enolate. For the formation of *C*-bound Pd-enolate under relatively similar conditions, see: Fuchita, Y.; Harada, Y. *Inorg. Chim. Acta* **1993**, *208*, 43-47.

17. Recent studies suggest that aerobic oxidation of Pd^{II}-hydrides proceed via Pd⁰, as shown in Scheme 2-2. See: (a) Konnick, M. M.; Stahl, S. S. *J. Am. Chem. Soc.* **2008**, *130*, 5753-5762. (b) Popp, B. V.; Stahl, S. S. *Chem. Eur. J.* **2009**, *15*, 2915-2922.

18. Gas update experiments show that the product:O₂ stoichiometry is 2:1, consistent with Pd-mediated disproportionation of H₂O₂ under reaction conditions. For previous characterization of Pd-mediated H₂O₂ disproportionation under related conditions, see the Supporting Information for the following reference: Steinhoff, B. A.; Fix, S. R.; Stahl, S. S. *J. Am. Chem. Soc.*, **2002**, *124*, 766-767.

19. (a) Stahl, S. S. *Angew. Chem., Int. Ed.* **2004**, *43*, 3400-3420; (b) Gligorich, K. M.; Sigman, M. S. *Chem. Commun.* **2009**, 3854-3867. (c) Chen, X.; Engle, K. M.; Wang, D.-H.; Yu, J.-Q. *Angew. Chem. Int. Ed.* **2009**, *48*, 5094-5115.

20. Pd(OAc)₂/DMSO catalyst systems for aerobic oxidation reactions were pioneered by the groups of Hiemstra and Larock. For initial reports, see: (a) Larock, R. C.; Hightower, T. R. *J. Org. Chem.* **1993**, *58*, 5298-5300. (b) van Benthem, R. A. T. M.; Hiemstra, H.; Michels, J. J.; Speckamp, W. N. *J. Chem. Soc., Chem. Commun.* **1994**, 357-359.

21. For mechanistic characterization of this catalyst system, see: Steinhoff, B. A.; Stahl, S. S. *J. Am. Chem. Soc.*, **2006**, *128*, 4348-4355.

22. The other ligands, such as pyridine (entry 13), 2-F-pyridine (entry 15) and the bis-sulfoxide ligand (entry 19) were selected on the basis of their utility in other recent Pd-catalyzed oxidation reactions. See, for example: (a) Nishimura, T.; Onoue, T.; Ohe, K.; Uemura, S. *J. Org. Chem.* **1999**, *64*, 6750-6755. (b) Izawa, Y.; Stahl, S. S. *Adv. Synth. Catal.* **2010**, *352*, 3223-3229. (c) Chen, M. S.; Prabakaran, N.; Labenz, N. A.; White, M. C. *J. Am. Chem. Soc.* **2005**, *127*, 6970-6971.

-
23. Brasche, G.; García-Fortanet, J.; Buchwald, S. L. *Org. Lett.* **2008**, *10*, 2207-2210.
24. McDonald, R. I.; Stahl, S. S. *Angew. Chem. Int. Ed.*, **2010**, *49*, 5529-5532.
25. Kinetic fitting was carried with COPASI software: Hoops, S.; Sahle, S.; Gauges, R.; Lee, C.; Pahle, J.; Simus, N.; Singhal, M.; Xu, L.; Mendes, P.; Kummer, U. *Bioinformatics* **2006**, *22*, 3067-3074.
26. The kinetics of phenol formation (Figure 2-1(B)) show that this reaction is more complicated than a simple sequential $A \rightarrow B \rightarrow C$ process. Specifically, a kinetic "burst" is evident during the first catalytic turnover that leads to rapid conversion of cyclohexanone to cyclohexenone. The fit in Figure 1B reflects a fit of the data after this burst phase. Mechanistic studies to elucidate the origin of these observations are ongoing.
27. Catalyst decomposition appears to be more rapid when ethyl acetate is used as the solvent rather than acetic acid. Vigorous agitation of the reaction mixture to ensure good gas-liquid mixing, or the use of higher O₂ pressure improves the outcome. When using elevated O₂ pressure, we employ a mixture of O₂ (9%) in N₂ as the gas source to reduce flammability hazards. See Supporting Information for details.
28. Si, D.; Wang, Y.; Zhou, Y. H. *Drug. Metab. Dispos.* **2003**, *37*, 629-634.
29. Cermak, R.; Wolfram, S. *Curr. Drug. Metab.* **2006**, *7*, 729-44.
30. (a) Loudon, J. D.; Razdan, R. K. *J. Chem. Soc.* **1954**, 4299-4303. (b) Choudary, B. M.; Ranganath, K. V. S.; Yadav, J.; Lakshmi Kantam, M. *Tetrahedron Lett.* **2005**, *46*, 1369-1371.

-
31. Kurono, M.; Yamaguchi, T.; Usui, T.; Fukushima, M.; Mizuno, K.; Matsubara, A., 1986; Vol. EP0193415 (A2).
32. Kondo, T.; Oyama, K.-I.; Yoshida, K. *Angew. Chem. Int. Ed.* **2001**, *40*, 894-897.
33. Nakajima, R.; Ogino, T.; Yokoshima, S.; Fukuyama, T. *J. Am. Chem. Soc.* **2010**, *132*, 1236-1237.
34. Trost, B. M.; Dong, G.; Vance, J. A. *Chem. Eur. J.* **2010**, *16*, 6265-6277.
35. Arnett, E. M.; Harrelson, J. A. *J. Am. Chem. Soc.* **1987**, *109*, 809-812.
36. Dehydrogenation of substrate **2-1** has been carried out on a 10-gram scale using a prototype flow reactor donated to UW-Madison by Eli Lilly. See Supporting Information and the following reference for details: Ye, X.; Johnson, M. D.; Diao, T.; Yates, M. H.; Stahl, S. S. *Green Chem.* **2010**, *12*, 1180-1186.
37. Hoops, S., Sahle, S., Gauges, R., Lee, C., Pahle, J., Simus, N., Singhal, M., Xu, L., Mendes, P., and Kummer, U. *Bioinformatics* **2006**, *22*, 3067-3074.
38. AIST: Integrated Spectral Database System of Organic Compounds. (Data were obtained from the National Institute of Advanced Industrial Science and Technology (Japan))
39. Booker-Milburn, K. I.; Thompson, D. F. *Tetrahedron* **1995**, *51*, 12955-12962.
40. Uyanik, M.; Akakura, M.; Ishihara, K. *J. Am. Chem. Soc.* **2008**, *131*, 251-262.
41. Ojima, I.; Yatabe, M.; Fuchikami, T. *J. Org. Chem.* **1982**, *47*, 2051-2055.

-
42. Bayón, P.; Marjanet, G.; Toribio, G.; Alibés, R.; de March, P.; Figueredo, M.; Font, J. J. *Org. Chem.* **2008**, *73*, 3486-3491.
43. Felpin, F.-X. *J. Org. Chem.* **2005**, *70*, 8575-8578.
44. Marino, J. P.; Jaen, J. C. *J. Am. Chem. Soc.* **1982**, *104*, 3165-3172.
45. Kryshtal, G. V.; Kulganek, V. V.; Kucherov, V. F.; Yanovskaya, L. A. *Synthesis-Stuttgart* **1979**, 107-109.
46. Shibuya, M.; Tomizawa, M.; Iwabuchi, Y. *Org. Lett.* **2008**, *10*, 4715-4718.
47. Nicolaou, K. C.; Montagnon, T.; Baran, P. S.; Zhong, Y. L. *J. Am. Chem. Soc.* **2002**, *124*, 2245-2258.
48. Zhang, H.; Qiu, Z. *Steroids* **2006**, *71*, 1088-1090.
49. Collington, E. W.; Jones, G. *J. Chem. Soc.C.* **1969**, 2656-2661.
50. Zhao, Y.; Yeung, Y.-Y. *Org. Lett.* **2010**, *12*, 2128-2131.
51. Liang, B.; Huang, M.; You, Z.; Xiong, Z.; Lu, K.; Fathi, R.; Chen, J.; Yang, Z. *J. Org. Chem.* **2005**, *70*, 6097-6100.
52. Kurono, M.; Yamaguchi, T.; Usui, T.; Fukushima, M.; Mizuno, K.; Matsubara, A., 1986; Vol. EP0193415 (A2).
53. Miao, H.; Yang, Z. *Org. Lett.* **2000**, *2*, 1765-1768.

-
54. Guerry, P.; Neier, R. *Synthesis-Stuttgart* **1984**, 485-488.
55. Sebesta, R.; Pizzuti, M. G.; Boersma, A. J.; Minnaard, A. J.; Feringa, B. L. *Chem. Commun.* **2005**, 1711-1713.
56. Nakajima, R.; Ogino, T.; Yokoshima, S.; Fukuyama, T. *J. Am. Chem. Soc.* **2010**, *132*, 1236-1237.

CHAPTER 3

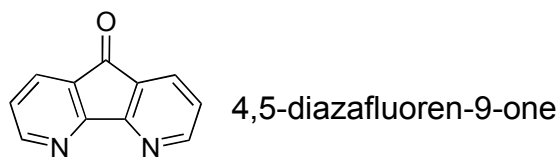
Palladium/4,5-Diazafluorenone-Catalyzed Aerobic α,β -Dehydrogenation of Carbonyl Compounds

This work has been published under the following:

Diao, T.; Wadzinski, T. J.; Stahl, S. S. *Chem. Sci.* **2012**, *3*, 887-891.

3.1 Introduction to Dehydrogenation of Carbonyl Compounds

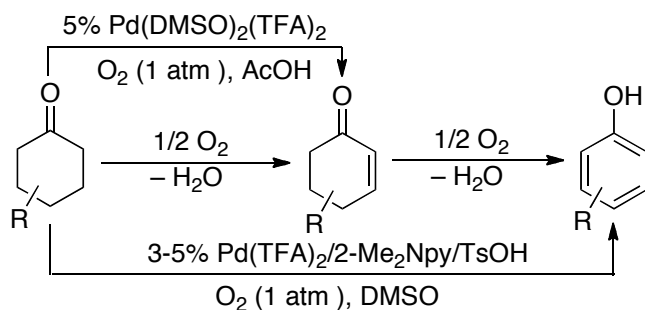
Enones and other α,β -unsaturated carbonyl compounds are important intermediates in the synthesis of pharmaceuticals and other complex organic molecules.¹ Such compounds are frequently prepared via stepwise protocols, including α -bromination-dehydrobromination,² α -selenylation followed by oxidation to a selenoxide and elimination,^{3,4} and formation of a silyl enol ether, followed by Pd^{II}-mediated dehydrosilylation ("Saegusa" oxidation).⁵ Direct α,β -dehydrogenation of ketones and aldehydes has also been achieved using stoichiometric reagents, such as 2,3-dichloro-5,6-dicyano-1,4-benzoquinone (DDQ)⁶ and 2-iodoxybenzoic acid (IBX).^{7,8} Pd^{II}-catalyzed direct dehydrogenation of carbonyl compounds with O₂ as the oxidant represents an appealing atom-economical alternative to these methods.^{9,10} Here, we report the discovery of a new Pd(TFA)₂/4,5-diazafluorenone (TFA = trifluoroacetate) catalyst system that overcomes key limitations of previously reported catalysts for these reactions. Comparison between this catalyst system and other catalysts, as well as preliminary mechanistic insights into these reactions are described below.



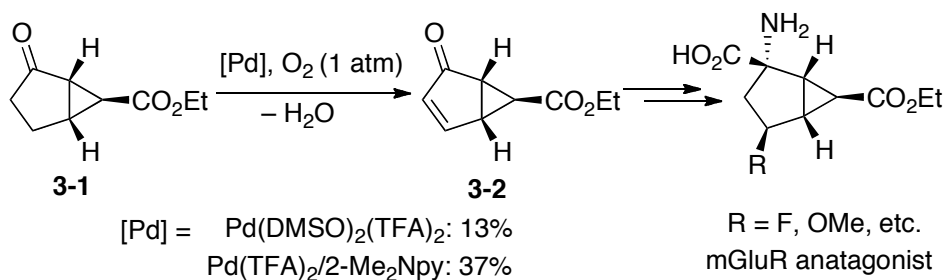
Early studies of Pd-catalyzed dehydrogenation reactions focused on cyclohexanone derivatives;¹¹ however, low yields and/or limited substrate scope restricted the synthetic utility of these methods. We recently reported a Pd(DMSO)₂(TFA)₂ catalyst system that overcomes many of these limitations and enables aerobic dehydrogenation of a variety of substituted cyclohexanones and other cyclic ketones, including heterocycles (Scheme 3-1).¹² Independently, we discovered a different Pd^{II} catalyst system, Pd(TFA)₂/2-Me₂Npy (2-Me₂Npy = 2-(N,N-

dimethylamino)pyridine), that affords substituted phenols via aerobic dehydrogenation of cyclohexanone and cyclohexenone derivatives (Scheme 3-1).¹³ Subsequent efforts in our lab to apply these methods to specific target molecules of interest have revealed limitations. In particular, the bicyclic cyclopentanone derivative **3-2** is a key precursor to a pharmaceutically important antagonist of the metabotropic glutamate receptor (mGluR) (Scheme 3-2).¹⁴ This molecule was previously prepared from **1** using IBX as the oxidant.^{14b} An aerobic dehydrogenation method could provide a scalable route to this molecule,¹⁵ but efforts to apply the Pd(DMSO)₂(TFA)₂ and Pd(TFA)₂/2-Me₂Npy catalyst systems to this reaction resulted in unsatisfactory yields ($\leq 37\%$, Scheme 3-2). Dehydrogenation of acyclic aldehydes and ketones have less precedent than reactions of cyclic ketones. 3-Arylpropanal (i.e., hydrocinnamaldehyde) derivatives were recently shown to undergo Pd(OAc)₂-catalyzed aerobic dehydrogenation in the presence of an amine cocatalyst, possibly via *in situ* formation of an enamine intermediate (Scheme 3-3).¹⁶ Analogous ketones (e.g., R = Me) were unreactive, however.

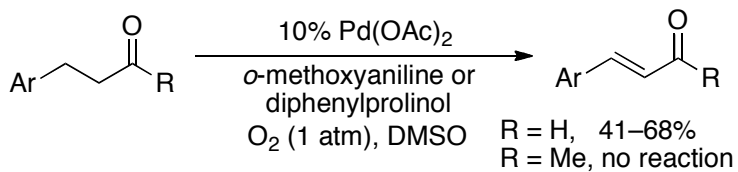
Scheme 3-1. Palladium-catalyzed Dehydrogenation of Cyclohexanones



Scheme 3-2. Attempted Dehydrogenation of a Pharmaceutically Important Cyclopentanone derivative



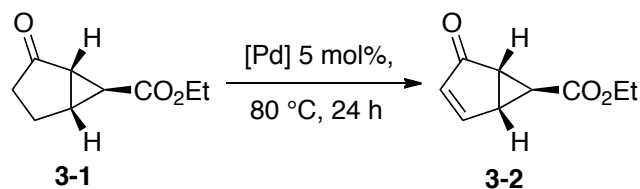
Scheme 3-3. Dehydrogenation of β-Aryl Carbonyl Compounds



3.2 Results and Discussions

3.2.1 Optimization of Catalyst and Reaction Conditions for Aerobic α,β -Oxidation of Cyclopentanone 3-1

Efforts to address these limitations were initiated by exploring possible Pd catalysts for aerobic dehydrogenation of cyclopentanone **3-1** at 80 °C under 1 atm of O₂. As noted above, the previously reported Pd(DMSO)₂(TFA)₂ catalyst exhibited poor reactivity (Table 3-1, entry 1). Use of the Pd(TFA)₂/2-Me₂Npy catalyst system in DMSO or Pd(TFA)₂ in the absence of an added ligand led to a slightly improved result (37% and 32% yield, respectively; entries 2 and 3). Other Pd^{II} sources were less effective than Pd(TFA)₂ (entries 4-7), and no reactivity was observed with traditional heterogeneous Pd catalysts (entries 8 and 9). A number of ancillary ligands were tested in combination with Pd(TFA)₂ (entries 10-19). In general, the ancillary ligands had little benefit or were deleterious relative to the reactivity of Pd(TFA)₂ alone. The best yield was observed with 4,5-diazafluorenone as a ligand; however, the yield maximized at 40% when the reaction was performed under 1 atm O₂ (entry 20). We reasoned that catalyst stability and turnover numbers could be improved by increasing the pressure of O₂ (used as a mixture of 9% O₂ in N₂ to minimize safety risks). Upon testing this hypothesis, a 61% yield of cyclopentenone product **2** was obtained with the Pd(TFA)₂/2-Me₂Npy catalyst system when the reaction was carried out under 7.2 atm O₂ (entry 21). The optimal yield, however, was achieved with the 4,5-diazafluorenone ligand (85% GC, 79% isolated yield; entry 22). The beneficial effect of diazafluorenone in this reaction complements our recent discovery of the utility of this ligand in other Pd-catalyzed aerobic oxidation reactions (allylic C–H oxidation and direct biaryl coupling).¹⁷

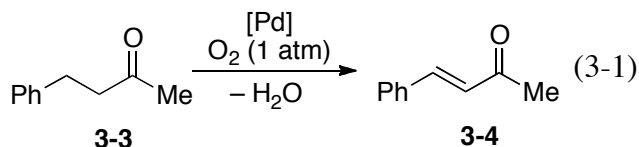
Table 3-1. Catalyst Optimization for the Aerobic Dehydrogenation of **3-1**^a

entry	Pd source	ligand	solvent	yield (%) ^b
1	Pd(TFA) ₂	DMSO	HOAc	13
2	Pd(TFA) ₂	2-Me ₂ Npy/TsOH	DMSO	37
3	Pd(TFA) ₂	none	DMSO	32
4	Pd(OAc) ₂	none	DMSO	21
5	Pd(BF ₄) ₂ (CH ₃ CN) ₄	none	DMSO	21
6	PdCl ₂	none	DMSO	6
7	Pd ₂ (dba) ₃	none	DMSO	8
8	Pd/C	none	DMSO	0
9	Pd(OH) ₂ /charcoal	none	DMSO	0
10	Pd(TFA) ₂	pyridine	DMSO	27
11	Pd(TFA) ₂	2-F pyridine	DMSO	31
12	Pd(TFA) ₂	2-MeO-pyridine	DMSO	32
13	Pd(TFA) ₂	3-NO ₂ -pyridine	DMSO	21
14	Pd(TFA) ₂	2,2'-bipyridine (bpy)	DMSO	33
15	Pd(TFA) ₂	6,6'-Me ₂ bpy	DMSO	15
16	Pd(TFA) ₂	5,5'-Me ₂ bpy	DMSO	12
17	Pd(TFA) ₂	phenanthroline	DMSO	36
18	Pd(TFA) ₂	2,9-Me ₂ phenanthroline	DMSO	14
19	Pd(TFA) ₂	bipyrimidine	DMSO	19
20	Pd(TFA) ₂	4,5-diazafluorenone	DMSO	40
21	Pd(TFA) ₂	2-Me ₂ Npy/TsOH	DMSO	61 ^c
22	Pd(TFA) ₂	4,5-diazafluorenone	DMSO	85 ^c [79] ^d

^a Conditions: [**3-1**] = 0.2 M (16.8 mg, 0.1 mmol), 5% catalyst (0.005 mmol), solvent (0.5 mL), 1 atm O₂, 80 °C, 24 h. ^b Determined by GC. ^c 7.2 atm O₂ (9% in N₂), 48 h. ^d Isolated yield.

3.2.2 Applications of the Pd(TFA)₂/4,5-Diazafluorenone Catalyst in the Dehydrogenation of Carbonyl Molecules

The success of Pd(TFA)₂/4,5-diazafluorenone in the dehydrogenation of **3-1** prompted us to explore the utility of this catalyst system in reactions of acyclic ketones. As noted above, previously reported catalyst systems were essentially unreactive in the dehydrogenation of benzylacetone (**3-3**, Eqn. (3-1)): 0% yield of **4** with Pd(OAc)₂/diphenylprolinol^{16a} and 4% yield with Pd(DMSO)₂(TFA)₂.¹² The poor reactivity of ketone **3** relative to hydrocinnamaldehyde (*cf.* Scheme 3-3) probably reflects the higher p*K*_a of the α-C–H bond of ketones relative to aldehydes (see further discussion below).¹⁸ In contrast, use of the optimized Pd(TFA)₂/diazafluorenone catalyst system to the dehydrogenation of **3** afforded enone **4** in 87% isolated yield (eqn (3-1)). With this substrate, the reaction was compatible with 1 atm O₂. To the best of our knowledge, this reaction represents the first example of aerobic dehydrogenation of acyclic ketones.



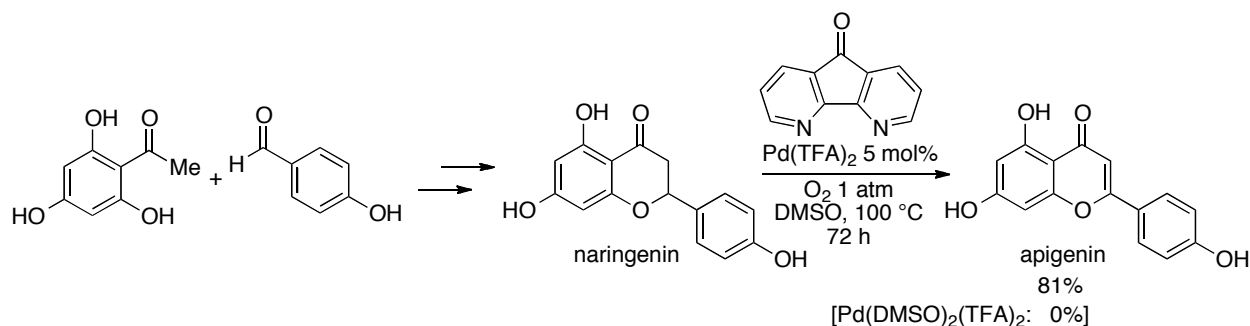
[Pd] = 10% Pd(OAc) ₂ /20% diphenylprolinol	0%
5% Pd(DMSO) ₂ (TFA) ₂	4%
5% Pd(TFA) ₂ /diazafluorenone	87%

(see Table 3-2 for reaction conditions)

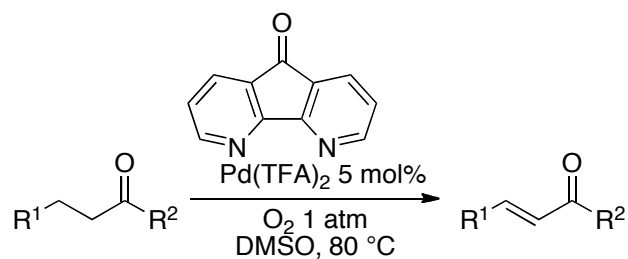
Apigenin is a flavone natural product that has attracted considerable interest as a cancer chemopreventative agent.¹⁹ The saturated precursor, naringenin, and related analogs can be readily obtained via condensation of simple benzaldehyde and *o*-acetylphenol precursors (Scheme 3-4).²⁰ An apigenin analog was recently prepared in 66% yield by DDQ-promoted dehydrogenation of the corresponding naringenin derivative.²¹ The Pd(DMSO)₂(TFA)₂ catalyst

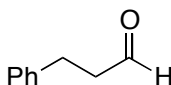
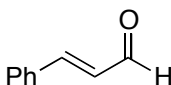
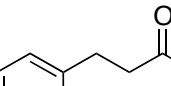
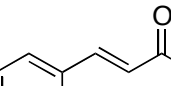
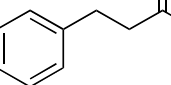
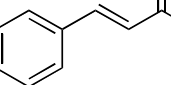
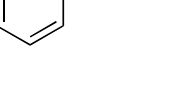
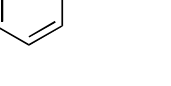
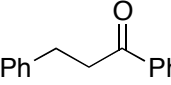
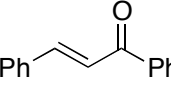
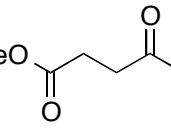
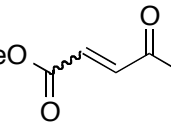
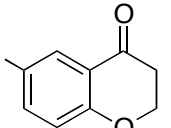
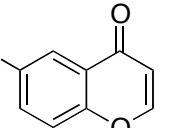
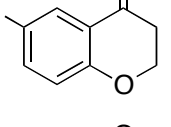
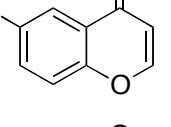
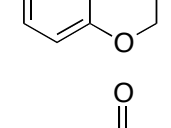
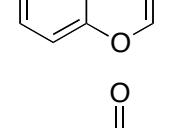
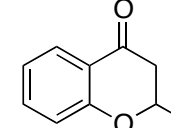
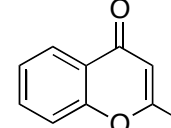
system was completely unreactive in an attempted dehydrogenation of naringenin, whereas the Pd(TFA)₂/4,5-diazafluorenone catalyst afforded the desired product in 81% yield (Scheme 3-4).

Scheme 3-4. Aerobic Dehydrogenation of Naringenin with the Pd(TFA)₂/4,5-Diazafluorenone Catalyst System



A number of related acyclic β -arylaldehyde and -ketone substrates and chroman-4-one and flavanone derivatives underwent successful aerobic dehydrogenation with this catalyst system (Table 3-2). Hydrocinnamaldehyde underwent facile dehydrogenation to afford cinnamaldehyde in 91% yield (entry 1). A small amount of benzaldehyde (8%) was formed as a by-product in this reaction. Other benzyl acetone derivatives, including those with electron-donating and electron-withdrawing substituents, and a phenyl ketone derivative underwent successful dehydrogenation (Table 3-2, entries 2-5). Dehydrogenation of methyl 3-benzoylpropanoate afforded the expected alkene in a 13:1 *trans:cis* isomeric ratio (entry 6). Chromones²² and flavones²³ have important biological activities, and the Pd(TFA)₂/4,5-diazafluorenone catalyst exhibits excellent reactivity in the dehydrogenative synthesis of these compounds (Table 3-2, entries 7-10), including chloro- and fluoro-substituted derivatives.

Table 3-2. Pd-Catalyzed Aerobic Dehydrogenation of Aldehydes and Ketones^a

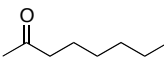
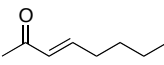
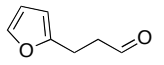
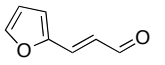
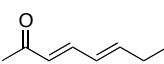
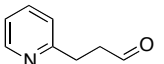
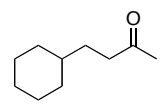
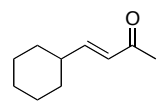
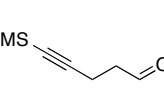
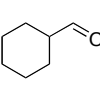
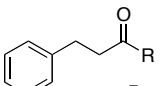
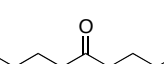
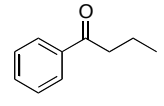
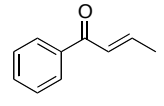
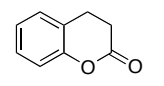
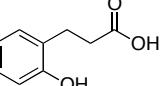
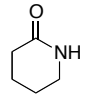
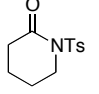
entry	substrate	time (h)	temp (°C)	enone	yield (%) ^b
1		8	80		91
2	 X = OMe	48	80		83
3	 = H	48	80		87
4	 = CF ₃	48	100		86
5		36	100		87
6		48	100	 <i>trans</i> : <i>cis</i> = 13 : 1	74
7	 X = H	32	80		96
8	 = Cl	32	80		94
9	 = F	32	80		94
10		24	100	 Flavone	88

^a Conditions: [substrate] = 0.8 M (0.4 mmol), Pd(TFA)₂ (6.6 mg, 0.02 mmol), 4,5-diazafluorenone (3.6 mg, 0.02 mmol), DMSO (0.5 mL), 1 atm O₂. ^b Isolated yield.

3.2.3 Limitations of the Pd(TFA)₂/4,5-Diazafluorenone Catalyst System

Preliminary efforts to expand the substrate scope beyond that indicated above have revealed some limitations. Acyclic substrates lacking an aryl group in the β position to the carbonyl are susceptible to further dehydrogenation at the γ,δ -position, resulting in a mixture of enone and dienone products. For example, an unoptimized reaction of 2-octanone afforded oct-3-en-2-one in 17% yield and octa-3,5-dien-2-one in 6% yield after 18 h, with 35% recovered starting material (Table 3-3, entry 1). 4-Cyclohexylbutan-2-one is sterically similar to benzylacetone and undergoes dehydrogenation to afford 4-cyclohexylbutenone (entry 2). However, 4-cyclohexylbutenone readily undergoes decomposition under oxidative conditions to form the cyclohexanecarboxaldehyde. 5-Nonanone exhibits no dehydrogenation reactivity, which may be due to steric hindrance (entry 3). The reaction of propyl phenyl ketone, which cannot undergo a second dehydrogenation step, afforded the enone in only low yield (20%) after 48 h (entry 4). The low substrate conversion in this reaction possibly reflects deactivation of the catalyst by formation of an inactive Pd- π -allyl species. Alternatively, the Pd catalyst could form inactive metallocycles via directed aryl C-H activation. Decompositions are observed in molecules containing heterocycles under the oxidative conditions (entries 5-7). Finally, esters such as ethyl hydrocinnamate were unreactive under the optimized conditions and increasing the reaction temperature to 100 °C failed to promote reactivity (entries 8-11). This lack of reaction probably reflects the reduced acidity of the α -C-H bond of esters relative to ketones and aldehydes.¹⁸ Lactones that have a more acidic α -C-H, however, undergo hydrolysis, which is likely to be catalyzed by Pd^{II} as a Lewis acid.

Table 3-3. Unsuccessful Substrates for Pd(TFA)₂/4,5-Diazafluorenone-Catalyzed Aerobic Dehydrogenation Reactions^a

Entry	Substrate	Major Product	Yield (%) ^b	Entry	Substrate	Major Product	Yield (%) ^b
1			17	5			33
			6	6		substrate decomposition	
2			8	7		substrate decomposition	
			10	8		no reaction	
3		no reaction			R = $\begin{matrix} \text{OH} \\ \text{SPh} \\ \text{OEt} \end{matrix}$		
4			20	9			75
				10		no reaction	
				11		no reaction	

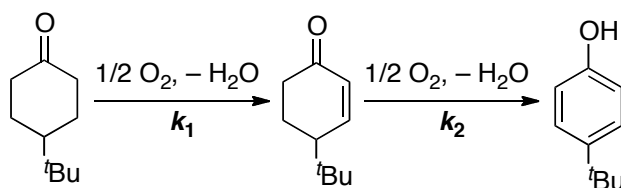
^a Reactions conditions: [substrate] = 0.8 M (0.4 mmol), [Pd(TFA)₂] = 0.04 M (0.005 mmol = 5 mol%), [4,5-diazafluorenone] = 0.01 M (0.02 mmol), solvent = DMSO (0.5 ml), 1 atm O₂.^b determined by GC or ¹H NMR spectroscopy.

3.2.4 Mechanistic Investigation of Pd(TFA)₂/4,5-diazafluorenone catalyzed Dehydrogenation Reaction

Future efforts to expand the scope of these reactions will benefit from mechanistic insights, and a thorough study of the different aerobic dehydrogenation catalysts has been initiated. A few preliminary results are worth noting. The Pd(TFA)₂/4,5-diazafluorenone catalyst was evaluated

in the dehydrogenation of 4-*tert*-butylcyclohexanone (Table 3-4) in order to compare its reactivity with the recently reported Pd(DMSO)₂(TFA)₂¹² and Pd(TFA)₂/2-Me₂Npy catalyst systems.¹³ Analysis of the reaction time courses for each of these reactions shows that the Pd(TFA)₂/4,5-diazafluorenone catalyst behaves similarly to the Pd(TFA)₂/2-Me₂Npy catalyst.²⁴ Both of these catalysts show a preference for formation of the phenol product, owing to faster dehydrogenation of the cyclohexenone to the phenol relative to the initial dehydrogenation step to afford the enone. In contrast, the first dehydrogenation step (k_1) is much faster than the second (k_2) when Pd(DMSO)₂(TFA)₂ is used as the catalyst, resulting in high selectivity for the enone product. The basis for these reactivity differences remains to be elucidated, but the results are consistent with the observation of single and double dehydrogenation products in the reaction of 2-octanone with the Pd(TFA)₂/4,5-diazafluorenone catalyst system.

Table 3-4. Comparison of Pd Catalysts in the Oxidation of 4-*tert*-Butylcyclohexanone^a



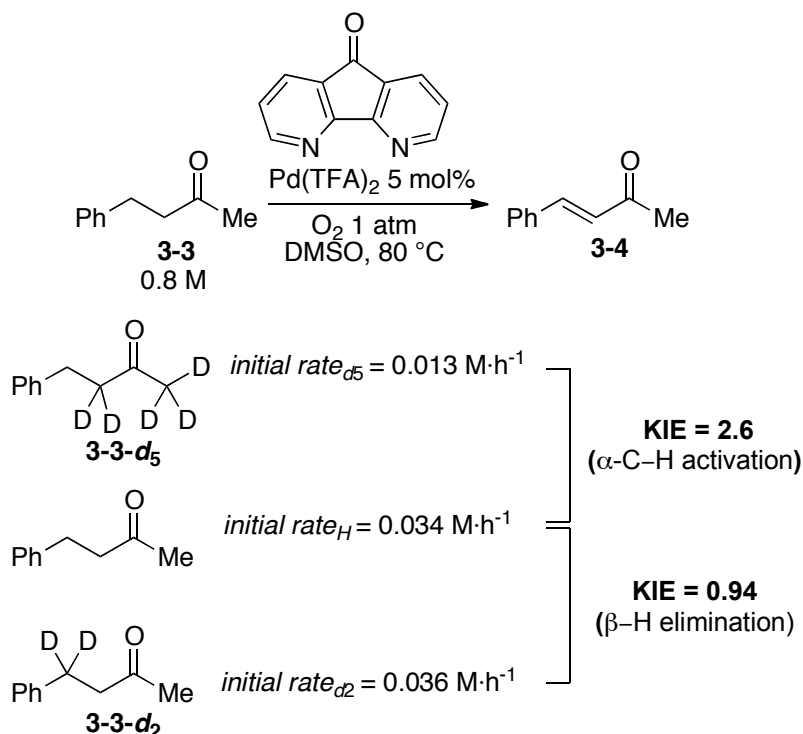
Catalyst	k_1 (h ⁻¹)	k_2 (h ⁻¹)	k_1/k_2
Pd(TFA) ₂ /2-Me ₂ Npy/TsOH	0.086	0.14	0.61
Pd(DMSO) ₂ (TFA) ₂	0.19	0.0057	33
Pd(TFA) ₂ /4,5-diazafluorenone	0.036	0.099	0.36

^a Conditions: [substrate] = 0.2 M (15.4 mg, 0.1 mmol), [catalyst] = 0.05 M (0.005 mmol), solvent (0.5 mL), 1 atm O₂, 80 °C.

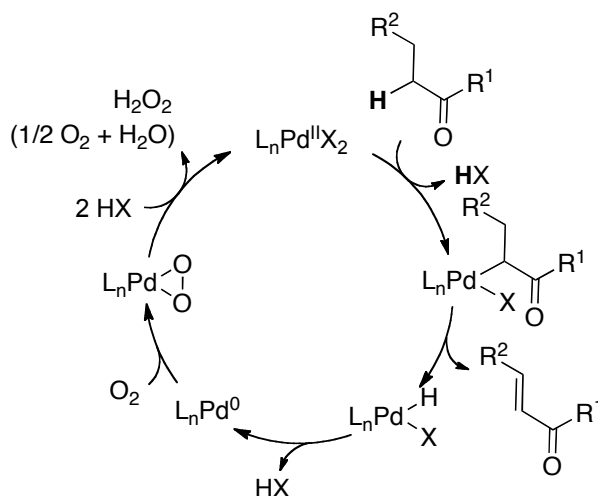
Deuterium kinetic isotope effects in the reaction of benzylacetone were evaluated by comparing the reaction rate of the parent substrate **3-3** with those of the α - and β -deuterated

derivatives **3-3-*d*₅** and **3-3-*d*₂** (Scheme 3-5).²⁵ A primary kinetic isotope effect ($k_H/k_D = 2.6$) was observed with the α -deuterated substrate, whereas a negligible isotope effect was observed from deuteration of the β position. This observation suggests that cleavage of the α -C–H bond is the turnover-limiting step of the catalytic reaction while β -hydride elimination from a presumed Pd-enolate intermediate is comparatively fast. These results are consistent with the correlation between the acidity of the α -C–H bond of the substrate and catalytic reactivity: aldehydes > ketones >> esters. A proposed catalytic cycle is shown in Scheme 6. The reaction is initiated by turnover-limiting "activation" (i.e., deprotonation) of the α -C–H bond. Subsequent fast β -hydride elimination from a Pd^{II}-enolate intermediate affords the enone product and a Pd^{II}-hydride intermediate.²⁶ The latter species can be oxidized by O₂ to regenerate the Pd^{II} catalyst (Scheme 3-6).²⁷

Scheme 3-5. Deuterium Kinetic Isotope Effects Based on Independent Initial-rate Measurements



Scheme 3-6. Proposed Catalytic Cycle for Pd-catalyzed α,β -Dehydrogenation of Carbonyl Compounds



3.2.5 Conclusion

In summary, we have identified a new catalyst, Pd(TFA)₂/4,5-diazafluorenone, that significantly expands the utility of direct aerobic dehydrogenation of carbonyl compounds. Noteworthy results include the first demonstration of aerobic dehydrogenation of acyclic ketones and the application of this catalyst to pharmaceutically important target molecules that were unreactive with previously reported catalysts.

3.3 Experimental

3.3.1 General Considerations

All commercially available compounds were used as received. Substrates that were not commercially available were prepared according to literature procedures: 4-(4-methoxyphenyl)-2-butanone (Table 3-2, entry 2) and 4-[4-(trifluoromethyl)phenyl]-2-butanone (Table 3-2, entry

4),²⁸ 1,3-diphenyl-propan-1-one (Table 3-2, entry 5),²⁹ and 4-methyl 3-benzoylpropionate (Table 3-2, entry 6).³⁰ The bicyclo[3.1.0]hexane-2-one-6-carboxylic acid ethyl ester **3-1** was donated by Eli Lilly.

¹H and ¹³C NMR spectra were recorded on a Bruker AC-300 MHz or a Varian Mercury-300 MHz spectrometer. The chemical shifts (δ) are given in parts per million and referenced to residual solvent peaks or a TMS internal standard. Gas chromatography was performed on a Shimadzu GC-17A using a Stabilwax®-DB column (15 m) and referenced to an internal standard (nitrobenzene). Flash column chromatography was performed on an Isco Combiflash system using silica gel 60 (Silicycle) and eluted with ethyl acetate/hexane.

The combination of organic solvents and O₂ creates the risk of an explosion. To minimize risks, all reactions carried out at pressures above 1 atm utilized a dilute oxygen gas mixture (9% O₂ in N₂) to ensure that the O₂ content remains below the lower explosive limit of O₂/organic mixtures.³¹ All reactions should be performed with care and carried out behind a blast shield.

3.3.2 General Procedure for Catalyst Optimization

Catalytic aerobic oxidation reactions were performed using a custom reaction apparatus that enabled several reactions to be performed simultaneously under a constant pressure of O₂ (approximately 1 atm) with controlled temperature and orbital agitation (Table 3-1). To a disposable 13 mm thick-walled culture tube was added **3-1** (0.1 mmol, 16.8 mg). The reaction tubes were placed in a 48-well parallel reactor mounted on a Glas-Col large capacity mixer. The headspace was purged with O₂ for 10 min, after which a stock solution of Pd(TFA)₂, (1.65 mg, 0.005 mmol, 0.05 equiv) and diazafluorenone (0.9 mg, 0.01 mmol, 0.1 equiv) in DMSO (0.5 mL) was injected via syringe. The solution was agitated vigorously at 80 °C for 24 h. After 24 h, the

reaction vessel was cooled to room temperature and vented. The solution was then diluted with CH_2Cl_2 and analyzed by GC.

3.3.3 Procedure for Dehydrogenation of 3-1 in a Parr Pressure Vessel and Product Isolation

The oxidation of **3-1** under 1 atm O_2 afforded 40% conversion due to catalyst decomposition. We speculated that the catalyst would be more stable with elevated pressures of O_2 , and the reaction was carried out in a Hastelloy Parr pressure vessel. A supply of dilute O_2 (9% in N_2) was used to avoid explosion hazard, and a typical protocol for this reaction format is as follows:

To a 2 ml GC vial with a stir bar was added **3-1** (33.6 mg, 0.2 mmol), followed by a solution of $\text{Pd}(\text{TFA})_2$ (3.3 mg, 0.01 mmol, 0.05 equiv) and 4,5-diazafluorenone (1.8 mg, 0.01 mmol, 0.05 equiv) in DMSO (0.5 mL). The vial was immediately placed in a 45 mL Hastelloy Parr pressure vessel, and sealed. 80 atm of 9% O_2 in N_2 (7.2 atm partial pressure of O_2) was introduced and the vessel was heated to 80 °C with vigorous stirring for 48 h. After 48 h, the vessel was vented. The solution was diluted with H_2O and extracted three times with CH_2Cl_2 . The CH_2Cl_2 solution was concentrated and loaded on silica gel and placed on Isco Combiflash column. The product was isolated with an eluent gradient of 10%-40% ethyl acetate in hexane, affording **3-2** in 79% as a white solid.

3.3.4 Procedure for Dehydrogenation of Benzylacetone 3-3

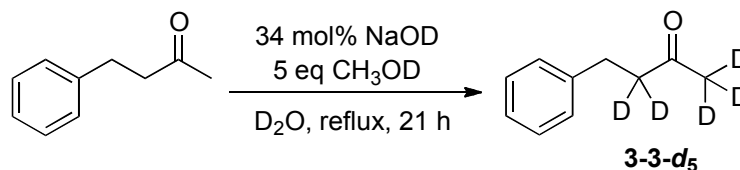
Good gas-liquid mixing is critical for these aerobic oxidation reactions. Analysis of different reaction formats showed that the best results are obtained with orbital agitation. Nevertheless, similar results can be obtained on bench using a standard cultured tube equipped with a balloon of O_2 and magnetic stir bar.

Dehydrogenation of 3-3 with orbital agitation. To a disposable 13 mm thick-walled culture tube were added Pd(TFA)₂ (6.6 mg, 0.02 mmol, 0.05 equiv), 4,5-diazafluorenone (3.6 mg, 0.02 mmol, 0.05 equiv), and DMSO (0.5 ml). The reaction tubes were placed in a 48-well parallel reactor mounted on a Glas-Col large capacity mixer. The headspace was purged with O₂ for 10 min, after which benzylacetone (60 µl, 0.4 mmol, 1 equiv) was added via syringe. The solution was agitated vigorously at 80 °C for 48 h. After 48 h, the reaction was cooled down, and O₂ was vented from the reactor. The reaction mixture was purified as described above. The 4-phenylbutenone product **3-4** was obtained in 87% yield as a colorless liquid. The by-product, benzaldehyde, was obtained as a colorless liquid in 8% yield.

Dehydrogenation of 3-3 in a cultured tube with magnetic stirring. To a cultured tube (VWR 89000-488) equipped with a stir bar was added Pd(TFA)₂ (6.6 mg, 0.02 mmol, 0.05 equiv), 4,5-diazafluorenone (3.6 mg, 0.02 mmol, 0.05 equiv), and DMSO (0.5 ml). The tube was sealed with a septum. A balloon was then attached via a long needle. The tube and balloon were purged and refilled with O₂ three times, submerging the needle in catalyst solution during purging to allow O₂ saturation via bubbling. After filling the balloon with O₂ a final time, the solution was stirred and benzylacetone **3-3** (60 µl, 0.4 mmol, 1 equiv) was injected via syringe. After reacting at 80 °C for 48 h, the mixture was cooled to room temperature, and an external standard (nitrobenzene, 10 µl, 0.097 mmol) was added. The mixture was diluted with CH₂Cl₂, and analyzed by GC to afford 79% GC yield.

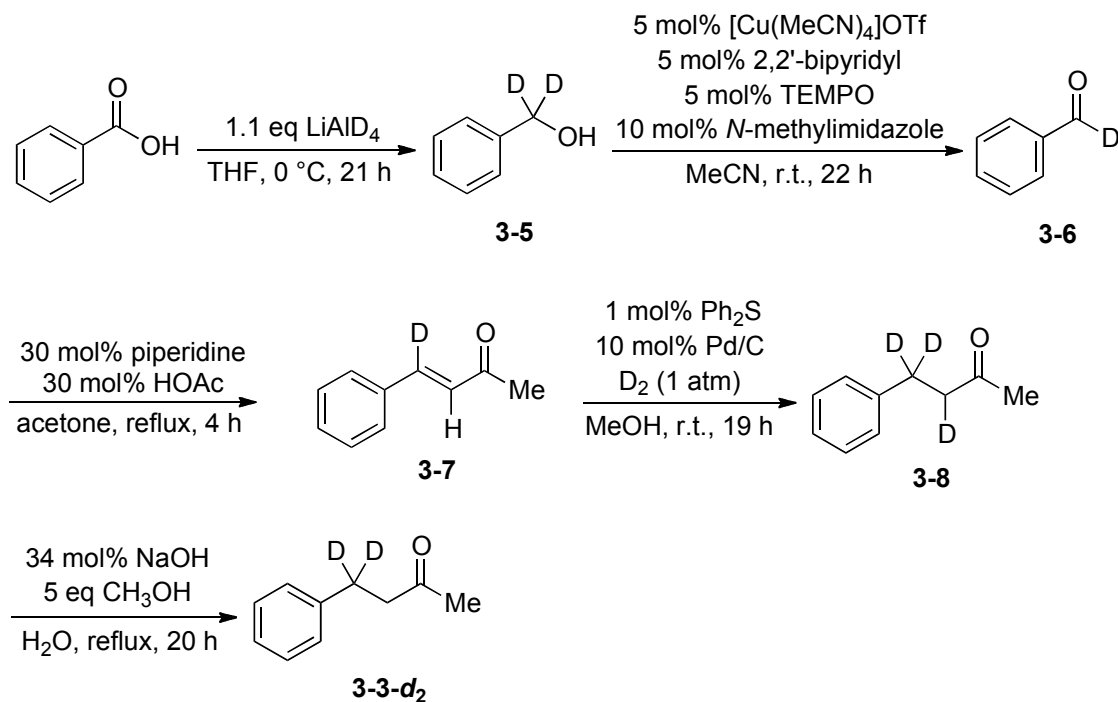
3.3.5 Synthesis of the Deuterated Substrates **3-3-*d*₅** and **3-3-*d*₂**

Synthesis of [1,1,1,3,3-*d*₅]-4-Phenyl-2-butanone (**3-3-*d*₅**)³²



An oven-dried 100 mL round bottom flask was equipped with a stir bar and condenser. After purging with N₂, the flask was charged with 8.5 mL D₂O, benzylacetone (1.48 g, 10.0 mmol), CH₃OD (1.72 g, 52.0 mmol, 5.2 equiv.), and a solution of 40% NaOD in D₂O (300 μL, 3.40 mmol, 0.34 equiv.) with stirring. The reaction mixture was stirred at reflux for 21 h and allowed to cool to room temperature before 8 mL diethyl ether was added via syringe. Following 1 h of stirring, the layers were separated and the aqueous layer was washed with ether (1 x 20 mL). The combined organic layers were washed with water (2 x 20 mL) and brine (1 x 20 mL), dried over Na₂SO₄, and concentrated by evaporation. The crude product was shown to be ca. 95 % deuterated material, and was distilled *in vacuo* to yield **3-*d*₅** (1.06 g, 70%) as a colorless oil. ¹H NMR data match previously reported data.³² ¹H NMR (CDCl₃): δ 7.31-7.17 (m, 5H), 2.88 (s, 2H).

Synthesis of [4,4-*d*₂]-4-Phenyl-2-butanone (**3-3-*d*₂**)



[1,1-*d*₂]-Benzyl alcohol (3-5). An oven-dried 250 mL round bottom flask was equipped with a stir bar. After purging with N₂, the flask was charged with LiAlD₄ (513 mg, 13.5 mmol, 1.1 equiv.) and 50 mL THF and stirred at 0 °C. A oven-dried 100 mL round bottom flask equipped with stir bar and septum was purged with N₂. A solution of benzoic acid (1.50 g, 12.3 mmol, 1 equiv) in 50 mL THF were added to the 100 mL flask and stirred at 0 °C. Above benzoic acid solution were added dropwise to the LiAlD₄ suspension at 0 °C using a cannula. The reaction mixture was slowly warmed to room temperature and allowed stirring for overnight. The mixture was diluted to 2 x its original volume with ethyl acetate and quenched by dropwise addition of water at 0 °C. The mixture was extracted with diethyl ether (3 x 50 mL), and the combined organic layers were washed with brine (2 x 50 mL), dried over Na₂SO₄, and concentrated by

evaporation. Distillation *in vacuo* yielded **3-5** (450 mg, 33%) as a colorless oil. ^1H NMR data match previously reported data.³³ ^1H NMR (CDCl_3): δ 7.37-7.25 (m, 5H), 1.73 (s, 1H).

[1-*d*]-Benzaldehyde (3-6).³⁴ A 100 mL round bottom flask equipped with a stir bar was charged with 20 mL acetonitrile and **S1** (380 mg, 3.44 mmol). A solution of $[\text{Cu}(\text{CH}_3\text{CN})_4]\text{OTf}$ (64 mg, 0.17 mmol, 0.05 equiv.) and 2,2'-bipyridine (27 mg, 0.17 mmol, 0.05 equiv.) in 4 mL acetonitrile, a solution of TEMPO (27 mg, 0.17 mmol, 0.05 equiv.) in 4 mL acetonitrile, and *N*-methylimidazole (27 μL , 0.34 mmol, 0.10 equiv.) were added with stirring. The solution was stirred at room temperature and consumption of starting material was monitored by TLC. Upon reaction completion, the reaction mixture was diluted to 2 x its original volume with a 1:1 ether:pentane solution, filtered through a plug of silica. Removal of solvent afforded **3-6** (330 mg, 90%) as a colorless oil. ^1H NMR data match previously reported data.³⁵ ^1H NMR (CDCl_3): δ 7.91-7.88 (m, 2H), 7.68-7.62 (m, 1H), 7.57-7.52 (m, 2H).

[4-*d*]-4-Phenyl-3-buten-2-one (3-7).³⁶ A 25 mL three-neck flask equipped with condenser and stir bar was purged with N_2 . An acetone (3 mL) solution of **3-6** (330 mg, 3.08 mmol) was added, followed by dropwise addition of piperidine (90 μL , 0.91 mmol, 0.30 equiv) and acetic acid (52 μL , 0.91 mmol, 0.30 equiv). The mixture was stirred under reflux for 4 h. The resulting mixture was diluted with EtOAc, quenched with saturated NaHCO_3 (1 x 10 mL), and washed with water (2 x 10 mL). The mixture was extracted with EtOAc (3 x 10 mL) and the combined organic layers were washed with brine (1 x 10 mL), dried over Na_2SO_4 and concentrated by evaporation. Purification by flash column chromatography (Hex:EtOAc, 0-15% EtOAc) yielded **3-7** (174 mg, 39%) as a colorless oil. ^1H NMR data match previously reported data.³⁷ ^1H NMR (CDCl_3) δ 7.56-7.53 (m, 2H), 7.41-7.38 (m, 3H), 6.71 (t, 1H, $J = 2.1$ Hz), 2.38 (s, 3H).

[3,4,4-*d*₃]-4-Phenyl-2-butanone (3-8).³⁸ A 50 mL round bottom flask equipped with stir bar and septum was charged with methanol (4 mL), **3-7** (174 mg, 1.19 mmol), diphenyl sulfide (2.2 mg, 0.012 mmol, 0.01 equiv.), and 5% Pd/C (20 wt % of the substrate). A balloon was purged three times with D₂, and introduced to the reaction via a needle. The reaction was allowed to stir at room temperature under D₂ (ca. 1 atm) for 19 h. Filtration through a plug of celite and concentration by evaporation afforded **3-8** (171 mg, 96%) as a colorless oil. ¹H NMR (CDCl₃): δ 7.31-7.26 (m, 2H), 7.22-7.16 (m, 3H), 2.75 (s, 1H), 2.14 (s, 3H).

[4,4-*d*₂]-4-Phenyl-2-butanone (3-3-*d*₂).³² A 50 mL round bottom flask equipped with a stir bar and condenser was charged **3-8** (171 mg, 1.13 mmol), 1 mL H₂O, CH₃OH (223 μL, 5.66 mmol, 5.0 equiv.), and a solution of NaOH (15.0 mg, 0.38 mmol, 0.34 equiv.) in 1 mL H₂O with stirring. The reaction mixture was stirred at reflux for 20 h and allowed to cool to room temperature. 2 mL diethyl ether was added via syringe. After stirring for 30 min, the solution was quenched with 0.1 M HCl. The aqueous layer was washed with ether (2 x 10 mL). The combined organic layers were washed with brine (1 x 10 mL), and dried over MgSO₄. Purification by flash column chromatography (Hex:EtOAc, 0-15% EtOAc) yielded **3-3-*d*₂** (53 mg, 31%) as a colorless oil. ¹H NMR (CDCl₃): δ 7.32-7.13 (m, 5H), 2.74 (s, 2H), 2.13 (s, 3H). ²H NMR (CHCl₃): δ 2.88 (s, 2D). ¹³C NMR (CDCl₃): δ 208.15, 141.12, 128.70, 128.48, 126.32, 45.24, 30.28. HRMS (ESI) [M + Na⁺]/z calcd. 150.1009, found 150.1010.

3.3.6 Reaction Profiles and Kinetic Fittings of Oxidizing 4-*tert*-Butylcyclohexanone with Different Catalysts^a

Oxidation of 4-*tert*-butylcyclohexanone was performed with three catalyst systems: Pd(TFA)₂/2-Me₂Npy/TsOH, Pd(DMSO)₂(TFA)₂ and Pd(TFA)₂/4,5-diazafluorenone. The timecourses were monitored by GC and fitted into an A→B→C kinetic model by Copasi® (Figure 3-1).

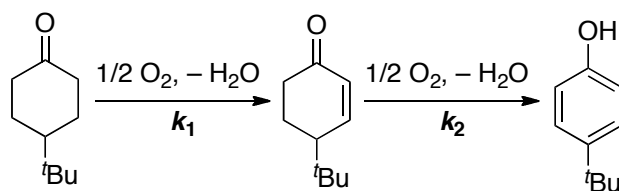
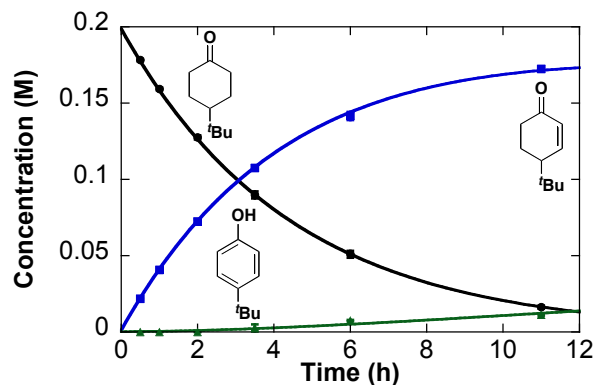
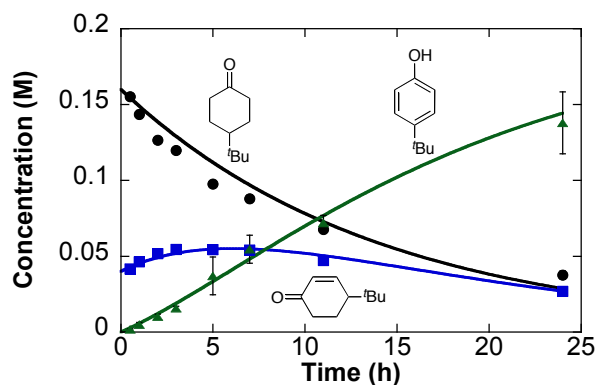
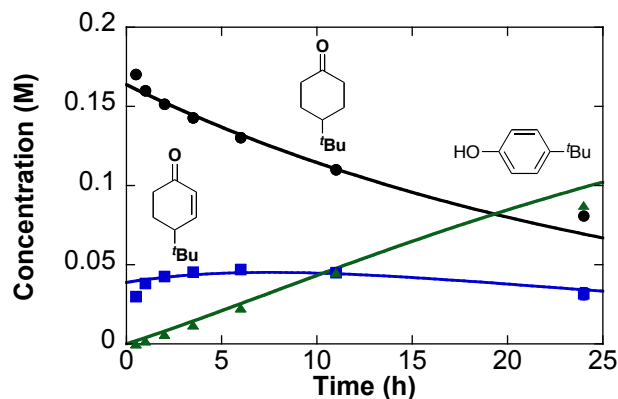
(A) Pd(TFA)₂/2-Me₂Npy/TsOH(B) Pd(DMSO)₂(TFA)₂(C) Pd(TFA)₂/4,5-diazafluorenone

Figure 3-1. Timecourses and fittings of Pd-catalyzed aerobic dehydrogenation of 4-*tert*-butylcyclohexanone. (A) Reactions catalyzed by the Pd(TFA)₂/2-Me₂Npy/TsOH system; (B) reactions catalyzed by the Pd(DMSO)₂(TFA)₂ catalyst system; (C) reactions catalyzed by the Pd(TFA)₂/4,5-diazafluorenone catalyst system. Conditions: [substrate] = 0.2 M (15.4 mg, 0.1 mmol), [catalyst] = 0.05 M (0.005 mmol), solvent (0.5 mL), 1 atm O₂, 80 °C.

3.3.7 Investigation of Kinetic Isotope Effects

Reactions were performed using orbital shakers under standard conditions, as described above. The catalyst was heated to 80 °C and the temperature was allowed to equilibrate for 5 min. Nitrobenzene (10 μ L) was injected via syringe as internal standard. Injection of substrates dissolved in solvent established the $t = 0$ point. At various time intervals, aliquots were withdrawn from the reaction mixture via pipet, diluted with CH_2Cl_2 and analyzed by GC. Accordingly, initial rates were determined as the slope of [3-4] vs. time at 10% conversion (Figure 3-2).

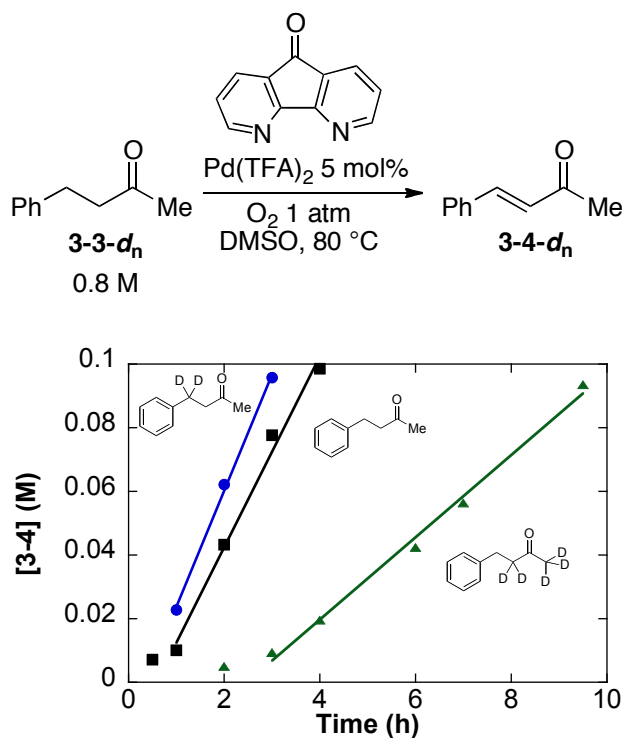
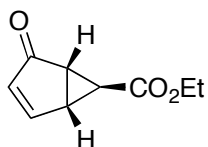


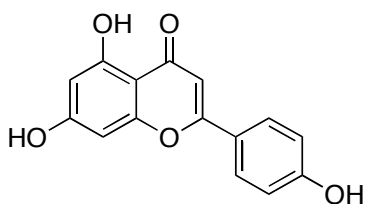
Figure 3-2. Initial rates of dehydrogenation of proteo- and deuterated benzylacetone. Conditions: [3-3] = 0.8 M (30 μ L, 0.2 mmol), [Pd(TFA)₂] = 0.04 M (0.01 mmol), [4,5-diazafluorenone] = 0.04 M (0.01 mmol), DMSO = 0.25 mL, 1 atm O₂, 80 °C.

3.3.8 ^1H NMR Spectroscopic Data

All compounds in Table 3-1, Scheme 3-4 and eqn 3-1 have been reported previously. In all cases, the product identities were established by comparison of the ^1H NMR spectra with previously reported data. In one case (scheme 3-5, **3-3- d_2**), full characterization was not previously reported; these data are included below.

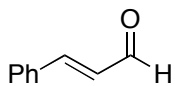


(**3-2**, Table 3-1, entry 22): Prepared as described above. Purified by silica gel column chromatography using a gradient of 10%-40% EtOAc in hexane elution to give 79% yield of the product as a white solid. ^1H NMR matches previously reported data.³⁹ ^1H NMR (CDCl_3): δ 7.61 (ddd, 1H, $J=5.6, 2.6, 0.7$ Hz), 5.74 (d, 1H, $J=5.6$ Hz), 4.15 (q, 2H, $J=7.2$ Hz), 2.85 (dt, 1H, $J=4.7, 2.6$ Hz), 2.47 (ddd, 1H, $J=4.7, 2.6, 0.7$ Hz), 2.26 (t, 1H, $J=2.6$ Hz), 1.27 (t, 3H, $J=7.2$ Hz).

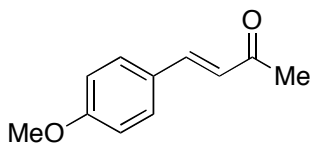


(apigenin, Scheme 3-4): Prepared as described above. The reaction mixture was washed with water and extracted with ethyl acetate. The mixture was purified by silica gel column chromatography using a gradient 30-70% EtOAc in hexane elution to give 81% yield of the product as a yellow solid. ^1H NMR matches previously reported data.⁴⁰ ^1H NMR ($\text{DMSO-}d_6$): δ

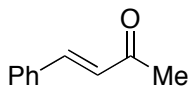
12.96 (s, 1H), 10.81 (br, 1H), 10.36 (br, 1H), 7.93 (d, 2H, J = 8.9 Hz), 6.92 (d, 2H, J = 8.9 Hz), 6.78 (s, 1H), 6.48 (d, 1H, J = 2.2), 6.19 (d, 1H, J = 2.2).



(Table 3-2, entry 1): Prepared as described with orbital agitation. Purified by silica gel column chromatography using a 10% EtOAc in hexane elution to give 91% yield of the product as a colorless solid. ¹H NMR matches previously reported data.⁴¹ ¹H NMR (CDCl₃): δ 9.71 (d, 1H, J = 7.6 Hz), 7.62-7.49 (m, 2H), 7.48 (d, 1H, J = 15.8 Hz), 7.46-7.41 (m, 3H), 6.72 (dd, 1H, J = 15.8, 7.6 Hz).

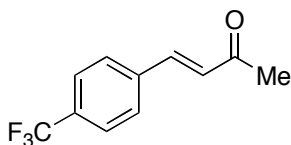


(Table 3-2, entry 2): Prepared as described above. Purified by silica gel column chromatography using a gradient 10%-20% EtOAc in hexane elution to give 83% yield of the product as a white solid. ¹H NMR matches previously reported data.⁴³ ¹H NMR (CDCl₃): δ 7.50 (d, 2H, J = 8.9 Hz), 7.48 (d, 1H, J = 16.5 Hz), 6.92 (d, 2H, J = 8.9 Hz), 6.61 (d, 1H, J = 16.5 Hz), 3.85 (s, 3H), 2.36 (s, 3H).

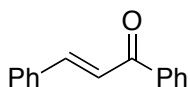


(Table 3-2, entry 3): Prepared as described above. Purified by silica gel column chromatography using a gradient 0%-15% EtOAc in hexane elution to give 87% yield of the

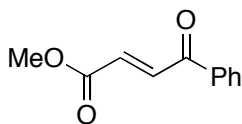
product as a colorless liquid. ^1H NMR matches previously reported data.⁴² ^1H NMR (CDCl_3): δ 7.60-7.49 (m, 3H), 7.46-7.37 (m, 3H), 6.72 (1H, d, $J = 16.2$ Hz), 2.39 (s, 3H).



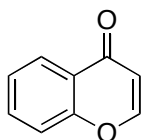
(Table 3-2, entry 4): Prepared as described above. Purified by silica gel column chromatography using a gradient 0%-20% EtOAc in hexane elution to give 86% yield of the product as a colorless oil. ^1H NMR matches previously reported data.⁴³ ^1H NMR (CDCl_3): δ 7.66 (s, 4H), 7.53 (d, 1H, $J = 16.1$ Hz), 6.78 (d, 1 H, $J = 16.1$ Hz), 2.42 (s, 3H).



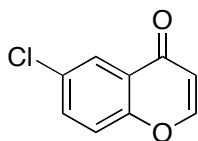
(Table 3-2, entry 5): Prepared as described above. Purified by silica gel column chromatography using a 20% EtOAc in hexane elution to give 87% yield of the product as a white solid. ^1H NMR matches previously reported data.⁴⁴ ^1H NMR (CDCl_3): δ 8.07-7.99 (m, 2H), 7.70-7.62 (m, 2H), 7.61-7.48 (m, 3H), 7.82 (d, 1H, $J = 15.8$ Hz), 7.54 (d, 1 H, $J = 15.8$ Hz), 7.46-7.39, (m, 3 H).



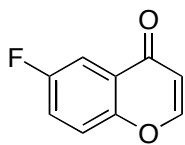
(Table 3-2, entry 6): Prepared as described above. Purified by silica gel column chromatography using a gradient 0%-15% EtOAc in hexane elution to give 74% yield of the product as a colorless liquid. ^1H NMR matches previously reported data.⁴⁵ ^1H NMR (CDCl_3): δ 8.03-7.80 (m, 2H), 7.94 (d, 1H, $J = 15.5$ Hz), 7.67-7.60 (m, 1H), 7.56-7.48 (2H, m), 6.90 (d, 1H, $J = 15.5$ Hz), 3.86 (s, 3H).



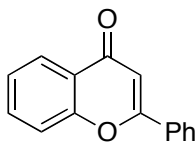
(Table 3-2, entry 7): Prepared as described above. Purified by silica gel column chromatography using a 20-40% EtOAc in hexane gradient elution to give 96% yield of the product as a white solid. ^1H NMR data match previously reported data.⁴⁶ ^1H NMR (CDCl_3): δ 8.22 (dd, 1H, $J = 8.0, 1.4$ Hz), 7.87 (d, 1H, $J = 6.1$ Hz), 7.68 (ddd, 1H, $J = 8.6, 8.0, 1.4$ Hz), 7.47 (d, 1H, $J = 8.6$ Hz), 7.42 (t, 1H, $J = 8.0$ Hz), 6.36 (d, 1H, $J = 6.1$ Hz).



(Table 3-2, entry 8): Prepared as described above. Purified by silica gel column chromatography using a 20-40% EtOAc in hexane gradient elution to give 94% yield of the product as a white solid. ^1H NMR data match previously reported data.⁴⁷ ^1H NMR (CDCl_3): δ 8.18 (d, 1H, $J = 2.6$ Hz), 7.86 (d, 1H, $J = 6.2$ Hz), 7.62 (dd, 1H, $J = 8.9, 2.6$ Hz), 7.43 (d, 1H, $J = 8.9$ Hz), 6.36 (d, 1H, $J = 6.2$ Hz).



(Table 3-2, entry 9): Prepared as described above. Purified by silica gel column chromatography using a 30% EtOAc in hexane gradient elution to give 94% yield of the product as a white solid. ^1H NMR data match previously reported data.⁴⁸ ^1H NMR (CDCl_3): δ 7.87 (d, 1H, $J = 6.0$ Hz), 7.85 (dd, 1H, $J = 8.2, 3.2$ Hz), 7.48 (dd, 1H, $J = 9.0, 4.4$ Hz), 7.40 (ddd, 1H, $J = 9.0, 7.5, 3.2$ Hz), 6.34 (d, 1H, $J = 6.0$ Hz).



(Table 3-2, entry 10): Prepared as described above. The reaction mixture was washed with water and extracted with ethyl acetate. The mixture was purified by silica gel column chromatography using a gradient 0%-30% EtOAc in hexane elution to give 88% yield of the product as a white solid. ^1H NMR matches previously reported data.⁴⁹ ^1H NMR (CDCl_3): δ 8.25 (dd, 1H, $J = 8.0, 1.6$ Hz), 7.99-7.89 (m, 2H), 7.72 (ddd, 1H, $J = 8.6, 7.1, 1.6$ Hz), 7.59 (dd, 1H, $J = 8.6, 1.0$ Hz), 7.57-7.49 (m, 3H), 7.44 (ddd, 1H, $J = 8.0, 7.1, 1.0$), 6.88 (s, 1H).

3.4 Contributions

Synthesis of deuterated compounds for the study of kinetic isotope effects, **3-3- d_2** and **3-3- d_5** , were performed by Tyler J. Wadzinski. T. J. Wadzinski also assisted in the synthesis of several

substrates, including the ketones in Table 3-2, entries 2, 4, 5 and 6, and Table 3-3, entries 5, 6, 7 and 11.

3.5 References

1. For reviews of methods for α,β -dehydrogenation of carbonyl compounds, see: (a) Buckle, D. R.; Pinto, I. L. Oxidation Adjacent to C=X Bonds by Dehydrogenation. In *Comprehensive Organic Synthesis - Selectivity, Strategy and Efficiency in Modern Organic Chemistry*; Trost, B. M., Fleming, I., Eds.; Elsevier 1991; Vol. 7, pp 119-149. (b) Larock, R. C. *Comprehensive Organic Transformations*; John Wiley & Sons: New York, 1999.
2. (a) Miller, B.; Wong, H.-S. *Tetrahedron* **1972**, 28, 2369-2376. (b) Stotter, P. L.; Hill, K. *A. J. Org. Chem.* **1973**, 38, 2576-2578.
3. For a leading reference and review of selenium based reagents, see: (a) Sharpless, K. B.; Lauer, R. F.; Teranishi, A. Y. *J. Am. Chem. Soc.* **1973**, 95, 6137-6139. (b) Reich, H. J. *Acc. Chem. Res.* **1979**, 12, 22-30.
4. Related sulfoxide elimination reactions are also used. For a leading reference, see: Trost, B. M.; Salzmann, T. N.; Hiroi, K. *J. Am. Chem. Soc.* **1976**, 98, 4887-4902.
5. The original report and many subsequent applications of the Saegusa oxidation protocol use 0.5-1 equiv of Pd^{II}, but catalytic examples have also been reported. See the following leading references: (a) Ito, Y.; Hirao, T.; Saegusa, T. *J. Org. Chem.* **1978**, 43, 1011-1013. (b) Larock, R.

C.; Hightower, T. R.; Kraus, G. A.; Hahn, P.; Zheng, D. *Tetrahedron Lett.* **1995**, *36*, 2423-2426.

(c) Yu, J. Q.; Wu, H. C.; Corey, E. J. *Org. Lett.* **2005**, *7*, 1415-1417.

6. (a) Walker, D.; Hiebert, J. D. *Chem. Rev.* **1967**, *67*, 153-195. (b) Buckle, D. R.; Collier, S. J.; McLaws, M. D. 2,3-Dichloro-5,6-dicyano-1,4-benzo-quinone. In *Encyclopedia of Reagents for Organic Synthesis*; John Wiley & Sons, Inc.: New York, 2005.

7. (a) Nicolaou, K. C.; Zhong, Y. L.; Baran, P. S. *J. Am. Chem. Soc.* **2000**, *122*, 7596-7597. (b) Nicolaou, K. C.; Montagnon, T.; Baran, P. S.; Zhong, Y. L. *J. Am. Chem. Soc.* **2002**, *124*, 2245-2258. (c) Nicolaou, K. C.; Montagnon, T.; Baran, P. S. *Angew. Chem. Int. Ed.* **2002**, *41*, 993-996. (d) Nicolaou, K. C.; Gray, D. L. F.; Montagnon, T.; Harrison, S. T. *Angew. Chem. Int. Ed.* **2002**, *41*, 996-999.

8. For a method employing catalytic 2-iodoxybenzene sulfonate (IBS) in combination with stoichiometric Oxone®, see: Uyanik, M.; Akakura, M.; Ishihara, K. *J. Am. Chem. Soc.* **2009**, *131*, 251-262.

9. For a recent review of efforts toward this goal, see: Muzart, J. *Eur. J. Org. Chem.* **2010**, 3779-3790.

10. For recent advances in Pd-catalyzed aerobic oxidation reactions, see the following references: (a) Stahl, S. S. *Angew. Chem. Int. Ed.* **2004**, *43*, 3400-3420. (b) Gligorich, K. M.; Sigman, M. S. *Chem. Commun.* **2009**, 3854-3867. (c) Chen, X.; Engle, K. M.; Wang, D.-H.; Yu, J.-Q. *Angew. Chem. Int. Ed.* **2009**, *48*, 5094-5115.

-
11. For leading references, see ref. 9 and the following: (a) Theissen, R. J. *J. Org. Chem.* **1971**, *36*, 752-757. (b) Muzart, J.; Pete, J. P. *J. Mol. Catal.* **1982**, *15*, 373-376. (c) Wenzel, T. T. *J. Chem. Soc., Chem. Commun.* **1989**, 932-933. (d) Park, Y. W.; Oh, H. H. *Bull. Korean Chem. Soc.* **1997**, *18*, 1123-1124. (e) Tokunaga, M.; Harada, S.; Iwasawa, T.; Obora, Y.; Tsuji, Y. *Tetrahedron Lett.* **2007**, *48*, 6860-6862.
12. Diao, T.; Stahl, S. S. *J. Am. Chem. Soc.* **2011**, 14566-14569.
13. Izawa, Y.; Pun, D.; Stahl, S. S. *Science* **2011**, *333*, 209-213.
14. (a) Massey, S. M.; Monn, J. A.; Valli, M. J.; office, E. p., Ed. 1998; Vol. EP 0 878 463 A1. (b) Zhang, F.; Moher, E. D.; Zhang, T. Y. *Tetrahedron Lett.* **2007**, *48*, 3277-3279.
15. For progress in the development of a safe and scalable flow process for aerobic oxidation, see: Ye, X. A.; Johnson, M. D.; Diao, T. N.; Yates, M. H.; Stahl, S. S. *Green Chemistry* **2010**, *12*, 1180-1186.
16. (a) Zhu, J.; Liu, J.; Ma, R. Q.; Xie, H. X.; Li, J.; Jiang, H. L.; Wang, W. *Adv. Synth. Catal.* **2009**, *351*, 1229-1232. (b) Liu, J.; Zhu, J.; Jiang, H. L.; Wang, W.; Li, J. *Chem. Asian J.* **2009**, *4*, 1712-1716.
17. (a) Campbell, A. N.; White, P. B.; Guzei, I. A.; Stahl, S. S. *J. Am. Chem. Soc.* **2010**, *132*, 15116-15119. (b) Campbell, A. N.; Meyer, E. B.; Stahl, S. S. *Chem. Commun.* **2011**, *47*, 10257-10259.

-
18. For pK_a values relevant to the present study, see: (a) Matthews, W. S.; Bares, J. E.; Bartmess, J. E.; Bordwell, F. G.; Cornforth, F. J.; Drucker, G. E.; Margolin, Z.; McCallum, R. J.; McCollum, G. J.; Vanier, N. R. *J. Am. Chem. Soc.* **1975**, *97*, 7006-7014. (b) Bordwell, F. G.; Bares, J. E.; Bartmess, J. E.; Drucker, G. E.; Gerhold, J.; McCollum, G. J.; Van der Puy, M.; Vanier, N. R.; Matthews, W. S. *J. Org. Chem.* **1977**, *42*, 326-332. (c) Bordwell, F. G.; Harrelson Jr, J. A. *Can. J. Chem.* **1990**, *68*, 1714-1718. (d) For a useful table of Bordwell pK_a values, see: <http://www.chem.wisc.edu/areas/reich/pkatable/>.
19. Patel, D.; Shukla, S.; Gupta, S. *Int. J. Oncol.* **2007**, *30*, 233-245.
20. Choudary, B. M.; Ranganath, K. V. S.; Yadav, J.; Lakshmi Kantam, M. *Tetrahedron Lett.* **2005**, *46*, 1369-1371.
21. Kondo, T.; Oyama, K.-i.; Yoshida, K. *Angew. Chem. Int. Ed.* **2001**, *40*, 894-897.
22. Si, D.; Wang, Y.; Zhou, Y.-H.; Guo, Y.; Wang, J.; Zhou, H.; Li, Z.-S.; Fawcett, J. P. *Drug Metab. Dispos.* **2009**, *37*, 629-634.
23. Cermak, R.; Wolffram, S. *Curr. Drug Metab.* **2006**, *7*, 729-744.
24. The reactions were monitored for 24 h, during which > 50% conversion was achieved for each reaction. The rate constants were obtained by kinetic simulation of the reaction timecourses to a simple $A \rightarrow B \rightarrow C$ sequential kinetic model. See Supplementary Information for kinetic profiles.

-
25. Oxidation of the **3-3-*d*₅** was carried out in DMSO-*d*₆ to avoid possible background α -H/D exchange.
26. A Pd⁰ species, formed from a Pd^{II}-H intermediate, has been isolated from a “Saegusa”-type oxidation reaction: Porth, S.; Bats, J. W.; Trauner, D.; Giester, G.; Mulzer, J. *Angew. Chem. Int. Ed.* **1999**, *38*, 2015-2016.
27. Recent studies suggest that aerobic oxidation of Pd^{II}-hydrides proceed via Pd⁰, as shown in Scheme 1. See: (a) Konnick, M. M.; Stahl, S. S. *J. Am. Chem. Soc.* **2008**, *130*, 5753-5762. (b) Popp, B. V.; Stahl, S. S. *Chem. Eur. J.* **2009**, *15*, 2915-2922. (c) Decharin, N.; Popp, B. V.; Stahl, S. S. *J. Am. Chem. Soc.* **2011**, *133*, 13268-13271.
28. Zou, G.; Guo, J.; Wang, Z.; Huang, W.; Tang, J. *Dalton Transactions* **2007**, 3055-3064.
29. Gooßen, Lukas J.; Ghosh, K. *Eur. J. Org. Chem.* **2002**, 2002, 3254-3267.
30. Jo, E.-A.; Jun, C.-H. *Eur. J. Org. Chem.* **2006**, 2006, 2504-2507.
31. (a) In *Perry's Chemical Engineers' Handbook*; 7th ed.; Perry, R. H.; Green, D. W. Eds.; McGraw-Hill: 1997, p 51-57. (b) Laut, P. B.; Johnstone, D.; *Chem. Eng.* **1994**, *101*, 96-105.
32. Kendall, J. T.; Spencer, T. A. *J. Labelled Compd. Radiopharmaceut.* **1993**, *12*, 1151-1154.
33. Golisz, S. R.; Labinger, J. A.; Bercaw, J. E. *Organometallics* **2010**, *29*, 5026-5032.
34. Hoover, J. M.; Stahl, S. S. *J. Am. Chem. Soc.* **2011**, *133*, 16901-16910.

-
35. Griesbeck, A. G.; Bondock, S.; Cygon, P. *J. Am. Chem. Soc.* **2003**, *125*, 9016-9017.
36. Zumbansen, K.; Döhring, A.; List, B. *Adv. Synth. Catal.* **2010**, *352*, 1135-1138.
37. Keinan, E.; Greenspoon, N. *J. Am. Chem. Soc.* **1986**, *108*, 7314-7325.
38. Mori, A.; Mizusaki, T.; Miyakawa, Y.; Ohashi, E.; Haga, T.; Maegawa, T.; Monguchi, Y.; Sajiki, H. *Tetrahedron* **2006**, *62*, 11925-11932.
39. Dominguez, C.; Prieto, L.; Valli, M. J.; Massey, S. M.; Bures, M.; Wright, R. A.; Johnson, B. G.; Andis, S. L.; Kingston, A.; Schoepp, D. D.; Monn, J. A. *J. Med. Chem.* **2005**, *48*, 3605-3612.
40. Li, W.; Dai, R.-J.; Yu, Y.-H.; Li, L.; Wu, C.-M.; Luan, W.-W.; Meng, W.-W.; Zhang, X.-S.; Deng, Y.-L. *Biol. Pharm. Bull.* **2007**, *30*, 1123-1129.
41. Velusamy, S.; Ahamed, M.; Punniyamurthy, T. *Org. Lett.* **2004**, *6*, 4821-4824.
42. Gottumukkala, A. L.; Teichert, J. F.; Heijnen, D.; Eisink, N.; van Dijk, S.; Ferrer, C.; van den Hoogenband, A.; Minnaard, A. J. *J. Org. Chem.* **2011**, *76*, 3498-3501.
43. Buszek, K. R.; Brown, N. *Org. Lett.* **2007**, *9*, 707-710.
44. Schmink, J. R.; Holcomb, J. L.; Leadbeater, N. E. *Org. Lett.* **2008**, *11*, 365-368.
45. Lu, H.-H.; Wang, X.-F.; Yao, C.-J.; Zhang, J.-M.; Wu, H.; Xiao, W.-J. *Chem. Commun.* **2009**, 4251-4253.

-
46. Liang, B.; Huang, M.; You, Z.; Xiong, Z.; Lu, K.; Fathi, R.; Chen, J.; Yang, Z. *J. Org. Chem.* **2005**, *70*, 6097-6100.
47. Ghosh, C. K.; Khan, S. *Synthesis-Stuttgart* **1981**, 719-721.
48. Kurono, M.; Yamaguchi, T.; Usui, T.; Fukushima, M.; Mizuno, K.; Matsubara, A. 1986; Vol. EP0193415 (A2).
49. Miao, H.; Yang, Z. *Org. Lett.* **2000**, *2*, 1765-1768.

CHAPTER 4

Characterization of DMSO Coordination to Palladium(II) in Solution

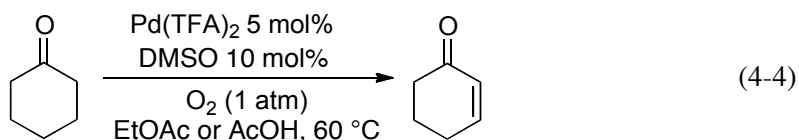
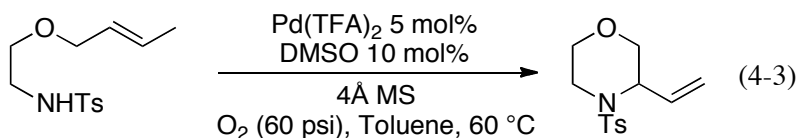
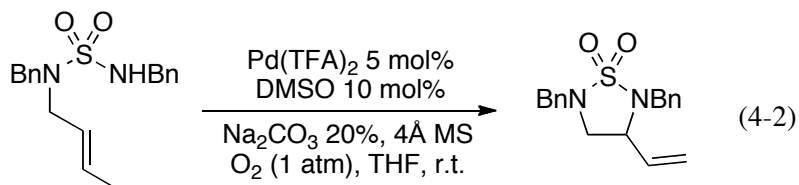
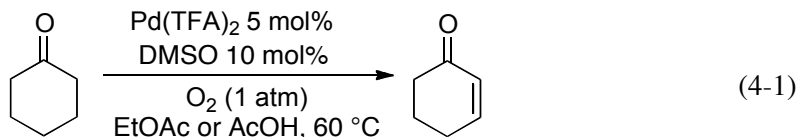
This work has been submitted for publication. The authors of the submitted manuscript are:

Diao, T.; White, P.; Guzei, I. and Stahl, S. S.

4.1 Introduction

A number of homogeneous palladium catalysts have been developed over the past decade for selective aerobic oxidation of organic molecules.¹ One of the earliest reported catalyst systems consists of Pd(OAc)₂ in DMSO as the solvent, which was first reported by the groups of Larock and Hiemstra in the mid-1990s.² This simple catalyst system has been used in a variety of oxidative transformations, including alcohol oxidation, intramolecular hetero- and carbocyclization of alkenes, and cycloalkenylation of silyl enol ethers.³ In these reactions, DMSO has been proposed to serve as a ligand and is believed to play a vital role in stabilizing Pd⁰ and promoting the reoxidation of Pd⁰ by O₂.⁴ Characterization of the coordination properties of DMSO in these reactions is complicated by the large excess of DMSO and insights thus far have been limited to computational studies.⁵

Sulfoxides, including DMSO, bis-sulfoxides, have been used as ligands or additives to promote a variety of Pd-catalyzed oxidation reactions, often using benzoquinone or Ag^I as the stoichiometric oxidants.⁶ Recently, we have reported that Pd(DMSO)₂(TFA)₂, in which DMSO is present in catalytic quantities, is an effective catalyst system for a number of oxidation reactions capable of using O₂ as the oxidant, including α,β -dehydrogenation of carbonyl compounds (eq 4-1)⁷ and oxidative amination of alkenes (eqs 4-2 and 4-3).⁸ A similar catalyst system has been reported by Buchwald and coworkers for chelate-directed C–H arylation of anilides (eq 4-4).⁹ Pd(TFA)₂ (TFA = trifluoroacetate) was the palladium source for dehydrogenation reactions and oxidative amination, while Pd(OAc)₂ in combination with trifluoroacetic acid was used as the catalyst in the biaryl-coupling reaction.



The coordination chemistry of DMSO to late transition metals has been the subject of considerable investigation.¹⁰ Depending on the identity of the metal and other ancillary ligands, DMSO can exhibit *S*-, *O*- or bridging μ -*S,O*-bound coordination modes. Soft metals, such as Ru^{II} , Os^{II} , Rh^{I} and Pt^{II} , typically favor DMSO coordination via the sulfur atom, but *O*-coordination has also been observed.¹⁰ Representative d^8 metal-DMSO complexes include $[\text{Rh}(\text{S-DMSO})_2(\text{O-DMSO})_2][\text{PF}_6]$,¹¹ $[\text{Pt}(\text{bpy})(\text{S-DMSO})\text{Cl}][\text{BF}_4]$ (bpy = 2,2'-bipyridine) and $[\text{Pd}(\text{phen})(\text{O-DMSO})\text{Cl}][\text{PF}_6]$ (phen = phenanthroline).¹² IR and ^1H NMR spectroscopic methods provide a valuable complement to X-ray crystallography in establishing the coordination mode of DMSO to transition metals.^{10,13} In the aforementioned complexes, *S*-coordinated DMSO ligands exhibit S–O stretching frequencies that range from 1080 to 1154 cm^{-1} , while *O*-bound DMSO ligands exhibit lower vibrational frequencies, ranging from 862 to 997 cm^{-1} (Table 4-1). In the ^1H NMR spectra, *S*-bound DMSO ligands exhibit ^1H NMR chemical shifts approximately 1 ppm downfield relative

to free DMSO (~2.53 ppm), whereas *O*-bound DMSO exhibits a smaller downfield shift (Table 4-1).¹⁴

Table 4-1. IR and ¹H NMR Spectroscopic Data of DMSO and Transition Metal-coordinated DMSO Reported in the Literature¹⁰

	IR (S–O) (cm ⁻¹)	¹ H NMR (ppm)
Free DMSO	1005	~ 2.53
<i>S</i> -DMSO ligands	1080 – 1154	3.80 – 3.30
<i>O</i> -DMSO ligands	862 – 997	3.03 – 2.59

Pd^{II} complexes have been identified with both *S*- and *O*-DMSO coordination. For example, in Pd(DMSO)₂Cl₂ both DMSO ligands are *S*-bound,¹⁵ whereas [Pd(phen)(*O*-DMSO)Cl][PF₆] features an *O*-bound DMSO.¹² Complexes containing both *S*- and *O*-bound DMSO ligands are also known, including [Pd(DMSO)₄](BF₄)₂, which has two *S*-bound and two *O*-bound DMSO ligands.¹⁵

Pd(DMSO)₂(TFA)₂ was first characterized by IR spectroscopy in the solid state in 1965 by Wilkinson and coworkers,¹⁶ and the data provided evidence for *S*-bound DMSO. Cotton and coworkers then reported a crystal structure of this complex, which revealed the presence of *trans*-DMSO ligands, one *S*-bound and one *O*-bound.¹⁷ In light of the growing significance of DMSO-ligated Pd^{II} complexes in aerobic oxidation reactions and the difficulty in characterizing the DMSO coordination chemistry in DMSO solvent, we wanted to establish the coordination chemistry of Pd(DMSO)₂(TFA)₂ in solution. Here, we report the characterization of this complex by ¹H and ¹⁹F NMR spectroscopy in catalytically relevant solvents, EtOAc, THF, AcOH and toluene. The results are supplemented by X-ray crystallographic and IR spectroscopic data, and they provide valuable insights into the structure and dynamic properties of this complex in solution.

4.2 Results and Discussion

4.2.1 Solid-State Structures of DMSO-Ligated Pd(TFA)₂ Complexes

Deep orange crystals were obtained from a solution of Pd(TFA)₂ and 2 equiv. of DMSO in EtOAc, and X-ray diffraction analysis established the structure of *trans*-Pd(*S*-DMSO)(*O*-DMSO)(TFA)₂ **4-3a(s)** (Figure 4-1), which exhibits only slight variations relative to the structure originally reported by Cotton and workers.¹⁷ The *S*-bound DMSO ligand has a shorter S–O bond [1.4633(17) Å] and the *O*-bound DMSO ligand has a longer S–O bond [1.5509(16) Å] relative to that of free DMSO (1.52 Å¹⁸). The solid-state infrared absorption spectrum of this complex reveals absorption bands at 1149 cm⁻¹ and 923 cm⁻¹ (Figure 4-2). These bands, which are blue- and red-shifted relative to free DMSO, $\nu_{\text{S-O}} = 1005 \text{ cm}^{-1}$, correspond to the S–O stretching frequencies of the *S*- and *O*-bound DMSO ligands, respectively.¹⁹

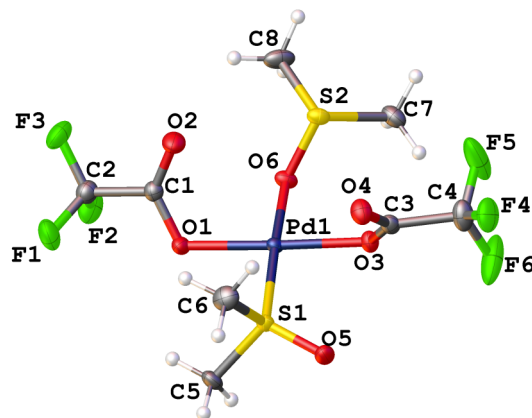


Figure 4-1. Molecular structure of Pd(*S*-DMSO)(*O*-DMSO)(TFA)₂ **4-3a(s)**, with 50% probability ellipsoids. Selected bond lengths, Å: Pd1-O1: 2.0158(15), Pd1-O3: 2.0170(16), Pd1-O6: 2.0554(16), Pd1-S1: 2.1994(5), S1-O5: 1.4633(17), S2-O6: 1.5509(16).

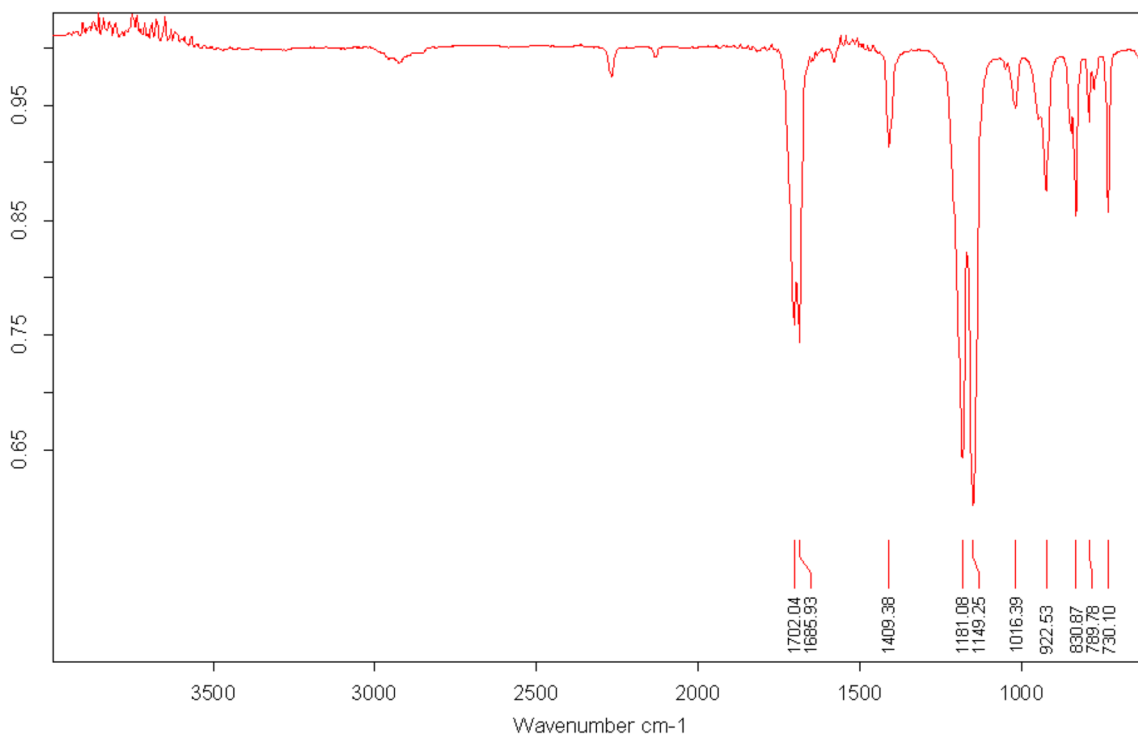


Figure 4-2. IR spectrum of Pd(*S*-DMSO)(*O*-DMSO)(TFA)₂ **4-3a(s)**. Infrared absorption bands (cm⁻¹): 1702, 1686, 1409, 1181, 1149, 1012, 922, 830, 789, 730.

A mono-DMSO-ligated Pd^{II} complex was obtained from an EtOAc solution of Pd(TFA)₂ containing only 1 equiv. of DMSO. X-ray diffraction analysis established the structure of *trans*-Pd(*S*-DMSO)(OH₂)(TFA)₂ **4-2a(s)** (Figure 4-3). The H₂O molecule, coordinated *trans* to the *S*-DMSO ligand, is hydrogen bonded to the carboxylates of adjacent molecules (see Supporting Information for details). An IR spectrum of the solid Pd(*S*-DMSO)(OH₂)(TFA)₂ **4-2a(s)** exhibits an absorption band at 1155 cm⁻¹ (Figure 4-4), consistent with *S*-coordination of DMSO (cf. Table 4-1). The lack of absorption bands between 860 and 1000 cm⁻¹ is consistent with the absence of an *O*-bound DMSO ligand.

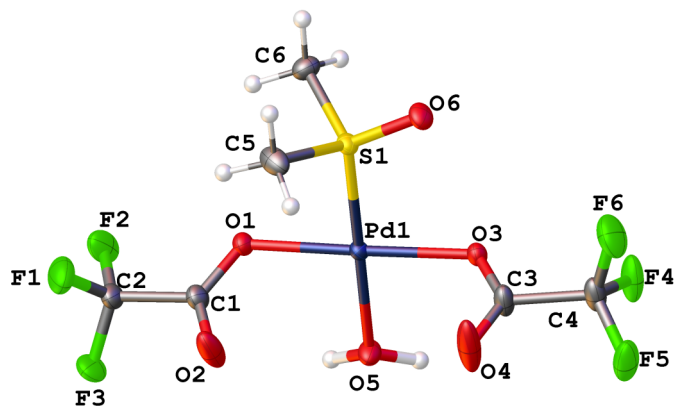


Figure 4-3. Molecular structure of Pd(*S*-DMSO)(OH₂)(TFA)₂ **4-2a(s)**, with 50% probability ellipsoids. The half molecule of co-crystallized solvent ethyl acetate is not shown. Selected bond lengths, Å: Pd1-O1: 2.0205(13), Pd1-O3: 2.0171(13), Pd1-O5: 2.0564(13), Pd1-S1: 2.1979(8), S1-O6: 1.4677(13).

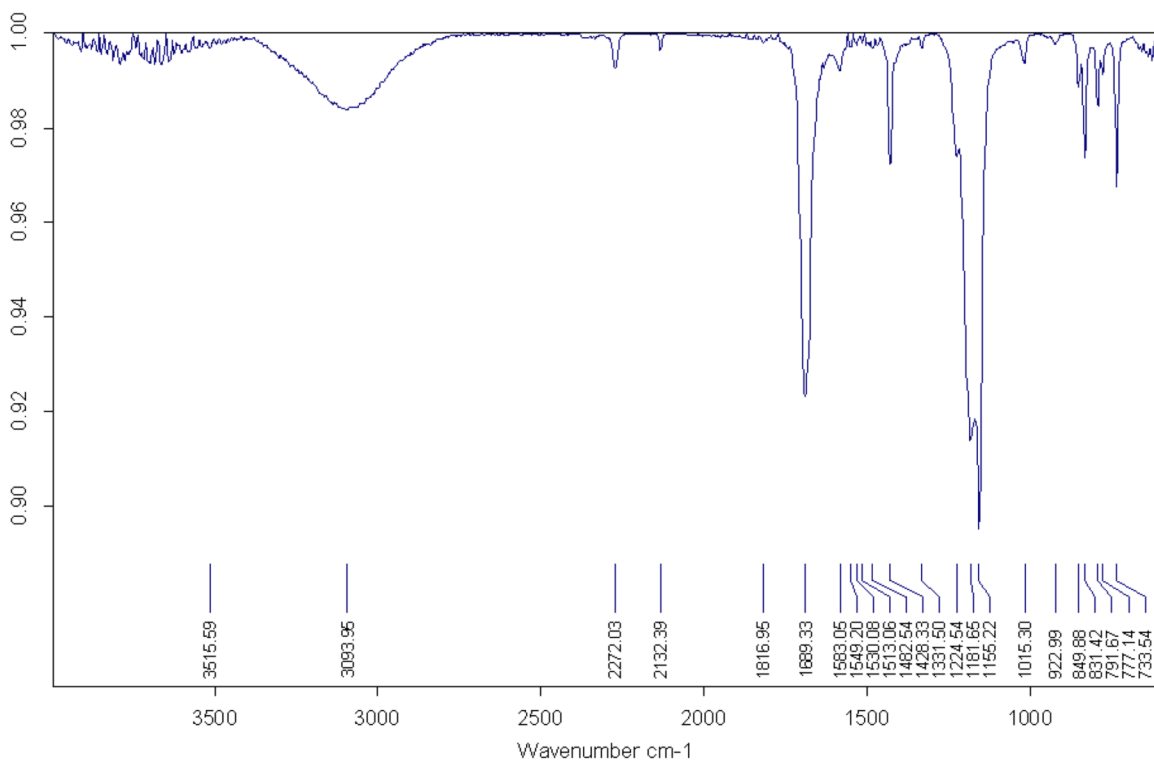


Figure 4-4. IR spectrum of Pd(*S*-DMSO)(OH₂)(TFA)₂ **4-2a(s)**. Infrared absorption bands (cm⁻¹): 3094 (br), 1689, 1428, 1182, 1155, 850, 792, 736.

4.2.2 The Solution-Phase Structure of Pd(TFA)₂/DMSO in EtOAc

Discrepancies can exist between solid-state and solution structures of transition-metal complexes. For example, the DMSO ligand in [Pd(bpy)(DMSO)Cl][PF₆] (bpy = 2,2'-bipyridine) was determined to be *O*-bound by X-ray crystallography; however, a mixture of *O*- and *S*-DMSO ligated species was observed in CD₃NO₂ by ¹H NMR spectroscopy.¹² In order to probe the similarities and differences between solid-state and solution structures of Pd(TFA)₂/DMSO complexes, a combination of ¹H and ¹⁹F NMR spectroscopy was used to determine the coordination properties of DMSO to Pd^{II} in catalytically relevant solvents.

The Pd(TFA)₂/DMSO-catalyzed dehydrogenation of cyclohexanone was performed in EtOAc (eq 4-1), and our initial spectroscopic studies were carried out in this solvent.⁷ A titration experiment was carried out by adding DMSO to a solution of Pd(TFA)₂ in EtOAc-*d*₀. The initial titration experiments were performed at -60 °C in order to slow dynamic processes. Pd(TFA)₂ completely dissolves in EtOAc and no ¹H resonances are observed in the ¹H NMR spectrum between 2.3 and 3.7 ppm (Figure 4-5). Addition of 0.5 equiv. of DMSO relative to Pd results in the appearance of a singlet at 3.47 ppm. This peak grows upon addition of another 0.5 equiv. of DMSO (1 equiv. total), with concomitant formation of three new smaller peaks at 3.58, 3.42 and 2.95 ppm. Further addition of DMSO results in diminishment of the peak at 3.47 ppm and growth of the peaks at 3.58, 3.42 and 2.95 ppm. With 2 equiv. of DMSO, the peak at 3.47 ppm is not present, but a new peak at 3.08 ppm is evident.²⁰ A broad peak, corresponding to free DMSO, appears at 2.64 ppm and the peak at 2.95 ppm is broadened in the presence of 3 equiv. DMSO.

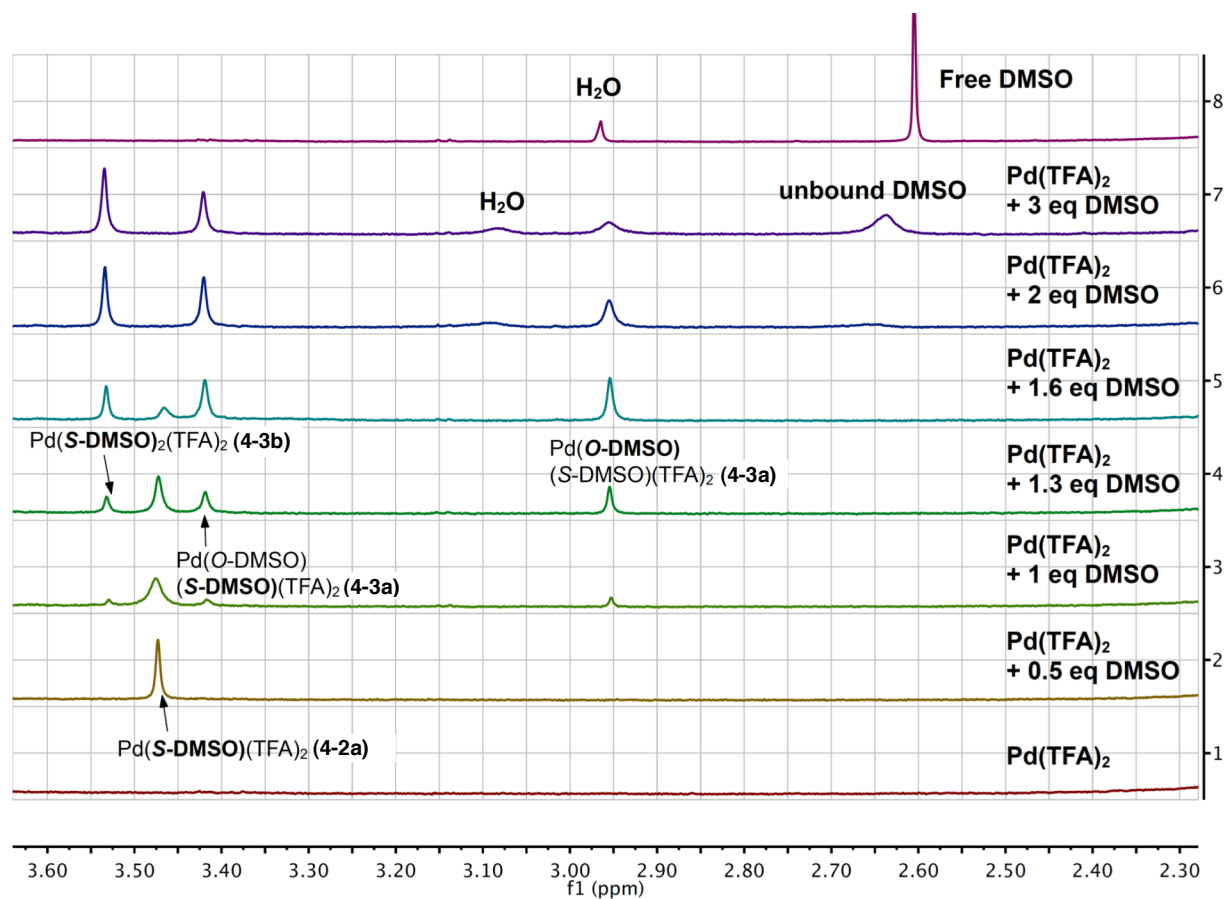


Figure 4-5. ^1H NMR spectra of $\text{Pd}(\text{TFA})_2$ in EtOAc in the presence of various quantities of DMSO at $-60\text{ }^\circ\text{C}$. Conditions: $[\text{Pd}(\text{TFA})_2] = 30\text{ mM}$ (6.6 mg, 0.02 mmol), EtOAc = 0.65 mL, $-60\text{ }^\circ\text{C}$, $[\text{DMSO}] = 0, 15, 30, 39, 48, 60$ and 90 mM .

The same DMSO titration solutions were analyzed by ^{19}F NMR spectroscopy (Figure 4-6). In EtOAc, $\text{Pd}(\text{TFA})_2$ exhibits a singlet at -76.76 ppm . Multiple minor species are evident between -73.50 and -75.30 ppm , the integrations of which vary at different temperatures and $\text{Pd}(\text{TFA})_2$ concentrations. A singlet at -74.74 ppm appears upon addition of 0.5 equiv. of DMSO. Further addition of DMSO leads to decreased integration of the $\text{Pd}(\text{TFA})_2$ peak at -76.76 ppm , with concomitant growth of the peak at -74.74 ppm and appearance of two new singlets at -74.80 and

–75.00 ppm. With 2 and 3 equiv. of DMSO, the peaks at –74.80 and –75.00 ppm are the sole peaks present in the ^{19}F NMR spectrum.

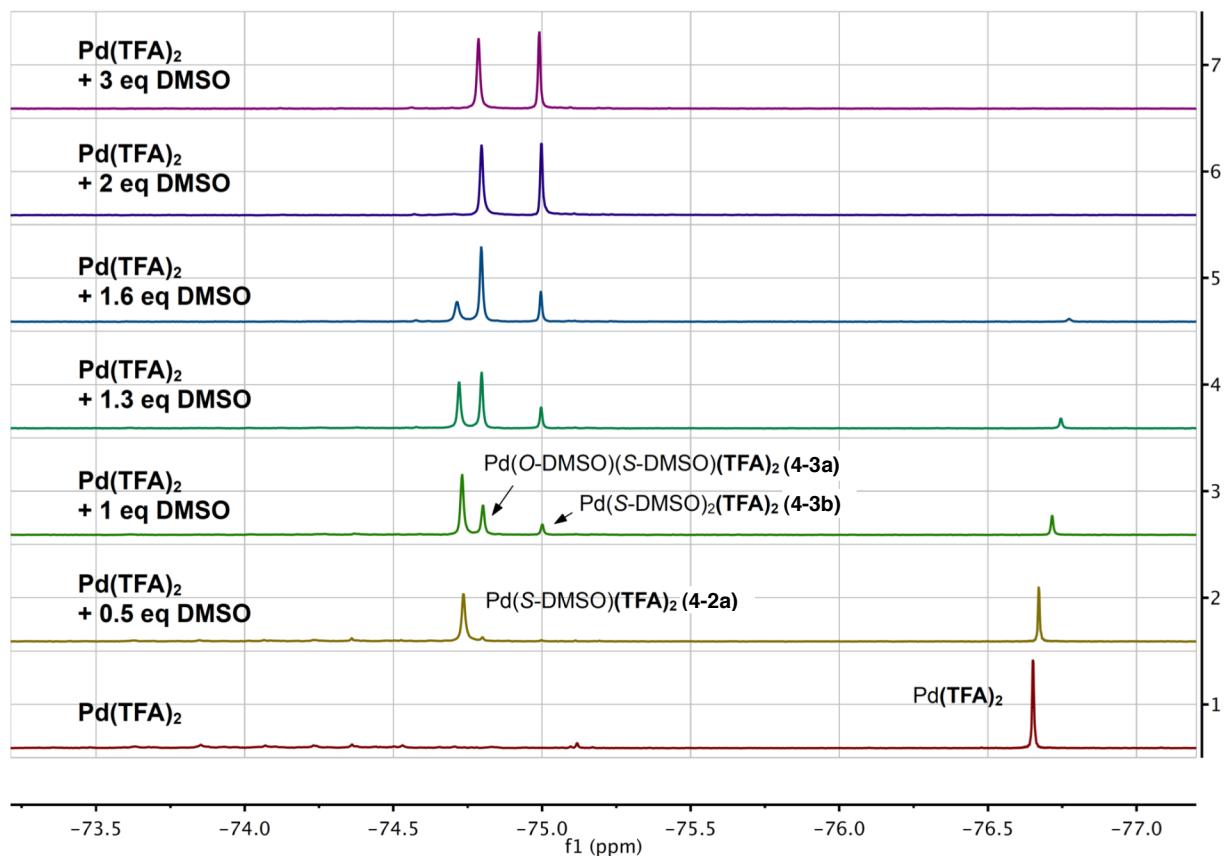


Figure 4-6. ^{19}F NMR spectra of $\text{Pd}(\text{TFA})_2$ in EtOAc in the presence of various quantities of DMSO at $-60\text{ }^\circ\text{C}$. Conditions: $[\text{Pd}(\text{TFA})_2] = 30\text{ mM}$ (6.6 mg, 0.02 mmol), EtOAc = 0.65 mL, $-60\text{ }^\circ\text{C}$, $[\text{DMSO}] = 0, 15, 30, 39, 48, 60$ and 90 mM .

The temperature dependence of equilibria between different $\text{Pd}(\text{TFA})_2/\text{DMSO}$ complexes has been investigated with the sample containing 1.6 equiv. of DMSO, in which multiple species are evident in the NMR spectra. Both ^1H and ^{19}F NMR spectra exhibit peak broadening as the temperature is increased (Figure 4-7). At temperatures above $-20\text{ }^\circ\text{C}$, the ^1H peaks at 3.47 and 3.42 ppm coalesce into one peak with concomitant broadening of the peak at 2.95 ppm. Similar

coalescence occurs for the ^{19}F peaks at -74.74 and -74.80 ppm. In contrast, the ^1H peak at 3.58 ppm and ^{19}F peak at -75.00 ppm remain sharp throughout the temperature range.

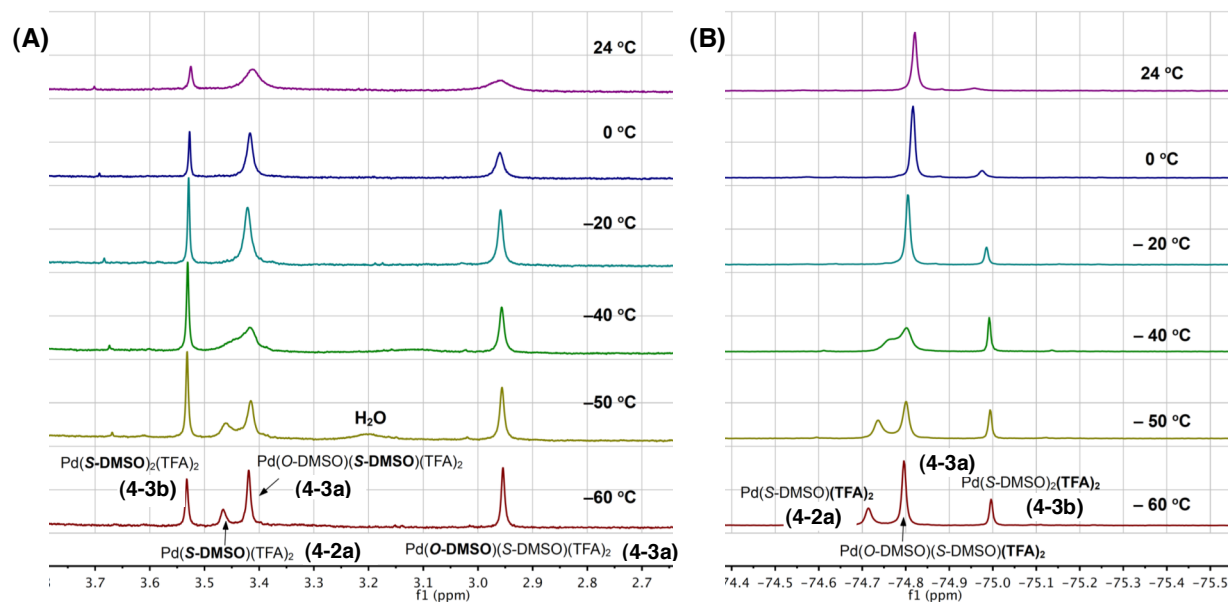
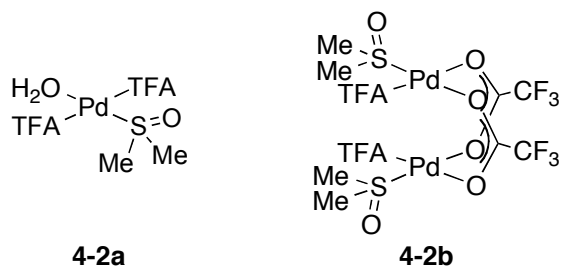
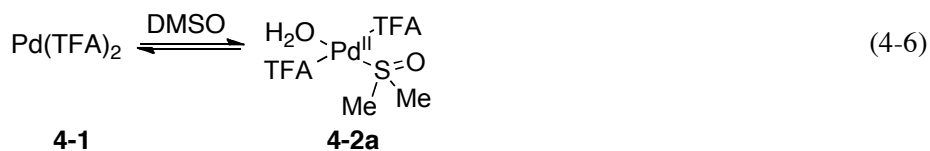
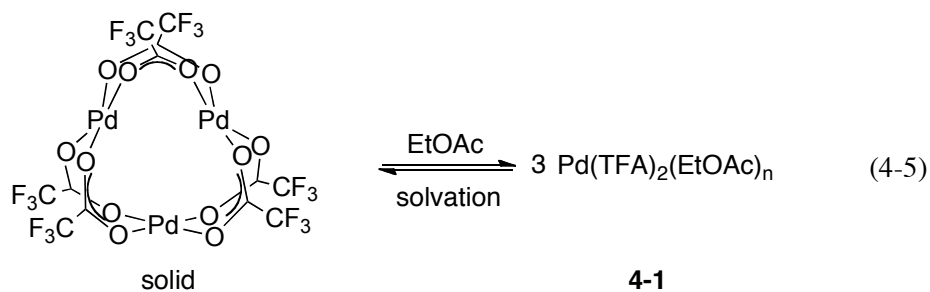


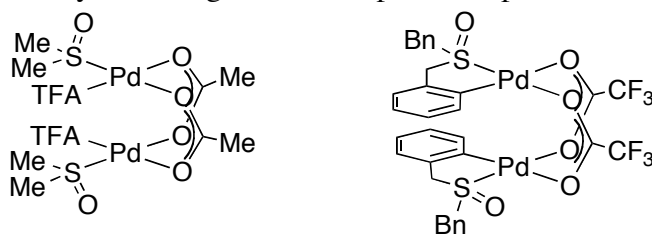
Figure 4-7. NMR spectra of Pd(TFA)₂/DMSO (1:1.6) in EtOAc at various temperatures. (A) ^1H NMR spectra; (B) ^{19}F NMR spectra. Conditions: [Pd(TFA)₂] = 30 mM (6.6 mg, 0.02 mmol), [DMSO] = 48 mM (1.6 equiv.), EtOAc = 0.65 mL, T = -60 , -50 , -40 , -20 , 0 and 24 °C.

Assignments of the peaks in the ^1H NMR spectra presented above are facilitated by the literature precedents, and peaks in the ^{19}F NMR spectra may be correlated to those in the ^1H NMR spectra and assigned accordingly. The solid-state structure of Pd(TFA)₂ is trimeric;²¹ however, Wilkinson has reported osmometry data suggesting that Pd(TFA)₂ dissociates into a monomer **4-1** in EtOAc (eq 4-5).¹⁶ The peak that appears at 3.47 ppm upon addition of DMSO is assigned to an *S*-bound DMSO ligand by analogy to previously characterized *S*-DMSO ligands (cf. Table 4-1), and integration of this peak and the corresponding new TFA peak in the ^{19}F NMR spectrum at -74.74 ppm relative to an internal standard (C₆H₅F) reflects formation of a 1:1 DMSO: Pd(TFA)₂

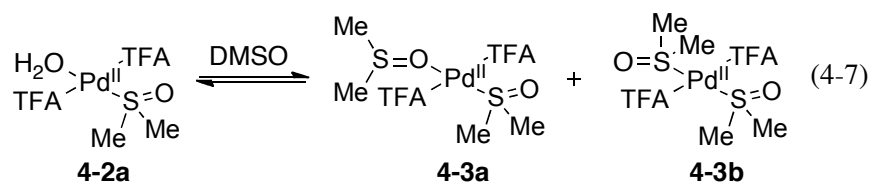
complex (**4-2a**, eq 4-6), analogous to Pd(*S*-DMSO)(OH₂)(TFA)₂ **4-2a(s)** (cf. Figure 4-3). An *S*-DMSO-ligated Pd(TFA)₂ dimer, such as **4-2b**, is an alternative possible structure, particularly in light of analogous crystallographically characterized structures, [Pd(*S*-DMSO)(OAc)₂]₂²² and the phenylsulfoxide-ligated Pd(TFA)₂ dimer (Scheme 4-1).^{23,24}



Scheme 4-1. Dimeric Carboxylate-Bridged Pd^{II} Complexes Reported in the Literature^{22,23}



The peaks that appear in the ^1H and ^{19}F NMR spectra upon addition of ≥ 1 equiv. of DMSO are consistent with bis-DMSO coordinated Pd species. The ^1H peaks at 3.54 ppm and 3.42 ppm represent two different *S*-bound DMSO ligands, whereas the peak at 2.95 ppm is consistent with an *O*-bound DMSO ligand. The ^1H resonances at 3.42 ppm and 2.95 ppm correlate with the peak at -74.80 ppm in the ^{19}F NMR spectra, and their respective integrations correspond to a ligand ratio of 1 *S*-DMSO : 1 *O*-DMSO : 2 TFA, consistent with the assignment of this species as $\text{Pd}(\text{S-DMSO})(\text{O-DMSO})(\text{TFA})_2$ **4-3a** (eq 4-7). The remaining *S*-bound DMSO peak at 3.58 ppm correlates with an ^{19}F peak at -75.00 ppm, and integrations of these peaks correspond to a 1:1 DMSO : TFA ligand ratio. This complex is assigned as $\text{Pd}(\text{S-DMSO})_2(\text{TFA})_2$ **4-3b**, in which both DMSO ligands coordinate via the sulfur atom (eq 4-7).



Based on above assignments, the ^1H and ^{19}F NMR data can be used to plot the concentrations as a function of added DMSO (Figure 4-8), and the plot derived from the ^1H NMR spectra is in good agreement with that derived from the ^{19}F NMR spectra. To summarize the results, initial addition of DMSO results in formation of a mono-DMSO-ligated $\text{Pd}(\text{TFA})_2$ complex with DMSO coordinated via the *S* atom. Higher concentrations of DMSO leads to conversion of this species into an equilibrium mixture of bis-DMSO-ligated $\text{Pd}(\text{TFA})_2$ complexes **4-3a** and **4-3b**. The bis-

DMSO coordination to Pd^{II} is sufficiently favored that unbound DMSO is not evident until >2 equiv. of DMSO is added.

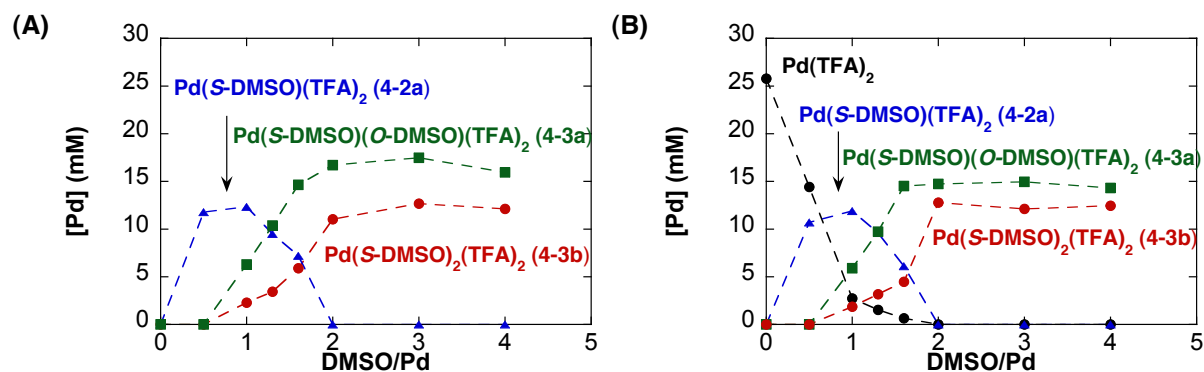
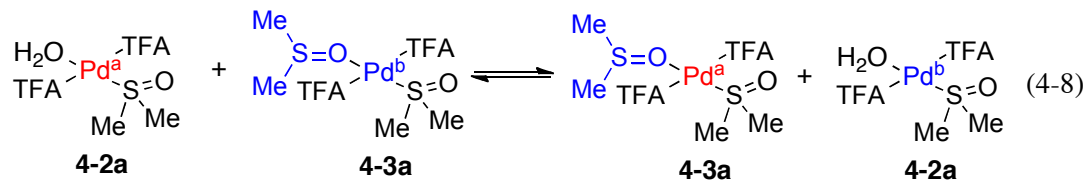


Figure 4-8. Plots of Pd(TFA)₂/DMSO complexes present in solution as a function of added [DMSO] on the basis of ¹H and ¹⁹F NMR data, (A) and (B), respectively. Conditions: [Pd(TFA)₂] = 30 mM (6.6 mg, 0.02 mmol), EtOAc = 0.65 mL, -60 °C, [DMSO] = 0, 15, 30, 39, 48, 60 and 90 mM.

In the presence of 3 equiv. of DMSO, the significant line broadening is evident for the peaks corresponding to unbound DMSO and the *O*-bound DMSO ligand in **4-3a**. This observation suggests that fast exchange takes place between them, and further implies that the *O*-bound DMSO ligand is more labile than the *S*-bound DMSO ligand. Complementary observations are obtained from the variable-temperature spectra of Pd(TFA)₂ in the presence of 1.6 equiv. of DMSO (Figure 4-7). This study reveals that **4-2a** and **4-3a** undergo fast exchange at elevated temperature (eq 4-8). Ligand exchange of the labile *O*-DMSO ligand in **4-3a** with **4-2a**, possibly catalyzed by the EtOAc solvent, can account for these observations. The kinetics of this exchange process will be discussed further below. The lack of peak broadening of **4-3b** suggests that analogous exchange of the *S*-bound DMSO ligands in **4-3b** does not take place on the NMR timescale.



The temperature dependence plots shown in Figure 4-9 also reveal that the concentration of **4-3b** decreased with concomitant increase of **4-3a** at increased temperature, indicating a temperature-dependent equilibrium between **4-3a** and **4-3b** (eq 4-9). The equilibrium constants at various temperatures are calculated based on the ^{19}F NMR spectra. van't Hoff analysis reveals a linear relationship between the $\ln(K_{\text{eq}})$ and $1/T$ (Figure 4-10) and enables determination of ΔH and ΔS , (-2.7 kcal/mol and -13 e.u., respectively). The relatively large negative ΔS suggests that **4-3b** has a more ordered structure than **4-3a**.

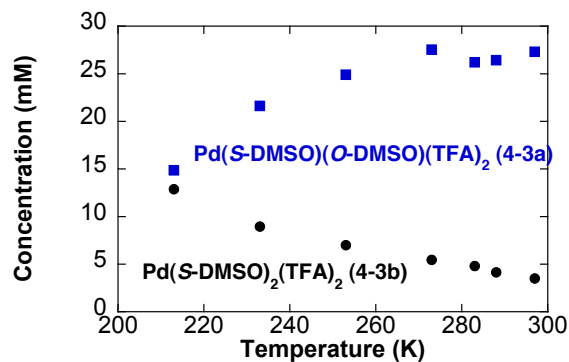


Figure 4-9. Concentrations of **4-3a** and **4-3b** at different temperatures, based on analysis of the ^{19}F NMR spectra. Conditions: $[\text{Pd}(\text{TFA})_2] = 15$ mM (3.3 mg, 0.01 mmol), $[\text{DMSO}] = 30$ mM (2 equiv.), $\text{EtOAc} = 0.65$ mL, $T = -60, -40, -20, 0, 10, 15$ and 24 °C.

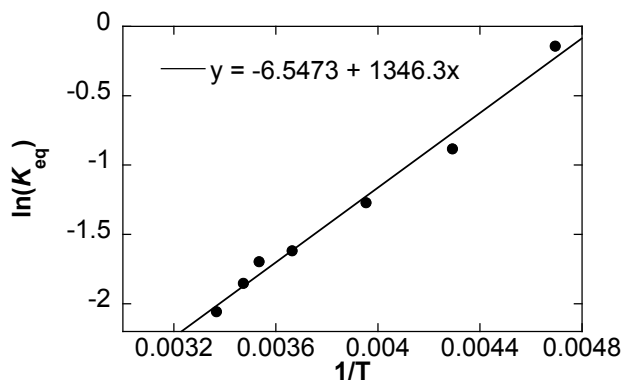
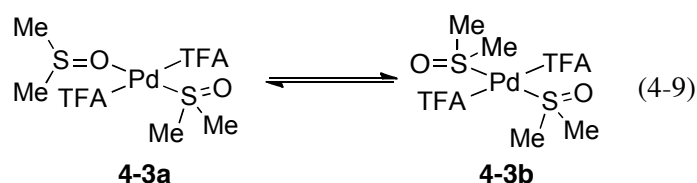
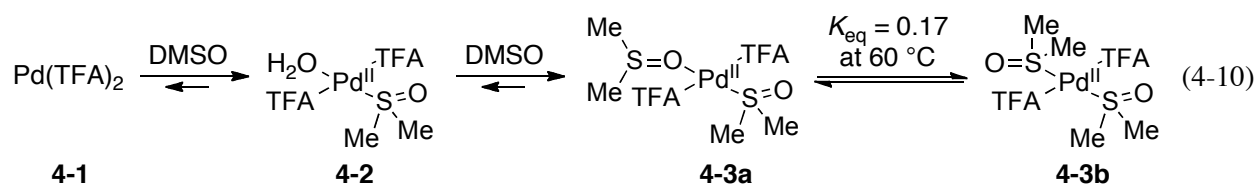


Figure 4-10. van't Hoff plot of the equilibrium between **4-3a** and **4-3b**. Conditions: $[\text{Pd}(\text{TFA})_2] = 15 \text{ mM}$ (3.3 mg, 0.01 mmol), $[\text{DMSO}] = 30 \text{ mM}$ (2 equiv.), $\text{EtOAc} = 0.65 \text{ mL}$, $T = -60, -40, -20, 0, 10, 15$ and $24 \text{ }^\circ\text{C}$.



The catalytic oxidation of cyclohexanone in EtOAc employs $\text{Pd}(\text{TFA})_2$ with 2 equiv. of DMSO at $60 \text{ }^\circ\text{C}$. The data presented above suggest that only bis-DMSO coordinated Pd compounds **4-3a** and **4-3b** are present under these conditions (eq 4-10). At $60 \text{ }^\circ\text{C}$, significant peak broadening is observed among all species (data not shown), suggesting that fast exchange can take place between both *S*- and *O*-bound DMSO ligands at this temperature. The equilibrium constant between **4-3a** and **4-3b** was calculated to be 0.17 at $60 \text{ }^\circ\text{C}$, based on the van't Hoff analysis described above (eq 4-9). Therefore, under the catalytic condition of dehydrogenation, **4-3a** is favored over **4-3b** by a 6:1 ratio.



4.2.3 Effect of the Anionic Ligand: Coordination Chemistry of DMSO to Pd(OAc)₂ in EtOAc

The use of trifluoroacetate as an anionic ligand is important to the success of the Pd/DMSO catalyst systems in eqs 4-1 to 4-3;^{7,8} replacement of Pd(TFA)₂ with Pd(OAc)₂ has been shown to result in decreased yields. These observations prompted us to analyze the coordination chemistry of DMSO to Pd(OAc)₂ in EtOAc. Pd(OAc)₂ fully dissolves in EtOAc to form an orange solution. Titration of DMSO into the solution results in the appearance of two broad peaks at 3.50 and 3.43 ppm in the ¹H NMR spectra, consistent with *S*-bound DMSO ligands, together with a peak at 2.60 ppm corresponding to free DMSO (Figure 4-11). Further addition of DMSO increases the concentration of bound DMSO ligands; however, the sum of the bound DMSO ligands maximizes at a DMSO: Pd^{II} ratio of approximately 2:3, when ≥ 10 equiv. of DMSO have been added (Figure 4-12).

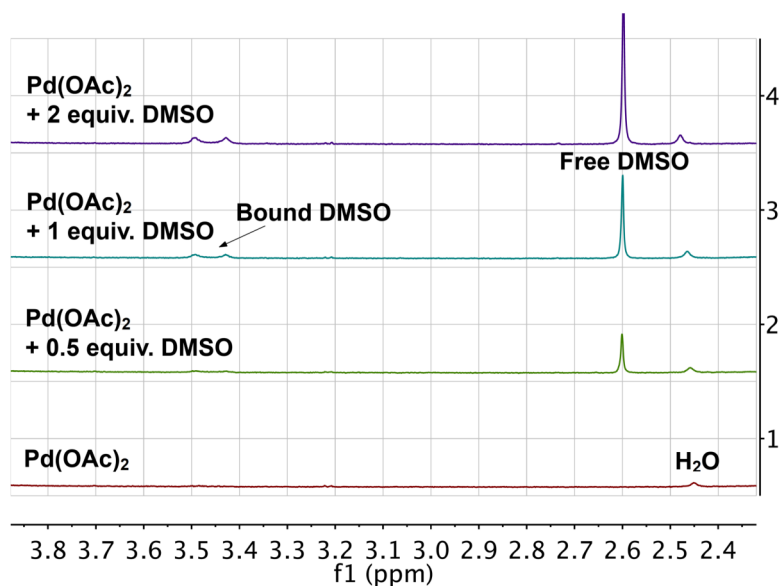


Figure 4-11. ^1H NMR spectra of $\text{Pd}(\text{OAc})_2$ in EtOAc with various quantities of DMSO at 24 °C. Conditions: $[\text{Pd}(\text{OAc})_2] = 30 \text{ mM}$ (4.4 mg, 0.02 mmol), EtOAc = 0.65 mL, 24 °C, $[\text{DMSO}] = 0, 7.5, 15$ and 30 mM.

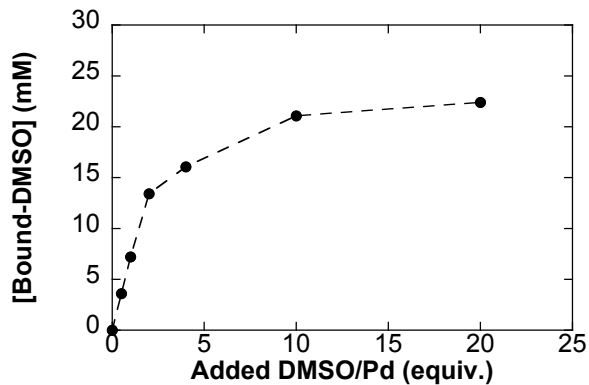
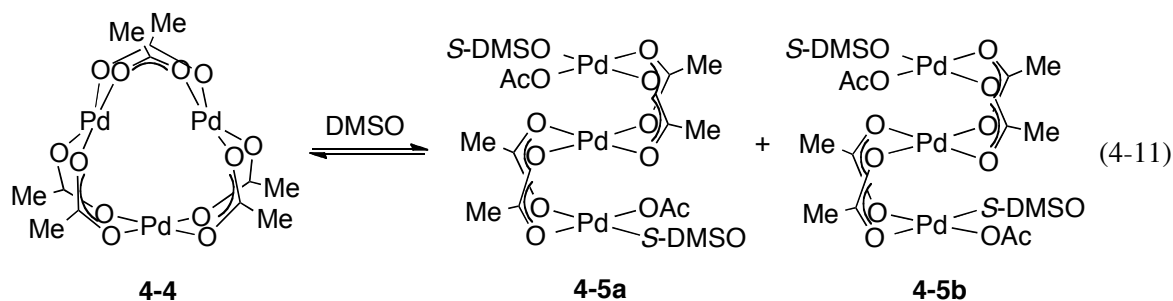


Figure 4-12. Titration curves of DMSO into the solution of $\text{Pd}(\text{OAc})_2$ in EtOAc at 24 °C. Conditions: $[\text{Pd}(\text{OAc})_2] = 30 \text{ mM}$ (4.4 mg, 0.02 mmol), EtOAc = 0.65 mL, 24 °C, $[\text{DMSO}] = 0, 15, 30, 60, 120, 300$ and 600 mM.

The solid state structures of $\text{Pd}(\text{TFA})_2$ and $\text{Pd}(\text{OAc})_2$ have both been characterized previously to be trimeric by X-ray crystallography,²¹ and $\text{Pd}(\text{OAc})_2$ has been proposed to remain trimeric in EtOAc.¹⁶ The 2:3 DMSO: Pd^{II} stoichiometry evident from the titration experiments in Figure 4-12

suggests that DMSO coordination might partially cleave the trimeric Pd(OAc)₂ structure forming linear trimers, such as complexes **4-5a** and **4-5b** (eq 4-11). A number of structurally similar acetate-bridged trimeric Pd complexes have been reported previously in the literature.²⁵ If this assignment is correct, the two distinct ¹H signals could arise from the C_s and C₂ isomers, **4-5a** and **4-5b**.

Despite the tentative nature of the Pd(OAc)₂/DMSO structural assignments, a distinction between DMSO coordination to Pd(TFA)₂ and Pd(OAc)₂ is clearly evident. The differences presumably reflect the different basicity of the carboxylate ligands. The more-basic acetate ligand should be a more effective bridging ligand, and cleavage of the trimeric structure by DMSO will be less favored. Such effects undoubtedly contribute to the different activities of Pd(TFA)₂ and Pd(OAc)₂ in the catalytic reactions. More detailed understanding of the catalytic implications of these observations requires further investigation.



4.2.4 The Solution Phase Structure of Pd(TFA)₂/DMSO in THF-*d*₈

Pd(DMSO)₂(TFA)₂ in THF serves as an effective catalyst for oxidative amination reactions (eq 4-2),⁸ and we performed DMSO titration experiments similar to those described above with a solution of Pd(TFA)₂ in THF-*d*₈. The spectra reveal trends similar to those observed in EtOAc, as well as differences associated with dynamics of the exchange processes (Figures 4-13 and 4-14). Addition of 0.5 equiv. of DMSO leads to the appearance of a resonance at 3.29 ppm in the ¹H

spectrum and a peak at -74.73 ppm in the ^{19}F NMR spectrum. These peaks are assigned to the mono-DMSO complex **4-2a**. Addition of more DMSO results in the appearance of peaks at 2.76 ppm and 3.35 ppm in the ^1H NMR spectra, and a peak at -74.97 ppm in the ^{19}F NMR spectra. Meanwhile, the peak at 3.29 ppm in the ^1H NMR spectra and -74.73 ppm in the ^{19}F NMR spectra shift upfield. Based upon the analysis of the EtOAc solutions, the peak at 3.35 ppm in the ^1H NMR spectra and -74.97 ppm in the ^{19}F NMR spectra are assigned to $\text{Pd}(\text{S-DMSO})_2(\text{TFA})_2$, **4-3b**. The peak at 2.76 ppm in the ^1H NMR spectra corresponds to an *O*-bound DMSO ligand, consistent with formation of $\text{Pd}(\text{S-DMSO})(\text{O-DMSO})(\text{TFA})_2$, **4-3a**.

The *S*-bound DMSO ligand of **4-3a** was not observed as an independent peak, but was manifested as an upfield shift of the *S*-bound DMSO resonance of **4-2a**. This observation reflects fast exchange between **4-2a** and **4-3a** (cf. eq 4-8), resulting in coalescence of their *S*-bound DMSO resonances. Similarly, **4-2a** and **4-3a** exhibit a single broadened peak at -74.73 ppm in the ^{19}F NMR spectra. Analogous coalescence of **4-2a** and **4-3a** has been observed in EtOAc at temperatures higher than 20 °C (cf. Figure 4-7). When >2 equiv. of DMSO are present, however, this peak appears at -74.81 ppm and is considerably sharpened, consistent with complete conversion of **4-2a** into **4-3a** (and **4-3b**). Complexes **4-2a** and **4-3a** do not interconvert rapidly with **4-3b** at -60 °C; however, when the spectra were recorded at room temperature, fast exchange was observed among all three species (**4-2a**, **4-3a** and **4-3b**; Figure 4-15).

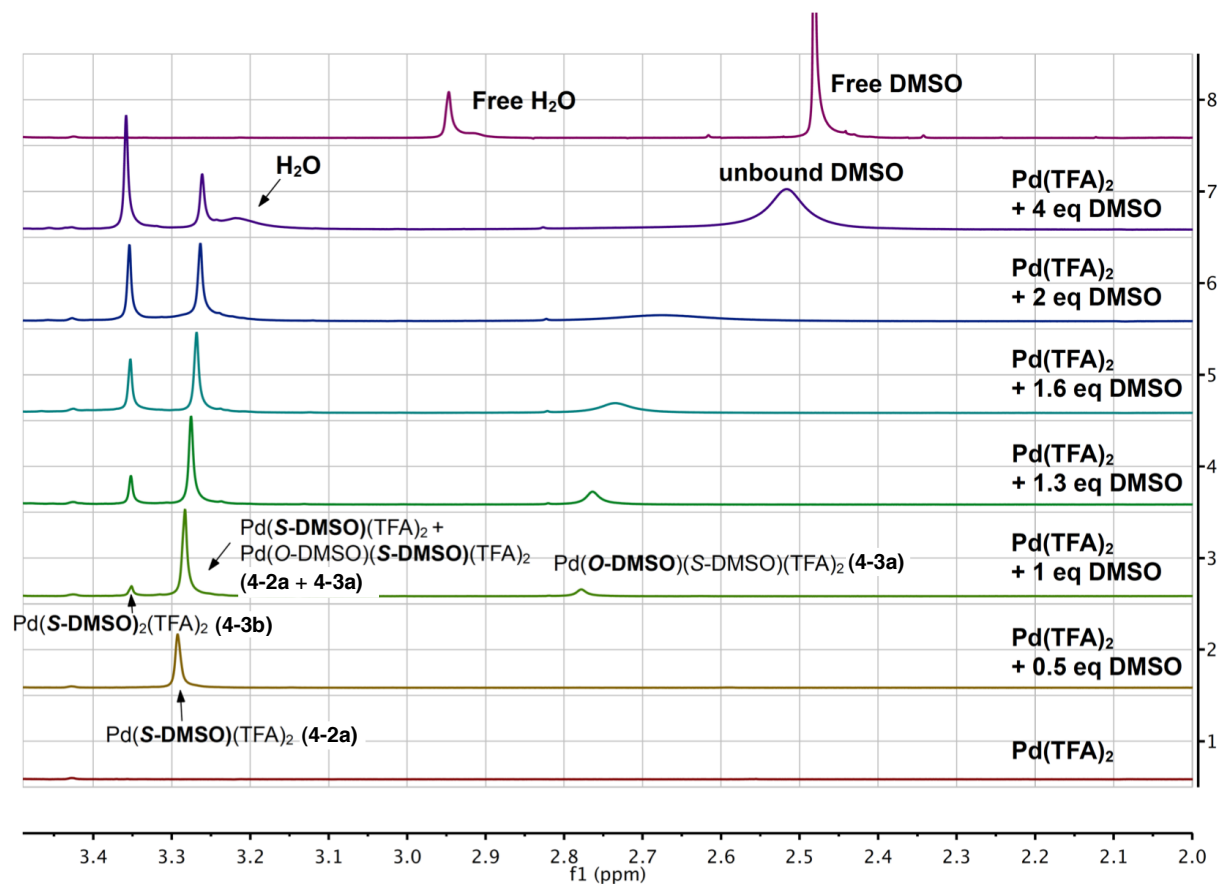


Figure 4-13. ^1H NMR spectra of $\text{Pd}(\text{TFA})_2$ in $\text{THF-}d_8$ with various quantities of DMSO at $-60\text{ }^\circ\text{C}$. Conditions: $[\text{Pd}(\text{TFA})_2] = 15\text{ mM}$ (3.3 mg, 0.01 mmol), $\text{THF-}d_8 = 0.65\text{ mL}$, $-60\text{ }^\circ\text{C}$, $[\text{DMSO}] = 0, 7.5, 15, 19.5, 24, 30$ and 60 mM .

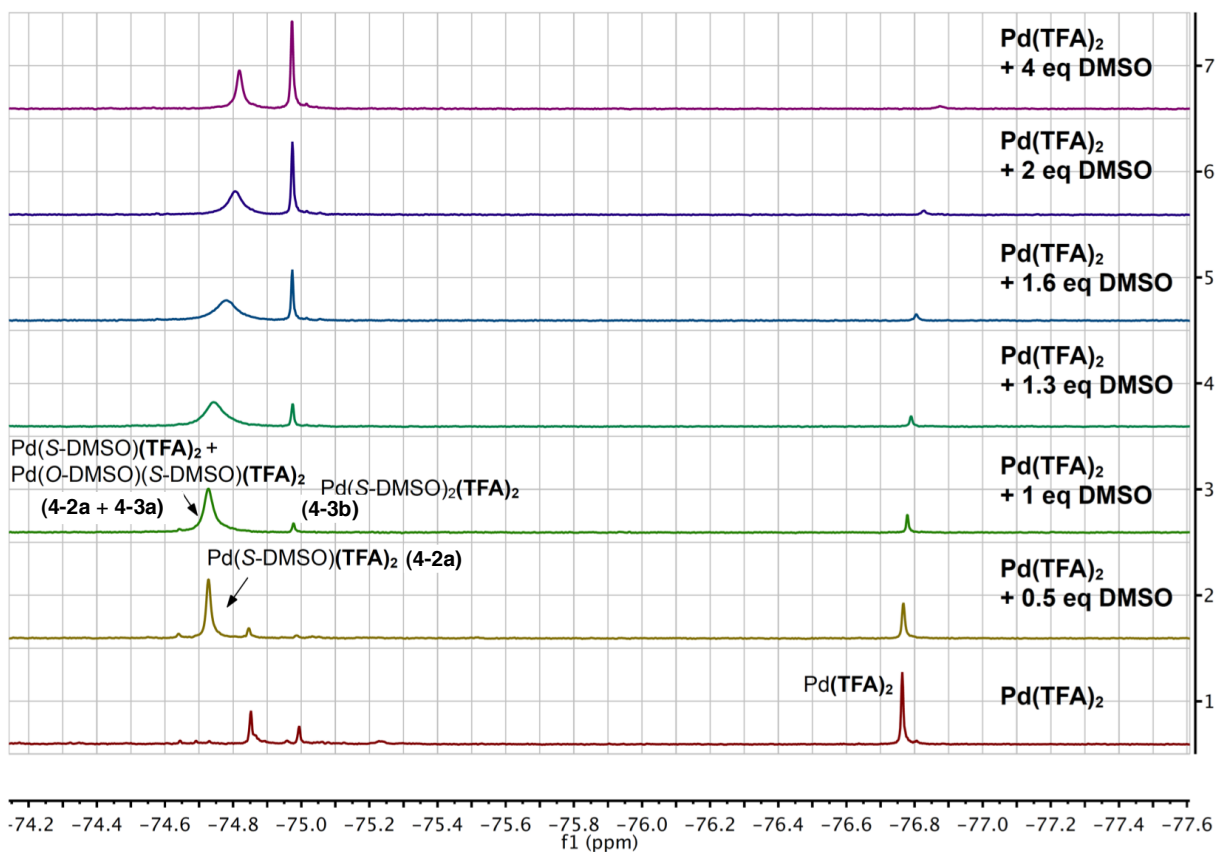


Figure 4-14. ^{19}F NMR spectra of $\text{Pd}(\text{TFA})_2$ in $\text{THF-}d_8$ with various quantities of DMSO at $-60\text{ }^\circ\text{C}$. Conditions: $[\text{Pd}(\text{TFA})_2] = 15\text{ mM}$ (3.3 mg, 0.01 mmol), $\text{THF-}d_8 = 0.65\text{ mL}$, $-60\text{ }^\circ\text{C}$, $[\text{DMSO}] = 0, 7.5, 15, 19.5, 24, 30$ and 60 mM .

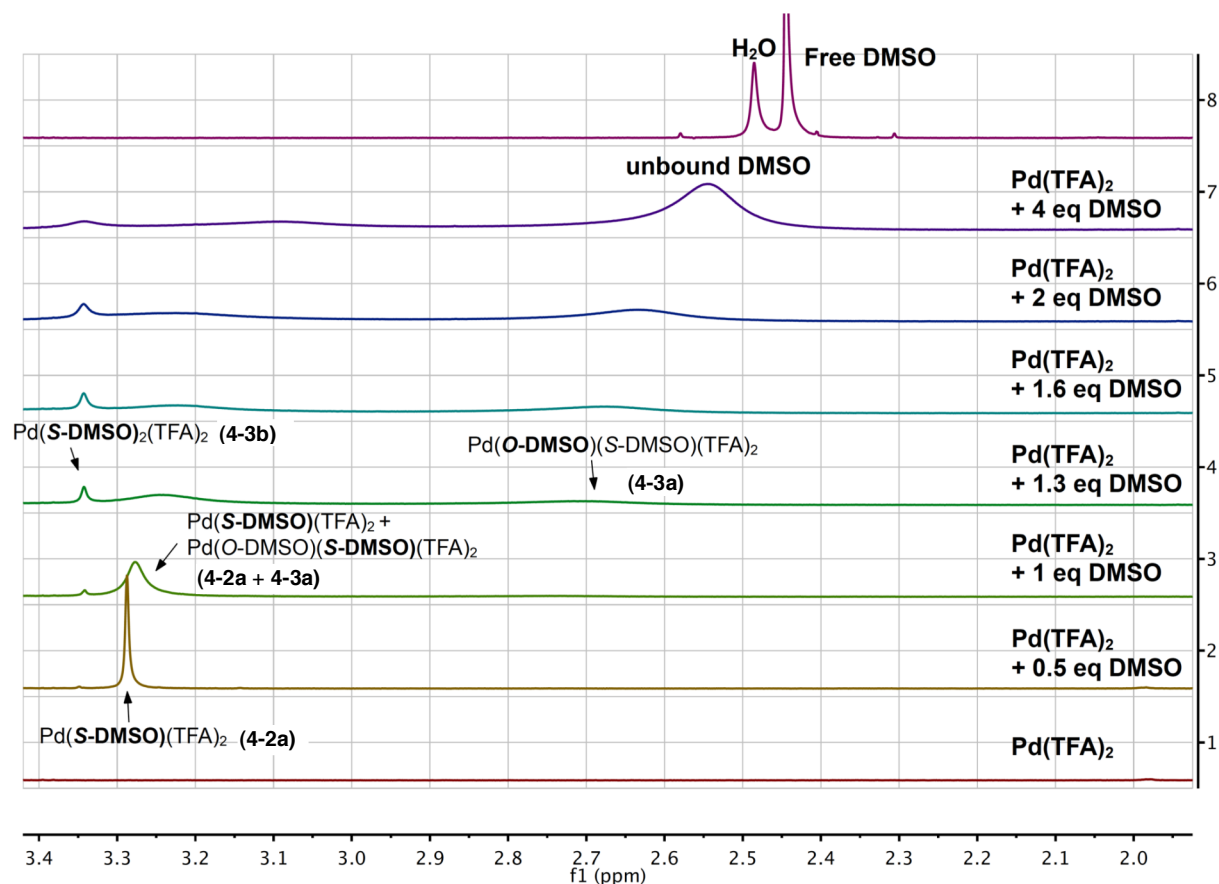


Figure 4-15. ^1H NMR spectra of $\text{Pd}(\text{TFA})_2$ in $\text{THF-}d_8$ with various quantities of DMSO at 24 °C. Conditions: $[\text{Pd}(\text{TFA})_2] = 15 \text{ mM}$ (3.3 mg, 0.01 mmol), $\text{THF-}d_8 = 0.65 \text{ mL}$, 24 °C, $[\text{DMSO}] = 0, 7.5, 15, 19.5, 24, 30$ and 60 mM .

The broad peak corresponding to **4-2a** and **4-3a** exhibits a chemical shift that depends on the relative concentrations of **4-2a** and **4-3a**. We reasoned that with 0.5 equiv. of DMSO, when **4-3a** has not yet started to form, the peak at 3.29 ppm in the ^1H NMR spectrum and -74.73 ppm in the ^{19}F NMR spectrum arise solely from **4-2a**. With 4 equiv. DMSO, when **4-2a** is consumed, the peaks at 3.26 ppm in the ^1H NMR spectrum and -74.81 ppm in the ^{19}F NMR spectrum solely represent **4-3a**. The concentrations of **4-2a** and **4-3a** can be calculated on the basis of the chemical shift of the merged peaks, and the concentrations of all of the individual species are plotted as a

function of added DMSO in Figure 4-16. In the presence of ≥ 2 equiv. of DMSO at -60 °C, and equilibrium mixture of the two bis-DMSO coordinated Pd^{II} complexes, **4-3a** and **4-3b**, is present in very similar concentrations.

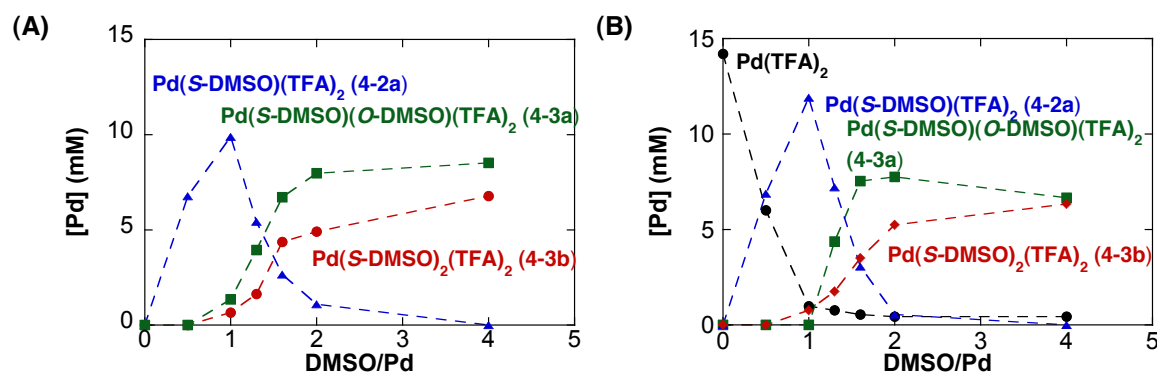
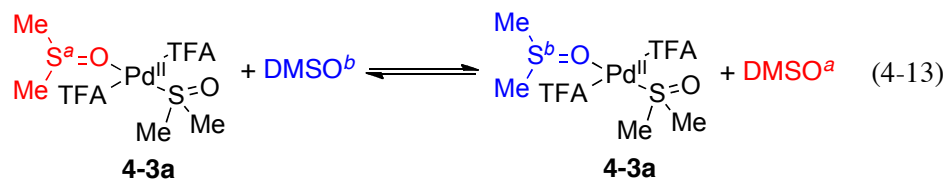
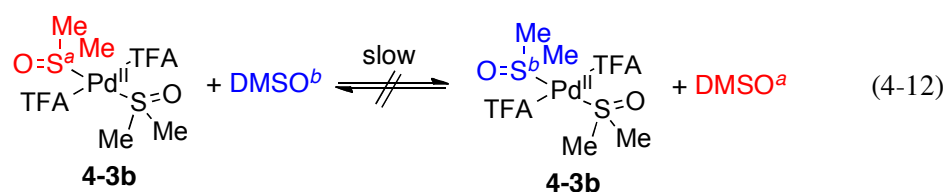


Figure 4-16. Titration curve of DMSO into the solution of Pd(TFA)₂ in THF-*d*₈. (A) Pd species derived from ¹H NMR spectra; (B) Pd species derived from ¹⁹F NMR spectra. Conditions: [Pd(TFA)₂] = 15 mM (3.3 mg, 0.01 mmol), THF-*d*₈ = 0.65 mL, -60 °C, [DMSO] = 0, 7.5, 15, 19.5, 24, 30 and 60 mM.

4.2.5 Comparison of the Kinetics of DMSO Ligand Exchange in EtOAc and THF-*d*₈

The interconversion between **4-2a** and **4-3a** (eq 4-8) resulted in line broadening of the separated peaks in EtOAc and coalescence of the peaks in THF-*d*₈. The rate of this process can be estimated by the peak width at half height, when the intensities of both peaks are equal.²⁶ At -60 °C, the concentrations of **4-2a** and **4-3a** are approximately equal when 1.3 and 1.4 equiv. of DMSO are present in EtOAc and THF-*d*₈, respectively. The exchange rates are calculated to be 3.3 sec⁻¹ and 116 sec⁻¹, in EtOAc and THF-*d*₈, respectively, based on the ¹⁹F NMR spectra under these conditions.²⁷ These results, showing that ligand exchange in THF-*d*₈ is substantially faster than in EtOAc, can be rationalized by a solvent-catalyzed ligand exchange mechanism, in which the better coordination ability of THF²⁸ relative to EtOAc leads to faster exchange.²⁹

The exchange between bound and unbound DMSO was analyzed by 1D NOESY saturation-transfer experiments, commonly called 1D EXSY (Exchange Spectroscopy).³⁰ When 3 equiv. of DMSO are added to Pd(TFA)₂ in EtOAc or THF-*d*₈, the solutions contain a mixture of **4-3a**, **4-3b** and unbound DMSO. The EXSY experiments performed on these solution at -60 °C reveal that saturation of the signal of **4-3b** does not affect other peaks. In contrast, excitation of **4-3a** causes inversion of the signal for the unbound DMSO (Figures 4-21 and 4-22). The lack of saturation transfer of **4-3b** to other species indicates that the DMSO ligands on **4-3b** are not exchanging with the unbound DMSO on the time scale of this experiment (eq 4-12). In contrast, the saturation transfer from **4-3a** to the unbound DMSO suggests that the DMSO ligand on **4-3a** undergoes fast exchange with the unbound DMSO (eq 4-13). These results have shown that the *O*-bound DMSO ligands are kinetically more labile than *S*-bound DMSO ligands. The exchange of both *O*- and *S*-bound DMSO ligands with free DMSO has been previously observed in a solution of [Pd(bpy)(DMSO)Cl][PF₆] in CD₃NO₂ at 35 °C.¹²



4.2.6 Solution Structures of Pd(TFA)₂/DMSO in AcOH-*d*₄ and Toluene-*d*₈

Pd-catalyzed aerobic oxidation reactions with Pd(TFA)₂/DMSO catalyst systems have also been carried out in AcOH and toluene (eqs 4-1 and 4-4); however, NMR spectroscopic analyses of mixtures of Pd(TFA)₂ and DMSO suggest that DMSO coordination to Pd^{II} is not as favorable in these solvents as in EtOAc and THF (Figure 4-17). Upon addition of 1 equiv. of DMSO to Pd(TFA)₂ in AcOH-*d*₄, unbound DMSO (2.77 ppm) is the major DMSO species, evident in the ¹H NMR spectrum. Smaller broad peaks present at 3.27–3.56 ppm suggest the presence of a mixture of minor *S*-bound DMSO-ligated Pd^{II} species (cf. Table 4-1). ¹⁹F NMR spectra obtained from the titration experiments similarly exhibit a mixture of different species (Figure 4-18). Integration of the bound DMSO peaks approaches a 1:1 DMSO:Pd stoichiometry, but only after addition 20 equiv. of DMSO (Figure 4-19). Possible structures consistent with a 1:1 DMSO:Pd stoichiometry include the monomeric and dimeric species **4-2a** and **4-2b** (see above). The high freezing point of AcOH-*d*₄ limits the utility of variable-temperature studies to gain further insights into this system.

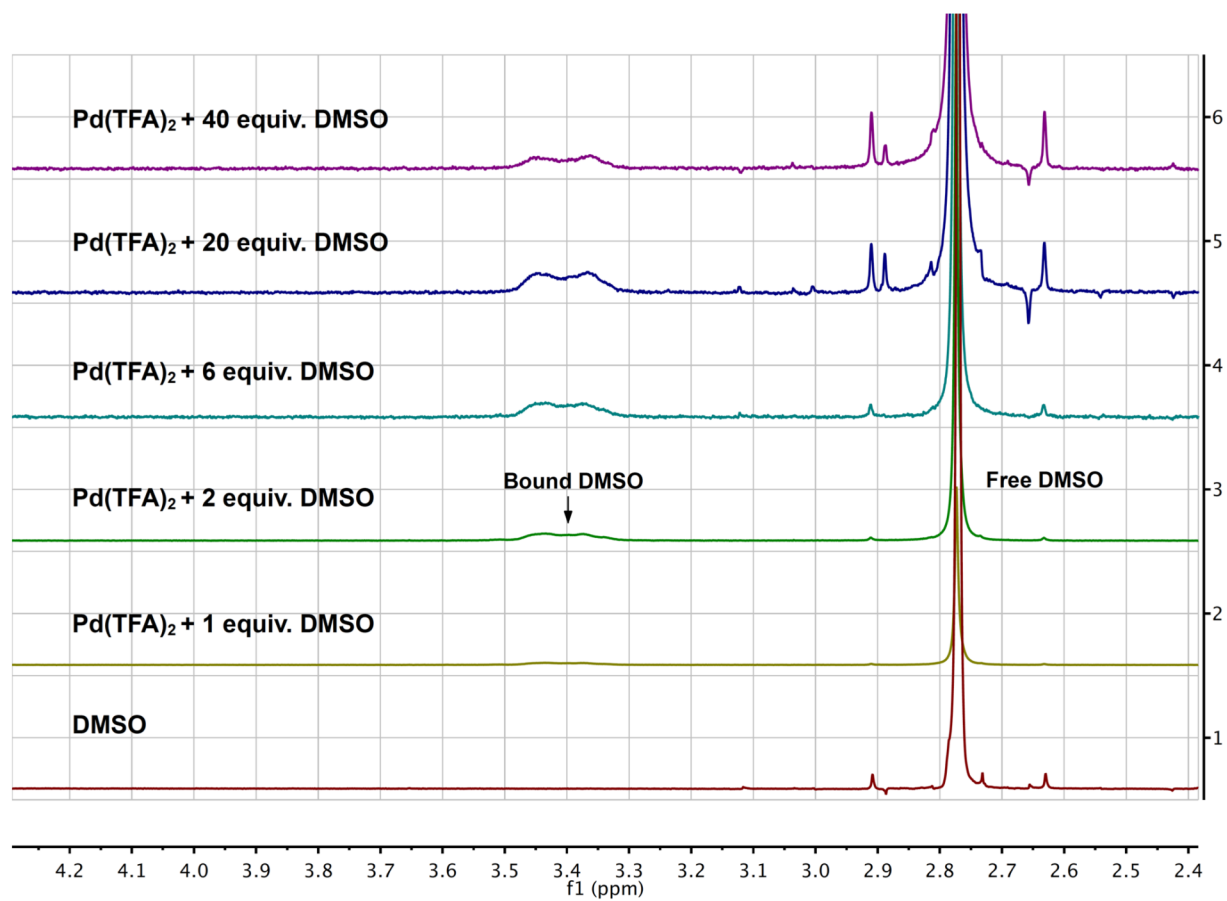


Figure 4-17. ^1H NMR spectra of $\text{Pd}(\text{TFA})_2$ in $\text{AcOH}-d_4$ with various quantities of DMSO at 24 $^\circ\text{C}$. Conditions: $[\text{Pd}(\text{TFA})_2] = 15$ mM (3.3 mg, 0.01 mmol), $\text{AcOH}-d_4 = 0.65$ mL, 24 $^\circ\text{C}$, $[\text{DMSO}] = 0, 15, 30, 90, 300$ and 600 mM.

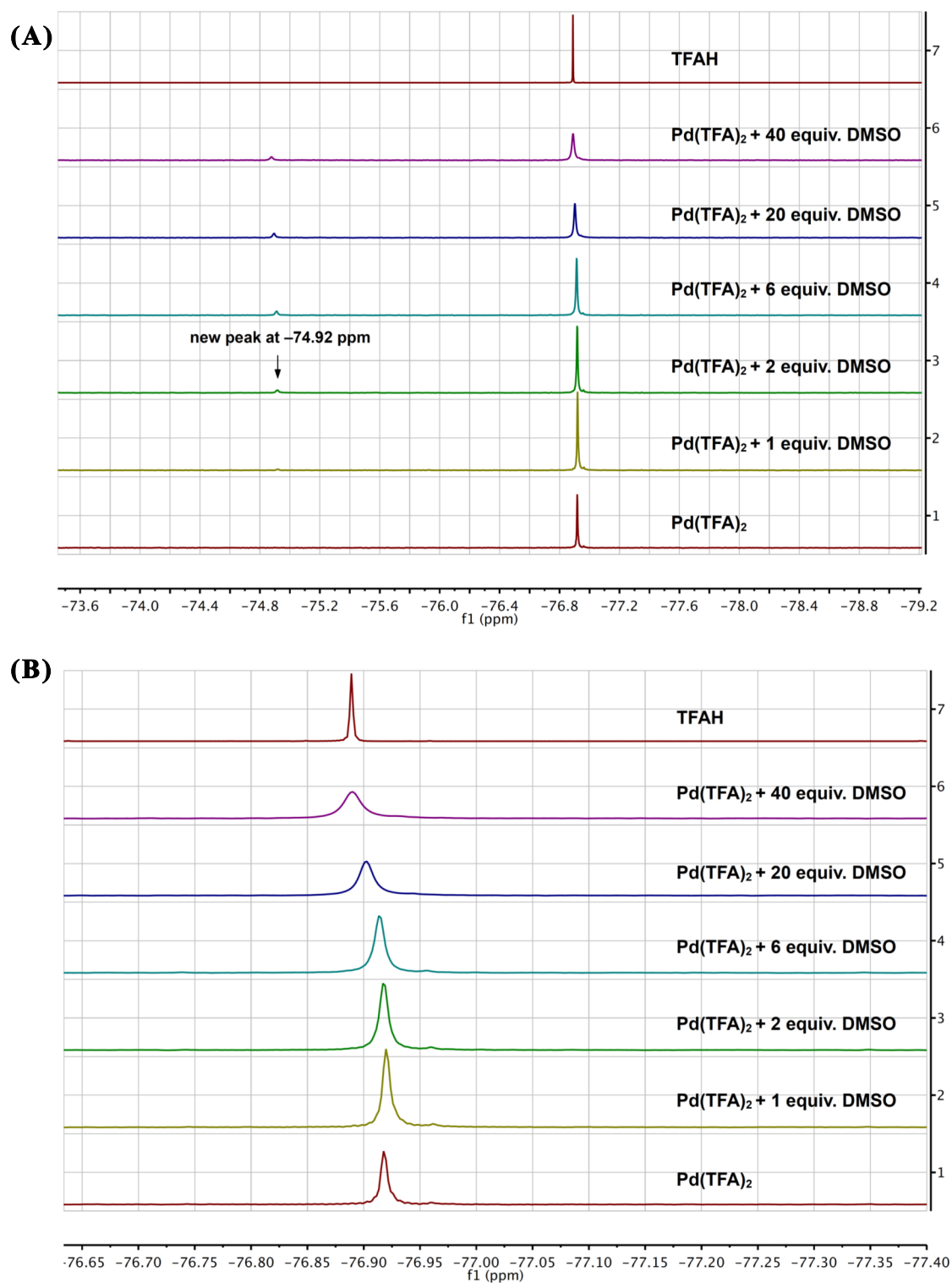


Figure 4-18. ^{19}F NMR spectra of $\text{Pd}(\text{TFA})_2$ in $\text{AcOH-}d_4$ with various quantities of DMSO at 24 $^\circ\text{C}$. (A) spectra on fully scale; (B) zoomed-in spectra. Conditions: $[\text{Pd}(\text{TFA})_2] = 15 \text{ mM}$ (3.3 mg, 0.01 mmol), $\text{AcOH-}d_4 = 0.65 \text{ mL}$, 24 $^\circ\text{C}$, $[\text{DMSO}] = 0, 15, 30, 90, 300$ and 600 mM.

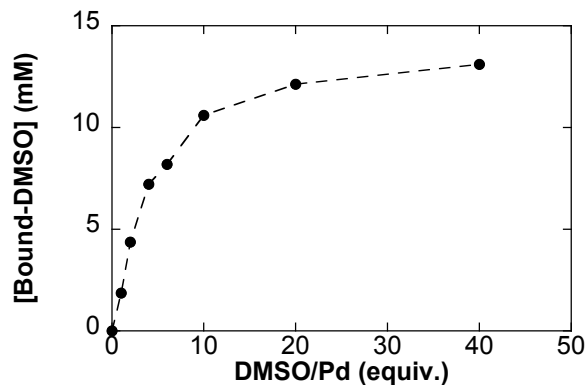


Figure 4-19. Titration curves of DMSO into the solution of Pd(TFA)₂ in AcOH-*d*₄ at 24 °C. Conditions: [Pd(TFA)₂] = 15 mM (3.3 mg, 0.01 mmol), AcOH-*d*₄ = 0.65 mL, 24 °C, [DMSO] = 0, 15, 30, 90, 300 and 600 mM.

Pd(TFA)₂ does not dissolve readily in toluene-*d*₈. Addition of 2 equiv. of DMSO to the suspension of Pd(TFA)₂ in toluene-*d*₈ leads to a bright yellow solution but does not fully dissolve Pd(TFA)₂. These observations indicate that DMSO coordinates to Pd(TFA)₂; however, a ¹H NMR spectrum of this suspension reveals a broad resonance in the region of free DMSO as the major species (Figure 4-20). A mixture of broad DMSO peaks approximately 0.6 ppm downfield of free DMSO supports the presence of *S*-bound DMSO ligands coordinated to Pd^{II}. Further characterization of this system was not pursued because of complications associated with the heterogeneity of this system.

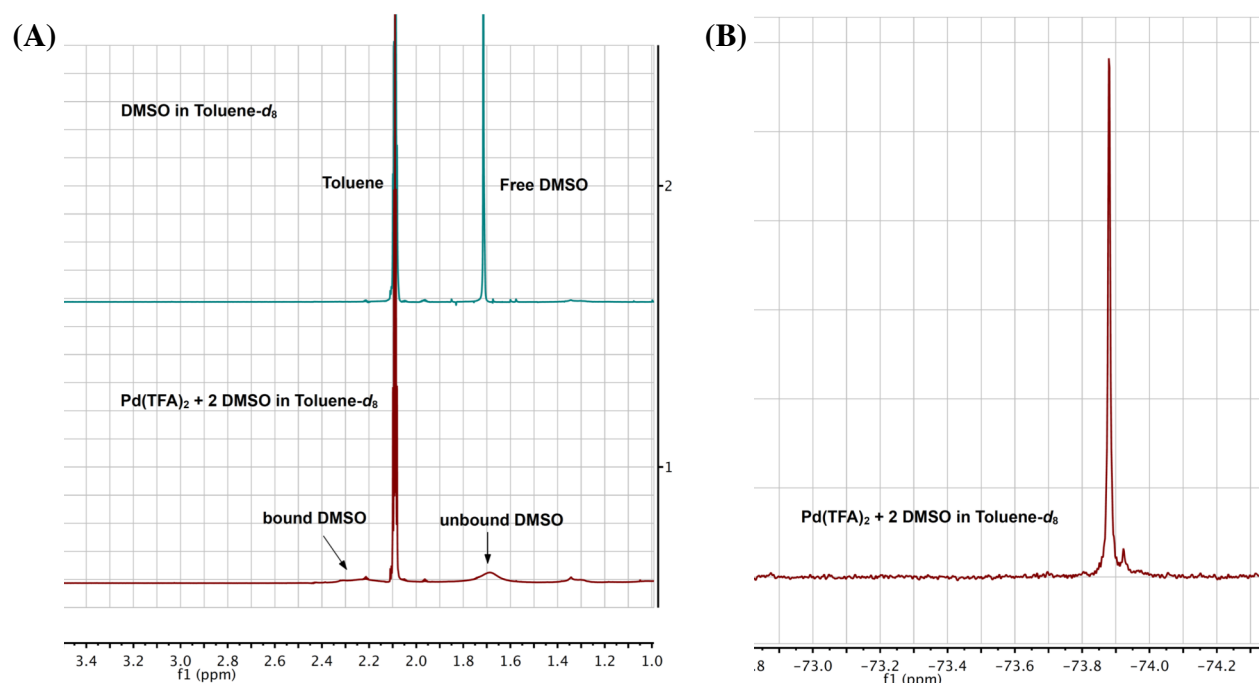


Figure 4-20. NMR spectra of Pd(TFA)₂/DMSO in toluene-*d*₈ at 24 °C. (A) ¹H NMR spectrum; (B) ¹⁹F NMR spectrum. Conditions: [Pd(TFA)₂] = 15 mM (3.3 mg, 0.01 mmol), [DMSO] = 30 mM (2 equiv.), toluene-*d*₈ = 0.65 mL, 24 °C.

4.2.7 Summary and Analysis

The coordination chemistry of the Pd(TFA)₂/DMSO catalyst system in various solvents highlights the complexity of DMSO coordination to Pd^{II} and subtle, but potentially important, difference between the linkage-isomer coordination modes of DMSO in solution relative to the solid state. The solid-state structure of *trans*-Pd(DMSO)₂(TFA)₂ exhibits one *S*- and one *O*-bound DMSO ligand, whereas our solution-state studies suggest that the structure with two *S*-bound DMSO ligands is nearly isoenergetic in EtOAc and THF (cf. Figures 4-6 and 4-13). When only 1 equiv. of DMSO is present, both the crystallographic and solution-phase spectroscopic data show that DMSO coordinates to Pd^{II} via the sulfur atom.

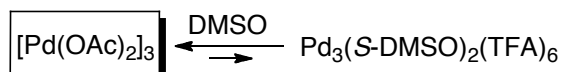
The solvent identity has a significant impact on the Pd(TFA)₂/DMSO coordination chemistry. In Scheme 4-2, the major Pd^{II} complexes formed in the presence of 2 equiv. of DMSO in different solvents are highlighted in boxes. In EtOAc and THF-*d*₈, DMSO coordination to Pd affords an equilibrium mixture of monomeric Pd(DMSO)₂(TFA)₂ linkage isomers. DMSO coordinates less effectively to Pd(OAc)₂, relative to Pd(TFA)₂, and also less effectively to Pd(TFA)₂ in AcOH and toluene, relative to EtOAc and THF-*d*₈. In these cases, the substoichiometric coordination of DMSO to Pd^{II} is evident from the spectroscopic data, probably reflecting the presence of bi- or trinuclear Pd^{II}-carboxylate species that are not fully cleaved by DMSO.

Scheme 4-2. Summary of Solution Structures of Pd(TFA)₂/DMSO in Various Solvents

Pd(TFA)₂/DMSO in EtOAc and THF



Pd(OAc)₂/DMSO in EtOAc



Pd(TFA)₂/DMSO in AcOH and Toluene



O-Bound DMSO ligands are considerably more labile than *S*-bound DMSO in Pd(TFA)₂/DMSO complexes. It seems reasonable that *O*- and *S*-bound DMSO ligands may work cooperatively in successful catalytic reactions. For example, a labile *O*-DMSO ligand might be important to enable weakly coordinating L-type ligands such as carbonyl oxygen atoms, alkenes,

sulfonamide nitrogen atoms, and arene C–H bonds (cf. eqs 4-1 to 4-4) to access the coordination sphere of Pd^{II}. This insight might explain the lack of catalytic activity exhibited by Pd(TFA)₂ coordinated with a bidentate bis(phenylsulfinyl)ethane ligand in dehydrogenation and oxidative amination.^{7,8} This ligand coordinates to Pd^{II} via the sulfur atom of the two sulfoxides.³¹ On the other hand, the more-strongly-coordinating *S*-DMSO ligand might be important in other steps of the catalytic mechanism. For example, the present studies do not address DMSO coordination to Pd⁰; however, the "softer" character of Pd⁰ relative to Pd^{II} suggests that DMSO will coordinate to Pd⁰ preferentially via the sulfur atom.⁵ Such coordination of DMSO to Pd⁰ should stabilize the Pd⁰ intermediate by inhibiting its aggregation into Pd black and facilitating oxidation of the catalyst by O₂. We speculate that the beneficial effect of DMSO in catalytic reactions carried out in AcOH and toluene might reflect this interaction of DMSO with Pd⁰, despite the poor coordinating ability of DMSO to Pd^{II} in these solvents.

4.3 Experimental

4.3.1 General Considerations and Procedures

All commercially available compounds were ordered from Sigma-Aldrich except for Pd(TFA)₂, which was obtained from Strem. EtOAc was purified by fractional distillation under N₂. All samples were prepared and experiments carried out in air.

¹H and ¹⁹F NMR spectra were acquired on a Varian INOVA-500 MHz spectrometer. The chemical shifts (δ) of ¹H NMR spectra are given in parts per million and referenced to solvent, non-deuterated CH₃CO₂Et (2.05 ppm) and the residual C3/C4 ethylene protons of THF-*d*₈ (1.73 ppm). The chemical shifts (δ) in the ¹⁹F NMR spectra were referenced relative to the corresponding ¹H spectra. Spectra were processed with MestReNovaTM software. Infrared spectra

were obtained with a Bruker Tensor 27 spectrometer equipped with a single reflection MIRacle Horizontal ATR ZnSe crystal by Pike Technologies.

Preparation of Pd(*S*-DMSO)(*O*-DMSO)(TFA)₂ 4-3a(s). Crystals of Pd(*S*-DMSO)(*O*-DMSO)(TFA)₂ were obtained by vapor diffusion of hexane into an EtOAc solution of Pd(TFA)₂ and 2 equiv. of DMSO at room temperature. Pd(TFA)₂ (8.4 mg, 0.25 mmol) was dissolved in 0.5 mL of EtOAc, forming a deep red solution. The solution turned bright yellow upon addition of DMSO (3.6 μL, 0.5 mmol). This solution was filtered through glass wool into a 4 mL vial and then transferred into a 15 mL vial containing 4 mL hexane. The vial was sealed with a Teflon cap and maintained at room temperature overnight. Deep orange crystalline needles formed.

Preparation of the Pd(*S*-DMSO)(OH₂)(TFA)₂ Complex 4-2a(s). Crystalline Pd(*S*-DMSO)(OH₂)(TFA)₂ was obtained by vapor diffusion of pentane into an EtOAc solution of Pd(TFA)₂ and 1 equiv. of DMSO at low temperature. Pd(TFA)₂ (8.4 mg, 0.25 mmol) was dissolved in 0.5 mL of EtOAc to form a deep red solution. Upon addition of DMSO (1.8 μL, 0.25 mmol), the solution turned bright yellow. The solution was filtered through glass wool into a 4 mL vial, and then transferred into a 15 mL vial containing 4 mL pentane. The vial was sealed with a Teflon cap and placed in refrigerator at -15 °C. After 4 days, orange crystalline needles formed.

NMR Spectroscopic Study of Pd(TFA)₂/DMSO in EtOAc. Pd(TFA)₂ (6.6 mg, 0.02 mmol) was weighed into a vial, followed by injection of EtOAc (0.64 mL). The suspension transformed into a deep red solution upon sonicating for 10 min. Fluorobenzene (4 μL, 0.041 mmol) was injected as an internal standard. The solution was transferred into an NMR tube. The spectrometer probe was pre-cooled to the desired temperature and allowed to equilibrate for 30 minutes. The sample was unlocked and the ¹H channel was used to perform gradient shimming. A ¹H NMR spectrum was acquired followed by tuning the probe for ¹⁹F and acquiring a ¹⁹F NMR spectrum.

Additional quantities of DMSO were then added from a stock solution into the same sample. The volume change caused by titration was controlled to be less than 5% over the course of the experiments.

NMR Spectroscopy Study of Pd(TFA)₂/DMSO in THF-*d*₈. Pd(TFA)₂ (3.3 mg, 0.01 mmol) was weighed into a vial. THF-*d*₈ (0.64 mL) was injected to form a deep red solution and then fluorobenzene (4 μL, 0.041 mmol) was added as an internal standard. The solution was transferred into an NMR tube. The spectrometer probe was pre-cooled to the desired temperature and allowed to equilibrate for 30 minutes. A ¹H NMR spectrum was acquired followed by tuning the probe for ¹⁹F and acquiring a ¹⁹F NMR spectrum. Additional quantities of DMSO were then added from a stock solution into the same sample. The volume change caused by titration was controlled to be less than 5% over the course of the experiments.

This procedure was also used for the NMR Spectroscopy studies of Pd(TFA)₂/DMSO in AcOH-*d*₄ and Pd(OAc)₂/DMSO in EtOAc.

NMR Spectroscopy Study of Pd(TFA)₂/DMSO in toluene-*d*₈. Pd(TFA)₂ (3.3 mg, 0.01 mmol) was weighed out in a vial and formed a suspension with addition of toluene-*d*₈ (0.64 mL). Pd(TFA)₂ dissolved to afford a yellow solution upon addition of 2 equiv. of DMSO. Fluorobenzene (4 μL, 0.041 mmol) was injected as the internal standard. The NMR spectra were acquired the same way as described above.

4.3.2 Investigation of the DMSO Ligand Exchange in EtOAc and THF-*d*₈

We performed 1D EXSY NMR experiments in order to determine if the equilibriums shown in eqs 4-12 and 4-13 are occurring in EtOAc or THF solutions of Pd(TFA)₂ in the presence of 3 equiv. of DMSO. At -60 °C, when 3 equiv. of DMSO are present, **4-3a**, **4-3b** and the unbound DMSO are the major species in both EtOAc and THF-*d*₈. Each peak of these species was excited

(denoted by an arrow in the spectra) (Figures 4-21 and 4-22). The 1D EXSY experiments reveal that saturation of the signal of **4-3b** does not affect other peaks. In contrast, when **4-3a** is excited, the unbound DMSO is inverted, which corresponds to saturation transfer from **4-3a** to the free DMSO. Consistently, saturation transfer from the free DMSO to **4-3a** was also observed when the free DMSO was excited, whereas the **4-3b** peak was not affected.

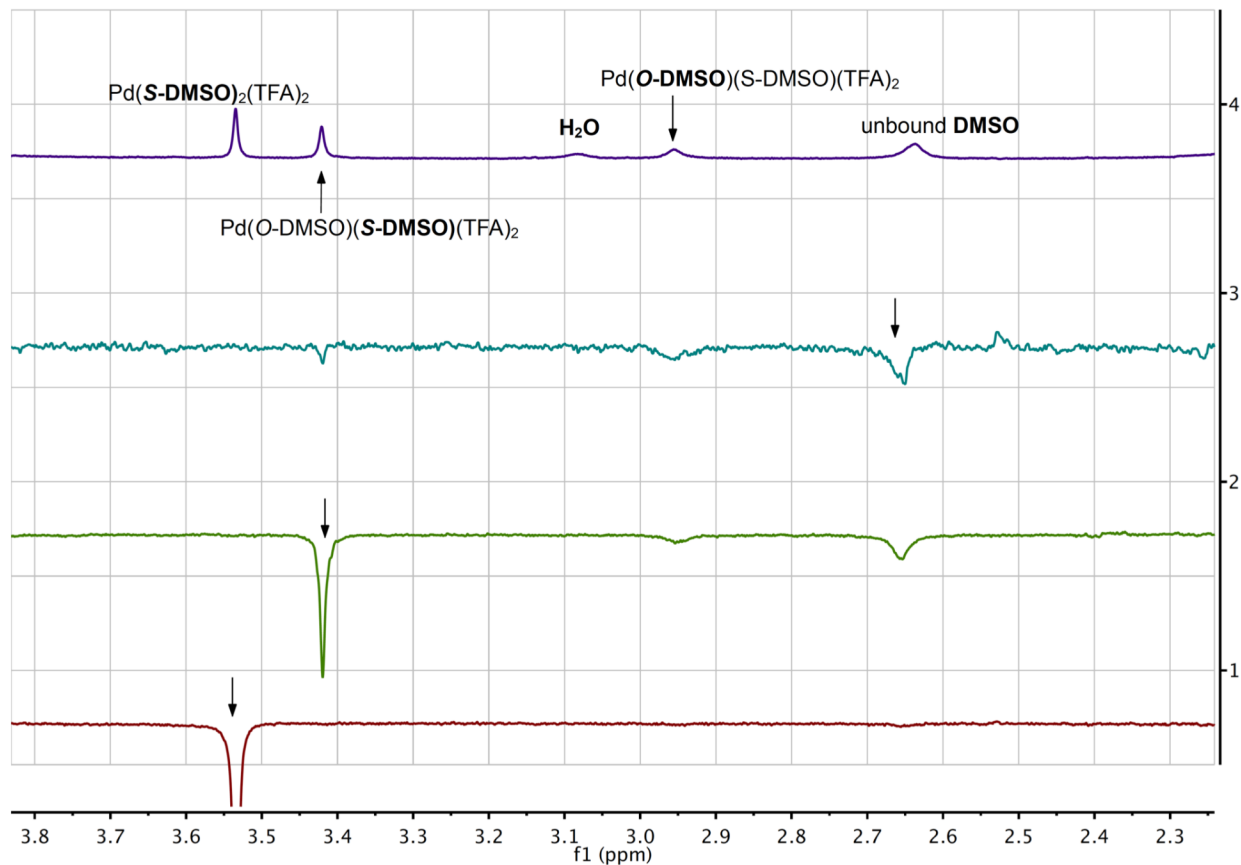


Figure 4-21. 1D EXSY NMR spectra of $\text{Pd}(\text{TFA})_2$ with 3 equiv. of DMSO in EtOAc (mix time = 0.28 sec). Conditions: $[\text{Pd}(\text{TFA})_2] = 30 \text{ mM}$ (6.6 mg, 0.02 mmol), $[\text{DMSO}] = 90 \text{ mM}$ (3 equiv.), EtOAc = 0.65 mL, $-60 \text{ }^\circ\text{C}$.

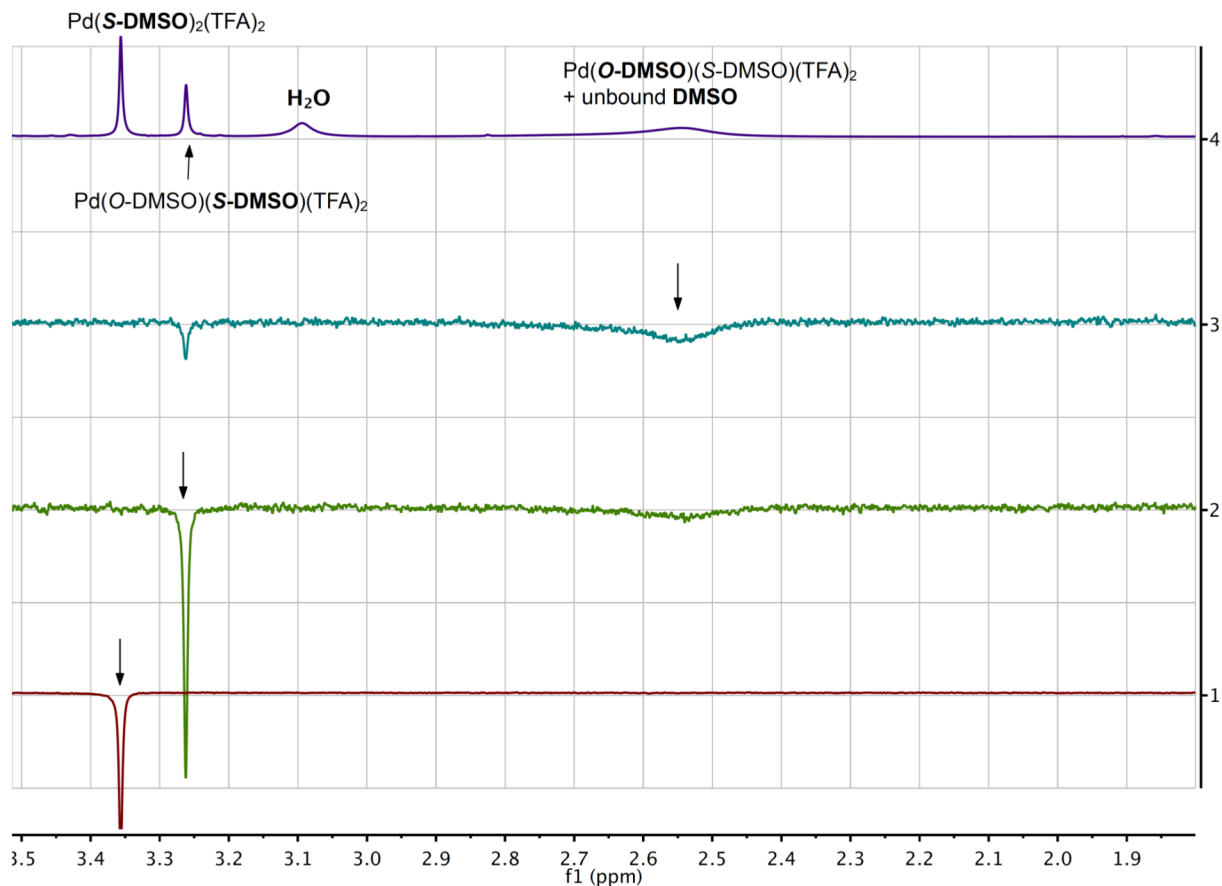


Figure 4-22. 1D EXSY NMR spectra of $\text{Pd}(\text{TFA})_2/\text{DMSO}$ in $\text{THF-}d_8$ (mix time = 0.25 sec). Conditions: $[\text{Pd}(\text{TFA})_2] = 15 \text{ mM}$ (3.3 mg, 0.01 mmol), $[\text{DMSO}] = 45 \text{ mM}$ (3 equiv.), $\text{THF-}d_8 = 0.65 \text{ mL}$, $-60 \text{ }^\circ\text{C}$.

Calculation of the rate constants for DMSO ligand exchange in EtOAc and $\text{THF-}d_8$ was based on the peak line broadening in NMR spectra. The Pd^{II} complexes, $\text{Pd}(\text{S-DMSO})(\text{TFA})_2$ **4-2a** and $\text{Pd}(\text{S-DMSO})(\text{O-DMSO})(\text{TFA})_2$ **4-3a**, undergo fast exchange on the NMR time scale (eq 4-8). This exchange process leads to line broadening of the ^1H peaks in EtOAc and a coalescence in $\text{THF-}d_8$ at $-60 \text{ }^\circ\text{C}$. The kinetics of the exchange process could be measured by the extent of line-broadening. Before coalescence, faster exchange results in broader peaks; after coalescence, faster exchange results in sharper peaks. When the intensities of the two exchanging species are equivalent, the following equations shown in Scheme 4-3 can be used to quantify the kinetics.

Scheme 4-3. Equations for Calculation of Ligand Exchange Rates Based on Line Broadening

For broadening of a single peak well before coalescence

$$k = \pi(\Delta\nu - \Delta\nu_{\text{ref}})$$

For residual broadening of a peak after coalescence

$$k = \frac{\pi \nu_{\text{AB}}^2}{2(\Delta\nu - \Delta\nu_{\text{ref}})}$$

$\Delta\nu$ = peak width at half height of exchanging singlet

$\Delta\nu_{\text{ref}}$ = peak width at half height of non-exchanging reference singlet

ν_{AB} = chemical shift (in Hz) between A and B

k = rate constant in sec^{-1}

The peak widths at half-height of the peaks of interest have been determined and are presented in Table 4-2. In EtOAc, peaks for both **4-2a** and **4-3a** are used in the calculation (Scheme 4-4). Since **4-3b** doesn't undergo ligand dissociation, the peak width of **4-3b** was used as the $\Delta\nu_{\text{ref}}$ for experiments in EtOAc. In THF, the ^{19}F singlet of trifluorotoluene was used as the internal standard for the ^{19}F NMR spectrum. The peak width of the internal standard was used as the $\Delta\nu_{\text{ref}}$.

Table 4-2. Estimated Rate Constants for the Equilibrium Between **4-2a** and **4-3a** Derived from the Peak Line Broadening^a

Solvent	Peak width at half height			k (sec^{-1})
	$\Delta\nu$ (Hz)			
EtOAc (before coalescence)	4-3b	4-2a	4-3a	4.02 (4-2a)
	4.22 ($\Delta\nu_{\text{ref}}$)	5.50	5.07	2.67 (4-3a)
				$k_{\text{avg}} = 3.34$
THF (after coalescence)	Trifluorotoluene	4-2a + 4-3a		
	4.64 ($\Delta\nu_{\text{ref}}$)	29.68		116

^aReaction conditions: in EtOAc, $[\text{Pd}(\text{TFA})_2] = 30$ mM (6.6 mg, 0.02 mmol), $[\text{DMSO}] = 39$ mM (1.3 equiv.), -60 °C. In THF- d_8 , $[\text{Pd}(\text{TFA})_2] = 15$ mM (3.3 mg, 0.01 mmol), $[\text{DMSO}] = 21$ mM (1.4 equiv.), internal standard: trifluorotoluene (^{19}F), -60 °C.

Scheme 4-4. Representative Equations for DMSO Ligand Exchange Rates

For Pd(TFA)₂/DMSO in EtOAc (before coalescence)

$$\begin{aligned} k &= \pi(\Delta\nu - \Delta\nu_{\text{ref}}) \\ &= \pi(5.50 - 4.22) \\ &= 4.02 \text{ sec}^{-1} \end{aligned}$$

For Pd(TFA)₂/DMSO in THF (after coalescence)

$$\begin{aligned} k &= \frac{\pi \nu_{\text{AB}}^2}{2(\Delta\nu - \Delta\nu_{\text{ref}})} \\ &= \frac{\pi 43.09^2}{2(29.64 - 4.64)} \\ &= 116 \text{ sec}^{-1} \end{aligned}$$

4.4 Contributions

Paul White performed calculations on the ground state structure of Pd(TFA)₂/DMSO complexes in various solvents. These results are not included in this chapter. Iliia Guzei solved the X-ray crystal structure of **4-2a(s)**. Lara Spencer solved the X-ray crystal structure of **4-3a(s)**.

4.5 References

-
- (a) Stahl, S. S. *Angew. Chem., Int. Ed.* **2004**, *43*, 3400-3420. (b) Stahl, S. S. *Science* **2005**, *309*, 1824-1826. (c) Gligorich, K. M.; Sigman, M. S. *Chem. Commun.* **2009**, 3854-3867. (d) Shi, Z.; Zhang, C.; Tang, C.; Jiao, N. *Chem. Soc. Rev.* **2012**, *41*, 3381-3430.
 - (a) Larock, R. C.; Hightower, T. R. *J. Org. Chem.* **1993**, *58*, 5298-5300. (b) van Benthem, R. A. T. M.; Hiemstra, H.; Michels, J. J.; Speckamp, W. N. *J. Chem. Soc., Chem. Commun.* **1994**, 357-359.

3. For representative examples, see refs 2a,b and the following: (a) Rönn, M.; Bäckvall, J.-E.; Andersson, P. G. *Tetrahedron Lett.* **1995**, *36*, 7749-7752. (b) R. C. Larock, T. R. Hightower, L. A. Hasvold, K. P. Peterson, *J. Org. Chem.* **1996**, *61*, 3584. (c) Toyota, M.; Ihara, M. *Synlett* **2002**, *8*, 1211-1222.

4. (a) Steinhoff, B. A.; Fix, S. R.; Stahl, S. S. *J. Am. Chem. Soc.* **2002**, *124*, 766-767. (b) Steinhoff, B. A.; Stahl, S. S. *J. Am. Chem. Soc.* **2006**, *128*, 4348-4355.

5. Zierkiewicz, W.; Privalov, T. *Organometallics* **2005**, *24*, 6019-6028.

6. For examples, see: (a) Grennberg, H.; Gogoll, A.; Bäckvall, J.-E. *J. Org. Chem.* **1991**, *56*, 5808-5811. (b) Bergstad, K.; Grennberg, H.; Bäckvall, J.-E. *Organometallics* **1998**, *17*, 45-50. (c) Chen, M. S.; White, M. C. *J. Am. Chem. Soc.* **2004**, *126*, 1346-1347. (d) Tanaka, D.; Romeril, S. P.; Myers, A. G. *J. Am. Chem. Soc.* **2005**, *127*, 10323-10333. (e) Hull, K. L.; Sanford, M. S. *J. Am. Chem. Soc.* **2007**, *129*, 11904-11905. (f) Delcamp, J. H.; Brucks, A. P.; White, M. C. *J. Am. Chem. Soc.* **2008**, *130*, 11270-11271. (g) Young, A. J.; White, M. C. *Angew. Chem. Int. Ed.* **2011**, *50*, 6824-6827.

7. Diao, T.; Stahl, S. S. *J. Am. Chem. Soc.* **2011**, *133*, 14566-14569.

8. (a) McDonald, R. I.; Stahl, S. S. *Angew. Chem. Int. Ed.* **2010**, *49*, 5529-5532. (b) Lu, Z.; Stahl, S. S. *Org. Lett.* **2012**, *14*, 1234-1237.

9. Brasche, G.; García-Fortanet, J.; Buchwald, S. L. *Org. Lett.* **2008**, *10*, 2207-2210.

10. For comprehensive reviews, see: (a) Calligaris, M.; Carugo, O. *Coord. Chem. Rev.* **1996**, *153*, 83-154. (b) Calligaris, M. *Coord. Chem. Rev.* **2004**, *248*, 351-375.

-
11. Dorta, R.; Rozenberg, H.; Milstein, D. *Chem. Commun.* **2002**, 710-711.
12. Annibale, G.; Cattalini, L.; Bertolasi, V.; Ferretti, V.; Gilli, G.; Tobe, M. L. *J. Chem. Soc., Dalton Trans.* **1989**, 1265-1271.
13. (a) Price, J. H.; Williamson, A. N.; Schramm, R. F.; Wayland, B. B. *Inorg. Chem.* **1972**, *11*, 1280-1284. (b) Davies, J. A.; Hartley, F. R.; Murray, S. G. *J. Chem. Soc., Dalton Trans.* **1979**, 1705-1708.
14. Davies, J. A. The Coordination Chemistry of Sulfoxides with Transition Metals. In *Advances in Inorganic Chemistry and Radiochemistry*; Emeléus, H. J., Sharpe, A. G., Eds.; Academic Press: New York, 1981; Vol. 24, pp. 115-187.
15. (A) Bennett, M. J.; Cotton, F. A.; Weaver, D. L.; Williams, R. J.; Watson, W. H. *Acta Crystallogr.* **1967**, *23*, 788-796. (b) Wayland, B. B.; Schramm, R. F. *Inorg. Chem.* **1969**, *8*, 971-976. (c) Price, J. H.; Schramm, R. F.; Wayland, B. B. *J. Chem. Soc. D: Chem. Comm.* **1970**, 1377-1378.
16. Stephenson, T. A.; Morehouse, S. M.; Powell, A. R.; Heffer, J. P.; Wilkinson, G. *J. Chem. Soc. (Resumed)* **1965**, 3632-3640.
17. Bancroft, D. P.; Cotton, F. A.; Verbruggen, M. *Acta Crystallogr. Sect. C* **1989**, *45*, 1289-1292.
18. Thomas, R.; Shoemaker, C. B.; Eriks, K. *Acta Crystallogr.* **1966**, *21*, 12-20.
19. Forel, M.-T.; Tranquille, M. *Spectrochim. Acta, A* **1970**, *26*, 1023-1034.

20. The peak at 3.08 ppm at $-60\text{ }^{\circ}\text{C}$ (Figure 4-5, spectrum 6) is assigned as unbound H_2O . This assignment is supported by the increased integration upon external addition of H_2O . The chemical shift of the unbound H_2O is 0.1 ppm downfield relative to the free H_2O in the absence of Pd complexes, possibly reflecting hydrogen-bonding interactions between H_2O and the carboxylate ligands on the Pd complexes.

21. Batsanov, A. S.; Timko, G. A.; Struchkov, Y. T.; Gerbeleu, N. V.; Indrichan, K. M.; Popovich, G. A. *Koord. Khim* **1989**, *15*, 688-693.

22. Stash, A. I.; Perepelkova, T. I.; Kravtsova, S. V.; Noskov, Yu. G.; Romm, I. P. *Russ. J. Coord. Chem.* **1998**, *24*, 36-39.

23. For an example of trifluoroacetate-bridged dimeric Pd sulfoxide complex, see: Ruger, R.; Rittner, W.; Jones, P. G.; Isenberg, W.; Sheldrick, G. M. *Angew. Chem. Int. Ed.* **1981**, *20*, 382-383.

24. For related complexes with other donor ligands, see: (a) Smith, R. C.; Woloszynek, R. A.; Chen, W.; Ren, T.; Protasiewicz, J. D. *Tetrahedron Lett.* **2004**, *45*, 8327-8330. (b) Vicente, J.; Saura-Llamas, I.; Palin, M. G.; Jones, P. G.; Ramrez de Arellano, M. C. *Organometallics* **1997**, *16*, 826-833.

25. (a) Ukhin, L. Yu.; Dolgoplova, N. A.; Kuz'mina, L. G.; Struchkov, Yu. T. *J. Organomet. Chem.* **1981**, *210*, 263-272. (b) Fuchita, Y.; Takahashi, K.; Kanehisa, N.; Shinkimoto, K.; Kai, Y.; Kasai, N. *Polyhedron* **1996**, *15*, 2777-2779. (c) Moyano, A.; Rosol, M.; Moreno, R. M.; Lpez, C.; Maestro, M. A. *Angew. Chem. Int. Ed.* **2005**, *44*, 1865-1869. (d) Giri, R.; Liang, J.; Lei, J.-G.; Li, J.-J.; Wang, D.-H.; Chen, X.; Naggar, I. C.; Guo, C.; Foxman, B. M.; Yu, J.-Q. *Angew. Chem.*

Int. Ed. **2005**, *44*, 7420-7424. (e) Friedlein, F. K.; Hampel, F.; Gladysz, J. A. *Organometallics* **2005**, *24*, 4103-4105. (f) Chitanda, J. M.; Prokopchuk, D. E.; Quail, J. W.; Foley, S. R. *Organometallics* **2008**, *27*, 2337-2345. (g) Bercaw, J. E.; Day, M. W.; Golisz, S. R.; Hazari, N.; Henling, L. M.; Labinger, J. A.; Schofer, S. J.; Virgil, S. *Organometallics* **2009**, *28*, 5017-5024. (h) Vázquez-García, D.; Fernández, A.; López-Torres, M.; Rodríguez, A.; Gómez-Blanco, N.; Viader, C.; Vila, J. M.; Fernández, J. J. *Organometallics* **2010**, *29*, 3303-3307.

26. (a) Gutowsky, H. S.; Holm, C. H. *J. Chem. Phys.* **1956**, *25*, 1228-1234. (b) Kost, D.; Carlson, E. H.; Raban, M. *J. Chem. Soc. D: Chem. Comm.* **1971**, 656-657.

27. Reaction conditions for exchange-rate studies: In EtOAc, [Pd(TFA)₂] = 30 mM (6.6 mg, 0.02 mmol), [DMSO] = 39 mM (1.3 equiv.), -60 °C. In THF-*d*₈, [Pd(TFA)₂] = 15 mM (3.3 mg, 0.01 mmol), [DMSO] = 21 mM (1.4 equiv.), -60 °C.

28. For studies of the coordinating ability of THF and the resulting effect on reactions, see: Lucht, B. L.; Collum, D. B. *Acc. Chem. Res.* **1999**, *32*, 1035-1042.

29. Crabtree, R. H. In *The Organometallic Chemistry of the Transition Metals*, 4th ed.; John Wiley & Sons: Hoboken, 2005.

30. Claridge, T. D. W. *High-Resolution NMR Techniques in Organic Chemistry*, 2nd ed.; Elsevier Science: Oxford, 2008.

31. Pettinari, C.; Pellei, M.; Cavicchio, G.; Crucianelli, M.; Panzeri, W.; Colapietro, M.; Cassetta, A. *Organometallics* **1999**, *18*, 555-563.

CHAPTER 5

Mechanistic Investigation of Pd(DMSO)₂(TFA)₂-Catalyzed Aerobic Dehydrogenation of Cyclohexanones

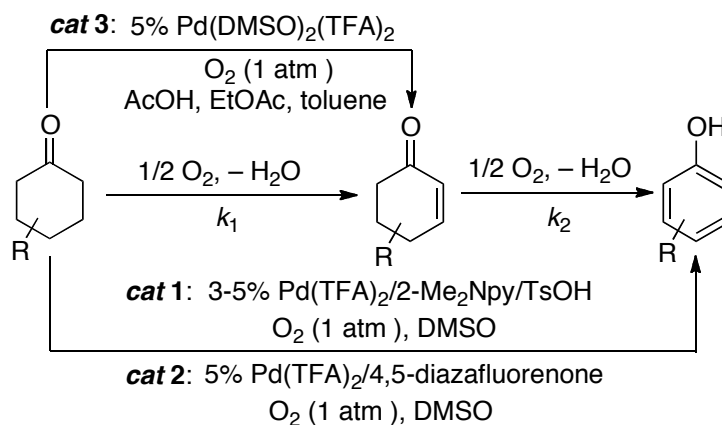
5.1 Introduction to Pd(DMSO)₂(TFA)₂-Catalyzed Aerobic Oxidation of Ketones

Dehydrogenation of saturated C–C bonds has emerged as an increasingly prominent approach to introduce C=C bonds into organic molecules. In particular, α,β -dehydrogenation of carbonyl compounds to prepare unsaturated carbonyl derivatives has found broad applications in organic syntheses.¹ Current stoichiometric oxidation methods, despite their wide utilities, produce large quantities of by-product.² Catalytic methods that use cheap and readily available oxidants would provide an appealing alternative, and could potentially have important impact in sustainable organic syntheses. While heterogeneous catalyzed H₂ evolution from ketones require high reaction temperatures and constant gas flow to remove H₂,^{3,4} transfer dehydrogenation employs a sacrificial alkene as the hydrogen acceptor to enhance the thermodynamic driving force.⁵ However, formation of inert metallacycles between α,β -unsaturated ketones and common transfer dehydrogenation catalysts, such as pincer ligated-Ir complexes, are shown to result in deactivation of the catalysts.^{6,7} Numerous studies of C–H activation by Pd, as well as β -hydride elimination from Pd-alkyls in recent decades⁸ provide the basis for Pd-mediated dehydrogenation of ketones.⁹ Employing O₂ as the hydrogen acceptor provides further leverage for Pd-mediated dehydrogenation, resulting in a sustainable and affordable catalytic approach for organic chemists.¹⁰

Catalytic dehydrogenation of a cyclohexanone could lead to cyclohexenone and/or phenol (Scheme 5-1). Both products are synthetically important, and we recently reported three different Pd^{II} catalyst systems for dehydrogenation adjacent to carbonyl groups, each of which exhibited somewhat different scope and utility. A Pd(TFA)₂/2-Me₂Npy (2-*N,N*-dimethylaminopyridine)/TsOH catalyst system exhibited good activity for dehydrogenation of cyclohexanones and cyclohexenones to phenols.¹¹ A Pd(TFA)₂/4,5-diazafluorenone catalyst

exhibited similar reactivity, but was especially useful for α,β -dehydrogenation of heterocyclic carbonyl compounds and showed some for dehydrogenation of acyclic carbonyl compounds.^{12,13} Finally, a $\text{Pd}(\text{DMSO})_2(\text{TFA})_2$ catalyst enabled highly selective dehydrogenation of cyclohexanones to cyclohexenones.¹⁴ The unique selectivity of $\text{Pd}(\text{DMSO})_2(\text{TFA})_2$ is clearly evident in the reactivity of cyclohexanone. The other two catalyst systems favor formation of phenol rather than cyclohexenone, and preliminary kinetic studies show that the first two catalysts promote further dehydrogenation of cyclohexenone to phenol (k_2) relative to the first dehydrogenation step (k_1). In contrast, with $\text{Pd}(\text{DMSO})_2(\text{TFA})_2$, the first step (k_1) is substantially faster than the second (k_2) (Scheme 5-1). These kinetic differences have important synthetic implications.

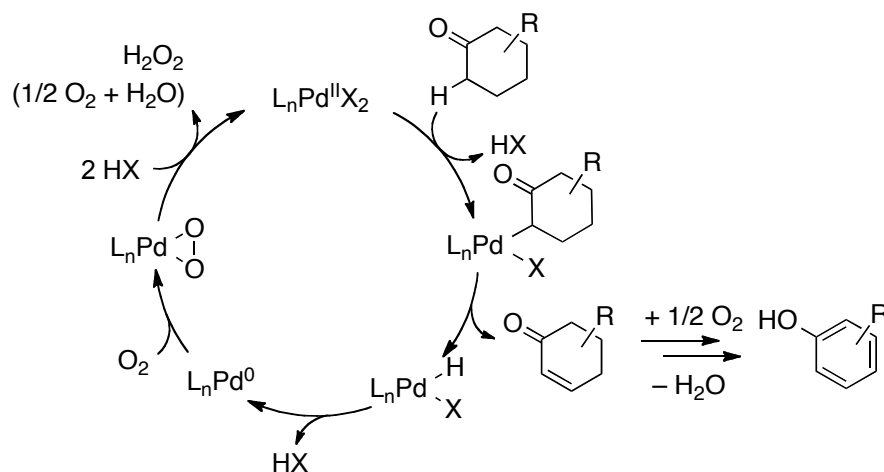
Scheme 5-1. Comparison of Rate Constants of the Oxidation of 4-*tert*-Butylcyclohexanone



Catalyst	Solvent	k_1/k_2
Cat. 1: $\text{Pd}(\text{TFA})_2/2\text{-Me}_2\text{Npy/TsOH}$	DMSO	< 1
Cat. 2: $\text{Pd}(\text{TFA})_2/4,5\text{-diazfluorenone}$	DMSO	< 1
Cat. 3: $\text{Pd}(\text{DMSO})_2(\text{TFA})_2$	AcOH, EtOAc, toluene	> 10

The mechanism of Pd-catalyzed α,β -dehydrogenation of carbonyl compounds is expected to be initiated by formation of a Pd-enolate intermediate,¹⁵ followed by β -hydride elimination to afford the enone (Scheme 5-2). Analogous to other Pd-catalyzed aerobic oxidation reactions, the resulting Pd-hydride intermediate can be oxidized to Pd^{II} by oxygen.¹⁶ A repeat of this sequence with the cyclohexenone as the substrate would lead to the corresponding phenol.¹⁷ We present here a detailed mechanistic study of the Pd(DMSO)₂(TFA)₂-catalyzed oxidation of cyclohexanone, aiming to shed light on three important mechanistic questions: (1) the identity of the turnover-limiting step; (2) the role of ligand in the catalyst system; (3) the origin of the chemoselectivity for enone relative to phenol.

Scheme 5-2. Proposed Mechanism for Pd-catalyzed Dehydrogenation of Cyclohexanones



5.2 Results

5.2.1 Kinetic Data of Pd(DMSO)₂(TFA)₂-Catalyzed Oxidation of Cyclohexanone

The catalytic dehydrogenation of cyclohexanone with Pd(DMSO)₂(TFA)₂ in EtOAc proceeds smoothly and reaches complete conversion after 24 h at 60 °C under 1 atm O₂ (Figure 5-1). The

time course data fit well to an $A \rightarrow B \rightarrow C$ kinetic model (Figure 5-1). Good mass balance reveals that negligible side reactions occur conservation of mass reveals that no side reaction is present. The rate constants for the first (k_1) and second (k_2) oxidation steps are estimated to be 0.131 h^{-1} and 0.125 h^{-1} , respectively, resulting in a ratio of 10 (k_1/k_2).

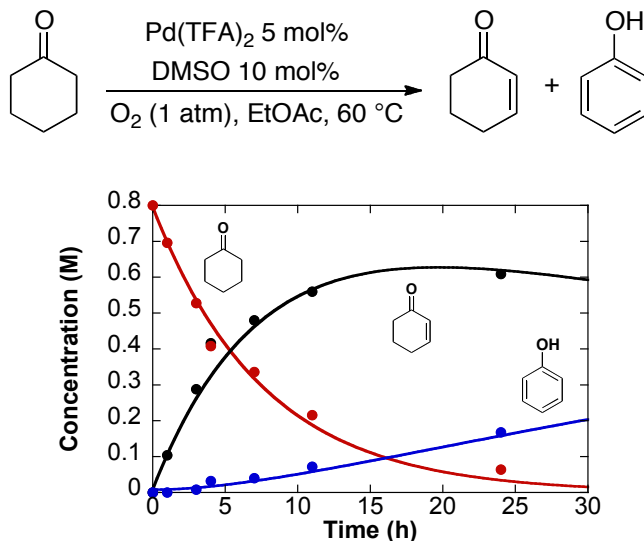


Figure 5-1. Reaction time course of Pd(DMSO)₂(TFA)₂-catalyzed aerobic oxidation of cyclohexanone. Reaction conditions: [cyclohexanone] = 0.8 M (0.8 mmol), [Pd(TFA)₂] = 0.04 M (0.04 mmol), [DMSO] = 0.08 M (0.08 mmol), O₂ (1 atm), EtOAc (1 mL), 60 °C.

The lack of an induction period in the reaction time course of Pd(DMSO)₂(TFA)₂-catalyzed oxidation of cyclohexanone allowed us to obtain kinetic orders of each reaction component via initial-rates methods. The conversion of enone to phenol was negligible within the first two turnovers and was thus neglected. The reaction exhibits a first order dependence on [substrate] and [catalyst] (Figure 5-2(A) and (B)). Attempts were made to assess the [O₂] dependence; however, the acquisition of results was complicated by Pd black formation in the gas-uptake apparatus used to monitor kinetics. Analysis of the O₂ dependence for 4-*tert*-

butylcyclohexanone under modified conditions, using AcOH as the solvent (cf. Figure 5-15), showed no dependence of the rate on $[O_2]$.

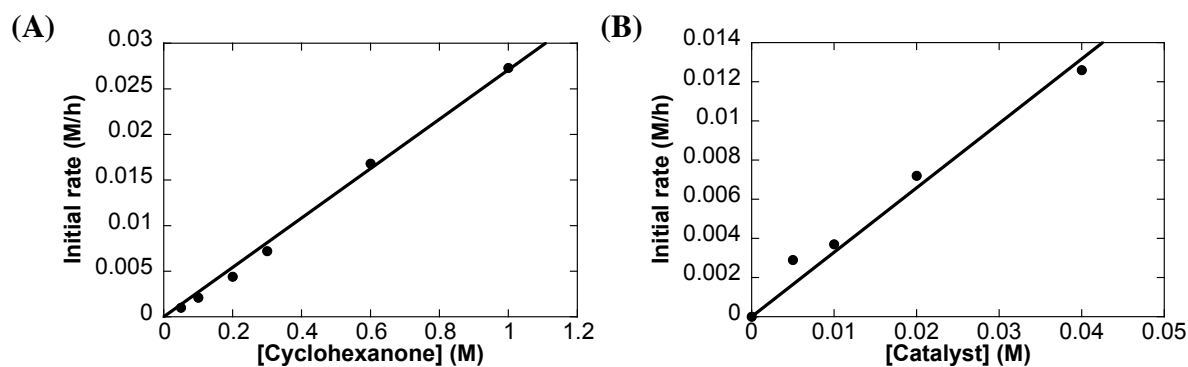


Figure 5-2. Kinetic orders for $Pd(DMSO)_2(TFA)_2$ -catalyzed oxidation of cyclohexanone to cyclohexenone: dependence of the initial rate on substrate concentration (A); dependence of the initial rate on catalyst concentration, where the “catalyst” is a 1:2 mixture of $Pd(TFA)_2$ and DMSO (B). Reaction conditions: EtOAc (1 mL), O_2 (1 atm), 60 °C; (A) $[Pd(TFA)_2] = 0.01$ M (0.01 mmol), $[DMSO] = 0.02$ M (0.02 mmol); (B) $[cyclohexanone] = 0.2$ M (0.2 mmol).

Variation of $[DMSO]$ at fixed $[cyclohexanone]$ and $[Pd(TFA)_2]$, revealed that changing the quantity of DMSO has minimal impact on the reaction rate (Figure 5-3(A)). Comparison of the time courses in the absence and presence of 2 equiv. of DMSO reveals that the catalyst undergoes rapid deactivation in the absence of DMSO (Figure 5-3(B)). Concomitant formation of Pd black was observed under these ligandless conditions. Increasing the concentration of DMSO results in less Pd black formation.

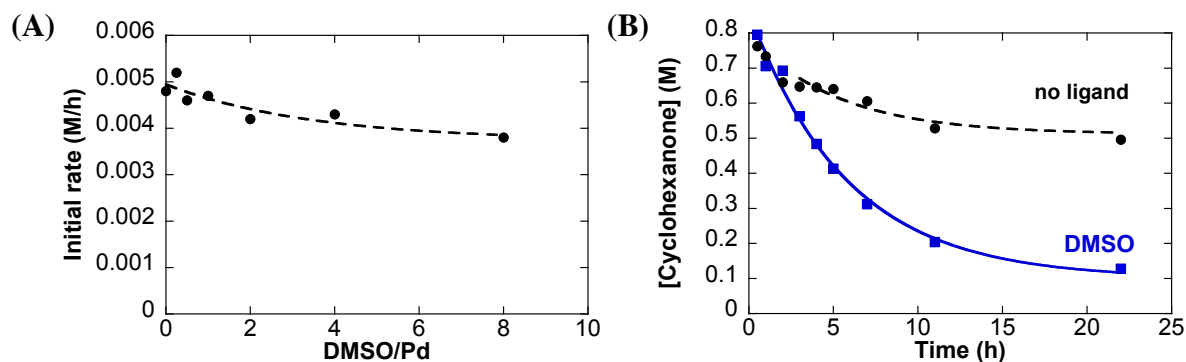
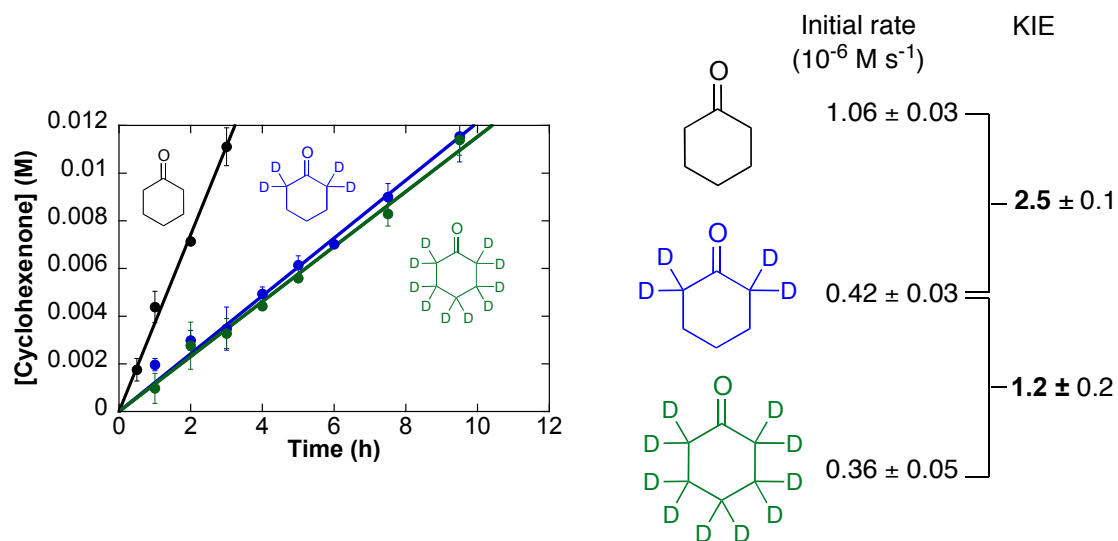


Figure 5-3. (A) Effect of the DMSO ligand on Pd-catalyzed oxidation of cyclohexanone to cyclohexenone evident from the dependence of the initial rate on the DMSO/Pd ratio. (B) Comparison of time courses for the dehydrogenation of cyclohexanone in the absence and presence of DMSO. Reaction conditions: EtOAc (1 mL), O₂ (1 atm), 60 °C; (A) [cyclohexanone] = 0.2 M (0.2 mmol), [Pd(TFA)₂] = 0.01 M (0.01 mmol); (B) [cyclohexanone] = 0.8 M (0.8 mmol), [Pd(TFA)₂] = 0.04 M (0.04 mmol), (DMSO = 0.08 M (0.08 mmol) (blue)).

Deuterium kinetic isotope effects (KIE) were determined by independent measurements of initial rates with the protio, α -deuterated (cyclohexanone-*d*₄) and fully deuterated (cyclohexanone-*d*₁₀) substrates (Scheme 5-3). Cyclohexanone reacts 2.5 (\pm 0.1) times faster than cyclohexanone-*d*₄, reflecting a primary KIE for cleavage of the α -C-H. The reaction time courses for cyclohexanone-*d*₄ and cyclohexanone-*d*₁₀ are nearly identical, and the ratio of the rates, 1.2 (\pm 0.2) reflects a negligible KIE for cleavage of the β -C-H. GC-MS and ¹H NMR spectroscopy reveal that no α -H/D scrambling of deuterated substrates takes place under the reaction conditions.

Scheme 5-3. Deuterium Kinetic Isotope Effects (KIE) Derived from Independent Measurement of Initial Rates of Dehydrogenation of Cyclohexanone to Cyclohexenone ^a



^a Reaction conditions: [Substrate] = 0.2 M (0.2 mmol), [Pd(TFA)₂] = 0.01 M (0.01 mmol), [DMSO] = 0.02 M (0.02 mmol), EtOAc (1 mL), O₂ (1 atm), 60 °C.

The identity of the carboxylate ligand on Pd influences the reaction rate. Replacement of Pd(TFA)₂ with Pd(OAc)₂ led to reduced initial rate (Figure 5-4). When a mixture of Pd(TFA)₂ and Pd(OAc)₂ was used as the Pd source, with the total [Pd] fixed to 5 mol%, increased initial rates were observed, with a maximum increase at an acetate:trifluoroacetate ratio of 1:1.

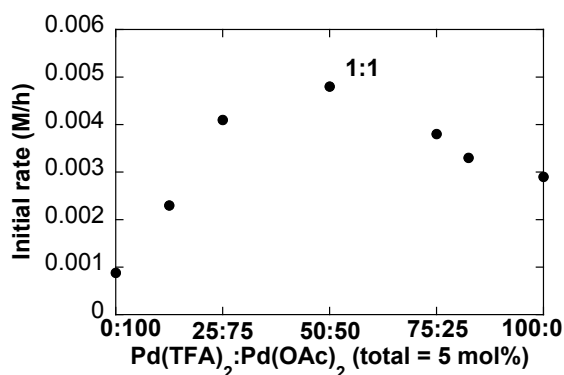


Figure 5-4. Dependence of the initial rate of Pd-catalyzed oxidation of cyclohexanone on different anionic ligands of Pd. Reaction conditions: [cyclohexanone] = 0.2 M (0.2 mmol), [Pd]_{total} = 0.01 M (0.01 mmol), [DMSO] = 0.02 M (0.02 mmol), EtOAc (1 mL), O₂ (1 atm), 60 °C.

5.2.2 Kinetic Study of Pd(DMSO)₂(TFA)₂-Catalyzed Oxidation of Cyclohexenone to Phenol

Independent examination of the second dehydrogenation step, which results in the conversion of cyclohexenone to phenol, was possible by increasing the catalyst loading to 10 mol%, in order to achieve good conversion at 60 °C. In contrast to the straightforward time course for Pd(DMSO)₂(TFA)₂-catalyzed dehydrogenation of cyclohexanone to cyclohexenone, the dehydrogenation of cyclohexenone exhibits an induction period at the beginning of the reaction (Figure 5-5). Accordingly, the time course for formation of phenol exhibits a sigmoidal curve (cf. Figure 5-13). When unligated-Pd(TFA)₂ was used as the catalyst, cyclohexenone dehydrogenation proceeds to high conversion without an induction period.

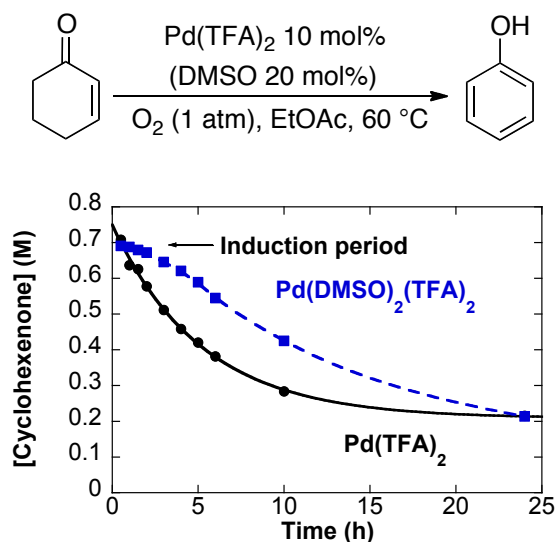


Figure 5-5. Time courses of $\text{Pd}(\text{TFA})_2$ -catalyzed oxidation of cyclohexenone to phenol in the presence (blue) and absence (black) of DMSO. Reaction conditions: [cyclohexenone] = 0.8 M (0.8 mmol), $[\text{Pd}(\text{TFA})_2]$ = 0.08 M (0.08 mmol), ([DMSO] = 0.16 M (0.16 mmol)), EtOAc (1 mL), O_2 (1 atm), 60 °C.

Product-associated auto catalysis is one possible origin of the sigmoidal time course; however control experiments reveal that addition of phenol or H_2O to the reaction mixture does not eliminate the induction period, and identical rates are observed relative to the standard reaction conditions (Figure 5-6).

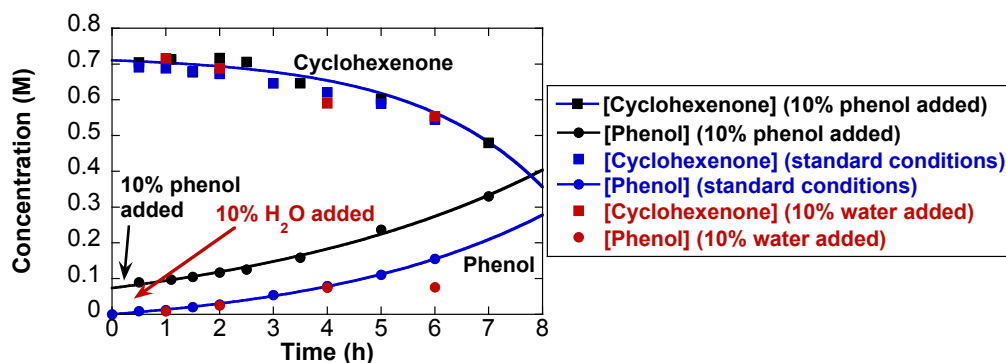


Figure 5-6. Effect of products on the induction period in $\text{Pd}(\text{DMSO})_2(\text{TFA})_2$ -catalyzed oxidation of cyclohexenone to phenol. Reaction conditions: $[\text{cyclohexenone}] = 0.8 \text{ M}$ (0.8 mmol), $[\text{Pd}(\text{TFA})_2] = 0.04 \text{ M}$ (0.04 mmol), $([\text{DMSO}] = 0.08 \text{ M}$ (0.08 mmol)), $\text{EtOAc} = 1 \text{ ml}$, 1 atm O_2 , $60 \text{ }^\circ\text{C}$.

The duration of the induction period increases as $[\text{DMSO}]$ is increased (Figure 5-7). Further analysis of the induction period reveals that DMSO has a dramatic inhibitory effect on the reaction (Figure 5-8). With 2 equiv. of DMSO, reflecting the stoichiometry used in the catalytic dehydrogenation of cyclohexanone, the reaction of cyclohexenone is almost 10-fold slower than the reaction carried out in the absence of DMSO.

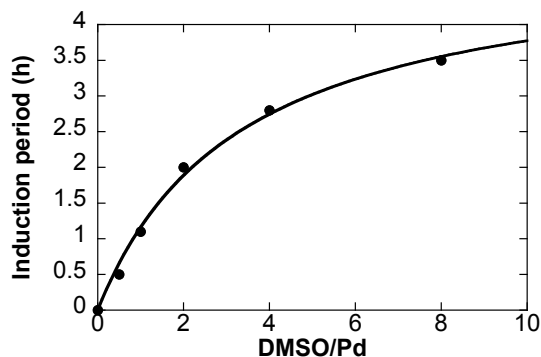


Figure 5-7. Dependence of the length of induction period on the Pd-catalyzed oxidation of cyclohexenone to phenol on [DMSO]. Reaction conditions: [cyclohexenone] = 0.8 M (0.8 mmol), [Pd(TFA)₂] = 0.08 M (0.08 mmol), EtOAc (1 mL), O₂ (1 atm), 60 °C.

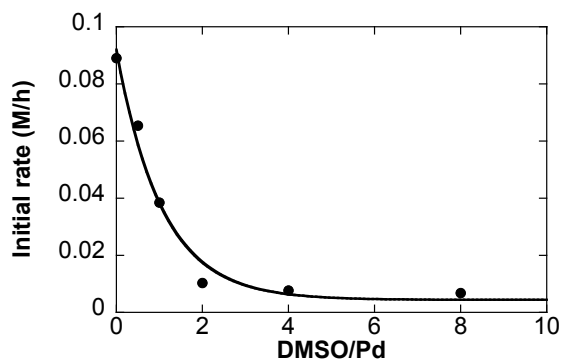
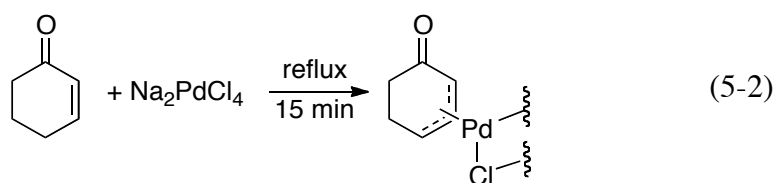
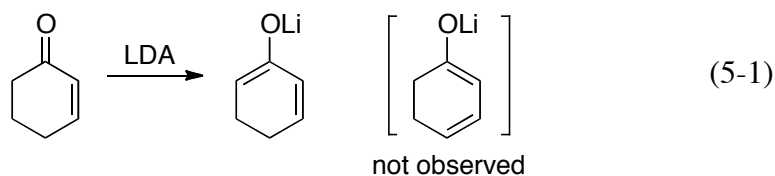


Figure 5-8. Dependence of the initial rate of Pd-catalyzed oxidation of cyclohexenone to phenol on the DMSO/Pd ratio. Reaction conditions: [cyclohexenone] = 0.8 M (0.8 mmol), [Pd(TFA)₂] = 0.08 M (0.08 mmol), EtOAc (1 mL), O₂ (1 atm), 60 °C.

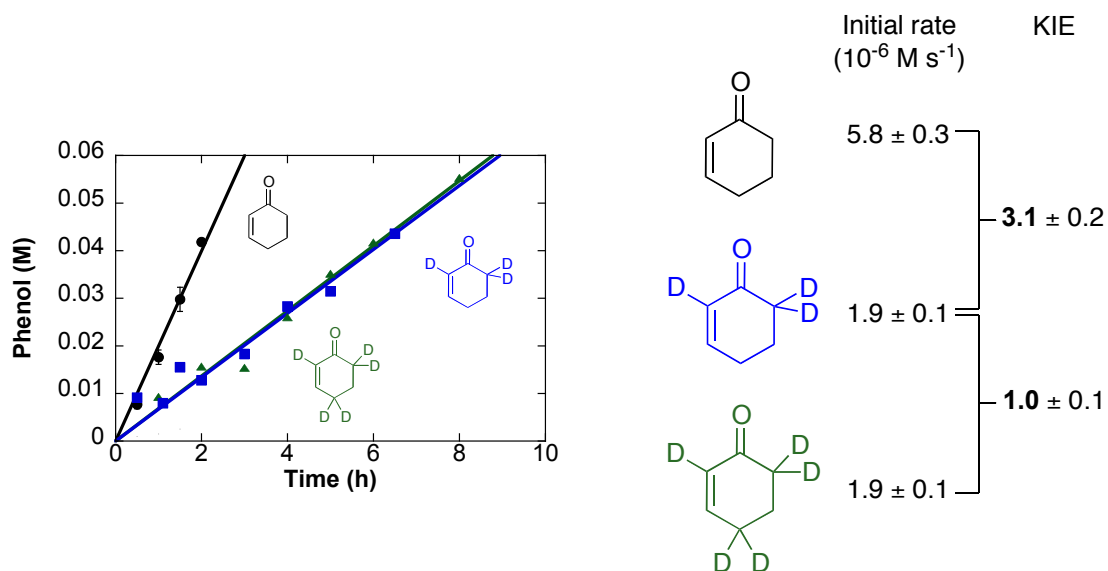
Cleavage of both the α -C-H and the C-H at the fourth position can occur as the key step for Pd(DMSO)₂(TFA)₂-catalyzed dehydrogenation of cyclohexenone. The α -C-H of cyclohexenone appears at 2.42 ppm in the ¹H NMR spectrum (CDCl₃), whereas the C-H at the fourth position displays a resonance at 2.37 ppm. Under basic conditions, for example in the presence of lithium diisopropylamide (LDA), cyclohexenone can be exclusively converted to the 2-oxycyclohexa-

1,3-dienyl lithium rather than the linear conjugated dienolate (eq 5-1), suggesting a more acidic α -C-H relative to the C-H at the fourth position.^{18,19} In addition, Brønsted acid conditions lead to H/D scrambling at the α -C-H, whereas the allylic C-H is unaffected.²⁰ In contrast, cyclohexenone is reported to react with sodium tetrachloropalladate to afford the di- μ -chloro-di-(6-oxo-cyclohex-2-enyl)-dipalladium, from cleavage of the allylic C-H (eq 5-2).^{21,22}



Deuterium kinetic isotope effects are used to probe the turnover-limiting step and the position at which the C-H cleavage of the key step takes place for $\text{Pd}(\text{DMSO})_2(\text{TFA})_2$ -catalyzed dehydrogenation of cyclohexenone. Cleavage of the α -C-H exhibits a primary kinetic isotope effect (3.1 ± 0.2), when comparing the independently acquired initial rates of cyclohexenone- d_0 versus 2,6,6-cyclohexenone- d_3 , with deuteration at the α -position (Scheme 5-4). Meanwhile, 2,4,4,6,6-cyclohexenone- d_5 , with deuteration at both allylic and α -position, reacts with a same rate as 2,6,6-cyclohexenone- d_3 (Scheme 5-4).²³

Scheme 5-4. Deuterium Kinetic Isotope Effects of Dehydrogenation of Cyclohexanone to Phenol
Derived from Independent Measurement of Initial Rates^a



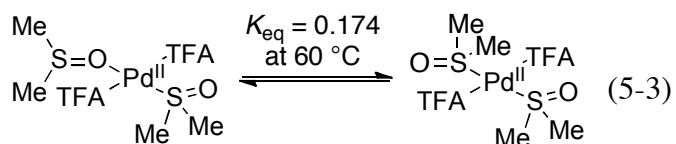
^a Reaction conditions: [substrate] = 0.8 M (0.4 mmol), [Pd(TFA)₂] = 0.08 M (0.04 mmol), ([DMSO] = 0.16 M (0.08 mmol)), EtOAc (0.5 mL), O₂ (1 atm), 60 °C.

5.3 Discussion

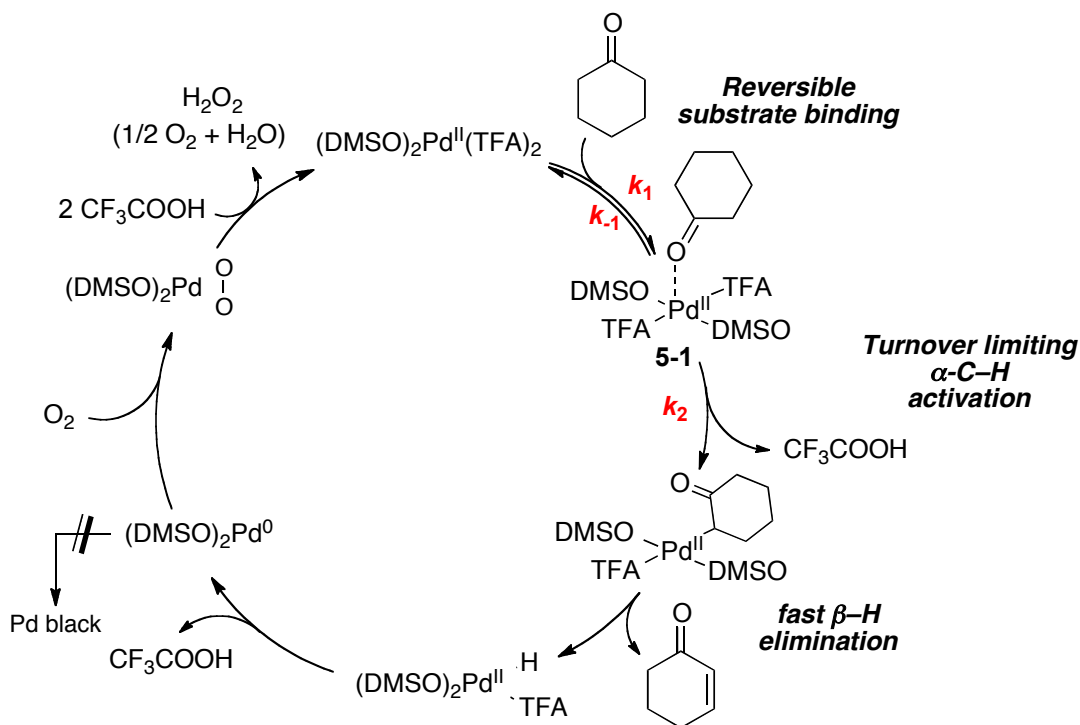
5.3.1 Mechanism of Pd(DMSO)₂(TFA)₂-Catalyzed Oxidation of Cyclohexanone to Cyclohexenone.

The mechanistic observations presented above for the catalytic dehydrogenation of cyclohexanone to cyclohexenone may be summarized as follows. The reaction exhibits first order dependences on [substrate] and [catalyst]. The concentration of DMSO has minimal effect on the reaction rate; however, the absence of DMSO results in significant decomposition of the Pd catalyst into the inactive Pd black. Cleavage of the α -C–H of cyclohexanone exhibits a primary KIE, whereas cleavage of β -C–H has a negligible KIE. No scrambling of the α -C–H with deuterium was observed at the end of the reaction.

In Scheme 5-5, we present a catalytic cycle that accounts for the above observations. Our study in chapter 4 has established the solution-phase structure of the $\text{Pd}(\text{DMSO})_2(\text{TFA})_2$ catalyst in EtOAc to be a mixture of $\text{Pd}(\text{S-DMSO})(\text{O-DMSO})(\text{TFA})_2$ and $\text{Pd}(\text{S-DMSO})_2(\text{TFA})_2$ (eq 5-3). Under the catalytic conditions at 60 °C, the $\text{Pd}(\text{S-DMSO})(\text{O-DMSO})(\text{TFA})_2$ is moderately favored over $\text{Pd}(\text{S-DMSO})_2(\text{TFA})_2$ by a ratio of 6:1. Cyclohexanone coordinates to the bis-DMSO ligated Pd catalyst via the carbonyl oxygen atom. This bis-DMSO ligated Pd catalyst via the carbonyl oxygen atom. This bis-DMSO ligated Pd catalyst undergoes turnover limiting $\alpha\text{-C-H}$ cleavage to afford a Pd^{II} -enolate intermediate, with concomitant release of TFAH. Subsequent $\beta\text{-H}$ elimination proceeds fast to afford cyclohexenone and a Pd^{II} -hydride. Oxidation of a Pd^{II} -hydride is expected to be initiated by reductive elimination of TFAH followed by aerobic oxidation of Pd^0 to regenerate the Pd^{II} catalyst.¹⁶



Scheme 5-5. Proposed Mechanism for Pd(DMSO)₂(TFA)₂-Catalyzed Dehydrogenation of Cyclohexanone



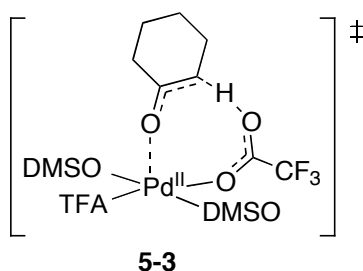
Application of the steady-state approximation to intermediate **5-1** results in the rate law shown in eq 5-4. The rate law exhibits a first-order dependence on [substrate] and [catalyst], as observed experimentally. Irreversible and turnover limiting α -C–H cleavage (k_2 step) is supported by the primary KIE observed (cf. Scheme 5-3).

$$\frac{d[\text{cyclohexenone}]}{dt} = \frac{k_1 k_2 [\text{cyclohexanone}] [\text{Pd}(\text{DMSO})_2(\text{TFA})_2]}{k_2 + k_{-1}} \quad (5-4)$$

The associative interaction between the Pd catalyst and cyclohexanone arises from the fact that DMSO is a better σ -donor relative to the carbonyl of a ketone, and is therefore unlikely to be

substituted by ketone.²⁴ The lack of a rate dependence on DMSO concentration supports this argument. If DMSO dissociates from Pd upon treatment with cyclohexanone, an inhibitory effect by DMSO would have been observed. In addition, formation of Pd-ketone adduct **5-1** is also evidenced by the slower reaction rate when Pd(TFA)₂ is replaced with Pd(OAc)₂ (cf. Figure 5-4), as the less electrophilic Pd center exhibits less favorable binding of the ketone.

The subsequent C–H cleavage from **5-1** is speculated to proceed via intramolecular deprotonation by the carboxylate ligand on Pd, for example, via transition-state structure **5-3**. The beneficial rate effect, when one of the TFA ligands in Pd(TFA)₂ is replaced with acetate (cf. Figure 5-4), may arise from the enhanced basicity of acetate relative to TFA. The maximized rate observed at a 1:1 OAc:TFA ratio could reflect the balance between basicity and electrophilicity. Analogous carboxylate-mediated cleavage of O–H bonds has been proposed for Pd(py)₂(OAc)₂-catalyzed (py = pyridine) alcohol oxidation.²⁵

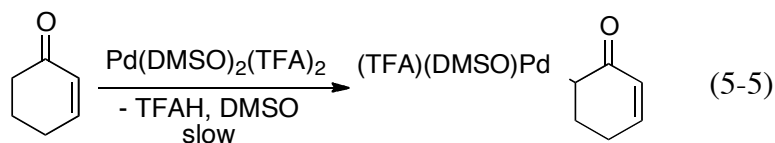


5.3.2 Mechanism of Pd(DMSO)₂(TFA)₂-Catalyzed Oxidation of Cyclohexenone and the Origin of the Chemoselectivity

An induction period is evident in the Pd(DMSO)₂(TFA)₂-catalyzed oxidation of cyclohexenone to phenol, the length of which increases as [DMSO] is increased at fixed [Pd(TFA)₂] and [substrate]. In contrast to the oxidation of cyclohexanone, where DMSO exhibits

negligible effect on the reaction rate, the oxidation of cyclohexenone is dramatically inhibited at increased [DMSO].

The precise origin of the induction period and the nature of the catalyst and/or catalytic mechanism following the induction period are not well understood and will require further investigation. However, the KIE studies show that cleavage of the α -C-H is associated with the induction period (eq 5-5). The absence of the activation at the allylic position is evident from the lack of a KIE for the allylic C-H. This selectivity is consistent with the higher acidity of the α -C-H relative to the C-H at the fourth position (cf. eq 5-1),¹⁹ but contradicts the formation of (π -allyl)Pd complexes from the reaction of cyclohexenone with Na_2PdCl_4 (cf. eq 5-2).²¹



The DMSO ligand to $\text{Pd}(\text{TFA})_2$ exhibits a dramatic inhibitory effect on dehydrogenation of cyclohexenone, whereas minimal effect of DMSO is observed for dehydrogenation of cyclohexanone. These remarkable kinetic observations provide the basis for the selective dehydrogenation of cyclohexanone to generate cyclohexenone relative to the formation of phenol. We speculate that this chemoselectivity is associated with the favorable coordination of cyclohexenone to Pd^{II} via the alkene relative to the carbonyl.²⁶ This coordination mode requires dissociation of the DMSO ligand to Pd^{II} . In contrast, cyclohexanone approaches the $\text{Pd}(\text{DMSO})_2(\text{TFA})_2$ catalyst via the carbonyl, forming a Pd-cyclohexanone adduct **5-1** (cf. Scheme 5-5). The DMSO ligands stay coordinated during this pathway, and therefore have minimal effect on the reaction rate.

5.3.3 Conclusion

Collectively, the dehydrogenation of cyclohexanone undergoes turnover-limiting α -C-H cleavage and fast β -H elimination to afford the cyclohexenone product. The chemoselectivity of Pd(DMSO)₂(TFA)₂-catalyzed oxidation of cyclohexanone to generate cyclohexenone relative to phenol originates from the different kinetic effect of DMSO on the two dehydrogenation steps. DMSO has minimal impact on the reaction rate in the first dehydrogenation step, whereas it strongly inhibits the second step. These results have important implications in understanding the role of ligands and design of catalysts for Pd-catalyzed dehydrogenation reactions.

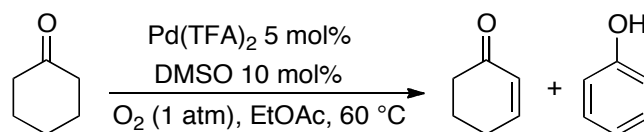
5.4 Experimental

5.4.1 General Considerations

All commercially available compounds were used as received and purchased from Sigma Aldrich. Cyclohexanone-*d*₁₀ was purchased from CDN Isotopes. The deuterated substrates 2,4,4,6,6-*d*₅-cyclohexenone and 2,6,6-*d*₃-cyclohexenone are not commercially available, and are prepared according to literature procedures.²³

¹H and ¹³C NMR spectra were recorded on a Bruker AC-300 MHz or a Varian Mercury-300 MHz spectrometer. The chemical shifts (δ) are given in parts per million and referenced to residual solvent peaks or a TMS internal standard. Gas chromatography was performed on a Shimadzu GC-17A using a Stabilwax®-DB column or an RTX-5MS column and referenced to an internal standard (tetradecane). Flash column chromatography was performed on an Isco Combiflash system using silica gel 60 (Silicycle) and eluted with ethyl acetate/hexane.

5.4.2 General Procedure for Acquiring Kinetic Data



Catalytic aerobic oxidation reactions were performed using a custom reaction apparatus that enabled several reactions to be performed simultaneously under a constant pressure of O₂ (approx. 1 atm) with controlled temperature and orbital agitation. To a disposable 13 mm thick-walled culture tube was added Pd(TFA)₂, (13.2 mg, 0.04 mmol, 0.05 equiv.), DMSO (5.6 μL, 0.04 mmol, 0.1 equiv), and 1 mL EtOAc to form a bright yellow solution. The reaction tube was placed in a 48-well parallel reactor mounted on a Glas-Col large capacity mixer. The headspace was purged with O₂ for 10 min, after which tetradecane (20 μL, 0.077 mmol) was added via syringe. The reactor temperature was set to 60 °C and allowed to equilibrate for 5 min. Injection of cyclohexanone (80 μL, 0.8 mmol) established the *t* = 0 point. After various time intervals, aliquots were withdrawn from the reaction mixture via pipette, diluted with CH₂Cl₂ and analyzed by GC.

5.4.3 Raw Kinetic Data

Most kinetic data and orders presented above are derived from the initial rates of the reactions. Unless specified, the initial rate was defined as the slope of [cyclohexenone] versus time from the beginning of the reaction to 10% conversion. Figures 5-9 to 5-12 represent the reaction time courses under different conditions, which are the raw data for Figures 5-2, 5-3(A), 5-4, 5-7 and 5-8. Experiments in each figure were performed in parallel using the same stock solutions and in the same large capacity mixer.

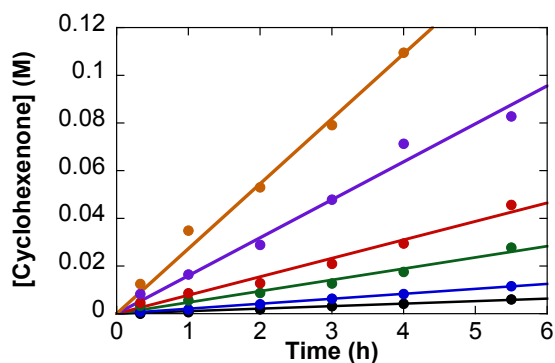


Figure 5-9. Time courses for the oxidation of cyclohexanone with varying concentrations in the presence of a fixed catalyst concentration. Reaction conditions: $[\text{Pd}(\text{TFA})_2] = 0.01 \text{ M}$ (0.01 mmol), $[\text{DMSO}] = 0.02 \text{ M}$ (0.02 mmol), EtOAc (1 mL), O_2 (1 atm), $60 \text{ }^\circ\text{C}$, $[\text{cyclohexanone}] = 0.05, 0.1, 0.2, 0.3, 0.6$ and 1 M .

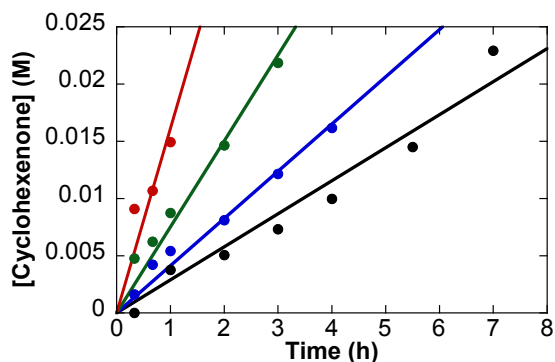


Figure 5-10. Time courses for oxidation of cyclohexanone in the presence of different catalyst loadings, where the “catalyst” is a 1:2 mixture of $\text{Pd}(\text{TFA})_2$ and DMSO. Reaction conditions: $[\text{cyclohexanone}] = 0.2 \text{ M}$ (0.2 mmol), EtOAc (1 mL), O_2 (1 atm), $60 \text{ }^\circ\text{C}$, $[\text{Pd}(\text{TFA})_2] = 0.005, 0.01, 0.02$ and 0.04 M , $[\text{DMSO}] = 0.01, 0.02, 0.04$ and 0.08 M , respectively.

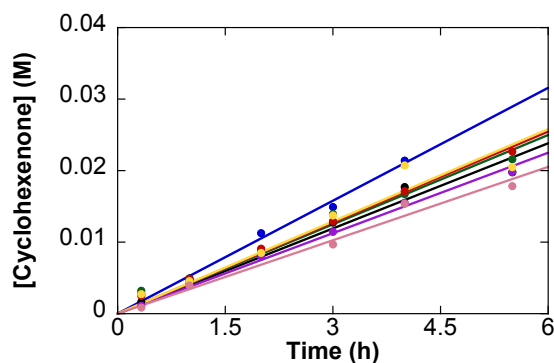


Figure 5-11. Time courses for oxidation of cyclohexanone in the presence of different quantities of DMSO with fixed $\text{Pd}(\text{TFA})_2$ concentration. Reaction conditions: $[\text{cyclohexanone}] = 0.2 \text{ M}$ (0.2 mmol), $[\text{Pd}(\text{TFA})_2] = 0.01 \text{ M}$ (0.01 mmol), EtOAc (1 mL), O_2 (1 atm), $60 \text{ }^\circ\text{C}$, $[\text{DMSO}] = 0, 0.0025, 0.005, 0.01, 0.02, 0.04$ and 0.08 M .

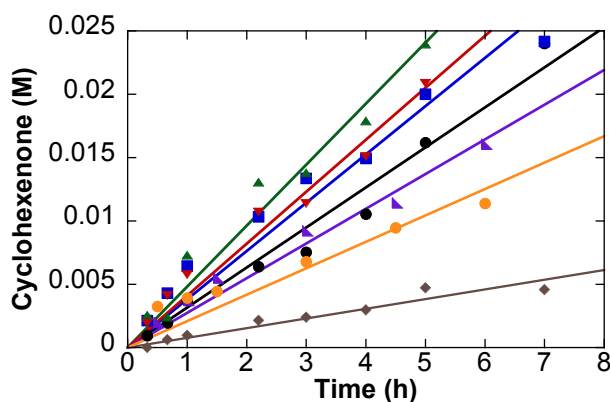


Figure 5-12. Time courses of Pd-catalyzed oxidation of cyclohexanone on different anionic ligands of Pd. Reaction conditions: $[\text{cyclohexanone}] = 0.2 \text{ M}$ (0.2 mmol), $[\text{Pd}]_{\text{total}} = 0.01 \text{ M}$ (0.01 mmol), $[\text{Pd}(\text{TFA})_2]:[\text{Pd}(\text{OAc})_2] = 0:100, 12:88, 25:75, 50:50, 75:25, 88:12, 100:0$. $[\text{DMSO}] = 0.02 \text{ M}$ (0.02 mmol), EtOAc (1 mL), O_2 (1 atm), $60 \text{ }^\circ\text{C}$.

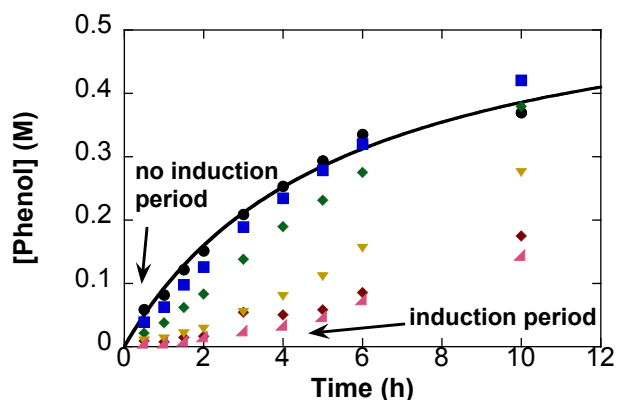


Figure 5-13. Dependence of the initial rate of Pd-catalyzed oxidation of cyclohexenone to phenol on the DMSO/Pd ratio. Reaction conditions: [cyclohexenone] = 0.8 M (0.8 mmol), [Pd(TFA)₂] = 0.08 M (0.08 mmol), EtOAc (1 mL), O₂ (1 atm), 60 °C, [DMSO] = 0, 0.04, 0.08, 0.16, 0.32 and 0.64 M.

5.4.4 Methods for Determining the Length of Induction Period

Figure 5-14 shows a representative reaction time course for oxidation of cyclohexenone to phenol under the standard conditions. The time course clearly consists of an induction period and a subsequent post-induction period. The data point at which the induction period ends is picked based on most linear points approximation. We fit the data from $t = 0$ to the end of induction period into a linear function, and the data from the end of induction period to the point of 10% conversion into a second linear function. The lengths of the induction period presented in Figure 5-7 are calculated as the time at intersection of the two lines. The initial rates presented in Figure 5-8 are calculated as the slope from $t = 0$ to the time at the intersection.

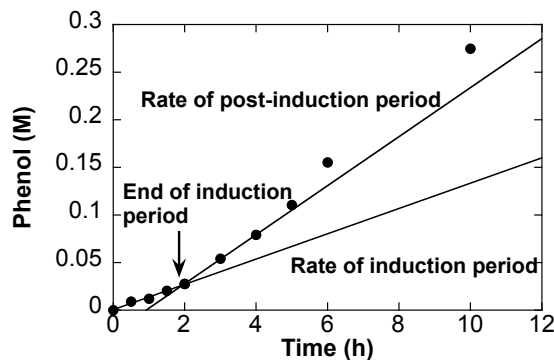


Figure 5-14. Time course of $\text{Pd}(\text{DMSO})_2(\text{TFA})_2$ -catalyzed oxidation of cyclohexenone to phenol. Reaction conditions: $[\text{cyclohexenone}] = 0.8 \text{ M}$ (0.4 mmol), $[\text{Pd}(\text{TFA})_2] = 0.08 \text{ M}$ (0.04 mmol), $[\text{DMSO}] = 0.16 \text{ M}$ (0.08 mmol), $\text{EtOAc} = 0.5 \text{ mL}$, 1 atm O_2 , 60 °C.

5.4.5 O_2 Dependence for $\text{Pd}(\text{DMSO})_2(\text{TFA})_2$ -Catalyzed Oxidation of 4-*tert*-Butylcyclohexanone

The dependence of initial rates on O_2 has been investigated with 4-*tert*-butylcyclohexanone. Reactions were performed under different O_2 partial pressures, with N_2 to make up the total pressure to 700 torr. Reactions were allowed to stir at 60 °C in parallel for 3.5 h. GC analysis revealed that 10% conversion was achieved in each reaction, despite under different O_2 pressures. We employed the ratio of [product]:time to represent the initial rate for each reaction. The plot of the initial rates as a function of the O_2 pressure revealed a zero order dependence of the reaction on O_2 pressure (Figure 5-15). Catalyst decomposition, as Pd black, was observed for reactions with < 200 Torr O_2 . The lack of rate dependence on O_2 pressure suggests that substrate oxidation is the turnover-limiting stage of the reaction.

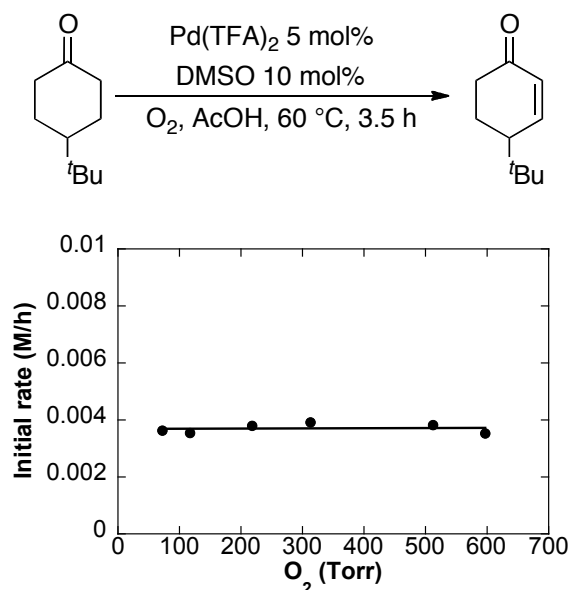


Figure 5-15. Dependence of the initial rate of Pd(DMSO)₂(TFA)₂-catalyzed aerobic oxidation of 4-*tert*-butylcyclohexanone on O₂ pressure. Reaction conditions: [4-*tert*-butylcyclohexanone] = 0.2 M, [catalyst] = 0.01 M, AcOH = 1 ml, 60 °C, time = 3.5 h.

5.5 References

1. (a) Buckle, D. R.; Pinto, I. L. Oxidation Adjacent to C=X Bonds by Dehydrogenation. In *Comprehensive Organic Synthesis - Selectivity, Strategy and Efficiency in Modern Organic Chemistry*; Trost, B. M., Fleming, I., Eds.; Elsevier 1991; Vol. 7, pp 119-149. (b) Larock, R. C. In *Comprehensive Organic Transformations*; John Wiley & Sons: New York, 1999; pp. 251-256.
2. Prominent methods include: hydrogenation-dehydrohalogenation, selenium and sulfur-based elimination and IBX (2-iodoxybenzoic acid)-mediated oxidation. For leading references, see: (a) Miller, B.; Wong, H.-S. *Tetrahedron* **1972**, 28, 2369-2376. (b) Stotter, P. L.; Hill, K. A.

J. Org. Chem. **1973**, *38*, 2576-2578. (c) Trost, B. M.; Salzmann, T. N.; Hiroi, K. *J. Am. Chem. Soc.* **1976**, *98*, 4887-4902. (d) Sharpless, K. B.; Lauer, R. F.; Teranishi, A. Y. *J. Am. Chem. Soc.* **1973**, *95*, 6137-6139. (e) Reich, H. J. *Acc. Chem. Res.* **1979**, *12*, 22-30. (f) Nicolaou, K. C.; Zhong, Y. L.; Baran, P. S. *J. Am. Chem. Soc.* **2000**, *122*, 7596-7597. (g) Nicolaou, K. C.; Montagnon, T.; Baran, P. S.; Zhong, Y. L. *J. Am. Chem. Soc.* **2002**, *124*, 2245-2258.

3. (a) Horning, E. C.; Horning, M. G. *J. Am. Chem. Soc.* **1947**, *69*, 1359-1361. (b) Newman, M. S.; Blum, J. *J. Am. Chem. Soc.* **1964**, 503-507. (c) Karakhanov, R. A.; Vartanyan, M. M.; Apandiev, R. B.; Karzhavina, N. P. *Izv. Akad. Nauk SSSR, Ser. Khim.* **1982**, 1905. (d) Jones, T. H.; Fales, H. M. *Tetrahedron Lett.* **1983**, *24*, 5439-5440.

4. (a) Williams, E. A.; Meikle, R. W.; Redemann, C. T. *J. Agric. Food. Chem.* **1965**, *13*, 210-213. (b) Hales, N. J.; Heaney, H.; Hollinshead, J. H.; Ley, S. V. *Tetrahedron* **1995**, *51*, 7741-7754. (c) Kamiguchi, S.; Nagashima, S.; Chihara, T. *Chem. Lett.* **2007**, *36*, 1340-1341.

5. Dobereiner, G. E.; Crabtree, R. H. *Chem. Rev.* **2009**, *110*, 681-703.

6. Zhang, X.; Wang, D. Y.; Emge, T. J.; Goldman, A. S. *Inorg. Chim. Acta.* **2011**, *369*, 253-259.

7. For an example of tetranuclear Ru-catalyzed transfer dehydrogenation of cyclohexanone with limited success, see: Yi, C. S.; Lee, D. W. *Organometallics* **2009**, *28*, 947-949.

8. (a) Hartwig, J. In *Organotransition Metal Chemistry: From Bonding to Catalysis*; Hartwig, J., Ed.; University Science Books: Sausalito, 2010. pp. 825-870. (b) Hartwig, J. In

Organotransition Metal Chemistry: From Bonding to Catalysis; Hartwig, J., Ed.; University Science Books: Sausalito, 2010, pp. 398-405.

9. For a review of early examples, see: Muzart, J. *Eur. J. Org. Chem.* **2010**, 3779-3790.
10. (a) Stahl, S. S. *Science* **2005**, *309*, 1824-1826. (b) Stahl, S. S. *Angew. Chem. Int. Ed.* **2004**, *43*, 3400-3420. (c) Gligorich, K. M.; Sigman, M. S. *Chem. Commun.* **2009**, 3854-3867. (d) Shi, Z.; Zhang, C.; Tang, C.; Jiao, N. *Chem. Soc. Rev.* **2012**, *41*, 3381-3430.
11. Izawa, Y.; Pun, D.; Stahl, S. S. *Science* **2011**, *333*, 209-213.
12. Diao, T.; Wadzinski, T. J.; Stahl, S. S. *Chem. Sci.* **2012**, *3*, 887-891.
13. For a simultaneously reported Pd/diazafluorenone-catalyzed dehydrogenation, see: Gao, W.; He, Z.; Qian, Y.; Zhao, J.; Huang, Y. *Chem. Sci.* **2012**, *3*, 883-886.
14. Diao, T.; Stahl, S. S. *J. Am. Chem. Soc.* **2011**, *133*, 14566-14569.
15. For the formation of Pd enolates, see the following review and references cited therein: Culkin, D. A.; Hartwig, J. F. *Acc. Chem. Res.* **2003**, *36*, 234-245.
16. Recent studies suggest that aerobic oxidation of Pd^{II}-hydrides proceed via Pd⁰, as shown in Scheme 5-2. See: (a) Konnick, M. M.; Stahl, S. S. *J. Am. Chem. Soc.* **2008**, *130*, 5753-5762. (b) Popp, B. V.; Stahl, S. S. *Chem. Eur. J.* **2009**, *15*, 2915-2922. (c) N. Decharin, B. V. Popp and S. S. Stahl *J. Am. Chem. Soc.*, **2011**, *133*, 13268-13271.

-
17. A similar mechanism with a Pd enolate intermediate has also been proposed for the analogous “Saegusa” reaction, Pd-catalyzed/mediated dehydrosilylation of silyl enol ethers. (a) Ito, Y.; Hirao, T.; Saegusa, T. *J. Org. Chem.* **1978**, *43*, 1011-1013. (b) Larock, R. C.; Hightower, T. R.; Kraus, G. A.; Hahn, P.; Zheng, D. *Tetrahedron Lett.* **1995**, *36*, 2423-2426. (c) Porth, S.; Bats, J. W.; Trauner, D.; Giester, G.; Mulzer, J. *Angew. Chem., Int. Ed.* **1999**, *38*, 2015-2016.
18. Rubottom, G. M.; Gruber, J. M. *J. Org. Chem.* **1977**, *42*, 1051-1056.
19. However, formation of the linear conjugated dienolate can be achieved by using KN(TMS)₂ as the base: Kawanisi, M.; Itoh, Y.; Hieda, T.; Kozima, S.; Hitomi, T.; Kobayashi, K. *Chem. Lett.* **1985**, 647-650.
20. Forsyth, D. A.; Botkin, J. H.; Osterman, V. M. *J. Am. Chem. Soc.* **1984**, *106*, 7663-7666.
21. Kasahara, A.; Tanaka, K.; Asamiya, K. *Bull. Chem. Soc. Jpn.* **1967**, *40*, 351-355.
22. For other related Pd-mediated cleavage of allylic C–H to form (π -allylPd) complexes, see: (a) Parshall, G. W.; Wilkinson, G. *Inorg. Chem.* **1962**, *1*, 896-900. (b) Trost, B. M.; Metzner, P. J. *J. Am. Chem. Soc.* **1980**, *102*, 3572-3577.
23. The syntheses of 2,6,6-cyclohexenone-*d*₃ and 2,4,4,6,6-cyclohexenone-*d*₅ are based on procedures described in following paper: Lambert, J. B.; Clikeman, R. R. *J. Am. Chem. Soc.* **1976**, *98*, 4203-4211. In this paper, the 2,6,6-cyclohexenone-*d*₃ is falsely assigned to 2,4,4-cyclohexenone-*d*₃. Our ¹H NMR and 1D NOSEY data confirm that the resulting deuterated substrate is 2,6,6-cyclohexenone-*d*₃.

-
24. The pK_a of the conjugated acid of DMSO and acetone are not found, but sulfur is expected to be more electron-rich and polarizable relative to carbon.
25. Steinhoff, B. A.; Guzei, I. A.; Stahl, S. S. *J. Am. Chem. Soc.* **2004**, *126*, 11268-11278.
26. Hartwig, J. *Organotransition Metal Chemistry: from Bonding to Catalysis*; University Science Books: Sausalito, 2009, Vol. 2.6.1.

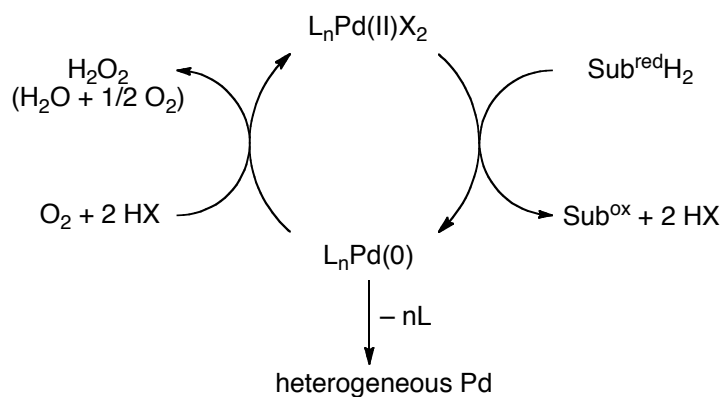
CHAPTER 6

Additional Results for Mechanistic Study of Pd(DMSO)₂(TFA)₂-Catalyzed Aerobic Oxidation of Cyclohexanone

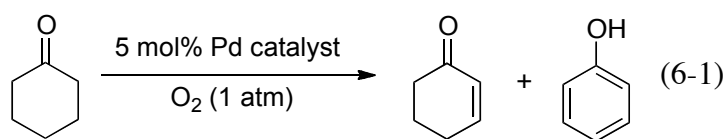
6.1 Introduction

Molecular oxygen represents a superior, sustainable and environmentally benign oxidant, and recent progresses in the development of Pd catalysts have enabled a wide variety of organic reactions using O_2 as the stoichiometric oxidant.¹ The generic catalytic cycle of Pd-catalyzed oxidative reactions consists of two independent half-reactions: Pd^{II} -mediated oxidation of the organic substrate and dioxygen-coupled oxidation of Pd^0 (Scheme 6-1).¹ The majority of these reactions features substrate oxidation as the turnover-limiting step. However, inefficient O_2 mixing of Pd^0 often leads to a competing catalyst decomposition pathway via Pd^0 -aggregation, which represents a common problem in Pd-catalyzed aerobic oxidation reactions.² The catalyst decomposition will reduce the population of the active homogeneous catalyst; however, in some cases, the resulting Pd^0 nanoparticles proved to be catalytically active.³ Critical investigation of several operational homogeneous transition metal catalysts revealed that they are no more than precursors to heterogeneous nanoparticle catalysts.^{4,5}

Scheme 6-1. The Generic Catalytic Cycle of Pd-Catalyzed Aerobic Oxidation Reactions



Pd-catalyzed aerobic dehydrogenation reactions have emerged as an appealing way to introduce unsaturation into molecules. Oxidation of a cyclohexanone could lead to phenol and/or cyclohexenone (eq 6-1), which are both synthetically important products. Until recently, only heterogeneous catalysts, such as Pd/C, were reported to catalyze the aromatization of cyclohexenone to phenol.⁶ With regards to cyclohexenone, early efforts of making cyclohexenone derivatives are limited with low yields and the narrow substrate scope.^{7,8} A more synthetically useful variation is the Pd-mediated/catalyzed Saegusa reaction, converting a broad range of silyl enol ethers to the corresponding α,β -enones, but this alternative does require multiple steps.⁹ Our recent discovery of three Pd catalyst systems have overcome some of the limitations presented above for the dehydrogenation of carbonyl compounds: (1) a Pd(TFA)₂/2-Me₂Npy (2-*N,N*-dimethylaminopyridine)/TsOH catalyst for full dehydrogenation of cyclohexanones/cyclohexenone to phenols;¹⁰ (2) a Pd(DMSO)₂(TFA)₂ catalyst for selective oxidation of cyclohexanones to cyclohexenones;¹¹ (3) a Pd(TFA)₂/4,5-diazafluorenone catalyst for dehydrogenation of β -benzylacetone derivatives into arylbutenone products.¹²



In this chapter, I present additional mechanistic data for Pd(DMSO)₂(TFA)₂-catalyzed aerobic dehydrogenation of cyclic ketones, with a focus on the kinetic data for oxidation of cyclohexenone to phenol and the characterization of the homogeneity of the reaction conditions. These results provide complementary insights into this catalyst system in addition to those described in Chapter 5.

6.2 Results

6.2.1 Variable Temperature Studies of Three Catalyst Systems for Dehydrogenation of Cyclohexanone

Oxidation of the parent cyclohexanone under a constant O₂ pressure (1 atm) is employed as the model reaction for the variable temperature study of three catalyst systems. The Pd(TFA)₂/2-Me₂Npy/TsOH-catalyzed dehydrogenation at 80 °C exhibits an initial “burst” with fast formation of cyclohexenone during the first catalytic turnover (Figure 6-1(A)). Similar “bursts” are observed at different temperatures: 40 and 60 °C. At 40 °C, the “burst” reactivity leads to a more rapid initial conversion of cyclohexanone than at 60 °C, reflected as an interception of the time courses for 40 and 60 °C. The irreproducible kinetics under identical conditions complicated further study of this catalyst system. Dehydrogenations catalyzed by the Pd(TFA)₂/4,5-diazafluorenone catalyst exhibit initial “bursts” as well, at 60 and 80 °C. At 40 °C, however, the reaction proceeds with an induction period. In contrast to these two catalysts, the time courses of Pd(DMSO)₂(TFA)₂-catalyzed dehydrogenations fit well to an exponential-decay function at different temperatures (Figure 6-1(C)). At 60 °C, the substrate half-life is about 2 h, considerably shorter than that with former two catalysts. The ΔH^\ddagger and ΔS^\ddagger for Pd(DMSO)₂(TFA)₂-catalyzed dehydrogenation of cyclohexanone are calculated to be 12.7 kcal/mol and 40.9 e.u. based on Eyring analysis of the temperature dependence of the reaction (Figure 6-2).

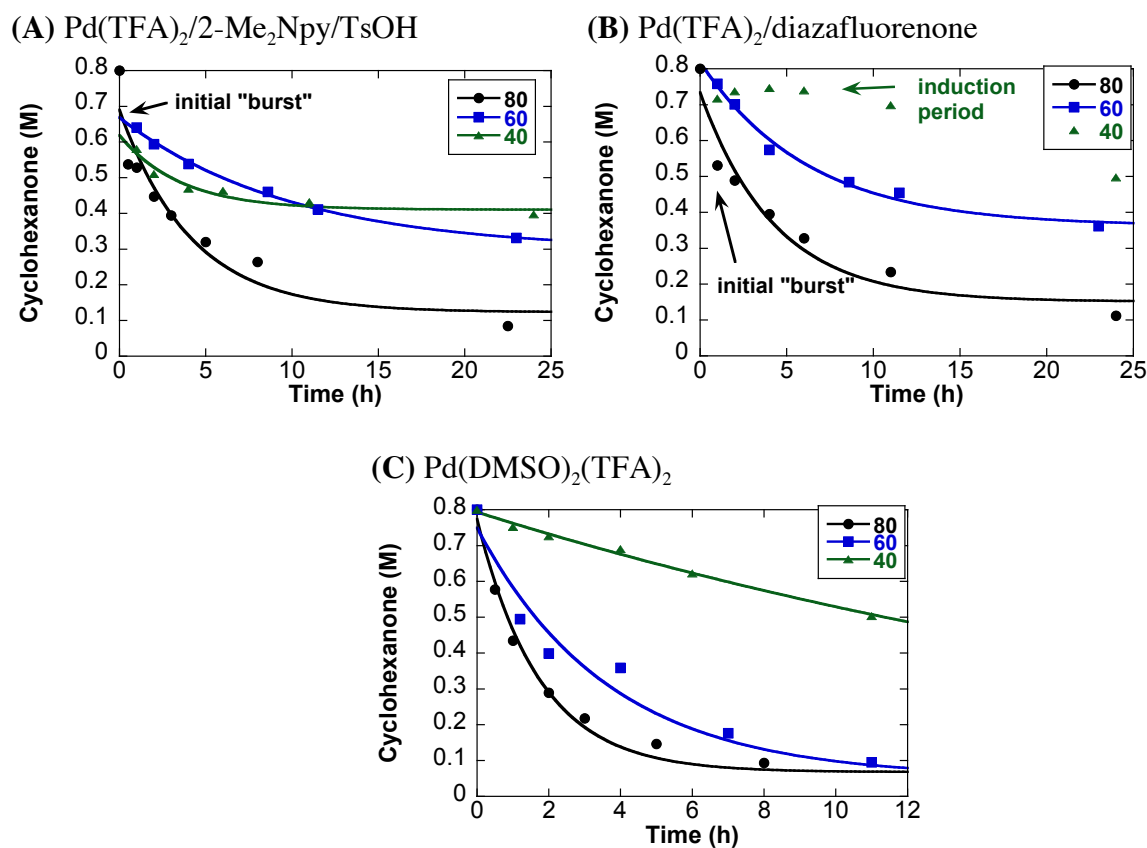


Figure 6-1. Reaction time courses for the dehydrogenation of cyclohexanone with different catalyst systems. Reaction conditions: [cyclohexanone] = 0.8 M (0.4 mmol), [Pd(TFA)₂] = 0.04 M (0.02 mmol), 1 atm O₂, T = 40, 60, 80 °C; (A) [Me₂Npy] = 0.08 M (0.04 mmol), [TsOH] = 0.16 M (0.08 mmol), DMSO = 0.5 mL; (B) [diazafluorenone] = 0.04 M (0.02 mmol), DMSO = 0.5 mL; (C) [DMSO] = 0.08 M (0.08 mmol), AcOH = 0.5 mL.

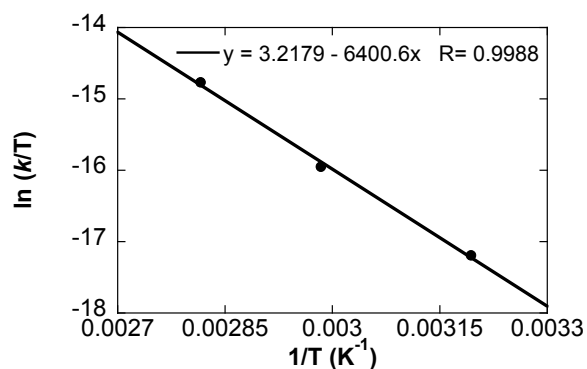


Figure 6-2. Eyring plot for Pd(DMSO)₂(TFA)₂-catalyzed dehydrogenation of cyclohexanone. Reaction conditions: [cyclohexanone] = 0.8 M (0.4 mmol), [Pd(TFA)₂] = 0.04 M (0.02 mmol), [DMSO] = 0.08 M (0.08 mmol), AcOH = 0.5 mL, 1 atm O₂, T = 40, 60, 80 °C.

6.2.2 Additional Kinetic Data for Pd(DMSO)₂(TFA)₂-Catalyzed Dehydrogenation of Cyclohexanone

Pd(DMSO)₂(TFA)₂-catalyzed oxidation of most cyclohexanone substrates has been carried out in AcOH in order to obtain the best selectivity for enones.¹¹ The plot in Figure 6-3 suggests that Pd(DMSO)₂(TFA)₂-catalyzed oxidation of the parent cyclohexanone proceeds with a good selectivity in AcOH. However, decomposition of cyclohexenone is observed at a longer reaction time (Figure 6-3). As discussed in Chapter 5, we employed Pd(DMSO)₂(TFA)₂ in EtOAc as the catalyst system for our kinetic investigation. The use of EtOAc as the solvent features several advantages for mechanistic investigations: (1) the lower selectivity for generating cyclohexenone relative to phenol in EtOAc ($k_1/k_2 = 10$) is not as good as that in AcOH, facilitates investigation of the second dehydrogenation step leading to phenol; (2) the neutral conditions avoid mechanistic complications arising from an acidic solvent, which could play a role in formation of the enolate intermediate.

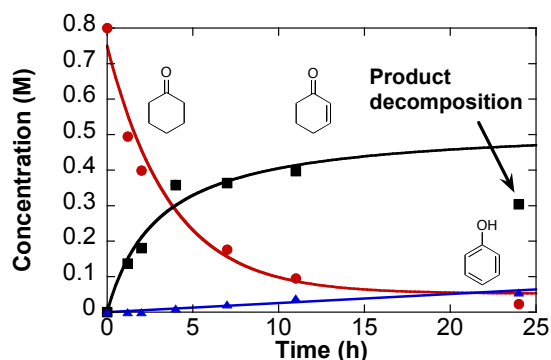


Figure 6-3. Reaction time course of $\text{Pd}(\text{DMSO})_2(\text{TFA})_2$ -catalyzed aerobic oxidation of cyclohexanone in AcOH. Reaction conditions: $[\text{cyclohexanone}] = 0.8 \text{ M}$ (0.8 mmol), $[\text{Pd}(\text{TFA})_2] = 0.04 \text{ M}$ (0.04 mmol), $[\text{DMSO}] = 0.08 \text{ M}$ (0.08 mmol), AcOH = 1 mL, 1 atm O_2 , 60 °C.

The conversion of [cyclohexanone] in $\text{Pd}(\text{TFA})_2$ -catalyzed dehydrogenations exhibits a strong dependence on the sulfoxide ligand (Figure 6-4). Replacement of DMSO with tetramethylene sulfoxide leads to a comparable reaction rate and conversion, whereas other sulfoxide ligands, including methyl methylsulfinate, methyl phenyl sulfoxide, diphenyl sulfoxide and trimethylene sulfoxide, result in substantially decreased yields.

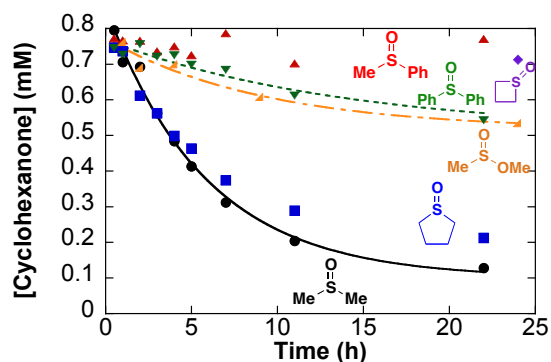


Figure 6-4. Dependence of $\text{Pd}(\text{TFA})_2$ -catalyzed oxidation of cyclohexanone on sulfoxide ligands. Reaction conditions: $[\text{cyclohexanone}] = 0.8 \text{ M}$ (0.8 mmol), $[\text{Pd}(\text{TFA})_2] = 0.04 \text{ M}$ (0.04 mmol), $[\text{ligand}] = 0.08 \text{ M}$ (0.08 mmol), EtOAc = 1 mL, 1 atm O_2 , 60 °C.

Addition of catalytic quantities (10 mol%) of carboxylic acids into the standard reaction conditions leads to faster reaction rates for converting cyclohexanone to cyclohexenone (Figure 6-5). Addition of more acidic TFAH results in faster rate relative to AcOH. However, a stronger acid TsOH¹³ almost completely inhibits the reaction. Addition of a non-coordinating base, 1,2,2,6,6-pentamethylpiperidine, is also detrimental.

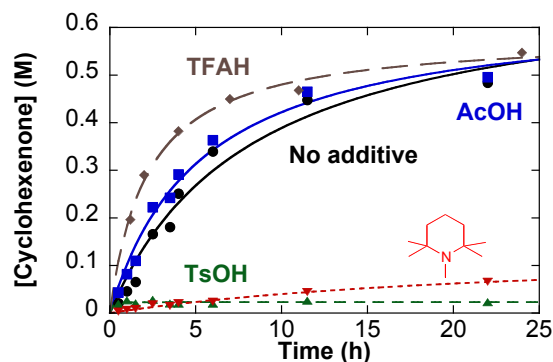


Figure 6-5. Dependence of Pd(DMSO)₂(TFA)₂-catalyzed oxidation of cyclohexanone on acid and base additives. Reaction conditions: [cyclohexanone] = 0.8 M (0.8 mmol), [Pd(TFA)₂] = 0.04 M (0.04 mmol), [DMSO] = 0.08 M (0.08 mmol), [additive] = 0.08 M (0.08 mmol), EtOAc = 1 ml, 1 atm O₂, 60 °C.

6.2.3 Additional Kinetic Data for Pd(DMSO)₂(TFA)₂-Catalyzed Dehydrogenation of Cyclohexenone

Pd(DMSO)₂(TFA)₂-catalyzed dehydrogenation of cyclohexenone to phenol proceeds with an induction period (cf. Figure 5-5). The kinetics from different runs appear to be reproducible, allowing us to explore the mechanism by further examining the kinetic orders for both induction and post-induction periods. The plot in Figure 6-6 reveals that both induction and post-induction periods exhibit an approximately first order dependence on [cyclohexenone].

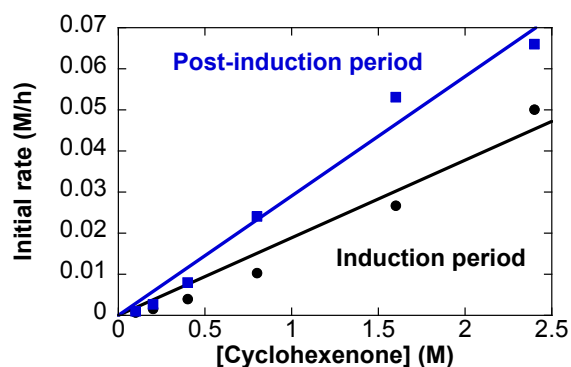


Figure 6-6. Dependence of the initial rate on [cyclohexenone] for Pd(DMSO)₂(TFA)₂-catalyzed oxidation of cyclohexenone to phenol. Reaction conditions: [Pd(TFA)₂] = 0.08 M (0.04 mmol), [DMSO] = 0.16 M (0.08 mmol), EtOAc = 0.5 mL, 1 atm O₂, 60 °C.

When [Pd(TFA)₂] and [DMSO] are varied at a 1:2 ratio, representing [catalyst], the reaction rate exhibits a non-linear dependence on [catalyst] (Figure 6-7(A)). Fitting the rate versus [catalyst]^{1/2} reveals a linear relationship for both induction and post-induction periods (Figure 6-7(B)). When [Pd(TFA)₂] is varied at a fixed [DMSO], 1 equiv. relative to [substrate], the reaction rates for both induction and post-induction periods still exhibits a half-order dependence on [Pd(TFA)₂] (Figure 6-8).

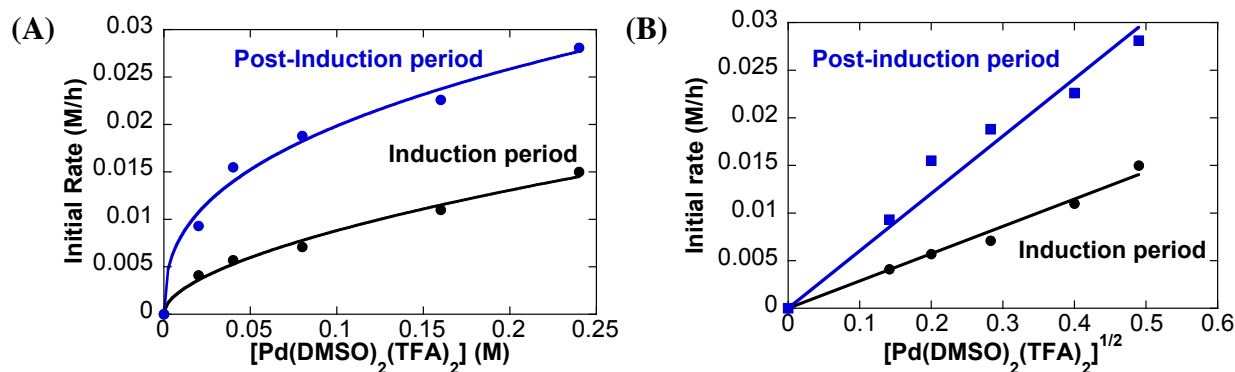


Figure 6-7. Dependence of the initial rate on the [catalyst], where the “catalyst” is an 1:2 mixture of $\text{Pd}(\text{TFA})_2$ and DMSO, for $\text{Pd}(\text{DMSO})_2(\text{TFA})_2$ -catalyzed oxidation of cyclohexenone to phenol. Reaction conditions: [cyclohexenone] = 0.8 M (0.4 mmol), EtOAc = 0.5 mL, 1 atm O_2 , 60 °C.

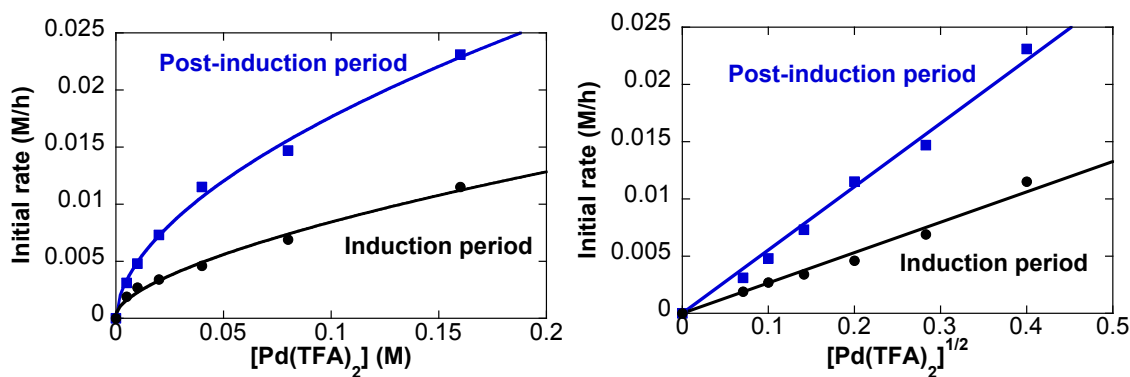


Figure 6-8. Dependence of the initial rate on the $[\text{Pd}(\text{TFA})_2]$ in the presence of excess DMSO ligand for $\text{Pd}(\text{DMSO})_2(\text{TFA})_2$ -catalyzed oxidation of cyclohexenone to phenol. Reaction conditions: [cyclohexenone] = 0.8 M (0.4 mmol), [DMSO] = 0.8 M (0.4 mmol), EtOAc = 0.5 mL, 1 atm O_2 , 60 °C.

The dependence of the rate on [DMSO] for the post-induction period is similar to that for the induction period (cf. Figure 5-8). Increasing [DMSO] dramatically inhibits the reaction rate

(Figure 6-9). At high [DMSO], noticeably less precipitation of Pd black was observed relative to at low [DMSO].

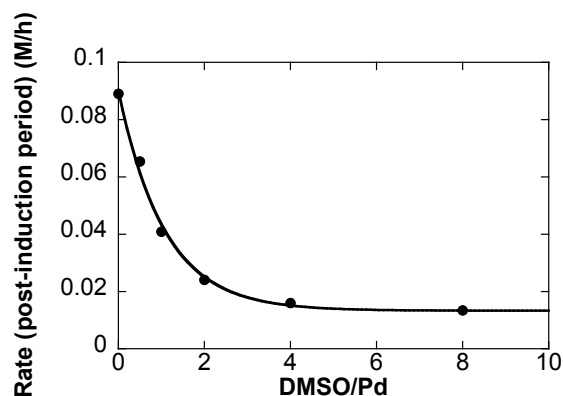


Figure 6-9. Dependence of the initial rate of $\text{Pd}(\text{DMSO})_2(\text{TFA})_2$ -catalyzed oxidation of cyclohexenone to phenol on the ratio of DMSO/Pd. Reaction conditions: [cyclohexenone] = 0.8 M (0.8 mmol), $[\text{Pd}(\text{TFA})_2]$ = 0.08 M (0.08 mmol), EtOAc = 1 mL, 1 atm O_2 , 60 °C, [DMSO] = 0, 0.04, 0.08, 0.16, 0.32 and 0.64 M.

The dependence of the length of the induction period on various components of the reaction reveals important insights into the origin of the induction period. The length of the induction period increases as [DMSO] is increased (Figure 6-10). Increasing [cyclohexenone] leads to a shorter induction period (Figure 6-11). The inverse half-life of the induction period, $1/t_{1/2}$, which was used as an estimation of the rate constant, exhibits a second order dependence on [cyclohexenone] (Figure 6-10, insert). The catalyst concentration also demonstrates a strong effect on the length of the induction period. In the presence of excess DMSO, higher $[\text{Pd}(\text{TFA})_2]$ leads to a shorter induction period, with $1/t_{1/2}$ exhibiting a linear dependence on $[\text{Pd}(\text{TFA})_2]$ (Figure 6-12(A)). When $[\text{Pd}(\text{TFA})_2]$ and [DMSO] are varied at a 1:2 ratio, however, the length of the induction period exhibits no dependence on $[\text{Pd}(\text{DMSO})_2(\text{TFA})_2]$ (Figure 6-12(B)).

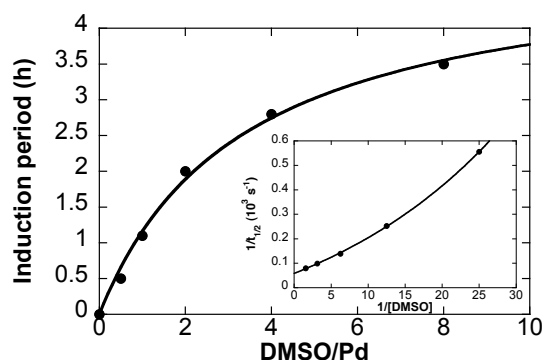


Figure 6-10. Dependence of the length of induction period on the Pd-catalyzed oxidation of cyclohexenone to phenol on [DMSO]. The curve-fit reflects a nonlinear least-squares fit to a generic hyperbolic function of [DMSO]/[Pd]: $y = c_1x/(c_2+x)$. Reaction conditions: [cyclohexenone] = 0.8 M (0.8 mmol), [Pd(TFA)₂] = 0.08 M (0.08 mmol), EtOAc (1 mL), O₂ (1 atm), 60 °C.

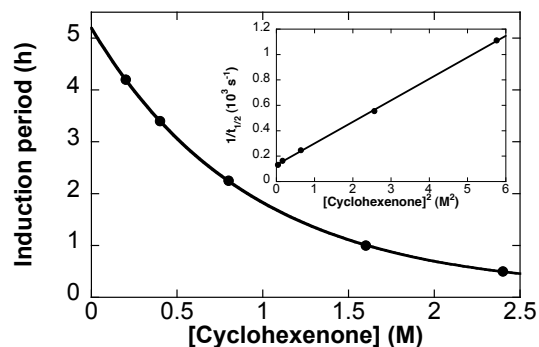


Figure 6-11. Dependence of the length of induction period on [cyclohexenone] for Pd(DMSO)₂(TFA)₂-catalyzed oxidation of cyclohexenone to phenol. Reaction conditions: [Pd(TFA)₂] = 0.08 M (0.04 mmol), [DMSO] = 0.16 M (0.08 mmol), EtOAc = 0.5 mL, 1 atm O₂, 60 °C.

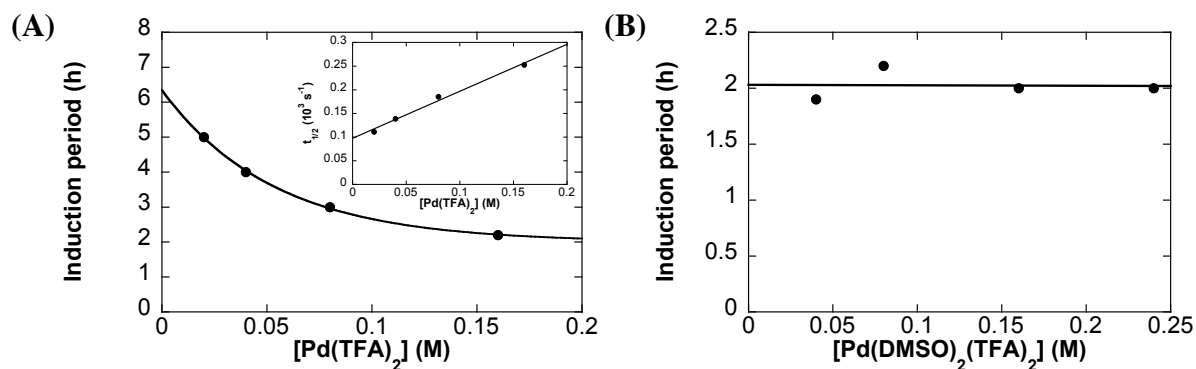


Figure 6-12. Dependence of the length of induction period on catalyst concentration, where $[\text{Pd}(\text{TFA})_2]$ is varied at fixed $[\text{DMSO}]$ in excess (A) and the “catalyst” is an 1:2 mixture of $\text{Pd}(\text{TFA})_2$ and DMSO (B). Reaction conditions: $[\text{cyclohexenone}] = 0.8 \text{ M}$, $\text{EtOAc} = 0.5 \text{ mL}$, 1 atm O_2 , $60 \text{ }^\circ\text{C}$, (A) $[\text{DMSO}] = 0.8 \text{ M}$.

Addition of 10% trifluoroacetic acid to the reaction mixture eliminates the induction period (Figure 6-13). The resulting initial time course almost overlays with the unligated $\text{Pd}(\text{TFA})_2$ -catalyzed reaction. However, addition of trifluoroacetic acid to the unligated $\text{Pd}(\text{TFA})_2$ -catalyzed reaction does not affect the initial rate.

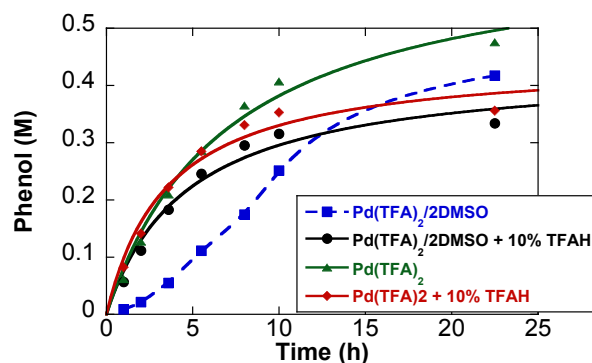


Figure 6-13. Reaction time courses of Pd-catalyzed oxidation of cyclohexenone to phenol. Reaction conditions: [cyclohexenone] = 0.8 M (0.4 mmol), [Pd(TFA)₂] = 0.04 M (0.02 mmol), ([DMSO] = 0.08 M (0.04 mmol)), ([TFAH] = 0.08 M (0.04 mmol)), EtOAc = 0.5 mL, 1 atm O₂, 60 °C.

6.2.4 Kinetic Studies of Dehydrogenation of Cyclohexenone Catalyzed by Unligated Pd(TFA)₂

The lack of an induction period observed with unligated Pd(TFA)₂ as the catalyst for dehydrogenation of cyclohexenone allowed us to probe the kinetic orders under these conditions by using initial rates. The plots in Figure 6-14 reveal a first order dependence of the reaction rate on [cyclohexenone] and [Pd(TFA)₂]. This first order dependence on [Pd(TFA)₂] contrasts the half-order dependence observed for Pd(DMSO)₂(TFA)₂-catalyzed reactions. The kinetic isotope effect, however, resembles that of Pd(DMSO)₂(TFA)₂-catalyzed reactions (cf. Scheme 5-4). The α-C–H exhibits a primary deuterium kinetic isotope effect (3.9 ± 0.58), when comparing the initial rates of dehydrogenation of cyclohexenone-*d*₀ versus 2,6,6-cyclohexenone-*d*₃ (Scheme 6-2). Negligible KIE is detected for the C–H at the 4-position, based on comparison of the rates of 2,6,6-cyclohexenone-*d*₃ and 2,4,4,6,6-cyclohexenone-*d*₅ (Scheme 6-2).

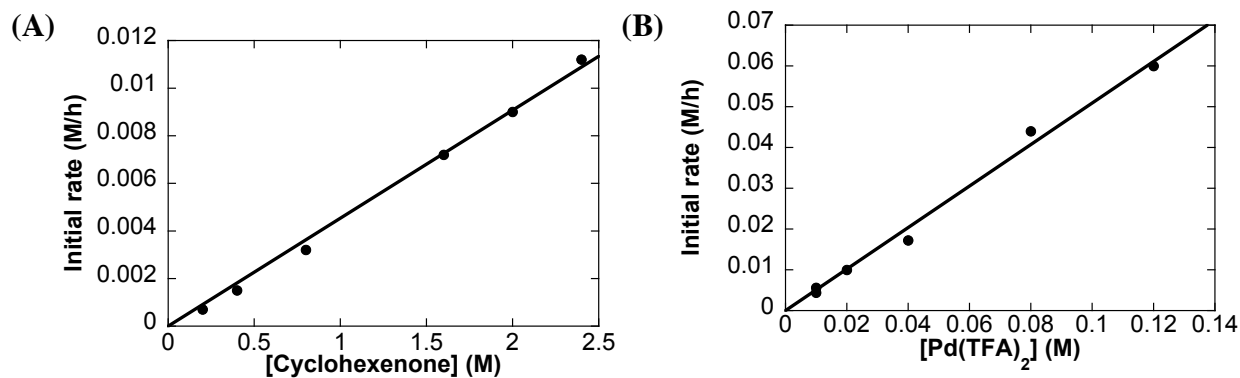
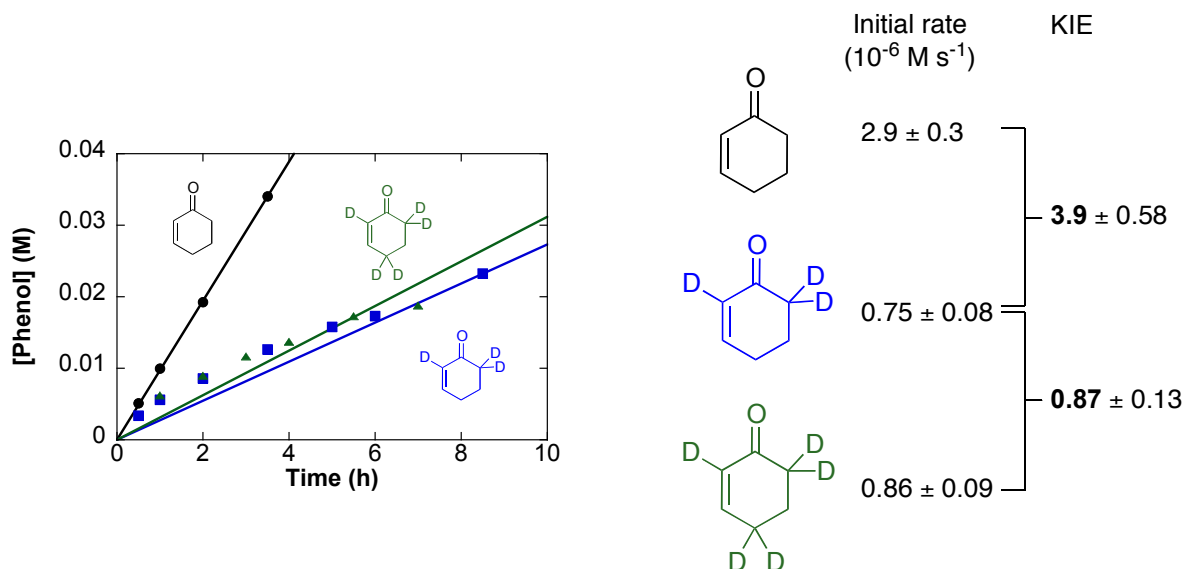


Figure 6-14. Kinetic orders for unligated-Pd(TFA)₂ catalyzed dehydrogenation of cyclohexenone to phenol, dependence of initial rate on [cyclohexenone] (A) and on [Pd(TFA)₂] (B). Reaction conditions: EtOAc = 0.5 mL, 1 atm O₂, 60 °C; (A) [Pd(TFA)₂] = 0.04 M (0.02 mmol); (B) [cyclohexenone] = 0.4 M (0.2 mmol).

Scheme 6-2. Deuterium Kinetic Isotope Effects (KIE) Derived from Independent Measurement of Initial Rates of Pd(TFA)₂-Catalyzed Dehydrogenation of Cyclohexenone to Phenol^a



^a Reaction conditions: [Substrate] = 0.4 M (0.2 mmol), [Pd(TFA)₂] = 0.02 M (0.01 mmol), EtOAc (0.5 mL), O₂ (1 atm), 60 °C.

6.2.5 Assessment of the Homogeneity of Pd(DMSO)₂(TFA)₂-Catalyzed Dehydrogenation

The induction period of Pd(DMSO)₂(TFA)₂-catalyzed dehydrogenation of cyclohexenone could arise from an in-situ formation of a second catalyst. In the absence of DMSO ligands, the reaction furnishes Pd black with concomitant fading of the yellow color of the solution, suggesting that the homogeneous Pd⁰ may decompose or aggregate into heterogeneous clusters of Pd. Under the catalytic conditions with DMSO ligands, Pd black was also formed, but the yellow color of the solution was retained. Numerous precedents for conversion of homogeneous Pd^{II} into nanoparticles prompted us to investigate the homogeneity of the catalyst system during the dehydrogenation of cyclohexanone and cyclohexenone.^{3,4} The Hg poisoning test is a common method for probing whether a transition metal-catalyzed reaction is homogeneous or heterogeneous, as formation of an amalgam between a M⁰ catalyst and Hg can terminate the activity of a heterogeneous catalyst.⁴ Addition of approximately 100 equiv. of Hg into a Pd(DMSO)₂(TFA)₂-catalyzed dehydrogenation of cyclohexanone at $t = 0.5$ h results in no immediate change in activity, but after two turnovers, a diminished reactivity was observed (Figure 6-15).

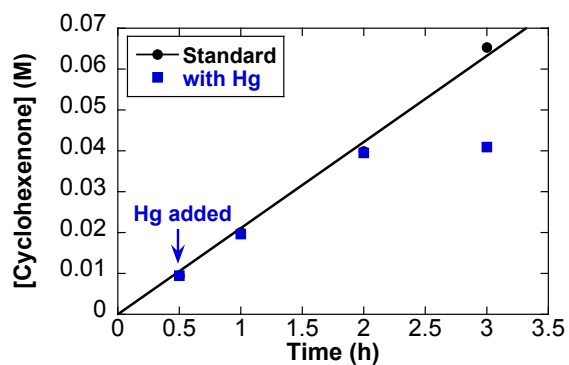


Figure 6-15. Hg test for $\text{Pd}(\text{DMSO})_2(\text{TFA})_2$ -catalyzed aerobic dehydrogenation of cyclohexanone to cyclohexenone. Reaction conditions: $[\text{cyclohexanone}] = 0.4 \text{ M}$ (0.2 mmol), $[\text{Pd}(\text{TFA})_2] = 0.02 \text{ M}$ (0.01 mmol), $[\text{DMSO}] = 0.04 \text{ M}$ (0.02 mmol), $\text{EtOAc} = 0.5 \text{ mL}$, 1 atm O_2 , $60 \text{ }^\circ\text{C}$.

Addition of Hg has a similar effect on $\text{Pd}(\text{DMSO})_2(\text{TFA})_2$ -catalyzed dehydrogenation of cyclohexenone. For both DMSO-ligated and unligated Pd catalyst systems, addition of Hg did not cause an immediate loss of activity (Figure 6-16), but a reduced reaction rate was observed after several hours.

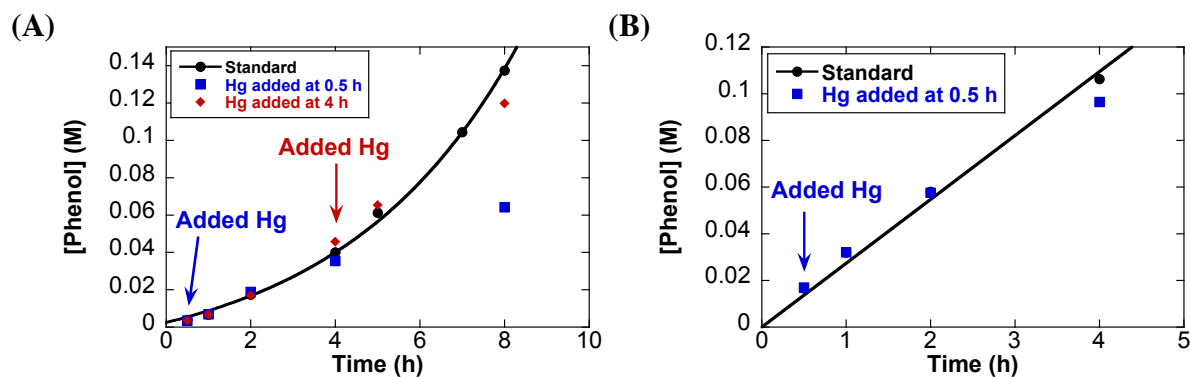


Figure 6-16. Mercury test for Pd(TFA)₂-catalyzed aerobic oxidation of cyclohexenone to phenol in the presence of DMSO ligands (A) and the absence of DMSO ligands (B). Reaction conditions: [cyclohexenone] = 0.8 M (0.4 mmol), [Pd(TFA)₂] = 0.04 M (0.02 mmol), EtOAc = 0.5 mL, 1 atm O₂, 60 °C; (A): [DMSO] = 0.08 M (0.02 mmol).

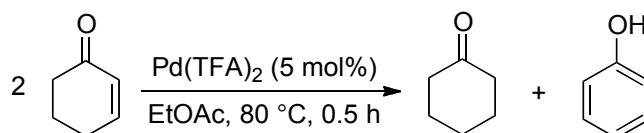
Dynamic light scattering (DLS) provides information about the particle size in solution without invading the system. Before addition of substrates, the solution of Pd(DMSO)₂(TFA)₂ in EtOAc displays particle sizes of < 1 nm. After a 24 h aerobic oxidation of cyclohexenone, particles ranging from 1.8 to 5.6 nm had formed. In contrast, the same experiment with the solution of Pd(DMSO)₂(TFA)₂ in AcOH reveals no detectable Pd nanoparticles after 24 h.

6.2.6 Pd-Catalyzed Disproportionation of Cyclohexenone to Cyclohexanone and Phenol

During our investigation of the Pd-catalyzed dehydrogenation of cyclohexenone, we observe a parallel Pd-catalyzed disproportionation reaction, where cyclohexenone is converted to cyclohexanone and phenol (Table 6-1). No cyclohexanone is detected in the unligated-Pd(TFA)₂ catalyzed dehydrogenation of cyclohexenone at 60 °C. At 80 °C, however, the reaction mixture affords cyclohexanone in 16% yield after 0.5 h, indicating the presence of a disproportionation pathway (Table 6-1, entry 1). This pathway is favored when the reaction is performed under N₂ atmosphere. Complete disproportionation is achieved after 0.5 h (entry 2) under N₂. The

presence of DMSO ligands in the system substantially inhibits the disproportionation reaction. No cyclohexenone disproportionation is observed under aerobic conditions, and 26% cyclohexenone disproportionation is observed under N₂ (entries 3 and 4). Large quantities of Pd black is observed under anaerobic conditions, whereas less Pd black is present under aerobic conditions.

Table 6-1. Disproportionation of Cyclohexenone to Cyclohexanone and Phenol ^a



Entry	Atmosphere	DMSO (mol%)	Ketone (%)	Enone (%)	Phenol (%)
1	O ₂	0	16	55	34
2	N ₂	0	50	0	50
3	O ₂	10	0	95	5
4	N ₂	10	13	73	13

^a Reaction conditions: [Cyclohexenone] = 0.8 M (0.4 mmol), [Pd(TFA)₂] = 0.04 M (0.02 mmol), EtOAc = 1 mL, 1 atm O₂, 80 °C, 0.5 h.

6.3 Discussion

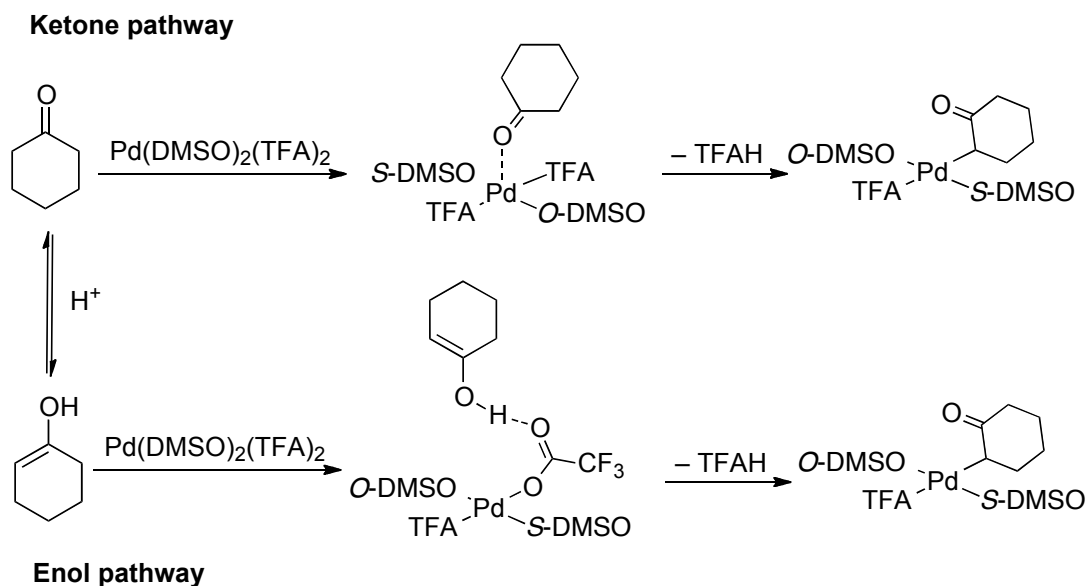
6.3.1 Additional Insights into Pd(DMSO)₂(TFA)₂-Catalyzed Dehydrogenation of Cyclohexanone

Our study in Chapter 5 established that the concentration of DMSO ligand has a minimal influence on the initial rate of Pd(DMSO)₂(TFA)₂-catalyzed dehydrogenation of cyclohexanone (cf. Figure 5-3(A)). The identity of sulfoxide ligands does affect the rate, however (Figure 6-4). Tetramethylene sulfoxide is most similar to DMSO with respect to sterics as well as electronics,^{14,15} and exhibits similar reactivity to DMSO. The larger sulfoxide ligands, such as diphenyl sulfoxide and methylphenyl sulfoxide are believed to sterically disfavor association of the ketone at the Pd^{II} center (cf. Scheme 5-5).

The dramatic inhibitory effect of TsOH supports the intramolecular deprotonation pathway for α -C–H cleavage that we propose in Chapter 5 (cf. structure **5-3**). TsOH is expected to react with the TFA ligand in-situ to generate $\text{Pd}(\text{OTs})_2$ and 2TFAH .¹⁶ We speculate that the inhibitory effect arises from the different basicity between tosylate and trifluoroacetate anion ligands on Pd, as the less basic tosylate is incapable of deprotonating the α -C–H.

The beneficial effect of AcOH and TFAH additives may be associated with the acid-catalyzed enolization of ketone to generate its enol form. As discussed in Chapter 5, $\text{Pd}(\text{TFA})_2$ -catalyzed dehydrogenation of cyclohexanone proceeds via a penta-coordinated ketone-Pd intermediate under neutral conditions (Scheme 6-3, ketone pathway). Formation of enol under acidic conditions may lead to an enol pathway, in which the enol interacts with the carboxylate ligand on Pd^{II} via hydrogen-bonding (Scheme 6-3, enol pathway). An analogous mechanism has been proposed for $\text{Pd}(\text{py})_2(\text{OAc})_2$ -catalyzed (py = pyridine) alcohol oxidation.¹⁷

Scheme 6-3. Possible Pathways for Acid-Accelerated Dehydrogenation of Cyclohexanone



6.3.2 The Homogeneous/Heterogeneous Characterization of Pd-Catalyzed Dehydrogenation of Cyclohexenone

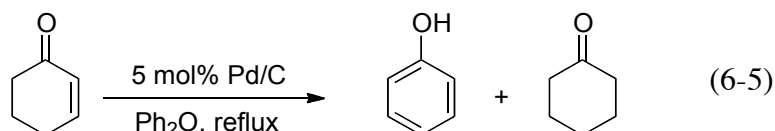
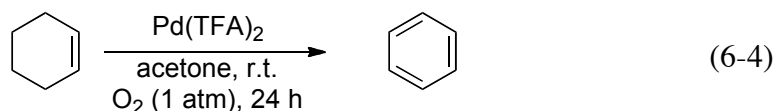
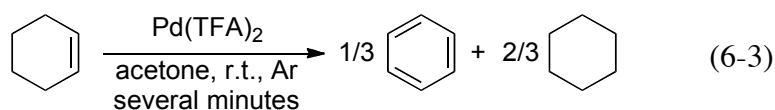
The induction period of $\text{Pd}(\text{DMSO})_2(\text{TFA})_2$ -catalyzed dehydrogenation of cyclohexenone raises suspicion that in-situ formed nanoclusters serve as the active catalyst species.⁴ The catalyst that forms following the induction period favors conversion of cyclohexenones to phenols, which is consistent with the chemoselectivity of heterogeneous Pd catalysts in the literature.⁶ Several qualitative observations support formation of nanoparticles as the active catalytic species. The observed precipitation of Pd black during the reaction confirms that catalyst aggregation pathway is taking place, and generation of nanoparticles in EtOAc solvent is also evident from DLS experiments. The Hg poisoning test reveals an inhibitory effect of the reaction rate by addition of Hg, although the effect is not observed immediately.

None of the above observations is definitive with respect to establishing whether the catalyst system is heterogeneous or homogeneous. Formation of Pd black is commonly observed in Pd-catalyzed reactions that proceed via a $\text{Pd}^{\text{II}}\text{-Pd}^0$ cycle. It is difficult to verify that these heterogeneous Pd particles are responsible for the catalytic reactivity. Similarly, the detection of nanoparticles by DLS only suggests the existence of aggregated Pd, but does not provide information about the reactivity of the species. The Hg poisoning test is inconclusive as well. The inhibitory effect of Hg^0 could arise from reaction of homogeneous Pd^0 intermediates with Hg^0 , thereby removing active homogeneous catalysts from the reaction. In addition, the time-scale for amalgamation is unclear. The lack of a Hg^0 effect at early stages of the reaction may be due to the fact that steady-state of the interaction between Hg and Pd has yet been reached.

On the other hand, the reproducible kinetics for this catalyst system supports a homogeneous catalyst. The formation of nanoparticles can be affected by random perturbations of the system,

and irreproducible kinetics are often observed for nanoparticle-catalyzed reactions. Furthermore, strong influences of ligand on the reaction rate are consistent with a homogeneous catalyst system as well.

The disproportionation reactivity of the Pd catalyst under anaerobic conditions at elevated temperatures illustrates the complexity and subtle condition dependence for the formation of a nanoparticle catalyst from an operationally homogeneous Pd catalyst. A rapid Pd-catalyzed disproportionation of cyclohexene to cyclohexane and benzene under Ar (eq 6-3), analogous to our observations, is first reported by Trost.¹⁸ It is then studied further and proposed to arise from a heterogeneous catalyst by Bercaw.^{19,20} The same Pd catalyst, under 1 atm O₂, oxidizes cyclohexene to benzene as the sole product (eq 6-4), and was proposed to be homogeneous by Bercaw and coworkers.²¹ The disproportionation under anaerobic conditions is considerably faster than the oxidation under aerobic conditions. In addition, Horning and coworkers reported the disproportionation of cyclohexenone to cyclohexanone and phenol under anaerobic conditions, using a heterogeneous catalyst, Pd/C (eq 6-5).²²



The reaction involving unligated Pd(TFA)₂ in EtOAc for oxidation of cyclohexenone resembles the conditions of Pd(TFA)₂ in acetone in eq 6-3 and 6-4, as well as the selectivity and

reaction rates under both aerobic and anaerobic conditions. While it is unclear whether the catalyst for oxidation of cyclohexenone under aerobic conditions is homogeneous or heterogeneous, the disproportionation catalyst under anaerobic conditions is expected to be heterogeneous, evident from the formation of bulk Pd black and exceptionally fast reactivity. The DMSO ligands considerably inhibit the disproportionation pathway, providing additional support that DMSO stabilizes the Pd catalyst.

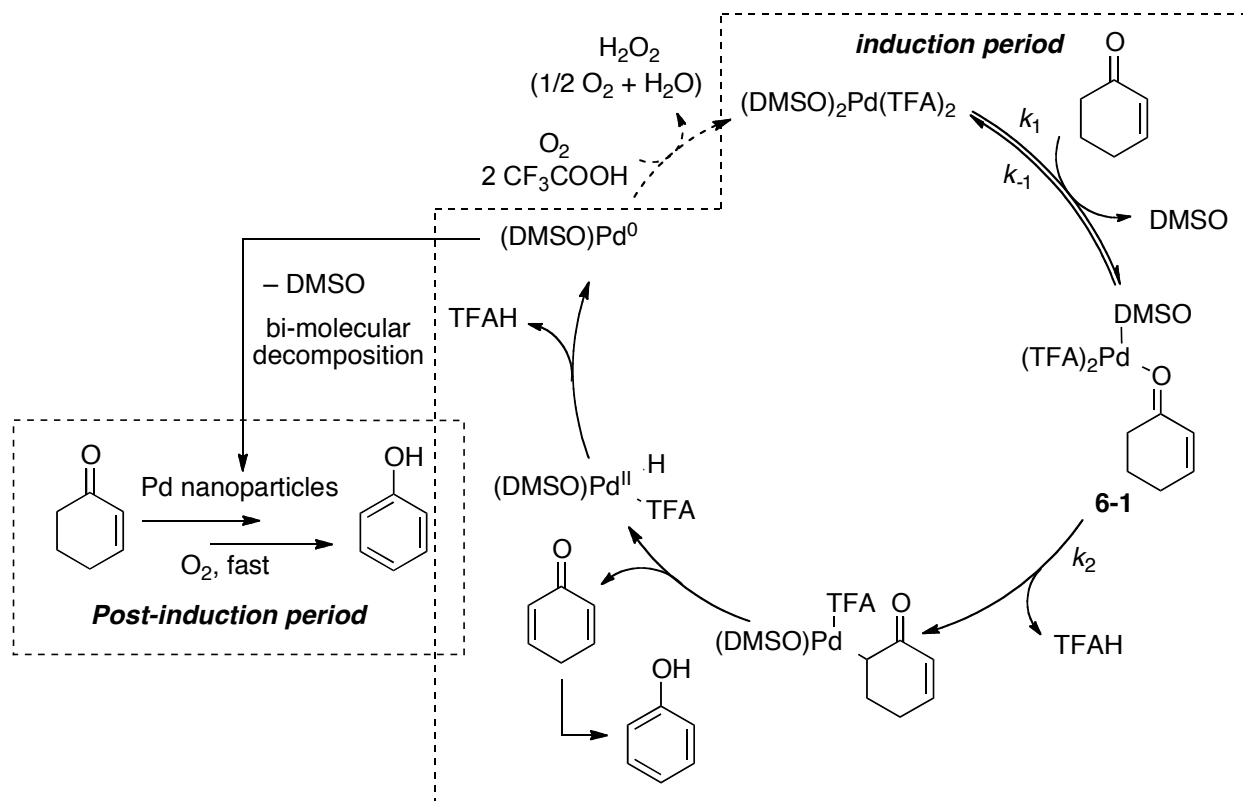
Despite the ambiguity of the homogeneity of the catalyst system in EtOAc, the solvent used for most of our mechanistic studies, the absence of nanoparticles for reactions taking place in AcOH, based on DLS data, suggests that the reactions carried out in this solvent are likely to be homogeneous. The formation and lack of nanoparticles in EtOAc and AcOH, respectively, correlates with the selectivity observed with each solvent for the formation of cyclohexenone or phenol in the dehydrogenation of cyclohexanone. While a definitive conclusion has not been reached, the collective data suggest that the conversion of cyclohexenone to phenol is most efficiently catalyzed by Pd nanoparticles that arise from *in situ* aggregation of Pd⁰. The AcOH solvent appears to inhibit Pd⁰ aggregation, thereby enabling high selectivity for cyclohexenone over phenol.

6.3.3 Proposed Mechanism for Pd(DMSO)₂(TFA)₂-Catalyzed Dehydrogenation of Cyclohexenone

Pd(DMSO)₂(TFA)₂-catalyzed oxidation of cyclohexenone consists of two stages: induction and post-induction periods. For both periods, the reaction rates exhibit a first order dependence on [cyclohexenone] and a half-order dependence on [catalyst]. The α-C–H exhibits a primary KIE, whereas the allylic C–H displays a negligible KIE. Collectively, the above results and

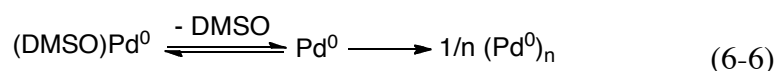
observations support a mechanism shown in Scheme 6-4. Dissociation of a DMSO ligand from Pd results in coordination of the cyclohexenone with Pd^{II}. The rate-limiting deprotonation of the α -C-H affords a Pd enolate intermediate, followed by fast β -H elimination to generate the dienone, which can rapidly tautomerize to the phenol, and a Pd-hydride. The resulting Pd-hydride undergoes reductive elimination to form the Pd⁰ intermediate. The Pd⁰ could be oxidized by O₂ to regenerate Pd^{II}, but competing aggregation upon dissociation of the DMSO ligands is fast under these conditions to generate Pd nanoparticles. These nanoparticles catalyze fast conversion of cyclohexenone to phenol, resulting in the post-induction stage. In the absence of the DMSO ligands, the formation of Pd nanoparticles is fast and results in no induction period.

Scheme 6-4. Proposed Mechanism for Pd(DMSO)₂(TFA)₂-Catalyzed Oxidation of Cyclohexenone to Phenol



The initial ligand dissociation step during the induction period accounts for the half-order dependence in [catalyst] and the sharp DMSO inhibitory effect. Because the DMSO and Pd(DMSO)(TFA)₂ are formed simultaneously, the reverse step formally exhibits a bimolecular dependence on [catalyst]. As a result, [Pd(DMSO)(TFA)₂] is proportional to the square root of [Pd(DMSO)₂(TFA)₂]. Accordingly, the reaction rate is proportional to the square root of [catalyst]. A similar half-order dependence on [catalyst] associated with ligand dissociation has been observed previously with Pd(py)₂(OAc)₂-catalyzed alcohol oxidation reactions.²³ According to the above analysis, in the presence of excess DMSO, a first order dependence of the rate on [Pd(TFA)₂] should be observed. Conversely, a half-order dependence was still observed under these conditions. We attribute this inconsistency to a change of mechanism in the presence of excess DMSO. Under these conditions, the dissociation of DMSO from Pd is inhibited, and instead, the trifluoroacetate ligand may dissociate from Pd to form a cationic Pd intermediate and open the coordination site for cyclohexenone.

The inverse half-life ($1/t_{1/2}$) of the induction period is decreased as [DMSO] increases, and is proportional to [cyclohexenone]² and [Pd(TFA)₂] in the presence of excess DMSO (eq 6-7). When [Pd(TFA)₂] and [DMSO] are varied together, the length of the induction period exhibits no dependence on [Pd(DMSO)₂(TFA)₂]. We attribute the induction period to the formation of Pd nanoparticles. This process is associated with pre-dissociation of DMSO from the Pd⁰(DMSO) intermediate (eq 6-6), resulting in inhibition of the aggregation rate by increasing [DMSO]. The second order dependence of $1/t_{1/2}$ on [cyclohexenone] may result from the coordination of cyclohexenone to Pd⁰(DMSO), which competes with O₂ oxidation of Pd⁰(DMSO) and hence facilitates the aggregation.²⁴ However, due to the lack of methods for precise measurement of the length of the induction period, the above analyses are primarily qualitative speculations.



The enhanced rate of dehydrogenation following the induction period is believed to be catalyzed by Pd nanoparticles. The rate at this stage exhibits a first-order dependence on [cyclohexenone] and a half-order dependence on [catalyst]. The precise nature of the Pd nanoparticle and the mechanism of the dehydrogenation reaction are unclear. However, it is reasonable to speculate that two molecules of substrate react on the surface of an aggregated Pd nanoparticle. In this scenario, one catalyst molecule produces two molecules of the phenol product, leading to the observed half-order dependence of the rate on [catalyst].

6.3.4 Conclusion

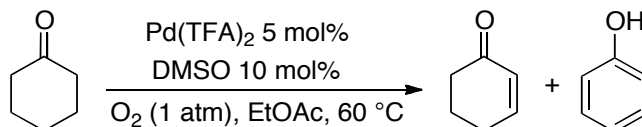
Additional kinetic results reveal the complexity of the $\text{Pd}(\text{DMSO})_2(\text{TFA})_2$ catalyst system in the dehydrogenation of cyclohexanone and cyclohexenone. Starting with an operationally homogeneous catalyst, the Pd^0 intermediate formed from the initial turnover is possibly converted into a nanoparticle via a bi-molecular pathway. The nanoparticles serve as a more efficient catalyst for aromatization of cyclohexenone to afford phenol. These results have important implications in understanding Pd-catalyzed aerobic oxidation reactions. Future work in the development of superior catalysts selective for oxidation of cyclohexanone to cyclohexenone requires ligands that can better stabilize the homogeneous Pd catalyst.

6.4 Experimental

6.4.1 General Procedures and Considerations

All commercially available compounds were used as received and purchased from Sigma Aldrich. ^1H NMR spectra were recorded on a Bruker AC-300 MHz or a Varian Mercury-300 MHz spectrometer. The chemical shifts (δ) are given in parts per million and referenced to

residual solvent peaks or a TMS internal standard. Gas chromatography was performed on a Shimadzu GC-17A using a Stabilwax®-DB column or a RTX-5MS column and referenced to an internal standard (tetradecane). Flash column chromatography was performed on an Isco Combiflash system using silica gel 60 (Silicycle) and eluted with ethyl acetate/hexane.



Catalytic aerobic oxidation reactions were performed using a custom reaction apparatus that enabled several reactions to be performed simultaneously under a constant pressure of O_2 (approx. 1 atm) with controlled temperature and orbital agitation. To a disposable 13 mm thick-walled culture tube was added Pd(TFA)_2 , (13.2 mg, 0.04 mmol, 0.05 equiv.), DMSO (5.6 μL , 0.04 mmol, 0.1 equiv), and 1 mL EtOAc to form a bright yellow solution. The reaction tube was placed in a 48-well parallel reactor mounted on a Glas-Col large capacity mixer. The headspace was purged with O_2 for 10 min, after which tetradecane (20 μL , 0.077 mmol) was added via syringe. The reactor temperature was set to 60 $^\circ\text{C}$ and allowed to equilibrate for 5 min. Injection of cyclohexanone (80 μL , 0.8 mmol) established the $t = 0$ point. After various time intervals, aliquots were withdrawn from the reaction mixture via pipettes, diluted with CH_2Cl_2 and analyzed by GC.

As illustrated in Figure 5-14, for dehydrogenation of cyclohexenone to phenol, when an induction period is present, the slope of [phenol]/time within the initial linear regime, starting from $t = 0$, represents the rate of the initial period. The initial rate for the post-induction period was calculated based on data from the last point of the induction period to the point at 10% conversion.

6.4.2 Procedures for Dynamic Light Scattering (DLS) Measurements

Dynamic light scattering (DLS) measures the time-dependent autocorrelation function of the scattered light intensity related to the particle's Brownian motion. DLS samples were prepared by using 1 μm PFTE filtered solvents and filtering the solution of palladium and/or catalytic reaction mixture through a pad of glass wool into a dust free culture tube. DLS experiments were carried out with a 100 mW, 532 nm laser (Compass 315-100, Coherent, Santa Clara, CA) illuminating a temperature controlled glass cell at 25 °C filled with a refractive-index matching fluid (decahydronaphthalene, Fisher Scientific, 30 Pittsburgh, PA) and the sample. The scattering of light was measured at 90° and the autocorrelation functions were obtained using a BI-9000AT digital autocorrelator (Brookhaven Instruments, Holtsville, NY). A calibration procedure was carried out on a diluted monodispersed suspension of polystyrene beads dissolved in water.

6.5 Contributions

Dr. Doris Pun performed the dynamic light scattering (DLS) measurements.

6.6 References

-
1. (a) Stahl, S. S. *Science* **2005**, *309*, 1824-1826. (b) Stahl, S. S. *Angew. Chem. Int. Ed.* **2004**, *43*, 3400-3420. (c) Gligorich, K. M.; Sigman, M. S. *Chem. Commun.* **2009**, 3854-3867. (d) Shi, Z.; Zhang, C.; Tang, C.; Jiao, N. *Chem. Soc. Rev.* **2012**, *41*, 3381-3430.
 2. (a) Steinhoff, B. A.; Guzei, I. A.; Stahl, S. S. *J. Am. Chem. Soc.* **2004**, *126*, 11268-11278. (b) Steinhoff, B. A.; Stahl, S. S. *J. Am. Chem. Soc.* **2006**, *128*, 4348-4355.
 3. For characterization of the decomposition of homogeneous Pd catalysts into nanoparticle catalysts in aerobic oxidation reactions, see: (a) van Benthem, R. A. T. M.; Hiemstra, H.; van

Leeuwen, P. W. N. M.; Geus, J. W.; Speckamp, W. N. *Angew. Chem. Int. Ed.* **1995**, *34*, 457-460.

(b) Mifsud, M.; Parkhomenko, K. V.; Arends, I. W. C. E.; Sheldon, R. A. *Tetrahedron* **2010**, *66*, 1040-1044.

4. For reviews about distinguishing homogeneous and heterogeneous catalysis, see: (a) Widegren, J. A.; Finke, R. G. *J. Mol. Catal. A: Chem.* **2003**, *198*, 317. (b) Crabtree, R. H. *Chem. Rev.* **2011**.

5. For deliberate synthesis of Pd nanoparticles and their application in aerobic alcohol oxidation, see: (a) Vargaftik, M. N.; Zagorodnikov, V. P.; Stolarov, I. P.; Moiseev, I. I.; Kochubey, D. I.; Likholobov, V. A.; Chuvilin, A. L.; Zamaraev, K. I. *J. Mol. Catal.* **1989**, *53*, 315. (b) Kaneda, K.; Fujii, M.; Morioka, K. *J. Org. Chem.* **1996**, *61*, 4502. (c) Kaneda, K.; Fujie, Y.; Ebitani, K. *Tetrahedron Lett.* **1997**, *38*, 9023. (d) Kovtun, G.; Kameneva, T.; Hladyi, S.; Starchevsky, M.; Pazdersky, Y.; Stolarov, I.; Vargaftik, M.; Moiseev, I. *Adv. Synth. Catal.* **2002**, *344*, 957. (e) Choi, K.-M.; Akita, T.; Mizugaki, T.; Ebitani, K.; Kaneda, K. *New J. Chem.* **2003**, *27*, 324.

6. (a) Horning, E. C.; Horning, M. G. *J. Am. Chem. Soc.* **1947**, *69*, 1359. (b) Downes, A. M.; Gill, N. S.; Lions, F. *J. Am. Chem. Soc.* **1950**, *72*, 3464. (c) Chitwood, H. C.; Fitzpatrick, J. T.; Fowler, G. W.; Freure, B. T. *Eng. Proc. Dev.* **1952**, *44*, 1696. (d) Zimmerman, H. E.; Schuster, D. I. *J. Am. Chem. Soc.* **1962**, *84*, 4527. (e) Newman, M. S.; Blum, J. *J. Am. Chem. Soc.* **1964**, *86*, 503. (f) Jacobsen, S. E.; C07C 213/00, 215/76 ed. US Patent, **1993**. Manitto, P.; Speranza, G.; Monti, D.; (g) Fontana, G.; Panosetti, E. *Tetrahedron* **1995**, *51*, 11531.

-
7. For a recent review, see: Muzart, J. *Eur. J. Org. Chem.* **2010**, 3779.
8. (a) Theissen, R. J. *J. Org. Chem.* **1971**, *36*, 752. (b) Muzart, J.; Pete, J. P. *J. Mol. Catal.* **1982**, *15*, 373. (c) Wenzel, T. T. *J. Chem. Soc., Chem. Commun.* **1989**, 932. (d) Park, Y. W.; Oh, H. H. *Bull. Kor. Chem. Soc.* **1997**, *18*, 1123. (e) Tokunaga, M.; Harada, S.; Iwasawa, T.; Obora, Y.; Tsuji, Y. *Tetrahedron Lett.* **2007**, *48*, 6860.
9. (a) Ito, Y.; Hirao, T.; Saegusa, T. *J. Org. Chem.* **1978**, *43*, 1011-1013. (b) Larock, R. C.; Hightower, T. R.; Kraus, G. A.; Hahn, P.; Zheng, D. *Tetrahedron Lett.* **1995**, *36*, 2423-2426. (c) Yu, J. Q.; Wu, H. C.; Corey, E. J. *Org. Lett.* **2005**, *7*, 1415-1417.
10. Izawa, Y.; Pun, D.; Stahl, S. S. *Science* **2011**, *333*, 209.
11. Diao, T.; Stahl, S. S. *J. Am. Chem. Soc.* **2011**, *133*, 14566.
12. Diao, T.; Wadzinski, T. J.; Stahl, S. S. *Chem. Sci.* **2012**, *3*, 887-891.
13. For a comprehensive summary of pK_a s:
<http://www.chem.wisc.edu/areas/reich/pkatable/index.htm>
14. Thomas, R.; Shoemaker, C. B.; Eriks, K. *Acta Crystallogr.* **1966**, *21*, 12-20.
15. Srivastava, R. S.; Fronczek, F. R. *Inorg. Chim. Acta.* **2001**, *322*, 32-36.
16. The pK_a of TsOH is lower than TFAH by 2 pK_a units.
17. Steinhoff, B. A.; Guzei, I. A.; Stahl, S. S. *J. Am. Chem. Soc.* **2004**, *126*, 11268.
18. Trost, B. M.; Metzner, P. J. *J. Am. Chem. Soc.* **1980**, *102*, 3572-3577.

-
19. Williams, T. J.; Caffyn, A. J. M.; Hazari, N.; Oblad, P. F.; Labinger, J. A.; Bercaw, J. E. *J. Am. Chem. Soc.* **2008**, *130*, 2418-2419.
20. Disproportion is often reported with heterogeneous catalysts. For an example of Pd nanoparticle-catalyzed disproportionation of alcohols, see: Kovtun, G.; Kameneva, T.; Hladyi, S.; Starchevsky, M.; Pazdersky, Y.; Stolarov, I.; Vargaftik, M.; Moiseev, I. *Adv. Synth. Catal.* **2002**, *344*, 957-964.
21. Bercaw, J. E.; Hazari, N.; Labinger, J. A. *J. Org. Chem.* **2008**, *73*, 8654-8657.
22. Horning, E. C.; Horning, M. G.; Walker, G. N. *J. Am. Chem. Soc.* **1949**, *71*, 169-171.
23. Steinhoff, B. A.; Guzei, I. A.; Stahl, S. S. *J. Am. Chem. Soc.* **2004**, *126*, 11268-11278.
24. (a) Stahl, S. S.; Thorman, J. L.; de Silva, N.; Guzei, I. A.; Clark, R. W. *J. Am. Chem. Soc.* **2002**, *125*, 12-13. (b) Popp, B. V.; Thorman, J. L.; Morales, C. M.; Landis, C. R.; Stahl, S. S. *J. Am. Chem. Soc.* **2004**, *126*, 14832-14842.

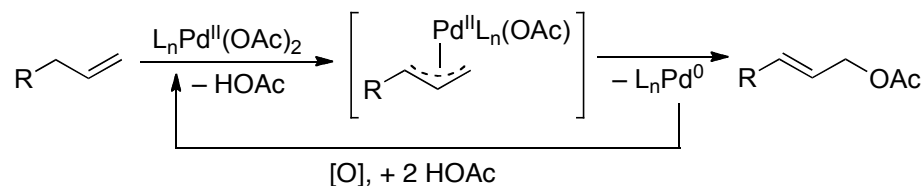
CHAPTER 7

O₂-Promoted Allylic Acetoxylation of (π -Allyl)Pd Complexes

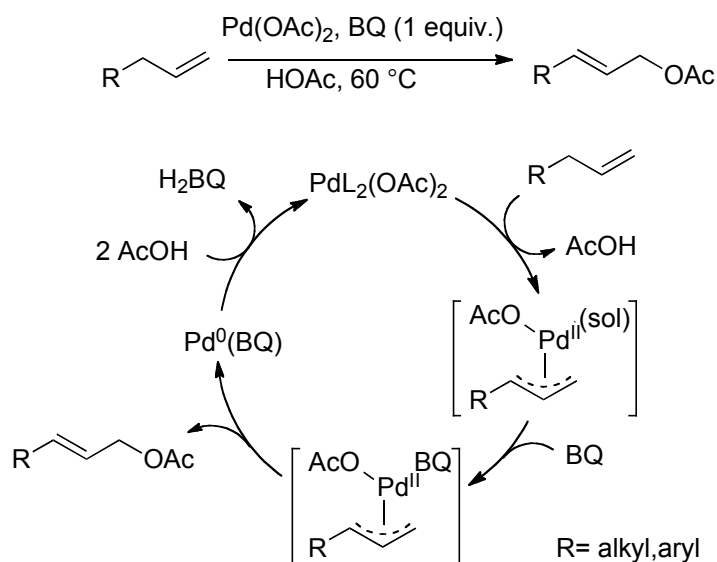
7.1 Introduction

Palladium-catalyzed acetoxylation of allylic C–H bonds is a reaction that has been the subject of extensive historical¹ and recent attention (Scheme 7-1).^{2,3} The vast majority of these reactions employ benzoquinone (BQ) as the stoichiometric oxidant, although reactions with O₂, hypervalent iodine and other reagents have also been used.⁴

Scheme 7-1. Pd-Catalyzed Oxidative Allylic Acetoxylation Reactions

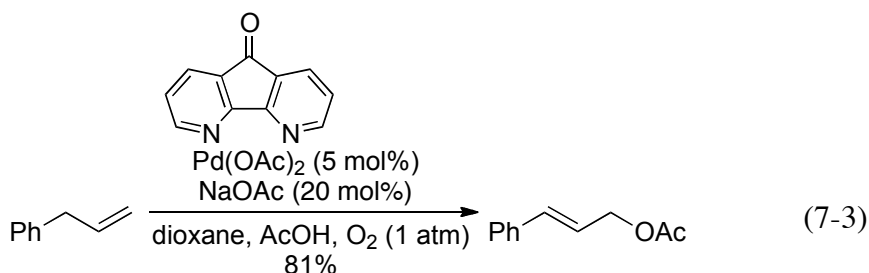
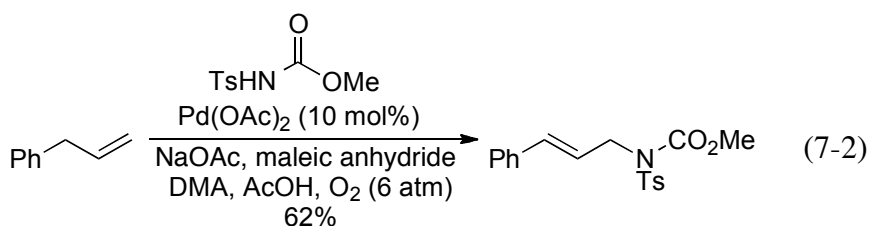
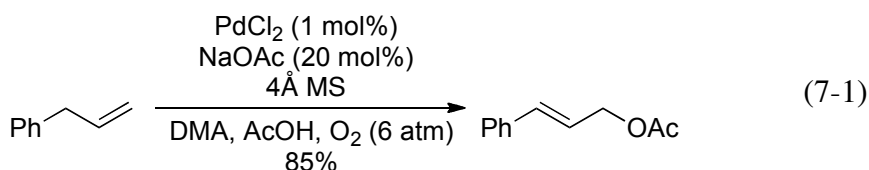


Fundamental studies of the oxidative acetoxylation reactions indicate that BQ promotes C–O reductive elimination from the (π -allyl)Pd^{II} intermediate (Scheme 7-2).^{5,6} These observations provide insights into the requirement of BQ for high yielding allylic acetoxylation reactions even when other stoichiometric oxidants are present.⁴ BQ may promote the acetoxylation of (π -allyl)Pd^{II} intermediates via two possible pathways: (1) BQ coordinates to (π -allyl)Pd^{II} intermediates and increase their electrophilicity (BQ-Pd^{II} interaction), proposed by Bäckvall and coworkers on the basis of kinetic data^{5c} and NMR spectroscopic studies;^{7,8} or (2) BQ displaces the allylic acetate product from Pd⁰ following reversible C–O bond formation (BQ-Pd⁰ interaction), proposed by Bercaw and coworkers on the basis of kinetic studies and acetate scrambling experiments.^{2c}

Scheme 7-2. BQ-Promoted Oxidative Allylic C-H Acetoxylation

Replacement of a traditional stoichiometric oxidant such as BQ with O_2 presents an environmentally benign alternative method.⁹ In light of the recent report of O_2 -promoted reductive elimination of hydrogen halide from Ir^{III} complexes by coordination to Ir,¹⁰ we ask whether O_2 is capable of interacting with Pd^{II} in a similar way, replacing BQ in promoting the acetoxylation of $(\pi\text{-allyl})\text{Pd}$ intermediates. If so, considering the capability of oxidizing Pd^0 to Pd^{II} with O_2 ,^{11,12} it is likely that, under the right conditions, O_2 can replace BQ in Pd-catalyzed oxidative allylic functionalization reactions. Recently, Kaneda and coworkers reported an aerobic Pd-catalyzed oxidative allylic acetoxylation reaction (eq 7-1).¹³ This unligated Pd method contradicts the argument that BQ is required to assist the acetoxylation of $(\pi\text{-allyl})\text{Pd}$ intermediates in allylic acetoxylation. Shortly after Kaneda's report, Liu and coworkers reported an aerobic Pd-catalyzed allylic amination reaction that uses maleic anhydride in place of BQ to promote cleavage of the Pd–C bond (eq 7-2).¹⁴ Subsequently, aerobic oxidative allylic acetoxylation

reactions have been achieved by employing a 4,5-diazafluorenone ligand (eq 7-3).¹⁵ It is likely that the bidentate 4,5-diazafluorenone ligand forms a cationic Pd^{II} intermediate, which undergoes facile acetoxylation.¹⁶ With the interesting O₂-mediated allylic oxidation reactions above, a systematic study of the mechanism of acetoxylation of unligated (π -allyl)Pd complexes with O₂ has not been reported.

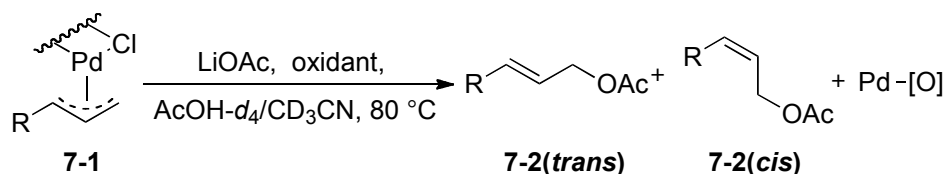


Here we investigate O₂-promoted acetoxylation of "ligand-free" (π -allyl)Pd complexes and palladium-catalyzed oxidative allylic acetoxylation using O₂ as the sole oxidant. The kinetic investigation on this reaction resulted in important insights into the mechanism of O₂-promoted acetoxylation processes. Our study of this O₂ promoted allylic acetoxylation in a simple "ligand-free" system also provides a foundation for our recent development of a ligand-based approach to achieve Pd-catalyzed C–H acetoxylation under aerobic conditions in the absence of BQ.¹⁵

7.2 Results

7.2.1 O₂-Promoted Acetoxylation of the (π -allyl)PdCl Complexes

We initiated our investigation of O₂-promoted acetoxylation by probing the effect of different oxidants on the acetoxylation reaction of various (π -allyl)PdCl complexes (Table 7-1).¹⁷ A mixture of AcOH-*d*₄ and CD₃CN in a ratio of 4:2.5 was used as the working solvent. AcOH-*d*₄ was employed by Bäckvall as the solvent for the study of BQ-promoted acetoxylation of (π -allyl)Pd complexes.⁵ The use of CD₃CN ensures solubility of the Pd complexes and LiOAc, as the acetate source. Alkyl, aryl and ester derived (π -allyl)PdCl complexes **7-1a**, **7-1b**, **7-1c** and **7-1d**, respectively, in the presence of BQ afford the terminal allylic acetate in high yields (Table 7-1, entries 1, 4, 7 and 10). A by-product, benzene, is observed in 3% yield from the reaction of **7-1b**, which possibly arises from over-oxidation or disproportionation of the allylic product **7-2b**. When investigating O₂ as the oxidant under the same conditions, the propenyl and cyclohexenyl PdCl complexes **7-1a** and **7-1b** only yield trace acetate product (entries 2 and 5), whereas electron-withdrawing (π -allyl)PdCl complexes **7-1c** and **7-1d** are converted to the allylic acetate product **7-2c** and **7-2d** in 31% and 94% yields, respectively. The O₂-promoted acetoxylation of **7-1c** proceeds to form the **7-2c** during the first five hours (about 30% conversion); however, multiple unidentified by-products emerge after 5 hours. These unexpected by-products likely inhibit the further conversion of **7-1c** to **7-2c**. In the absence of an oxidant, **7-1a**, **7-1b** and **7-1c** appear to be stable towards nucleophilic attack by acetate (entries 3, 6 and 9). The electron-withdrawing methyl butenoate derived (π -allyl)PdCl complex **7-1d** undergoes slow acetoxylation, and generates the acetoxylation product **7-2d** in 19% yield. While Pd black was generated in this reaction of **7-1d** under an N₂ atmosphere, none was observed in the reactions with O₂ or BQ present.

Table 7-1. Acetoxylation of (π -allyl)Pd Complexes in the Presence of BQ or O₂^a

Entry	(π -allyl)Pd complex	Oxidant	Product	NMR yield (%)
				7-2-trans(cis)
1	 7-1a	BQ	 7-2a	69
2		O ₂		2
3		none		1
4	 7-1b	BQ	 7-2b	(84)
5		O ₂		(7)
6		none		(0)
7	 7-1c	BQ	 7-2c(trans)	96 (0)
8		O ₂		31 (0)
9		none		1 (0)
10	 7-1d	BQ	 7-2d(trans)	93 (7)
11		O ₂		94 (6)
12		none		19 (0)
				7-2d(cis)

^a Reaction conditions: [Pd] = 10 mM, [LiOAc] = 12 mM, [Oxidant] = 30 mM, AcOH-*d*₄ = 0.4 mL, CD₃CN = 0.25 mL, 24 h. Reactions were performed in NMR tubes and monitored by INOVA-500MHz spectrometer with 1,3,5-tri-*tert*-butyl benzene as the internal standard.

The Hammett plot for the acetoxylation of *p*-substituted allylbenzene-derived (π -allyl)PdCl complexes in the presence of oxidants sheds light on the electronic effect of the Pd complexes on the reaction (eq 7-4). Formation of the allylic acetate product was monitored by ¹H NMR

spectroscopy, and the initial rate of each reaction (k_x) represents the rate from $t = 0$ to 5% conversion of the $(\pi\text{-allyl})\text{PdCl}$. The rho (ρ) values of $\ln(k_x/k_H)$ versus σ_{para} were determined to be 0.898 and 1.00 in the presence of BQ and O_2 , respectively (Figure 7-1).

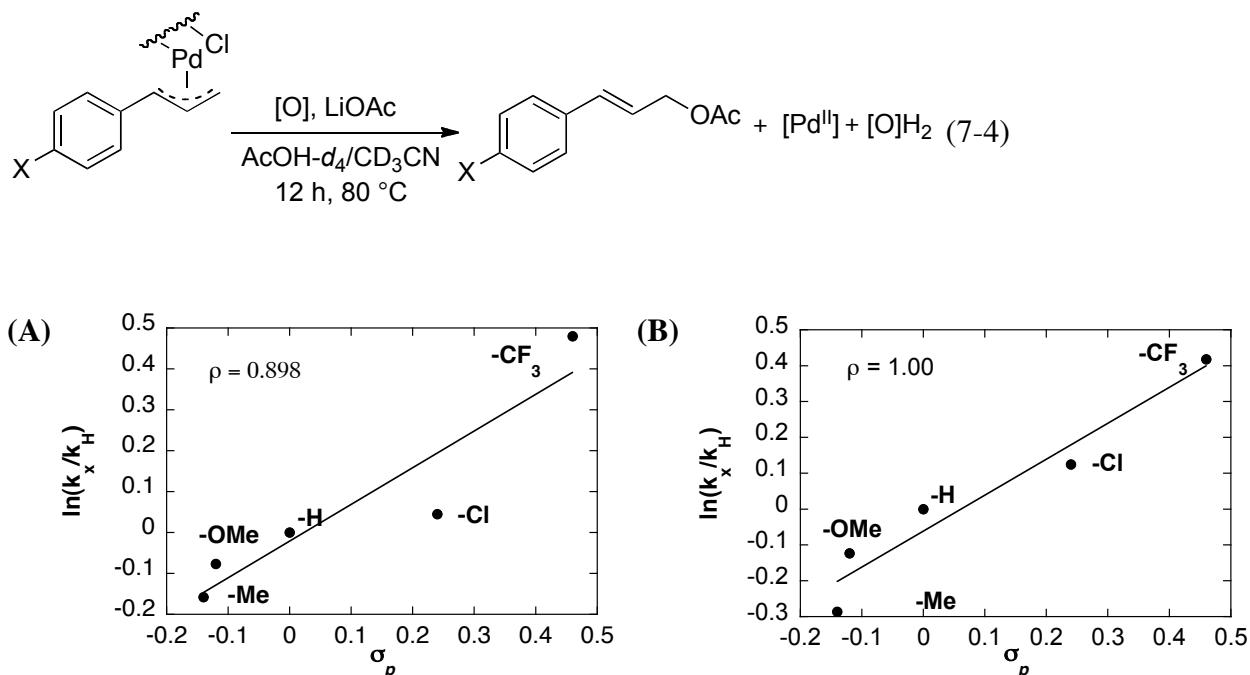


Figure 7-1. Hammett plot of the acetoxylation of p -substituted $(\pi\text{-Allyl})\text{PdCl}$ complexes in the presence of BQ (A) and O_2 (B). Reaction conditions: $[\text{Pd}]_0 = 3 \text{ mM}$, $[\text{LiOAc}] = 30 \text{ mM}$, $\text{AcOH-}d_4 = 0.4 \text{ mL}$, $\text{CD}_3\text{CN} = 0.25 \text{ mL}$, 80°C , (A) $[\text{BQ}] = 30 \text{ mM}$; (B) $[\text{O}_2] = 13 \text{ mM}$.

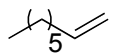
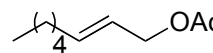
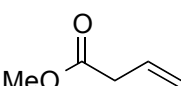
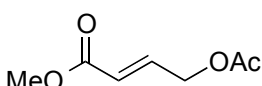
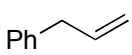
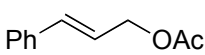
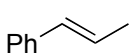
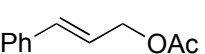
7.2.2 "Unligated" Pd Catalyzed Aerobic Allylic Acetoxylation of Terminal Alkenes

In light of the recent success in Pd-catalyzed aerobic acetoxylation reactions,^{13,15} we examined the allylic C–H acetoxylation reaction of alkenes with catalytic $\text{Pd}(\text{OAc})_2$ under the same conditions as our stoichiometric experiments, using an elevated O_2 pressure (Table 7-2). No acetoxylation product was observed from the reaction of 1-octene under 60 psi of O_2 after 24 hours (entry 1). Instead, the migration of the alkene through the aliphatic chain afforded a mixture of alkene isomers. Allyl benzene and methyl butenoate yield the desired allylic acetate

product in moderate yield (entries 2 and 3). ^1H NMR spectra of the crude reaction mixtures reveal that unreacted starting material is the remaining of the material. Allylic acetoxylation of β -methylstyrene proceeded with 30% conversion to the desired cinnamyl acetate (entry 4). The slower reaction rate of β -methylstyrene compared to that of allylbenzene can be attributed to the lower acidity of the allylic methyl proton relative to a benzylic allylic proton.

Table 7-2. Pd(OAc) $_2$ -Catalyzed Aerobic Allylic Acetoxylation Reactions^a

$$\text{R}^1\text{-CH}_2\text{-CH=CH-R}^2 \xrightarrow[\text{AcOH, CH}_3\text{CN}]{\text{Pd(OAc)}_2 \text{ 5 mol\%, LiOAc (2 equiv.)}, \text{O}_2 \text{ 60 psi, 80 }^\circ\text{C, 24 h}} \text{R}^1\text{-CH=CH-CH(R}^2\text{)-OAc}$$

Entry	Substrate	Product	yield ^b
1			0% ^c
2			75%
3			67%
4			30%

^a Reaction conditions: [substrate] $_0$ = 0.5 M, [LiOAc] = 1 M, AcOH- d_4 = 2 ml, CD $_3$ CN = 1.2 ml. ^b Yields were determined by ^1H NMR spectroscopy with 1,3,5-trimethoxybenzene as the internal standard. ^c Double bond migration was observed.

7.2.3 Characterization of the (π -allyl)PdCl Complexes in the AcOH/CH $_3$ CN Solvent Mixture

In order to probe the effect of O $_2$ on the acetoxylation of (π -allyl)PdCl complexes, the acetoxylation of allylbenzene-derived (π -allyl)PdCl complex **7-1c** was used as a model for mechanistic studies of this process. The UV-visible spectrum of the solution of **7-1c** in AcOH shows a strong absorption peak at 290 nm (Figure 7-2(A)). Upon titration of CH $_3$ CN into the

same solution, the species at 290 nm converts into a new species that absorbs at 270 nm. The plot of absorption at 270 nm versus $[\text{CH}_3\text{CN}]$ fits a hyperbolic function, suggesting saturation at high $[\text{CH}_3\text{CN}]$ (Figure 7-2(B)). The same titration experiments are performed in deuterated solvents and monitored by ^1H NMR spectroscopy. Titration of CD_3CN into the solution of **7-1c** in $\text{AcOH-}d_4$ leads to downfield shift of the ^1H peaks (Figure 7-3(A)). The doublet at 4.65 ppm represents the benzylic proton of **7-1c** ($[\text{C}_6\text{H}_5\text{CH}_2\text{CHCH}_2\text{PdCl}]_2$), and the plot of its chemical shift as a function of the $[\text{CD}_3\text{CN}]$ reflects a dramatic downfield shift at low $[\text{CD}_3\text{CN}]$ and a modest change at high $[\text{CD}_3\text{CN}]$ (Figure 7-3(B)). The data at low $[\text{CD}_3\text{CN}]$ fit a hyperbolic function, whereas the data at high $[\text{CD}_3\text{CN}]$ fit a linear function.

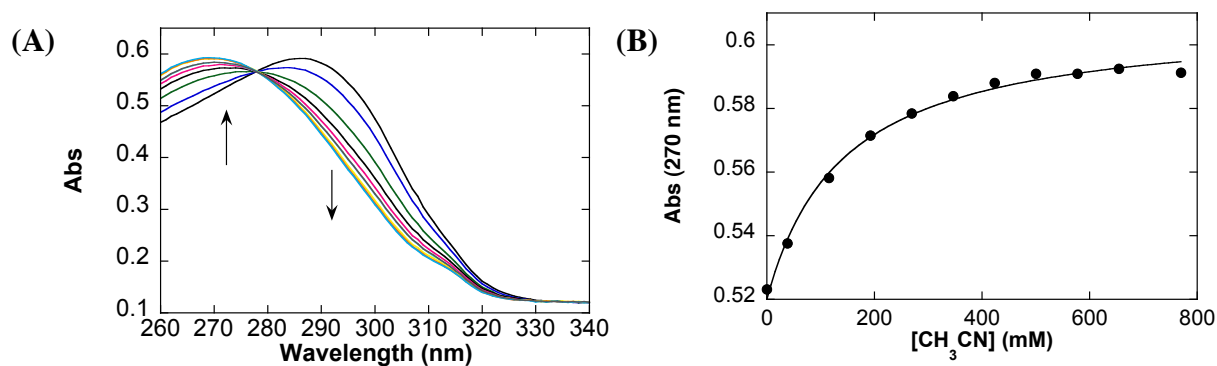


Figure 7-2. Titration of CH_3CN into a solution of **7-1c** in AcOH determined by UV-Visible spectroscopy, UV-Visible spectra (A) and the absorption of the peak at 270 nm as a function of $[\text{CH}_3\text{CN}]$ (B). Conditions: $[\text{7-1c}]_0 = 0.025 \text{ mM}$, solvent = AcOH , $22 \text{ }^\circ\text{C}$.

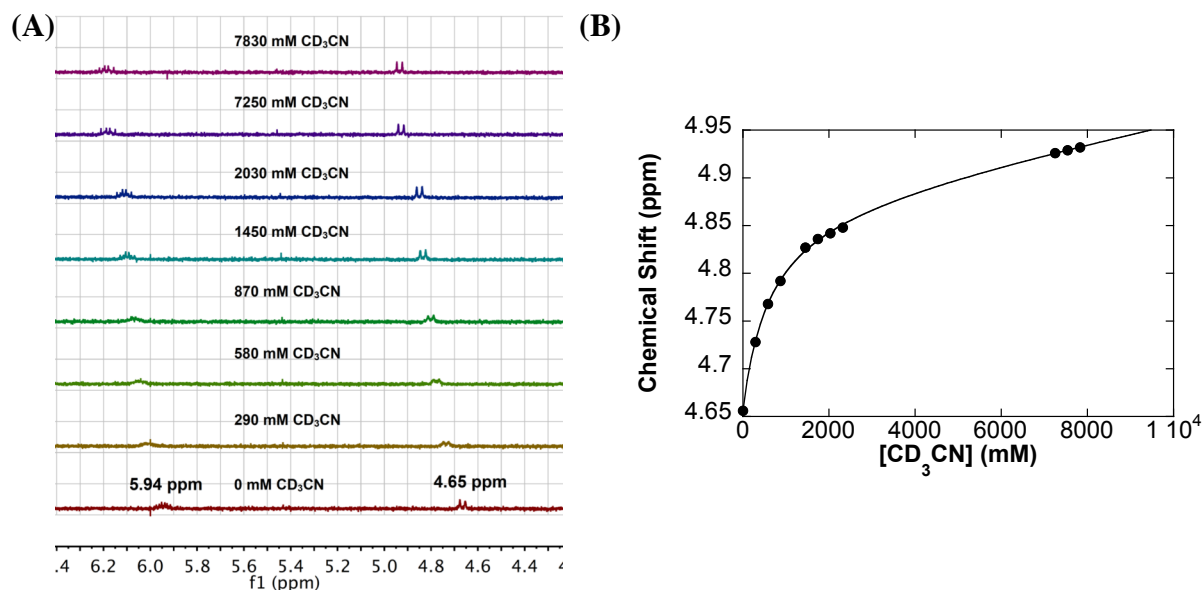


Figure 7-3. Titration of CD₃CN into a solution of **7-1c** in AcOH-*d*₄ determined by ¹H NMR spectroscopy: ¹H NMR spectra (A) and the integration of the peak at 4.65 ppm ([C₆H₅CH₂CHCH₂PdCl₂]) as a function of [CD₃CN] (B). The curve fit reflects a nonlinear least-squares fit to a modified hyperbolic function of [CD₃CN]: $\delta = [\text{CD}_3\text{CN}]/(c_1 + c_2[\text{CD}_3\text{CN}]) + c_3[\text{CD}_3\text{CN}] + \delta_0$. Reaction conditions: [**7-1c**] = 0.25 mM, solvent = AcOH-*d*₄, total solution volume = 0.65 mL, 24 °C.

We continued our investigation by examining the effect of LiOAc on the ground state structure of **7-1c**. Addition of LiOAc leads to an upfield shift of ¹H peaks of **7-1c** in a solvent mixture of AcOH-*d*₄ and CD₃CN in a ratio of 4 : 2.5 (corresponding to 8000 mM CD₃CN in AcOH-*d*₄). For example, the benzylic proton ([C₆H₅CH₂CHCH₂PdCl₂]) is a doublet at 4.945 ppm in the absence of LiOAc. Increasing the LiOAc concentration results in upfield shift of this peak, which plateaus at high [LiOAc] (Figure 7-4).

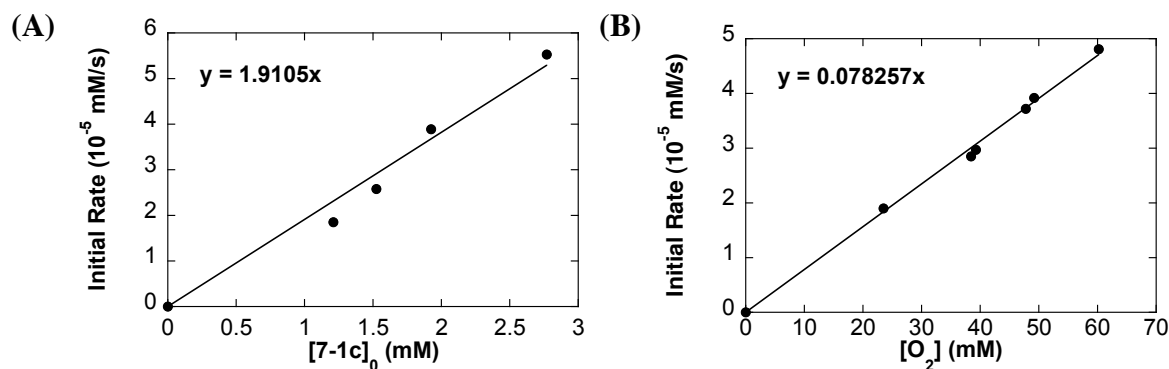


Figure 7-5. Kinetic orders of O₂-promoted acetoxylation of **7-1c**: dependence of the initial rate on $[7-1c]$ (A) and $[O_2]$ (B). Reaction conditions: AcOH-*d*₄ = 0.4 mL, CD₃CN = 0.25 mL, 80 °C, $[LiOAc]$ = 30 mM, (A) $[O_2]$ = 13 mM and (B) $[7-1c]_0$ = 1.5 mM.

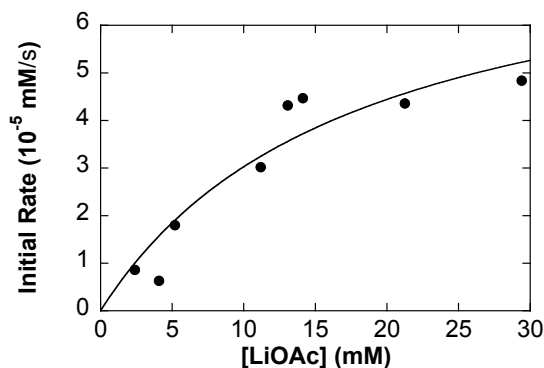


Figure 7-6. Rate dependence of the acetoxylation of **7-1c** on $[LiOAc]$. Reaction conditions: $[1c]_0$ = 3 mM, $[O_2]$ = 13 mM, AcOH-*d*₄ = 0.4 mL, CD₃CN = 0.25 mL, 80 °C.

The effect of BQ on the acetoxylation of **7-1c** was determined under analogous reaction conditions. The initial rate displays a first order dependence on $[7-1c]$ and $[BQ]$ (Figure 7-7). The slope of the reaction rate as a function of $[BQ]$ is almost 10 times greater relative to the rate as a function of $[O_2]$.

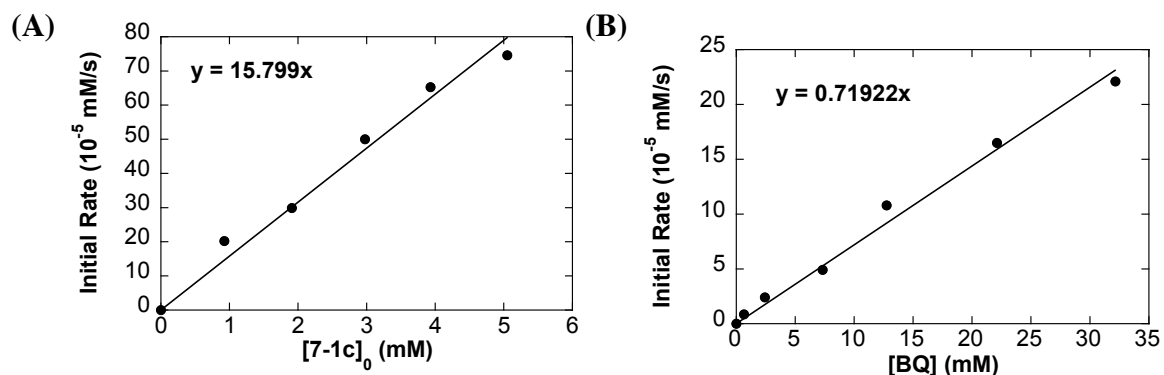
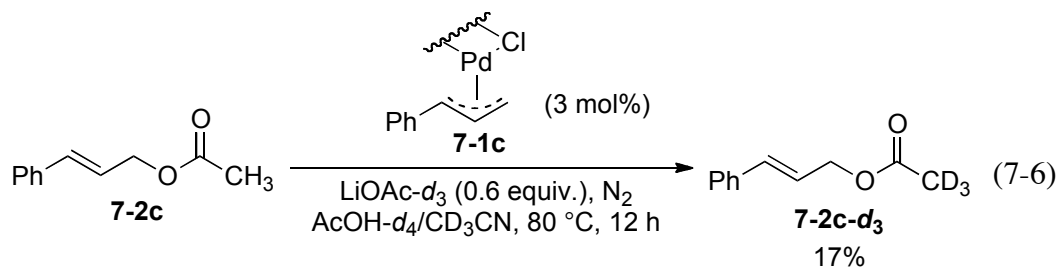


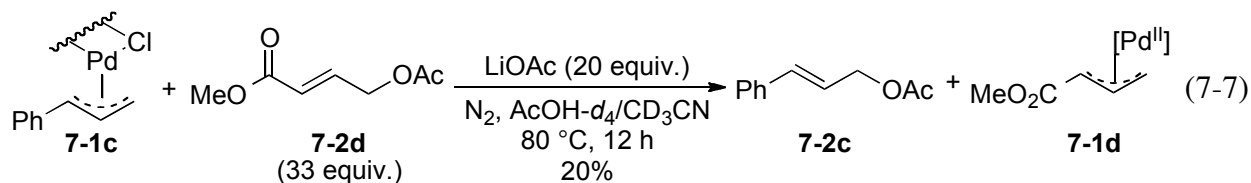
Figure 7-7. Kinetic orders of BQ-promoted acetoxylation of **7-1c**: dependence of the initial rate on **[7-1c]** (A) and **[BQ]** (B). Reaction conditions: $\text{AcOH-}d_4 = 0.4$ mL, $\text{CD}_3\text{CN} = 0.25$ mL, 80°C , (A) $[\text{LiOAc}] = 12$ mM, $[\text{BQ}] = 30$ mM (B) $[\text{LiOAc}] = 30$ mM, $[\text{7-1c}]_0 = 1.5$ mM.

7.2.5 Acetate Exchange Experiments

In order to probe the reversibility of formation of C–O bond in the acetoxylation process, we conducted an acetate scrambling experiment of **7-2c**. Cinnamyl acetate, **7-2c**, and a catalytic quantity of **7-1c** were introduced into the reaction conditions with deuterium-labeled $\text{LiOAc-}d_3$ (eq 7-6). After 12 hours, in the absence of an oxidant, the overall concentration of cinnamyl acetate **7-2c** and **7-1c** remained constant, but 17% of the total cinnamyl acetate **7-2c** was converted to the d_3 -labeled cinnamyl acetate **7-2c-}d_3. Comparable quantity of free $\text{AcOH-}d_3$ was formed concomitantly.**



We also performed an analogous experiment with **7-2c** replaced by the more electron-deficient **7-2d** under the same conditions. After 12 h, **7-1c** was converted to **7-2c** in 20% yield (eq 7-7). Meanwhile, the same quantity of the Pd complex **7-1d** was observed, arising from **7-2d**.

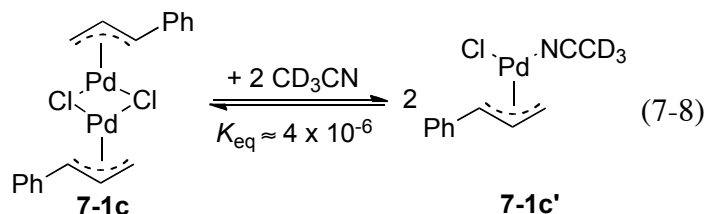


7.3 Discussion

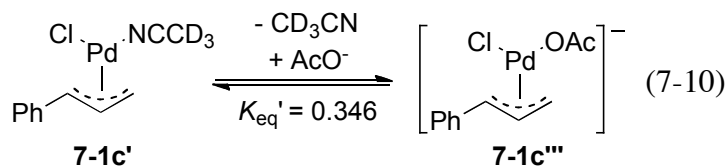
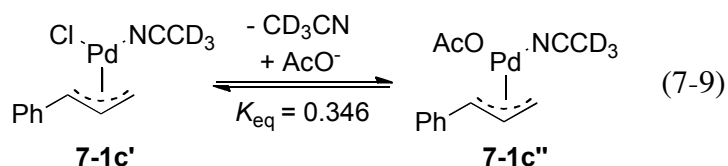
7.3.1 The Identity of 7-1c under the Reaction Conditions

(π -Allyl)PdCl complexes have been reported to be dimers in AcOH, and neutral donor ligands, such as pyridine, have been shown to break the dimeric (π -allyl)PdCl into monomers.¹⁸ As observed in Figures 7-2 and 7-3, the addition of CH₃CN leads to changes in the UV-visible and ¹H NMR spectra of **7-1c** in AcOH. We speculate that **7-1c** is a dimer in AcOH, and formation of the monomeric **7-1c'** upon coordination to CH₃CN is the origin of the change in the spectra (eq 7-8). This proposed equilibrium process is consistent with the saturation of the UV-visible absorbance at high [CH₃CN]. Based on the UV-visible spectra, the equilibrium constant of this dimer-monomer (K_{eq}) is calculated to be 4.28×10^{-6} . The fitting of the CD₃CN titration curve, derived from the ¹H NMR spectra, consists a hyperbolic term and a linear term, reflecting two types of influences that CD₃CN has on the ¹H NMR spectra. We reason that the initial change of the chemical shift upon addition of CD₃CN is caused by formation of **7-1c'** from **7-1c** (eq 7-8). In contrast, at the linear phase where **7-1c'** is the predominant species, the change of chemical shift is directly proportional to the [CD₃CN], suggesting a solvent-associated change of chemical shifts. The equilibrium constant of eq 7-8 is calculated to be 3.74×10^{-6} based on above

analysis of the ^1H NMR spectra. Collectively, the two independent measurements match each other and the equilibrium constant (K_{eq}) of eq 7-8 is determined to be 4×10^{-6} .



Addition of LiOAc into a solution of **7-1c'** in the mixed solvent system, AcOH and CH_3CN , led to a gradual change of the ^1H NMR spectra, which plateaus at high $[\text{LiOAc}]$. The interaction of LiOAc with **7-1c'** suggests a ligand exchange process. The chloride ligand can be replaced by acetate to form **7-1c''** (eq 7-9). Alternatively, substitution of CH_3CN with acetate will lead to the anionic Pd complex **7-1c'''** (eq 7-10). The neutral **7-1c''** is expected to have lower energy than the anionic **7-1c'''**, and the high CH_3CN concentration favors formation of **7-1c''**. However, we are unable to completely rule out eq 7-10 with our current data. The equilibrium constant (K_{eq}) is calculated to be 0.346 based the plot in Figure 7-4.

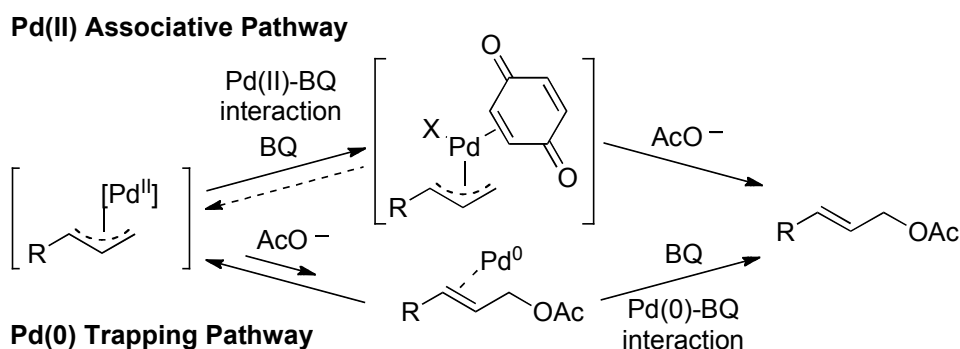


7.3.2 Mechanism of O_2 -Promoted Acetoxylation of **7-1c** and the Comparison with BQ

Two possible pathways for BQ-promoted acetoxylation of $(\pi\text{-allyl})\text{Pd}^{\text{II}}$ complexes have been proposed by Bäckvall⁵ and Bercaw (Scheme 7-2).^{2c} The electrophilic BQ can coordinate side-on through the alkene to $(\pi\text{-allyl})\text{Pd}^{\text{II}}$ complexes and facilitate the rate-determining nucleophilic

attack by acetate, presented as Pd^{II} associative pathway in Scheme 7-2. The alternative Pd⁰ trapping pathway involves reversible C–O bond formation to afford the Pd⁰-alkene intermediate, followed by dissociation of the alkene via trapping of Pd⁰ with BQ. In this Pd⁰-trapping mechanism, the reversible formation of alkene-Pd⁰ adduct is independent from BQ, and BQ serves as an oxidant to trap the Pd⁰-alkene adduct.

Scheme 7-2. Proposed Pathways for BQ-Promoted Acetoxylation of (π -allyl)Pd Complexes

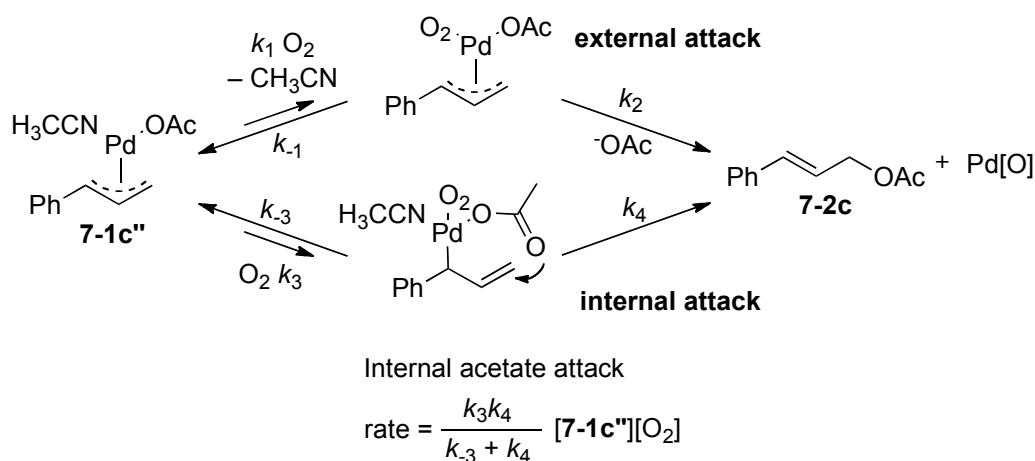


We envisioned two analogous pathways for O₂-promoted acetoxylation of **7-1c**. The mechanistic studies described above provide important constraints to distinguish between the Pd^{II} associated pathway and Pd⁰ trapping pathway. To summarize the kinetic data, the rate of O₂-promoted acetoxylation of **7-1c** is determined to be first order dependent on [**7-1c**] and [O₂] in the presence of excess LiOAc. The increase of [LiOAc] leads to a faster rate of acetoxylation, which reaches saturation at high [LiOAc]. In comparison, the BQ-promoted acetoxylation of **7-1c** under similar conditions displays first order dependence on [**7-1c**] and [BQ], as well.

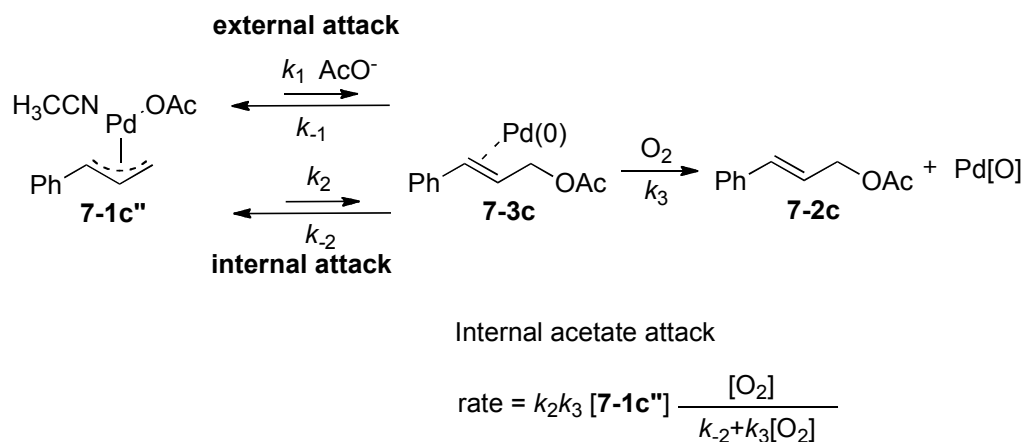
Under the reaction conditions of our study, excess LiOAc and CH₃CN as a co-solvent with AcOH resulted in complete conversion of **7-1c** into **7-1c''** or **7-1c'''**. Scheme 7-3 and 7-4 illustrate two pathways for acetoxylation of **7-1c''**, Pd^{II} associative pathway and Pd⁰ trapping

pathway, respectively. The nucleophilic attack of acetate to the π -allyl Pd complex can precede both intramolecularly and intermolecularly. The effect of LiOAc on the ground state structure of **7-1c** (Figure 7-4) and the kinetic rate of the acetoxylation reaction (Figure 7-6) correlate with each other. Saturation was reached at 15 mM of LiOAc in both plots. This observation suggests that the effect of LiOAc on the kinetic rate arises from the change of ground state structure of **7-1c** upon addition of LiOAc, and the formation of C–O bond is likely via intramolecular attack of the acetate ligand to the allylic C.

Scheme 7-3. Acetoxylation of **7-1c** via the Pd^{II} Associative Pathway and Derived Rate Laws



Scheme 7-4. Acetoxylation of **7-1c** via the Pd⁰ Trapping Pathway and Derived Rate Laws

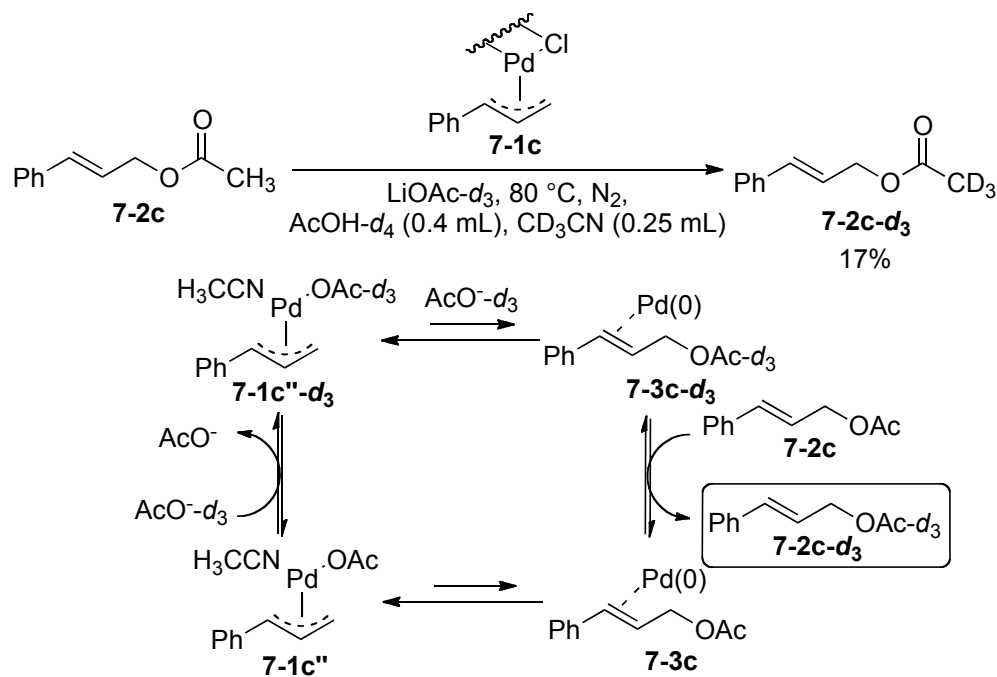


We derived the rate law for the Pd^{II} associative pathway and Pd⁰-trapping pathway based on intramolecular attack of the acetate, by applying the steady-state approximation. The rate law of the Pd^{II} associative pathway exhibits first order dependence on [O₂] and [**7-1c''**], which is consistent with our kinetic data. The rate law for the Pd⁰ trapping pathway displays a first order dependence on [**7-1c''**] and saturation dependence on [O₂]. However, if the O₂ trapping step (*k*₃) is much slower than the reverse step of C–O formation (*k*₂), the reaction would exhibit a first order in [O₂], consistent with our kinetic data. The lack of the presence of the Pd⁰-cinnamyl acetate adduct **7-3c** in the ¹H NMR spectra supports a large *k*₂. Collectively, both pathways are consistent with our observed kinetic data.

Despite the ambiguity of rate laws of the two pathways, the acetate scrambling experiments suggest that Pd⁰ trapping pathway is possible. In the absence of an oxidant, the presence of **7-1c** has led to the formation of deuterium labeled cinnamyl acetate **7-2c-d₃** from **7-2c**, implying a sequence of reversible steps: (1) C–O bond formation to afford Pd⁰-alkene adduct **7-3-d₃** from **7-1c''**; (2) replacement of **7-2c-d₃** from Pd⁰ with a molecule of **7-2c**; ^{19,20} (3) conversion of **7-3** to **7-1c''**, namely oxidative cleavage of the C–O bond (Scheme 7-5). The acetate scrambling serves as evidence for the formation of a **7-3c** intermediate, as attempts to observe **7-3c** by ¹H NMR spectroscopy fail due to the low equilibrium constant for forming **7-3c** from **7-1c''**. Formation of allylic acetates in the presence of Pd⁰ trapping reagents can be correlated to their coordination capability to Pd⁰. In the cases when oxidants are present, trapping of intermediate **7-3c** by oxidants becomes irreversible, and thus affords the acetate product and a reoxidized Pd^{II}. This hypothesis has found support in formation of **7-1d** from **7-2d** in the presence of **7-1c** (cf. eq 7-7). Under these conditions, the electron deficient alkene **7-2d** serves as the trapping reagent that

exchanges with the **7-3c** intermediate to release **7-2c** and form **7-1d**. **7-2d** in this process can be regarded as an oxidant in the context of converting the Pd⁰ of **7-3c** into Pd^{II} complex **7-1d**.

Scheme 7-5. Reversible Pathways for Formation of **7-2c-d₃** from **7-2c**



The interaction of O₂ with Pd⁰ proposed above for the Pd⁰-trapping mechanism is consistent with previous studies from our group,^{11,20} where O₂ and electron-deficient alkenes can exchange with each other in coordination to Pd⁰ complexes. Although the trapping of Pd⁰ intermediates by O₂ validates the possibility of aerobic allylic acetoxylation in the absence of BQ in a ligand-free system, the reactions rates can be accelerated in the presence of electron-deficient ancillary ligands such as 4,5-diazafluorenone.¹⁵ Mechanistic investigation revealed that 4,5-diazafluorenone facilitated the formation of C-O bond by coordination to π-allyl palladium complexes.

7.3.3 Conclusion

Stoichiometric and catalytic studies have revealed that O₂ is capable of promoting oxidative allylic acetoxylation of alkenes. Our kinetic investigation suggests that the O₂-promoted acetoxylation of (π -allyl)PdCl complexes could proceed via either a Pd^{II} associative pathway, where O₂ coordinates to Pd^{II}, or a Pd⁰ trapping pathway, in which O₂ interacts with an Pd⁰ intermediate. Acetate scrambling experiments verifies that the Pd⁰ trapping pathway is plausible under the reaction condition. These results presented above have important implications in replacing BQ with O₂ in oxidative allylic acetoxylation reactions.

7.4 Experimental

7.4.1 General Procedures and Considerations

All commercially available compounds and deuterated solvents were used as received, and were purchased from Sigma-Aldrich. All NMR experiments were acquired on a Varian INOVA-500 MHz spectrometer. The chemical shifts (δ) of ¹H NMR spectra are given in parts per million and referenced to the residual acetate proton of AcOH-*d*₄ (2.04 ppm). Unless specified, all experiments used recrystallized 1,3,5-tri-(*tert*-butyl)benzene as the internal standard. All reactions were conducted in J-Young tubes, except for experiments in Figure 7-5(B) for determining the dependence the initial rate on [O₂], which were performed in thick wall NMR tubes with a flame sealed top.

General Procedure for Synthesis of π -allyl Palladium Complexes. All π -allyl palladium complexes are prepared according to literature procedures.¹⁷ A representative procedure for the synthesis of cinnamyl derived π -allyl palladium complex **7-1c** is presented here. To an oven-

dried round bottom flask equipped with a magnetic stir bar was added palladium trifluoroacetate (154 mg, 0.5 mmol). The flask was wrapped with aluminum foil, and then put under an N₂ atmosphere. Dry THF (5 mL) and allyl benzene (66 μ L, 0.5 mmole) was added via syringe. The flask was stirred for 1 hour at room temperature. Tetrabutylammonium chloride (150 mg, 0.55 mmol) was added, and the solution was allowed to stir for another 30min. After the reaction, the mixture was filtered through Celite to remove palladium black, purified by silica gel column chromatography, and recrystallized from CH₂Cl₂ and hexane. The ¹H NMR spectrum of this compound is consistent with the literature.

General Procedure for Pd(OAc)₂-Catalyzed Aerobic Allylic Acetoxylation of Alkenes.

Allylbenzene (132 μ L, 1 mmol), LiOAc (130 mg, 3 mmol) and Pd(OAc)₂ (10 mg, 5 mol%) were weighed out in a thick walled pressure tube. 1.2 ml HOAc and 0.8 ml CH₃CN were then added. The tube was equipped with a pressure regulator. 30 psi of O₂ was charged into the tube and released 10 times to fully purge the system. The tube was then pressurized with 60 psi O₂ and allowed to stir at 80 °C overnight. The reaction was then cooled to room temperature and trimethoxybenzene (50 mg, 0.3 mmol) was added as internal standard. Solvent was then removed by rotovap and the sample was analyzed by ¹H NMR spectroscopy. Reactions with other alkene substrates applied the same procedure as allylbenzene.

7.4.2 ¹H NMR Spectra and Timecourse of O₂-Promoted Acetoxylation of 7-1c

Solutions of internal standard (1,3,5-tri-(*tert*-butyl)benzene) in deuterated solvents, AcOH-*d*₄ and CD₃CN were prepared on a 10-mL scale. The palladium complex **7-1c** and lithium acetate stock solutions were prepared immediately before use on a 1-mL scale using the internal standard solution. To a J-Young NMR tube, stock solutions were added via gas-tight syringe.

After preparation of the sample, the J-Young NMR tubes were immediately placed in an acetone/dry ice bath. Freeze-pump-thaw cycles were carried out three times to degas the solvent. The gas (O₂ or N₂) was then introduced to the tubes. When pressurized oxygen was required, a liquid nitrogen bath was used instead of acetone/dry ice. The volume of oxygen was measured by a manometer. Before insertion into the NMR spectrometer, the tube was thawed and shaken well to allow good mixing of gas into solvent. The spectrometer probe was pre-heated to the desired temperature and allowed to equilibrate for 30 minutes.

The ¹H NMR spectrum of **7-1c** exhibits a doublet at 4.93 ppm, representing the benzylic proton ([C₆H₅CH₂CHCH₂PdCl]₂) (Figure 7-8(A)). This peak was used to determine [7-1c]. At high temperature the peaks at 4.13 and 3.19 ppm become broad, reflecting fast exchange between the two vinyl protons via an η¹ intermediate at elevated temperature. The acetate methylene doublet at 4.76 ppm (C₆H₅CHCHCH₂OAc) of **7-2c** was used to represent **7-2c** in measuring [7-2c].

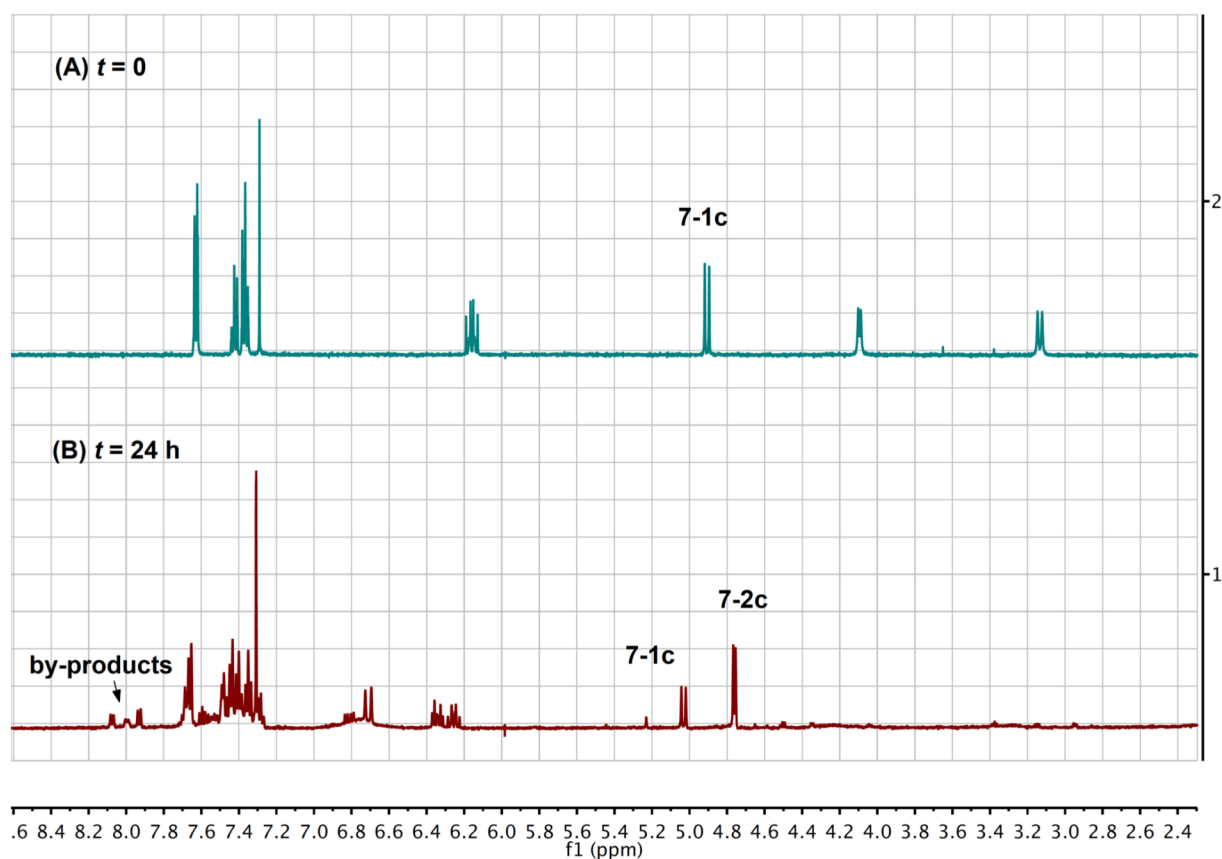


Figure 7-8. The ¹H NMR spectrum of **7-1c** under the reaction conditions (A) and crude spectrum of the same sample after 24 h (B). Reaction conditions: [**7-1c**]₀ = 3 mM, [O₂] = 48 mM, [LiOAc] = 30 mM, AcOH-*d*₄ = 0.4 mL, CD₃CN = 0.25 mL, 80 °C.

Despite formation of by-products at the late stage of the reaction, the reaction timecourse during the first 500 minutes suggests a clean conversion of **7-1c** to **7-2c** (Figure 7-9). Initial rate measurements based on the first 5% conversion have been used for the kinetic analyses above.

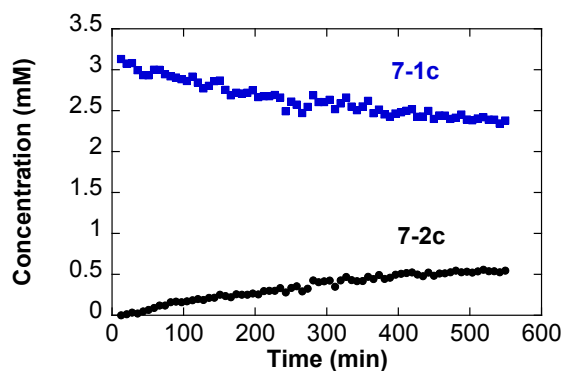


Figure 7-9. The initial time course of O_2 -promoted acetoxylation of **7-1c**. Reaction conditions: $[7-1c]_0 = 3$ mM, $[O_2] = 48$ mM, $[LiOAc] = 30$ mM, $AcOH-d_4 = 0.4$ mL, $CD_3CN = 0.25$ mL, 80 °C.

7.4.3 Procedure for the Acetate Exchange Experiments

The allylbenzene derived π -allyl palladium complex **7-1c** (2.2 mg, 4.0 μ mol), cinnamyl acetate **7-2c** (5.5 mg, 5.2 μ mol, 31 μ mol) and $LiOAc-d_3$ (2.7 mg, 40 μ mol) were weighed into a J-Young tube. The stock solution of internal standard in $AcOH-d_4$ and CD_3CN were added via gas-tight syringe. The NMR tube was immediately placed in an acetone/dry ice bath. Freeze-pump-thaw cycles were carried out three times to degas the solvent. 1 atm of N_2 was then introduced to the tube. With the probe of the NMR spectrometer pre-heated to 80 °C, the NMR tube was placed into the NMR spectrometer and data acquired over 12 h.

The integration of the acetate peak of **7-2c** (at 2.07 ppm) was reduced by 17% after 12 h, which was interpreted as conversion of 17% **7-2c** to **7-2c- d_3** (Figure 7-10). A singlet peak grows in at 2.04 ppm, the concentration of which corresponds to 17% acetate relative to **7-2c**. We assign this peak as the free $AcOH$, arising from exchange of the $AcOH-d_3$ with **7-2c**.

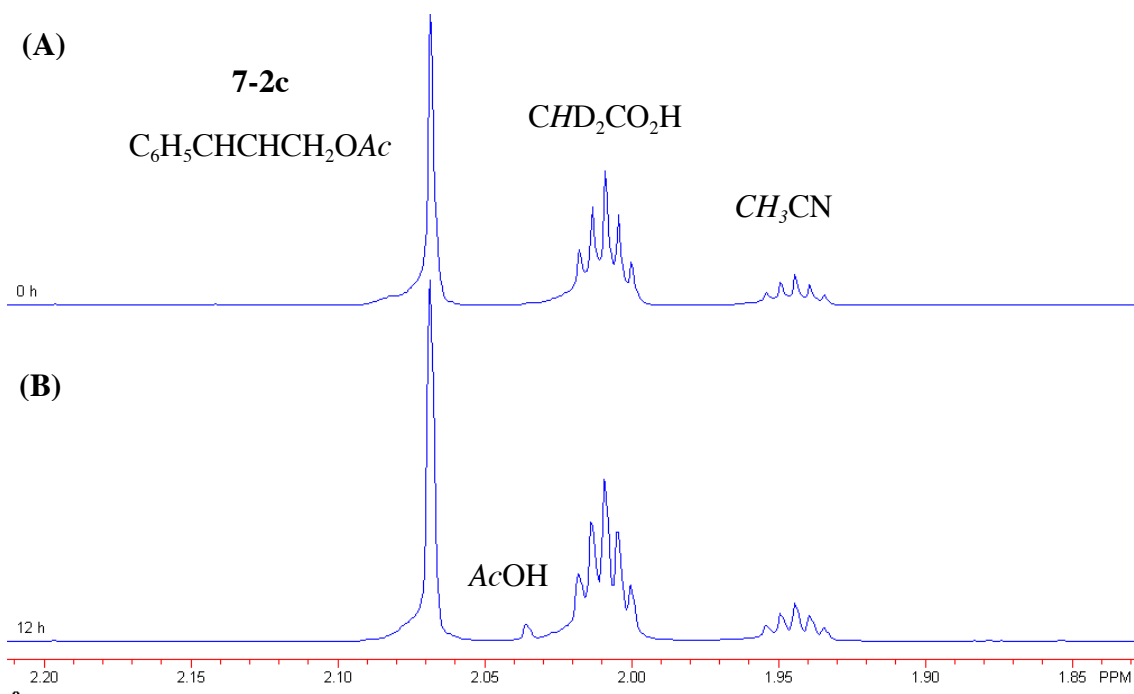
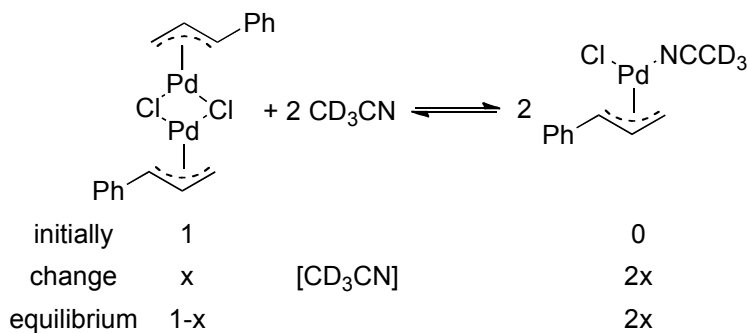


Figure 7-10. The acetate exchange experiment of allylbenzene **7-2c** in the presence of **7-1c** at $t = 0$ (A) and $t = 12$ h (B). Reaction conditions: $[\mathbf{7-1c}]_0 = 1.5$ mM, $[\text{LiOAc-}d_3] = 30$ mM, $[\mathbf{7-2c}]_0 = 50$ mM, $\text{AcOH-}d_4 = 0.4$ ml, $\text{CD}_3\text{CN} = 0.25$ ml, 80°C , N_2 , 12 h.

7.4.4 Derivation of the Equilibrium Constant Between **7-1c'** and **7-1c**

Scheme 7-6 illustrates the derivation of the equilibrium constant for conversion of **7-1c** into **7-1c'**. The results derived from UV-visible spectra and ^1H NMR spectra are consistent.

Scheme 7-6. Equations for Calculation of the Equilibrium Constant Between 7-1c' and 7-1c



Based on the UV-Visible spectra

$$A_{\text{obs}} = A_M \cdot X_M + A_D \cdot X_D$$

$$A_D = 0.5231$$

$$A_M = 0.5909$$

$$A_{\text{obs}} = 0.5231 \cdot (1-x) + 0.5909 \cdot x$$

Solve x for each of the data point

$$K_{\text{eq}} = \frac{[\text{Pd}_M]^2}{[\text{Pd}_D][\text{CD}_3\text{CN}]^2}$$

$$= \frac{4x^2 [\text{Pd}]_0}{(1-x) [\text{CD}_3\text{CN}]^2}$$

Based on the ¹H NMR spectra

$$\delta_{\text{obs}} = \delta_M \cdot X_M + \delta_D \cdot X_D + \Delta\delta_{[\text{CD}_3\text{CN}]}$$

$$\Delta\delta_{[\text{CD}_3\text{CN}]} = 1.56 \cdot 10^{-6} [\text{CD}_3\text{CN}] \quad (\text{By Linear correlation in excess CD}_3\text{CN})$$

$$\delta_D = 4.656 \text{ ppm}$$

$$\delta_M = 4.813 \text{ ppm}$$

$$\delta_{\text{obs}} = 4.656 \cdot (1-x) + 4.813 \cdot x + 1.56 \cdot 10^{-6} [\text{CD}_3\text{CN}]$$

Solve x for each of the data point

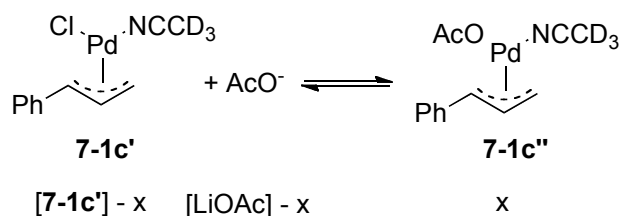
$$K_{\text{eq}} = \frac{[\text{Pd}_M]^2}{[\text{Pd}_D][\text{CD}_3\text{CN}]^2}$$

$$= \frac{4x^2 [\text{Pd}]_0}{(1-x) [\text{CD}_3\text{CN}]^2}$$

7.4.5 Rate Laws Derivations

Figure 7-4 revealed a hyperbolic function of the concentration of **7-1c''** relative to [LiOAc]. We proposed that this effect of [LiOAc] on the ground state structure of the (π -allyl)Pd complex was the origin of the saturation dependence of the rate on [LiOAc] (cf. Figure 7-6). Scheme 7-7 illustrates the derivation of the hyperbolic dependence of [**7-1c''**] on [LiOAc].

Scheme 7-7. Equations for Derivation of the Saturation Dependence of [**7-1c''**] on [LiOAc]



$$K_{\text{eq}} = \frac{x}{(1-x)([\text{LiOAc}] - x)}$$

$$[\mathbf{7-1c''}] = x$$

$$= \frac{[\mathbf{7-1c'}] + [\text{LiOAc}] - 1 - \left(([\mathbf{7-1c'}] + [\text{LiOAc}] - 1)^2 - 4K_{\text{eq}}[\mathbf{7-1c'}][\text{LiOAc}] \right)^{1/2}}{2K_{\text{eq}}}$$

$$\begin{array}{l} \text{when } [\text{LiOAc}] = 0 \\ [\mathbf{7-1c''}] = 0 \end{array}$$

$$\begin{array}{l} \text{when } [\text{LiOAc}] \gg [\mathbf{7-1c'}] \\ [\mathbf{7-1c''}] = [\mathbf{7-1c'}] \end{array}$$

Scheme 7-7 suggests that under our standard working conditions, when LiOAc is in excess, the (π -allyl)Pd complex is predominantly in the form of **7-1''**. The rate laws shown in Scheme 7-3 and 7-4 are based on above assumption about the form of **7-1c**, and are derived by applying the steady-state approximation (Scheme 7-8).

Scheme 7-8. Equations for Derivation of the Rate Laws**Pd(II) associative pathway**

External acetate attack

$$[\text{Pd}^{\text{II}}\text{-O}_2] = \frac{k_1[\mathbf{7-1c''}][\text{O}_2]}{k_{-1} + k_2[\text{LiOAc}]}$$

$$\text{rate} = k_2[\text{Pd}^{\text{II}}\text{-O}_2][\text{LiOAc}]$$

$$= k_1k_2[\mathbf{7-1c''}][\text{O}_2] \frac{[\text{LiOAc}]}{k_{-1} + k_2[\text{LiOAc}]}$$

Internal acetate attack

$$[\text{Pd}^{\text{II}}\text{-O}_2] = \frac{k_3[\mathbf{7-1c''}][\text{O}_2]}{k_{-3} + k_4}$$

$$\text{rate} = k_4[\text{Pd}^{\text{II}}\text{-O}_2]$$

$$= \frac{k_3k_4}{k_{-3} + k_4} [\mathbf{7-1c''}][\text{O}_2]$$

Pd(0) trapping pathway

External acetate attack

$$[\mathbf{7-3c}] = \frac{k_1[\mathbf{7-1c''}][\text{LiOAc}]}{k_{-1} + k_3[\text{O}_2]}$$

$$\text{rate} = k_3[\text{O}_2][\mathbf{7-1c''}]$$

$$= k_2k_3 [\mathbf{7-1c''}][\text{LiOAc}] \frac{[\text{O}_2]}{k_{-2} + k_3[\text{O}_2]}$$

Internal acetate attack

$$[\mathbf{7-3c}] = \frac{k_2[\mathbf{7-1c''}]}{k_{-2} + k_3[\text{O}_2]}$$

$$\text{rate} = k_3[\text{O}_2][\mathbf{7-1c''}]$$

$$= k_2k_3 [\mathbf{7-1c''}] \frac{[\text{O}_2]}{k_{-2} + k_3[\text{O}_2]}$$

7.5 References

-
1. (a) Kikukawa, K.; Sakai, K.; Asada, K.; Matsuda, T. *J. Organomet. Chem.* **1974**, *77*, 131-145. (b). Heumann, A.; Akermark, B. *Angew. Chem. Int. Ed.* **1984**, *23*, 453-454. (c) McMurry, J. E.; Kocotovský, P. *Tetrahedron Lett.* **1984**, *25*, 4187-4190. (d) Jia, C.; Müller, P.; Mimoun, H. *J. Mol. Catal. A: Chem.* **1995**, *101*, 127-136. (e) El Firdoussi, L.; Baqqa, A.; Allaoud, S.; Ait Allal, B.; Karim, A.; Castanet, Y.; Mortreux, A. *J. Mol. Catal. A: Chem.* **1998**, *135*, 11-22. (f) Grennberg, H.; Bäckvall, J. E. *Chem. Eur. J.* **1998**, *4*, 1083-1089. (g) Hansson, S.; Heumann, A.;

Rein, T.; Åkermark, B. *J. Org. Chem.* **1990**, *55*, 975-984. (e) Attolini, M.; Peiffer, G.; Maffei, M. *Tetrahedron* **2000**, *56*, 2693-2697.

2. (a) Chen, M. S.; White, M. C. *J. Am. Chem. Soc.* **2004**, *126*, 1346-1347. (b) Chen, M. S.; Prabakaran, N.; Labenz, N. A.; White, M. C. *J. Am. Chem. Soc.* **2005**, *127*, 6970-6971. (c) Lin, B.-L.; Labinger, J. A.; Bercaw, J. E. *Can. J. Chem.* **2009**, *87*, 264-271. (d) Pilarski, L. T.; Selander, N.; Böse, D.; Szabó, K. I. *J. Org. Lett.* **2009**, *11*, 5518-5521. (e) Henderson, W. H.; Check, C. T.; Proust, N.; Stambuli, J. P. *Org. Lett.* **2010**, *12*, 824-827. (f) Thiery, E.; Aouf, C.; Belloy, J.; Harakat, D.; Le Bras, J.; Muzart, J. *J. Org. Chem.* **2010**, *75*, 1771-1774.

3. For a leading reference: Dyker, G. *Handbook of C-H Transformations*; Wiley-VCH: Weinheim, Germany, **2005**; Chapter 4.

4. When stoichiometric oxidants other than BQ, such as MnO₂ or CuCl₂ are used, the reactions still require catalytic quantities of BQ, see: (a) Heumann, A.; Reglier, M.; Waegell, B. *Angew. Chem., Int. Ed. Engl.* **1982**, *21*, 366-367. (b) Heumann, A.; Åkermark, B. *Angew. Chem., Int. Ed. Engl.* **1984**, *23*, 453-454. (c) Hansson, S.; Heumann, A.; Rein, T.; Åkermark, B. *J. Org. Chem.* **1990**, *55*, 975-984. (d) Principato, B.; Maffei, M.; Siv, C.; Buono, G.; Peiffer, G. *Tetrahedron* **1996**, *52*, 2087-2096.

5. (a) Bäckvall, J. E.; Bystrom, S. E.; Nordberg, R. E. *J. Org. Chem.* **1984**, *49*, 4619-4631. (b) Bäckvall, J. E.; Nystrom, J. E.; Nordberg, R. E. *J. Am. Chem. Soc.* **1985**, *107*, 3676-3686. (c) Bäckvall, J. E.; Gogoll, A. *Tetrahedron Lett.* **1988**, *29*, 2243-2246.

-
6. For a BQ induce allylic chlorination, see: Szabó, K. J. *Organometallics* **1998**, *17*, 1677–1686.
7. For a study of the conversion of Pd⁰-BQ to Pd^{II}, see: Grennberg, H.; Gogoll, A.; Bäckvall, J. E. *Organometallics* **1993**, *12*, 1790-1793.
8. An analogous beneficial effect of BQ in promoting reductive bond formations has recently been reported in conversion of the (IMes)₂Pd^{II}(OOCPh)(H) complex into (IMes)₂Pd⁰ and PhCOOH: Decharin, N.; Stahl, S. S. *J. Am. Chem. Soc.* **2011**, *133*, 5732-5735.
9. (a) Stahl, S. S. *Science* **2005**, *309*, 1824-1826. (b) Stahl, S. S. *Angew. Chem. Int. Ed.* **2004**, *43*, 3400-3420. (c) Shi, Z.; Zhang, C.; Tang, C.; Jiao, N. *Chem. Soc. Rev.* **2012**, *41*, 3381-3430.
10. (a) Williams, D. B.; Kaminsky, W.; Mayer, J. M.; Goldberg, K. I. *Chem. Commun.* **2008**, 4195-4197. (b) Lin, B. L.; Clough, C. R.; Hillhouse, G. L. *J. Am. Chem. Soc.* **2002**, *124*, 2890-2891.
11. For discussion of Pd⁰ oxidation by O₂, see: (a) Stahl, S. S.; Thorman, J. L.; Nelson, R. C.; Kozee, M. A. *J. Am. Chem. Soc.* **2001**, *123*, 7188–7189. (b) Konnick, M. M.; Guzei, I. A.; Stahl, S. S. *J. Am. Chem. Soc.* **2004**, *126*, 10212–10213. (c) Landis, C. R.; Morales, C. M.; Stahl, S. S. *J. Am. Chem. Soc.*, **2004**, *126*, 16302-16303. (d) Muzart, J. *Chem. Asian J.* **2006**, *1*, 508–515. (e) Konnick, M. M.; Gandhi, B. A.; Guzei, I. A.; Stahl, S. S. *Angew. Chem. Int. Ed.*, **2006**, *45*, 2904-2907. (f) Popp, B. V.; Stahl, S. S. *J. Am. Chem. Soc.*, **2007**, *129*, 4410-4422. (g) Popp, B. V.; Wendlandt, J. E.; Landis, C. R.; Stahl, S. S. *Angew. Chem. Int. Ed.*, **2007**, *46*, 601-604. (h)

Konnick, M. M.; Stahl, S. S. *J. Am. Chem. Soc.* **2008**, *130*, 5753–5762. (i) Popp, B. V.; Stahl, S. S. *Chem. Eur. J.* **2009**, *15*, 2915–2922.

12. (a) Popp, B. V.; Thorman, J. L.; Stahl, S. S. *J. Mol. Catal. A: Chem.* **2006**, *251*, 2–7. (b) Popp, B. V.; Morales, C. M.; Landis, C. R.; Stahl, S. S. *Inorg. Chem.*, **2010**, *49*, 8200–8207.

13. Mitsudome, T.; Umetani, T.; Nosaka, N.; Mori, K.; Mizugaki, T.; Ebitani, K.; Kaneda, K. *Angew. Chem. Int. Ed.* **2006**, *45*, 481–485.

14. (a) Liu, G. S.; Yin, G. Y.; Wu, L. *Angew. Chem., Int. Ed.* **2008**, *47*, 4733–4736. (b) Yin, G.; Wu, Y.; Liu, G. *J. Am. Chem. Soc.* **2010**, *132*, 11978–11987.

15. Campbell, A. N.; White, P. B.; Guzei, I. A.; Stahl, S. S. *J. Am. Chem. Soc.* **2010**, *132*, 15116–15119.

16. (a) Åkermark, B.; Zetterberg, K. *Tetrahedron Lett.* **1975**, *16*, 3733–3736. (b) Trost, B. M.; Weber, L.; Strege, P. E.; Fullerton, T. J.; Dietsche, T. J. *J. Am. Chem. Soc.* **1978**, *100*, 3416–3426.

17. For synthetic routes to various Pd(π -allyl)Cl complexes, see: (a) Trost, B. M.; Metzner, P. J. *J. Am. Chem. Soc.* **1980**, *102*, 3572–3577. (b) Tsuji, J.; Imamura, S. *Bull. Chem. Soc. Jpn.* **1967**, *40*, 197–202. (c) Imaizumi, S.; Matsuhisa, T.; Senda, Y. *J. Organomet. Chem.* **1985**, *280*, 441–448.

18. Wolfe, S.; Campbell, P. G. C. *J. Am. Chem. Soc.* **1971**, *93*, 1499–1501.

19. The exchange of alkene ligands on Pd⁰ is assumed to be fast. The rate constant of the exchange of electron-deficient alkenes from Pd⁰ has been reported to be in the order of 10² (M⁻¹s⁻¹) at room temperature.

20. Popp, B. V.; Thorman, J. L.; Morales, C. M.; Landis, C. R.; Stahl, S. S. *J. Am. Chem. Soc.*, **2004**, *126*, 14832-14842.

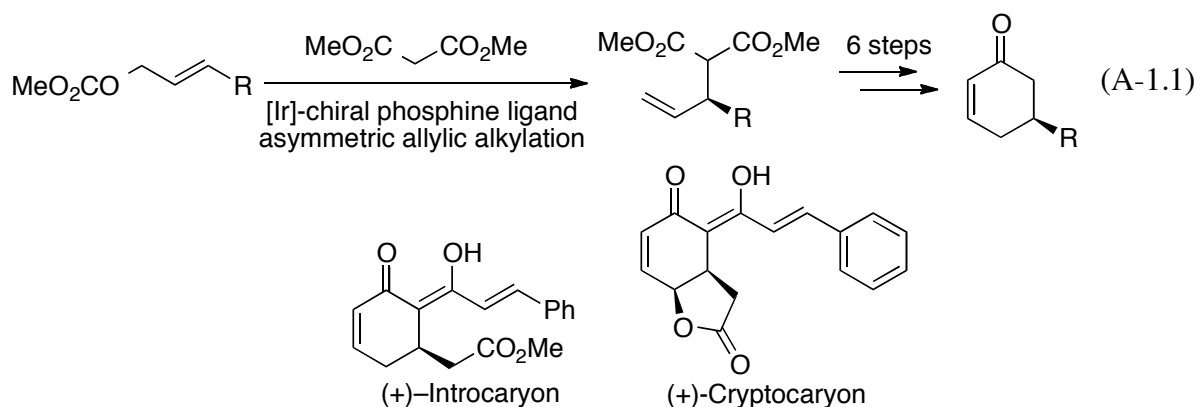
Appendix 1:

Efforts Towards Enantioselective Formal Synthesis of

(+) Infectocaryone and (+) Cryptocaryone via Aerobic Dehydrogenation

A.1.1 Introduction

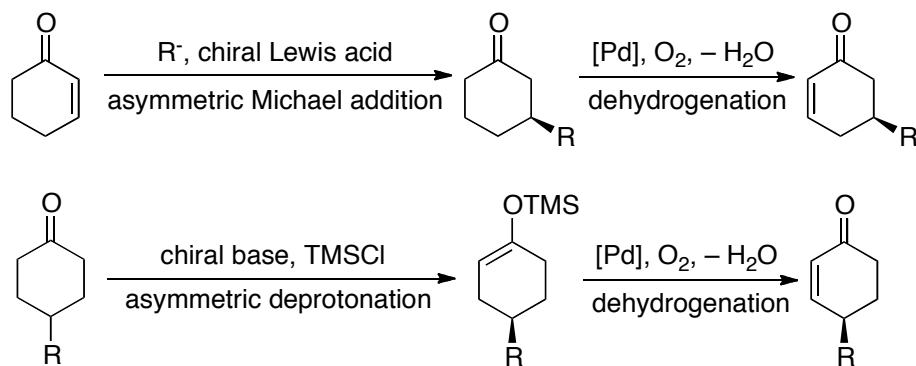
Chiral cyclohexenone derivatives are versatile synthetic intermediates in the syntheses of natural product and pharmaceuticals.¹ Recently, Helmchen and coworkers report an enantioselective strategy for preparing 5-alkyl cyclohexenones (eq A-1.1).² The chiral center is installed by Ir-catalyzed asymmetric allylic alkylation of allyl carbonates. This method is also utilized to synthesize natural products (+)-infecrocaryone and (+)-cryptocaryone. Despite the high enantioselectivity, however, this method requires multiple subsequent steps to convert the chiral alkenes into the corresponding cyclohexenones.



A large number of chiral Lewis acids have been developed for asymmetric Michael addition of cyclohexenones with various nucleophiles. In particular, BINOL-based heterobimetallic Lewis acid systems represent a class of superior, cheap and reliable catalysts.³ We envision that the combination of the asymmetric Michael addition of a simple cyclohexenone followed by Pd-catalyzed dehydrogenation reaction will efficiently afford chiral 5-substituted cyclohexenone (Scheme A-1.1). The development of asymmetric deprotonation methods enables the conversion of a *meso*-4-substituted cyclohexanone into a chiral silyl enol ether.⁴ A Saegusa type dehydrosilylation⁵ of the intermediate chiral silyl enol ether will readily result in the corresponding chiral 4-substituted cyclohexenone (Scheme A-1.1). Compared to the previous

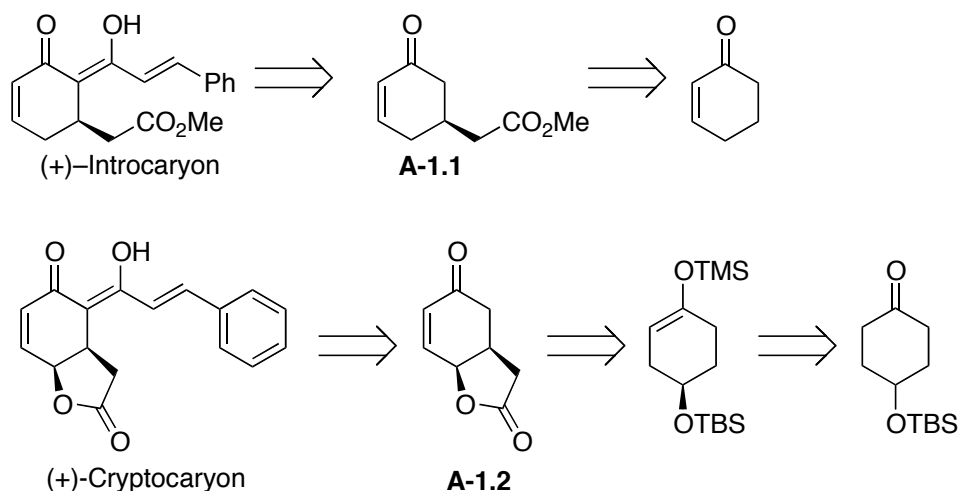
"AAA" method, the proposed methods bear shorter synthetic route and use cheaper reagents. In addition, due to the versatility of Micheal addition methods, a variety of substituents can be readily installed to cyclohexenones.

Scheme A-1.1. Proposed Strategies for Preparing Chiral Cyclohexenone Derivatives with Dehydrogenation as an Intermediate Step



Based on the dehydrogenation strategy proposed above, I envision retrosynthetic routes to (+)-infectocaryone and (+)-cryptocaryone (Scheme A-1.2). The key cyclohexenone intermediates **A-1.1** and **A-1.2** can be obtained from cheap sources, including cyclohexenone and 4-*tert*-butyldimethylcyclohexanone. I describe here my attempting efforts to synthesize **A-1.1** and **A-1.2** with Pd-catalyzed dehydrogenation methods.

Scheme A-1.2. Retrosynthetic Analysis for (+)-infectocaryone and (+)-cryptocaryone



A.1.2 Results and Discussion

A highly enantioselective Michael addition of dimethyl malonate to cyclohexenone is reported by Shibasaki and coworkers, using a $\text{LiAl}(\text{S-BINOL})_2$ catalyst.⁶ **A-1.3** is obtained in high yield with this catalyst (eq A-1.2). Aerobic dehydrogenation of **A-1.3** with the $\text{Pd}(\text{DMSO})_2(\text{TFA})_2$ catalyst (cf. Chapter 2) leads to considerable amount of over-oxidation product, phenol (Table A-1.1). The minor regio-isomer, **A-1.5**, is also observed as a by-product.

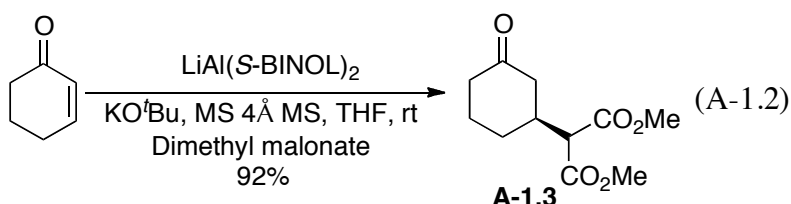


Table A-1.1. Pd-Catalyzed Aerobic Dehydrogenation of **A-1.3**

Entry	$\text{Pd}(\text{TFA})_2$ (%)	DMSO (%)	Solvent	Temp (°C)	Time (h)	A-1.3 (%) ^a	A-1.4 (%) ^a	Phenol (%) ^a
1	5	10	AcOH	80	24	54	12	24
2	5	10	AcOH	80	36	0	0	100
3	5	10	EtOAc	60	44	45	11	25

^aCrude yield determined by ^1H NMR spectroscopy.

The unsatisfactory yield of **A-1.4** from Pd-catalyzed dehydrogenation of **A-1.3** prompts us to prepare the less sterically hindered intermediate **A-1.6** from **A-1.3** and seek to obtain better dehydrogenation yield with **A-1.6**. The decarboxylation of **A-1.3** proceeds with a high yield in the presence of LiI (eq A-1.3). However, the $\text{Pd}(\text{DMSO})_2(\text{TFA})_2$ -catalyzed dehydrogenation of **A-1.6** in the solution of AcOH generates **A-1.1** in low yield (Table A-1.2). Longer reaction time leads to decomposition of the product. Change of the solvent to EtOAc provides a better mass

balance, however, the slow reaction rate requires high catalyst loading to achieve a reasonable conversion of A-1.6.

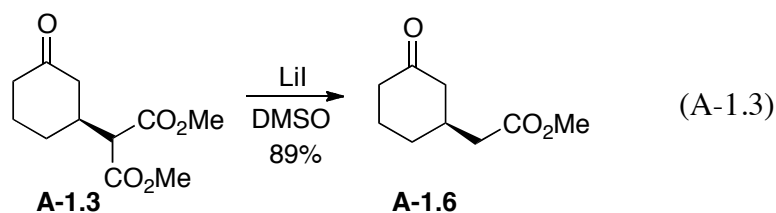
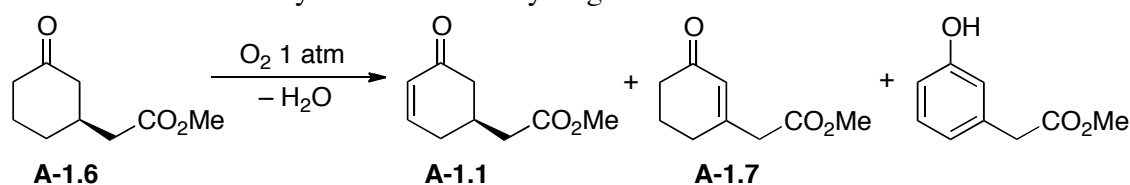


Table A-1.2. Pd-Catalyzed Aerobic Dehydrogenation of A-1.6



Entry	Pd(TFA) ₂ (%)	DMSO (%)	Solvent	Temp (°C)	Time (h)	Conv. (%) ^a	A-1.1 (%) ^a	A-1.7 (%) ^a	Phenol (%) ^a
1	5	10	HOAc	80	24 h	85	28	2	20
2	5	10	HOAc	80	48 h	100	0	0	0
3	20	40	EtOAc	60	18 h	65	44	6	13

^aCrude yield determined by ¹H NMR spectroscopy.

We also prepared the racemic bicyclic ketone intermediate A-1.8 in order to test the dehydrogenation conditions for converting A-1.8 to A-1.2, the precursor to (+)-cryptocaryone (Scheme A-1.3). The syn-addition of the silyl ketene acetal to 4-*tert*-butyldimethylsilyl cyclohexenone is achieved with good selectivity by employing HgI₂ as a Lewis acid additive.⁷ The resulting bicyclic A-1.8 intermediate undergoes rapid decomposition under the Pd-catalyzed dehydrogenation conditions, and only trace enone product is observed (Table A-1.3).

Scheme A-1.3. Preparation of the Racemic Bicyclic Intermediate A-1.8

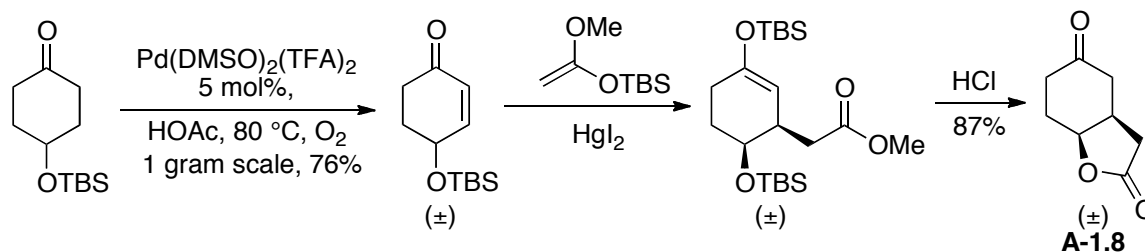
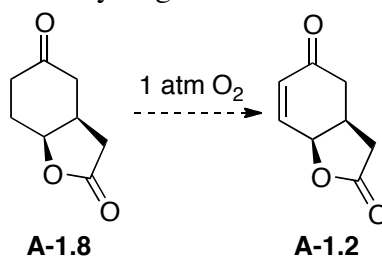
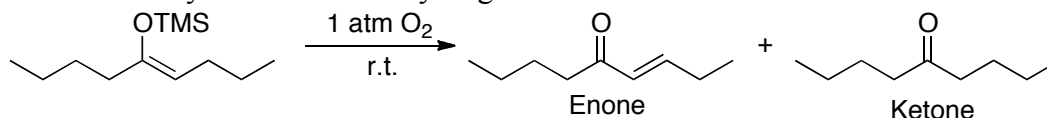


Table A-1.3. Pd-Catalyzed Aerobic Dehydrogenation of **A-1.8**

Entry	Pd(TFA) ₂ (%)	DMSO (%)	Solvent	Temp (°C)	Conv. (%) ^a	A-1.2 (%) ^a
1	5	10	AcOH	80	83	4
2	5	10	EtOAc	60	49	6

^aCrude yield determined by ¹H NMR spectroscopy.

We explored the dehydrosilylation of silyl enol ethers in parallel, in order to develop a Pd catalyst that allows mild dehydrosilylation with improved yields relative to the current conditions.⁵ A modified Pd(DMSO)₂(TFA)₂ catalyst, in combination with 4 Å MS (molecular sieves) and NaOAc, successfully catalyzes the oxidative dehydrosilylation of (trimethylsilyloxy)nonanene in high yield at room temperature (Table A-1.4), with a small amount of the hydrolysis product, 5-nonanone, formed as a by-product.

Table A-1.4. Pd-Catalyzed Aerobic Dehydrogenation of **A-1.8**

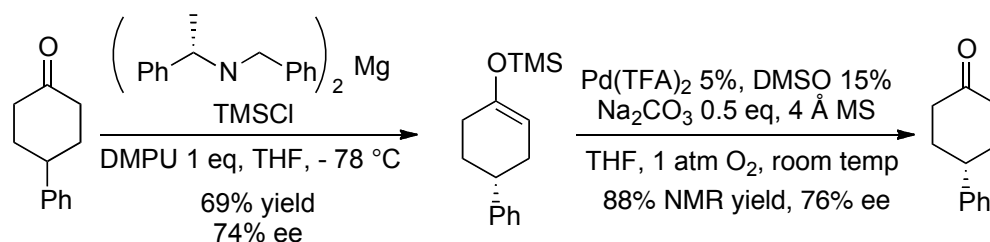
Entry	Pd (5%)	Ligand (mol%)	MS	Solvent	Additives(10%)	Yield (%) ^a (Enone)	Yield (%) ^a (Ketone)
1	Pd(TFA) ₂	DMSO (10)		THF	NaOBz	49	27
2	Pd(TFA) ₂	DMSO (10)	3 Å	THF	NaOBz	68	18
3	Pd(TFA) ₂	DMSO (10)	3 Å	THF		29	10
4	Pd(TFA) ₂	DMSO (10)	4 Å	THF	NaOBz	84	5
5	Pd(OAc) ₂	DMSO (10)	4 Å	THF	NaOBz	0	0
6	Pd(TFA)₂	DMSO (10)	4 Å	THF	NaOAc	95	4
7	Pd(OAc) ₂	DMSO (10)	4 Å	acetone	NaOAc	84	13
8	Pd(OAc) ₂	DMSO (10)	4 Å	dioxane	NaOAc	65	12

^aCrude yield determined by GC spectroscopy with tetradecane as the internal standard.

This identified Pd(DMSO)₂(TFA)₂ catalyst is submitted to dehydrosilylation of the chiral 4-phenylcyclohexanone, prepared according to literature procedures^a (Scheme A-1.4).⁸ The corresponding 4-phenylcyclohexenone is obtained in high yield, and the ee of the molecule

remains the same as the starting 4-phenylcyclohexanone. In fact, this tandem strategy has been applied in the enantioselective synthesis of a fragment of Labiatin⁹ and a fumagillin analogue, as a potential MetAP-2 Reversible Inhibitor.¹⁰ Stoichiometric Pd(OAc)₂ is used as the oxidant for this application.

Scheme A-1.4. Tandem Asymmetric Deprotonation of 4-Phenylcyclohexanone Followed by Pd-Catalyzed Dehydrosilylation to Prepare Chiral 4-Phenylcyclohexenone



A.1.3 Conclusion

We describe here an effort towards the formal synthesis of (+) infectocaryone and (+) cryptocaryone, using Pd-catalyzed dehydrogenation methods. The unsatisfactory yields for the desired cyclohexenone products suggest that more robust catalysts with high chemoselectivity and regioselectivity are required.

A.1.4 References

1. For an recent example of using chiral 4-methylcyclohexenone in synthesis, see: Tun, M. K. M.; Wustmann, D.-J.; Herzon, S. B. *Chem. Sci.* **2011**, *2*, 2251-2253.
2. Franck, G.; Brödner, K.; Helmchen, G. *Org. Lett.* **2010**, *12*, 3886-3889.
3. Shibasaki, M.; Sasai, H.; Arai, T. *Angew. Chem. Int. Ed.* **1997**, *36*, 1236-1256.

-
4. For leading references, see: (a) Aoki, K.; Tomioka, K.; Noguchi, H.; Koga, K. *Tetrahedron* **1997**, *53*, 13641-13656. (b) Graf, C.-D.; Malan, C.; Knochel, P. *Angew. Chem. Int. Ed.* **1998**, *37*, 3014-3016. (c) Anderson, J. D.; García García, P.; Hayes, D.; Henderson, K. W.; Kerr, W. J.; Moir, J. H.; Fondekar, K. P. *Tetrahedron Lett.* **2001**, *42*, 7111-7114.
5. (a) Ito, Y.; Hirao, T.; Saegusa, T. *J. Org. Chem.* **1978**, *43*, 1011-1013. (b) Larock, R. C.; Hightower, T. R.; Kraus, G. A.; Hahn, P.; Zheng, D. *Tetrahedron Lett.* **1995**, *36*, 2423-2426.
6. Xu, Y.; Otori, K.; Ohshima, T.; Shibasaki, M. *Tetrahedron* **2002**, *58*, 2585-2588.
7. Danishefsky, S. J.; Simoneau, B. *J. Am. Chem. Soc.* **1989**, *111*, 2599-2604.
8. Henderson, K. W.; Kerr, W. J.; Moir, J. H. *Chem. Comm.* **2000**, 479-480.
9. Clark, J. S.; Vignard, D.; Parkin, A. *Org. Lett.* **2011**, *13*, 3980-3983.
10. Rodeschini, V.; Van de Weghe, P.; Salomon, E.; Tarnus, C.; Eustache, J. *J. Org. Chem.* **2005**, *70*, 2409-2412.

Appendix 2:

Additional NMR Experiments and Spectroscopic Data for Chapter 4

Additional Data**Additional Spectra of DMSO Titration Experiments in EtOAc and THF-*d*₈****DOSY Experiments for Compounds 4-1, 4-2, 4-3a and 4-3b****Additional NMR Data for Pd(TFA)₂/DMSO in AcOH-*d*₄****Additional ¹H and ¹⁹F NMR Spectra of Pd(TFA)₂/DMSO in Toluene-*d*₈**

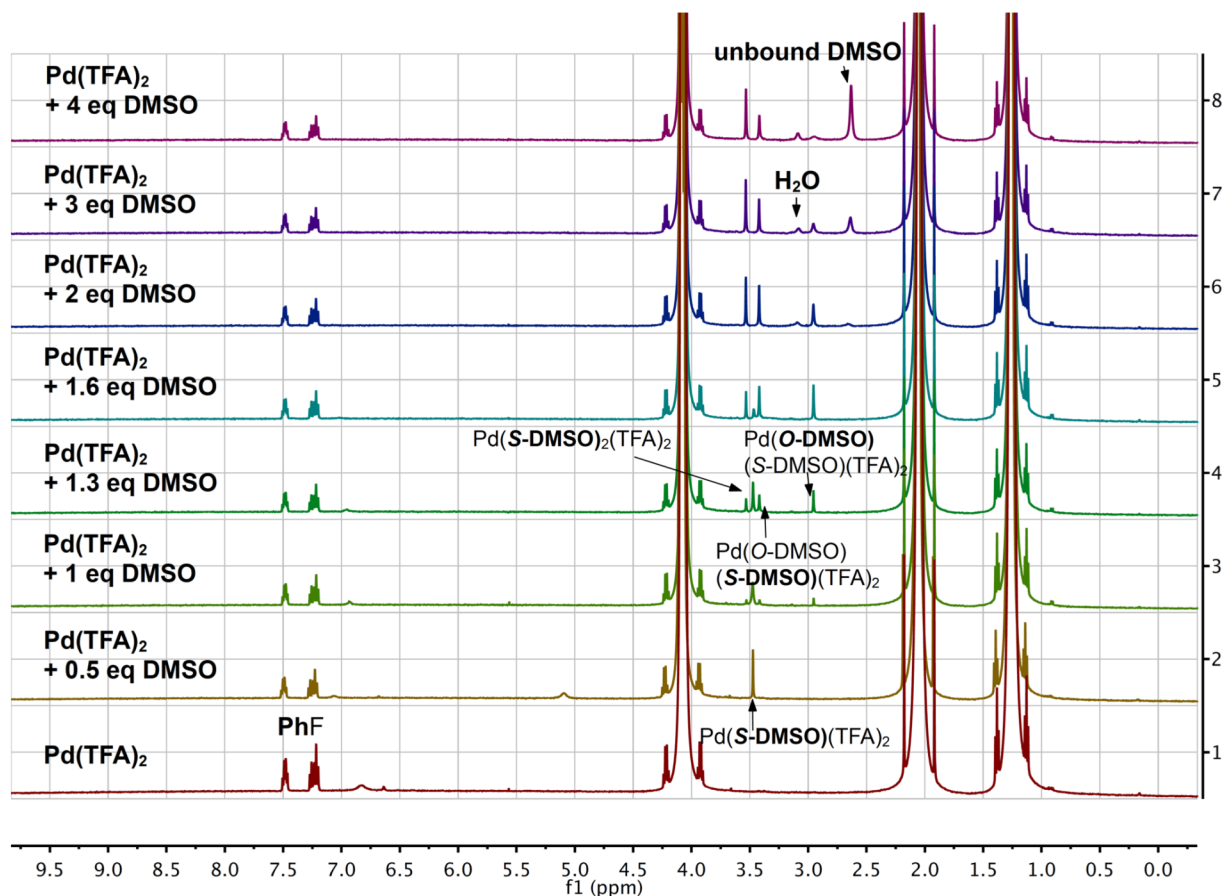
Additional Spectra of DMSO Titration Experiments in EtOAc and THF-*d*₈

Figure A-2.1. ¹H NMR spectra of Pd(TFA)₂ in EtOAc with various quantities of DMSO at -60 °C. Conditions: [Pd(TFA)₂] = 30 mM (6.6 mg, 0.02 mmol), EtOAc = 0.65 mL, -60 °C, [DMSO] = 0, 15, 30, 39, 48, 60, 90, 120 mM, PhF (internal standard) = 6.5 mM (4 μL).

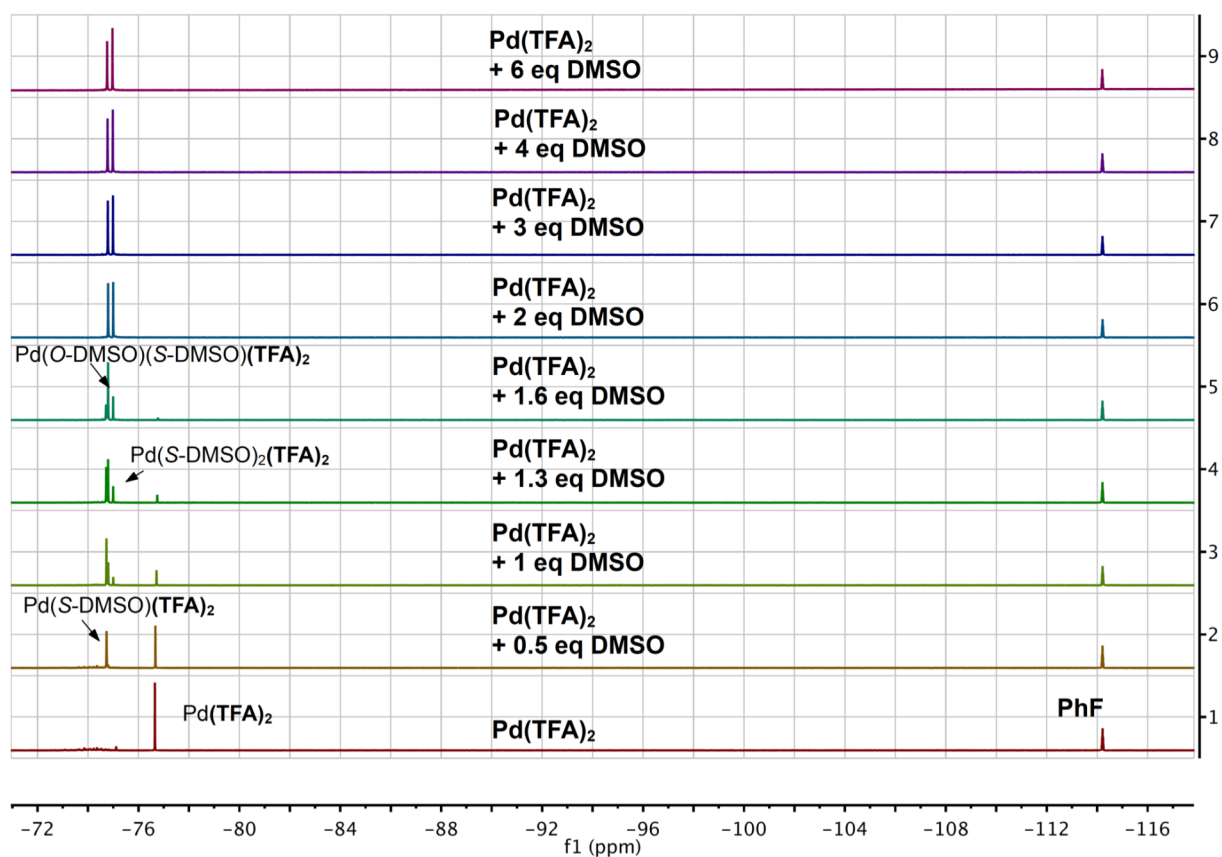


Figure A-2.2. ^{19}F NMR spectra of $\text{Pd}(\text{TFA})_2$ in EtOAc with various quantities of DMSO at -60 °C. Conditions: $[\text{Pd}(\text{TFA})_2] = 30$ mM (6.6 mg, 0.02 mmol), EtOAc = 0.65 mL, -60 °C, $[\text{DMSO}] = 0, 15, 30, 39, 48, 60, 90, 120, 180$ mM, PhF (internal standard) = 6.5 mM (4 μL).

The solution of $\text{Pd}(\text{OAc})_2$ with 2 equiv. DMSO in EtOAc has been analyzed by ^1H NMR spectroscopy at various temperatures. As the temperature is decreased, the two broad peaks at 24 $^\circ\text{C}$, corresponding to bound DMSO ligands, were sharpened and separated from each other (Figure A-2.3).

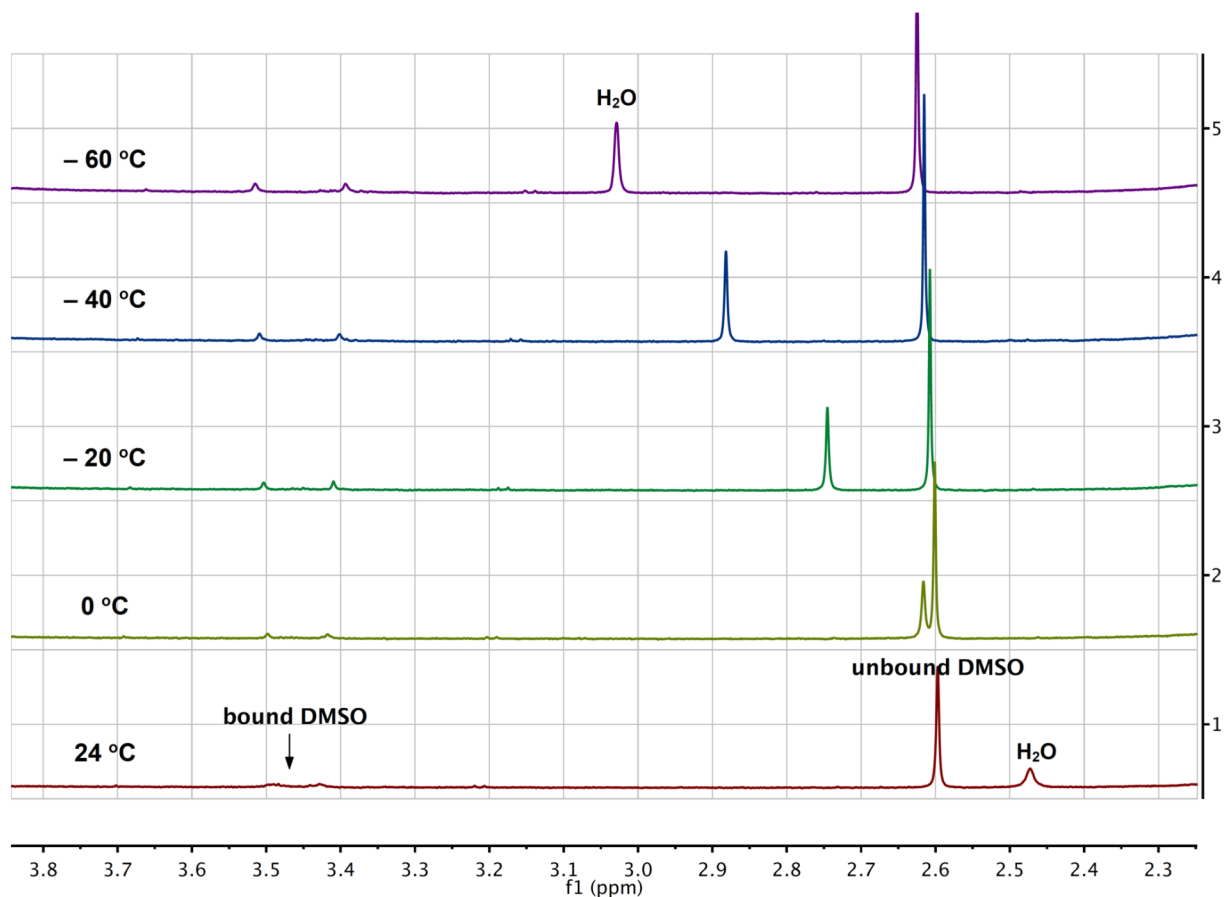


Figure A-2.3. ^1H NMR spectra of $\text{Pd}(\text{OAc})_2/\text{DMSO}$ in EtOAc at various temperatures. Conditions: $[\text{Pd}(\text{OAc})_2] = 15 \text{ mM}$ (2.2 mg, 0.01 mmol), $[\text{DMSO}] = 30 \text{ mM}$ (2 equiv.), EtOAc = 0.65 mL, temperature = $-60, -40, -20, 0, 24 \text{ }^\circ\text{C}$.

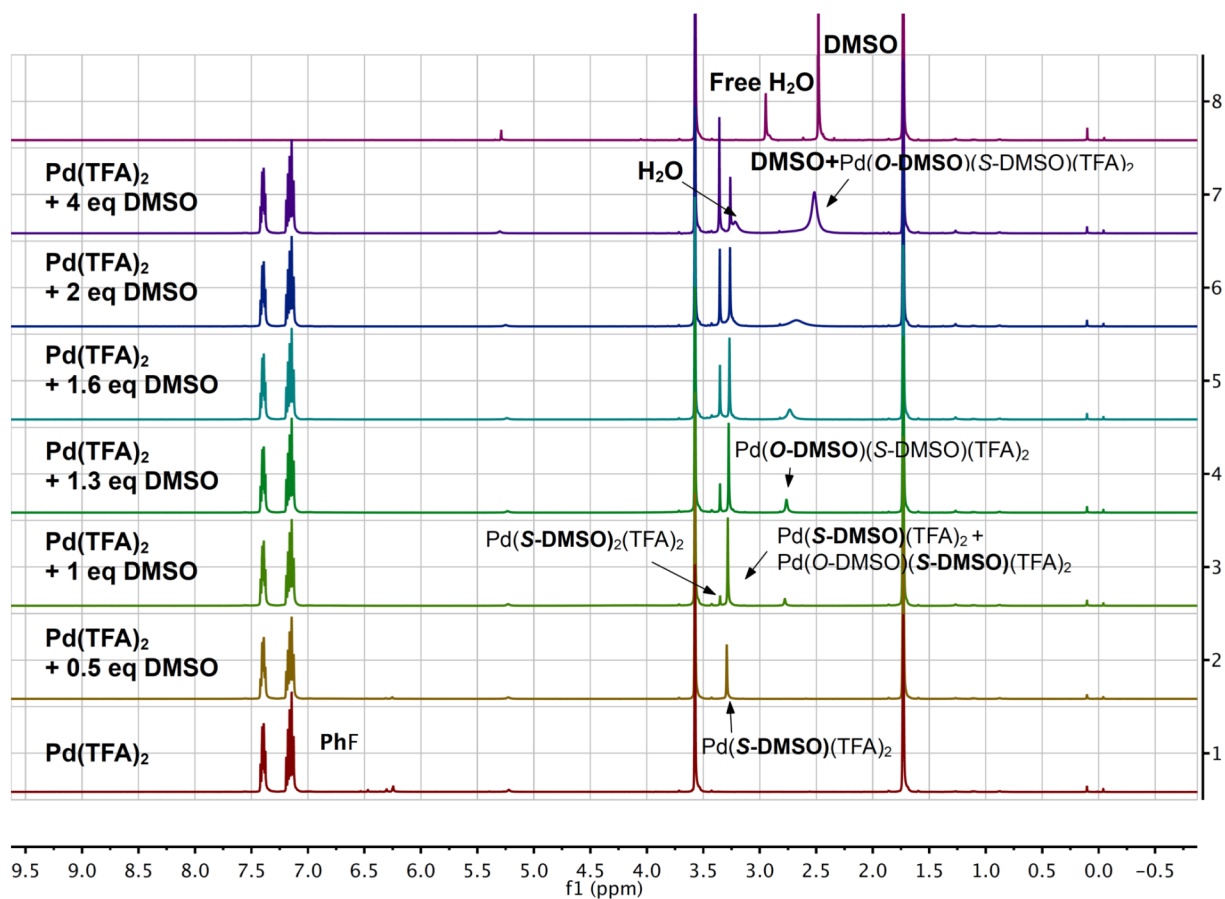


Figure A-2.4. ^1H NMR spectra of $\text{Pd}(\text{TFA})_2$ in $\text{THF-}d_8$ with various quantities of DMSO at -60 $^\circ\text{C}$. Conditions: $[\text{Pd}(\text{TFA})_2] = 15$ mM (3.3 mg, 0.01 mmol), $\text{THF-}d_8 = 0.65$ mL, -60 $^\circ\text{C}$, $[\text{DMSO}] = 0, 7.5, 15, 19.5, 24, 30, 60, 90, 120$ mM.

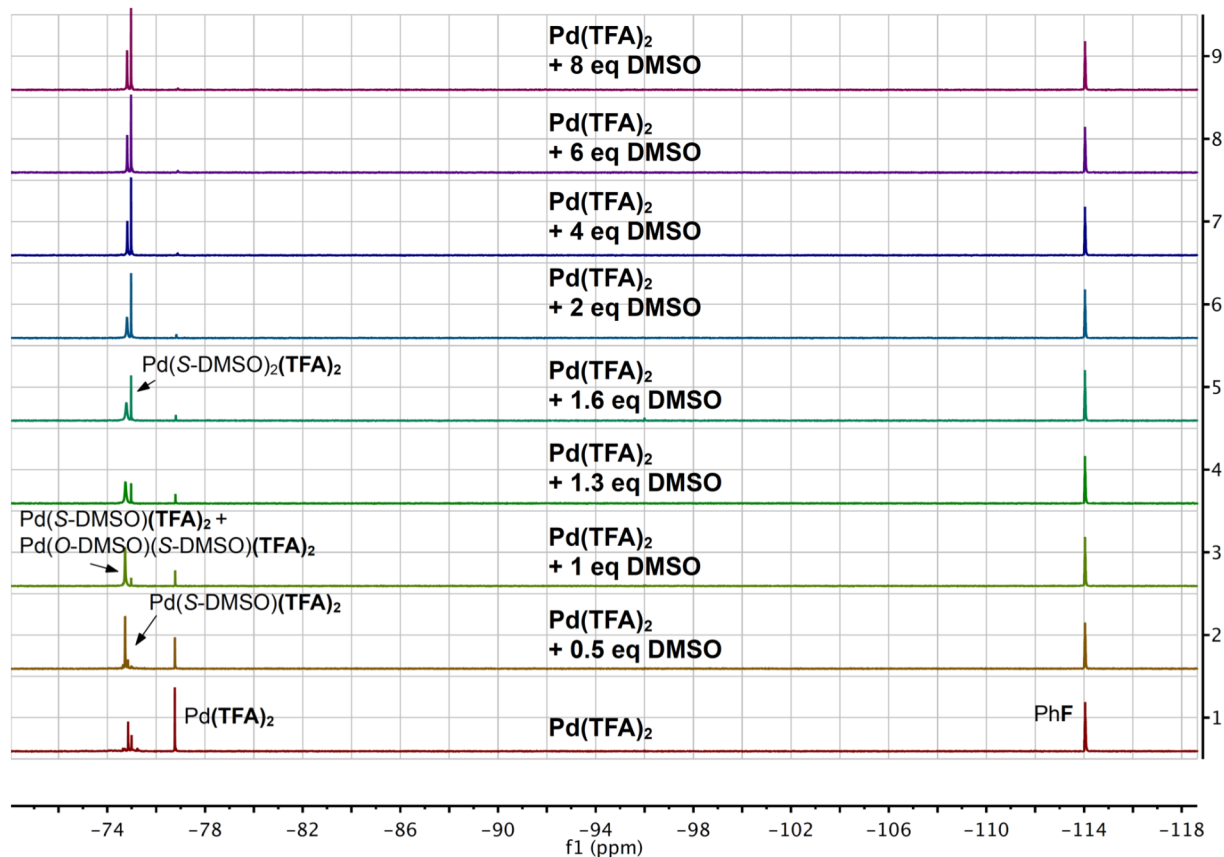


Figure A-2.5. ^{19}F NMR spectra of $\text{Pd}(\text{TFA})_2$ in $\text{THF-}d_8$ with various quantities of DMSO at -60 $^\circ\text{C}$. Conditions: $[\text{Pd}(\text{TFA})_2] = 15$ mM (3.3 mg, 0.01 mmol), $\text{THF-}d_8 = 0.65$ mL, -60 $^\circ\text{C}$, $[\text{DMSO}] = 0, 7.5, 15, 19.5, 24, 30, 60, 90, 120$ mM.

DOSY Experiments for Compounds 4-1, 4-2, 4-3a and 4-3b

The diffusion coefficient of a molecule in solution reflects the size of the molecule (radius). 1D DOSY (Diffusion Order Spectroscopy) experiments are known as a way to probe the molecular sizes by observing the attenuation of the NMR signals during a pulsed field gradient experiment. We performed a series of 1D DOSY experiments on the ^{19}F NMR spectra of $\text{Pd}(\text{TFA})_2$ in the presence of 0, 1 and 2 equiv. of DMSO in order to estimate the aggregation of

Pd complexes in solution. In particular, we sought to differentiate the monomeric **4-2a** from the dimeric **4-2b** in solution.

Figure A-2.6 shows a representative 1D DOSY spectra of the solution of Pd(TFA)₂ in EtOAc at 24 °C. The intensities of the ¹⁹F peaks decrease as increased gradient pulse strength G. Defined by the theory of 1D DOSY experiments, the ln(I/I₀) of peaks display a linear relationship versus the G² (Figure A-2.7). The slope of the resulting line is proportional to the diffusion coefficient, and inverse proportional to the size of the molecule, since the larger the size of a molecule, the slower it diffuses (Scheme A-2.1).

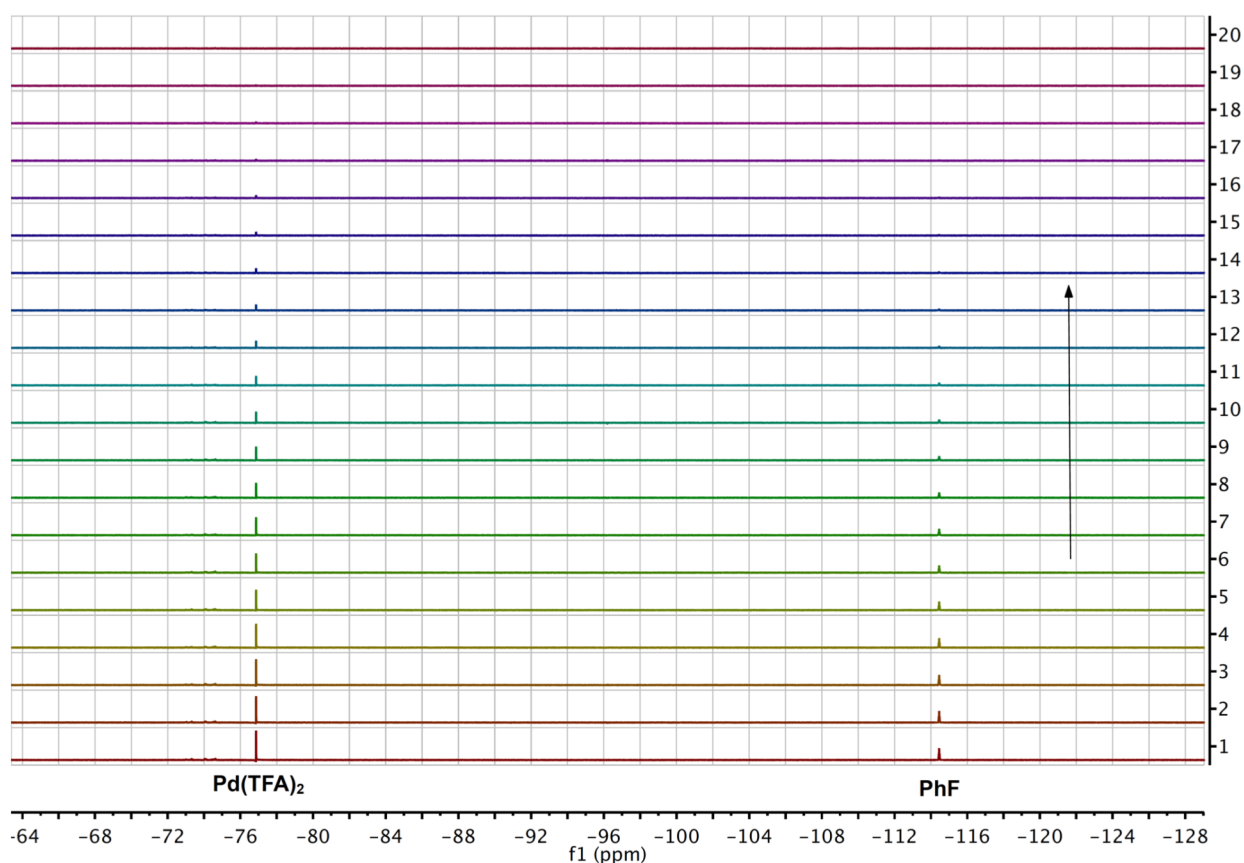


Figure A-2.6. 1D DOSY (Dbppste) experiments on the ¹⁹F peaks of Pd(TFA)₂ in EtOAc. Conditions: [Pd(TFA)₂] = 15 mM (3.3 mg, 0.01 mmol), EtOAc = 0.65 mL, temperature = 24 °C.

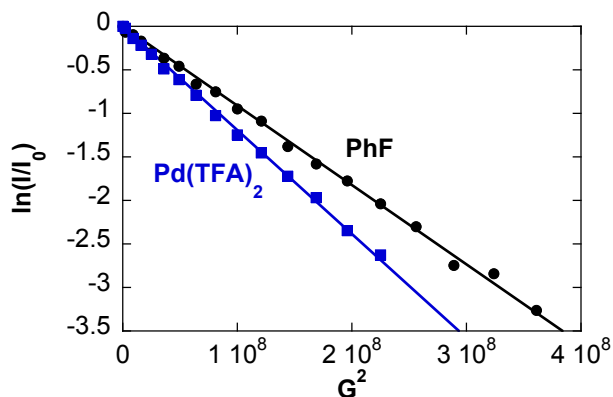


Figure A-2.7. $\ln(I/I_0)$ as a function of of $\text{Pd}(\text{TFA})_2$ in EtOAc with various quantities of DMSO at -40°C . Conditions: $[\text{Pd}(\text{TFA})_2] = 15\text{ mM}$ (3.3 mg, 0.01 mmol), EtOAc = 0.65 mL, 24°C .

Scheme A-2.1. Equations for Calculation of Relative Molecular Size of Pd Complexes Relative to Fluorobenzene based on 1D DOSY Data

$$\ln(I/I_0) \propto -G^2 \cdot D$$

I = intensity of peaks

G = Strength of the gradient pulse

D = Diffusion coefficient

$$\text{Molecular size} \propto 1/D$$

$$\text{Relative molecular size} = \frac{\text{slope } (\ln(I/I_0)/G^2) \text{ of PhF}}{\text{slope } (\ln(I/I_0)/G^2) \text{ of Pd}}$$

Four samples were determined, $\text{Pd}(\text{TFA})_2$, $\text{Pd}(\text{DMSO})(\text{TFA})_2$, $\text{Pd}(\text{DMSO})_2(\text{TFA})_2$ and $[\text{Pd}(\eta^3\text{-4-CF}_3\text{C}_6\text{H}_4\text{C}_3\text{H}_5)\mu\text{-Cl}]_2$. At room temperature, the ^{19}F NMR spectra of $\text{Pd}(\text{TFA})_2$ and $\text{Pd}(\text{TFA})_2/\text{DMSO}$ (1 equiv.) exhibit predominant species at -76.76 and -74.74 ppm, respectively. With 2 equiv. of DMSO, two ^{19}F peaks at -74.80 and -75.00 ppm were present, representing two different species. With an internal reference, fluorobenzene,¹ the molecular sizes of the complexes were calculated based on equations in Scheme A-2.1 and presented relative to PhF (Table A-2.1). The ratio of the molecular size of $\text{Pd}(\text{TFA})_2$:fluorobenzene is determined to be

1.5. This number increases to 2.3 for the complex formed in the presence of 1 equiv. of DMSO. The relative molecular sizes of the two peaks in the presence of 2 equiv. of DMSO are 1.4 and 1.7, respectively. The relative molecular size of (π -allyl)PdCl complex $[\text{Pd}(\eta^3\text{-4-CF}_3\text{C}_6\text{H}_4\text{C}_3\text{H}_5)\mu\text{-Cl}]_2$ is determined to be 2.4.

Table A-2.1. Relative Molecular Size of Pd Complexes Determined by 1D DOSY Experiments^a

Sample	Pd(TFA) ₂	Pd(DMSO)(TFA) ₂	Pd(DMSO) ₂ (TFA) ₂		$[\text{Pd}(\eta^3\text{-4-CF}_3\text{C}_6\text{H}_4\text{C}_3\text{H}_5)\mu\text{-Cl}]_2$
Molecular weight	332	410 or 820	488		654
Peak (ppm)	-76.76	-74.74	-74.80	-75.00	-63.51
	4-1	4-2a or 4-2b	4-3a	4-3b	
Relative molecular size Slope(PhF/Pd)					
run 1	1.3	2.9	1.3	1.7	2.2
run 2	1.2	1.9	1.4	1.8	2.5
run 3	1.8	2.3			
Average	1.5 ± 0.3	2.3 ± 0.3	1.4 ± 0.3	1.7 ± 0.3	2.4 ± 0.3

^a Conditions: [Pd] = 15 mM (3.3 mg, 0.01 mmol), [DMSO] = 0, 15, 30 mM (0, 1, 2 equiv.), EtOAc = 0.65 mL, temperature = 24 °C.

Wilkinson and coworkers have determined **4-1** to be a monomer in EtOAc,² whereas $[\text{Pd}(\eta^3\text{-4-CF}_3\text{C}_6\text{H}_4\text{C}_3\text{H}_5)\mu\text{-Cl}]_2$ is known as a chloro-bridged dimer in organic solvents. These two complexes can serve as benchmarks for monomeric and dimeric Pd species, respectively. In the presence of 2 equiv. of DMSO, the Pd species exhibit similar molecular sizes as **4-1**. These observations are consistent with our proposed monomeric Pd structures, **4-3a** and **4-3b**. In the presence of 1 equiv. of DMSO, however, the Pd complex displays a relative molecular size that is close to $[\text{Pd}(\eta^3\text{-4-CF}_3\text{C}_6\text{H}_4\text{C}_3\text{H}_5)\mu\text{-Cl}]_2$, suggesting that the mono-DMSO ligated Pd complex may exist as a dimer in solution.

Additional NMR Data for Pd(TFA)₂/DMSO in AcOH-*d*₄

The ¹⁹F NMR spectrum of Pd(TFA)₂ in AcOH-*d*₄ exhibits a singlet at -76.918 ppm, very close to the ¹⁹F peak of TFAH in AcOH at -76.923 ppm (cf. Figure 4-18). Addition of DMSO led to formation of a new ¹⁹F peak at -74.92 ppm and the slight upfield shift of the peak at -76.918 ppm. The integration of the peak at -74.92 ppm exhibits no correlation to bound DMSO peaks in ¹H NMR (Figure A-2.8). Instead, line broadening and shift of the peak at -76.918 ppm suggest formation of new species underneath the unligated-Pd(TFA)₂ peak.

In AcOH-*d*₄, the trifluoroacetate ligand on Pd^{II} could be replaced by acetate. This reaction has been ruled out by formation of a new ¹⁹F peak at -74.92 ppm and the slight upfield shift of the peak at -76.918 ppm upon addition of DMSO, as the ¹⁹F peak should exhibit no change if fully dissociated from Pd^{II} (cf. Figure 4-18).. The line broadening of peaks in the ¹⁹F NMR spectra is consistent with the broad bound-DMSO peaks in the ¹H NMR spectra, representing fast exchange between complexes. The precise identity of the ¹⁹F peak at -74.92 ppm is yet to be resolved.

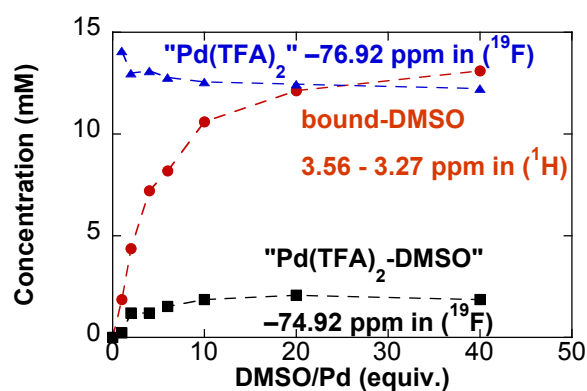


Figure A-2.8. Titration curves of DMSO into the AcOH-*d*₄ solution of Pd(TFA)₂ at 24 °C. Conditions: [Pd(TFA)₂] = 15 mM (3.3 mg, 0.01 mmol), [DMSO] = 30 mM (2 equiv.), AcOH-*d*₄ = 0.65 mL, 24 °C, [DMSO] = 0, 15, 30, 90, 300 and 600 mM.

Additional ^1H and ^{19}F NMR Spectra of $\text{Pd}(\text{TFA})_2/\text{DMSO}$ in Toluene- d_8

Attempts to resolve the coordination chemistry of DMSO to $\text{Pd}(\text{TFA})_2$ in toluene are shown in Figure A-2.9 and A-2.10 by acquiring the NMR spectra at $-60\text{ }^\circ\text{C}$. The mixture of $\text{Pd}(\text{TFA})_2$ with 1 equiv. of DMSO in toluene- d_8 was analyzed by ^1H and ^{19}F NMR spectroscopy. A ^1H peak at 1.36 ppm is upfield relative to the free DMSO. We are not able to assign this peak based on current data and the literature precedents. With excess DMSO, this peak merged with the free DMSO resonance, indicating that they are interconverting to each other. Another ^1H peak at 2.01 ppm may associate with the *O*-bound DMSO. Further addition of DMSO leads to downfield shift of the *O*-bound DMSO peak and formation of a mixture of *S*-bound DMSO species that are under fast exchange, evident as significant line broadening. The line broadening and the shift of peaks in the ^{19}F NMR spectra implicate fast exchange of different species. We are not able to quantify these species due to the unknown Pd concentration in the solution, but the clear increase of peak integration with > 3 equiv. of DMSO suggests that DMSO binding with 2 equiv. of DMSO is not complete. Formation of multiple species may arise from the solvation of $\text{Pd}(\text{TFA})_2$ in toluene. $\text{Pd}(\text{TFA})_2$ appears as a trimer in the solid state and doesn't dissolve readily in toluene by itself, since toluene is a non-polar solvent. The solvation possibly involves interaction between DMSO, $\text{Pd}(\text{TFA})_2$ and toluene, breakage of the trimer or formation of alternative oligomers that result in various species in the solution.

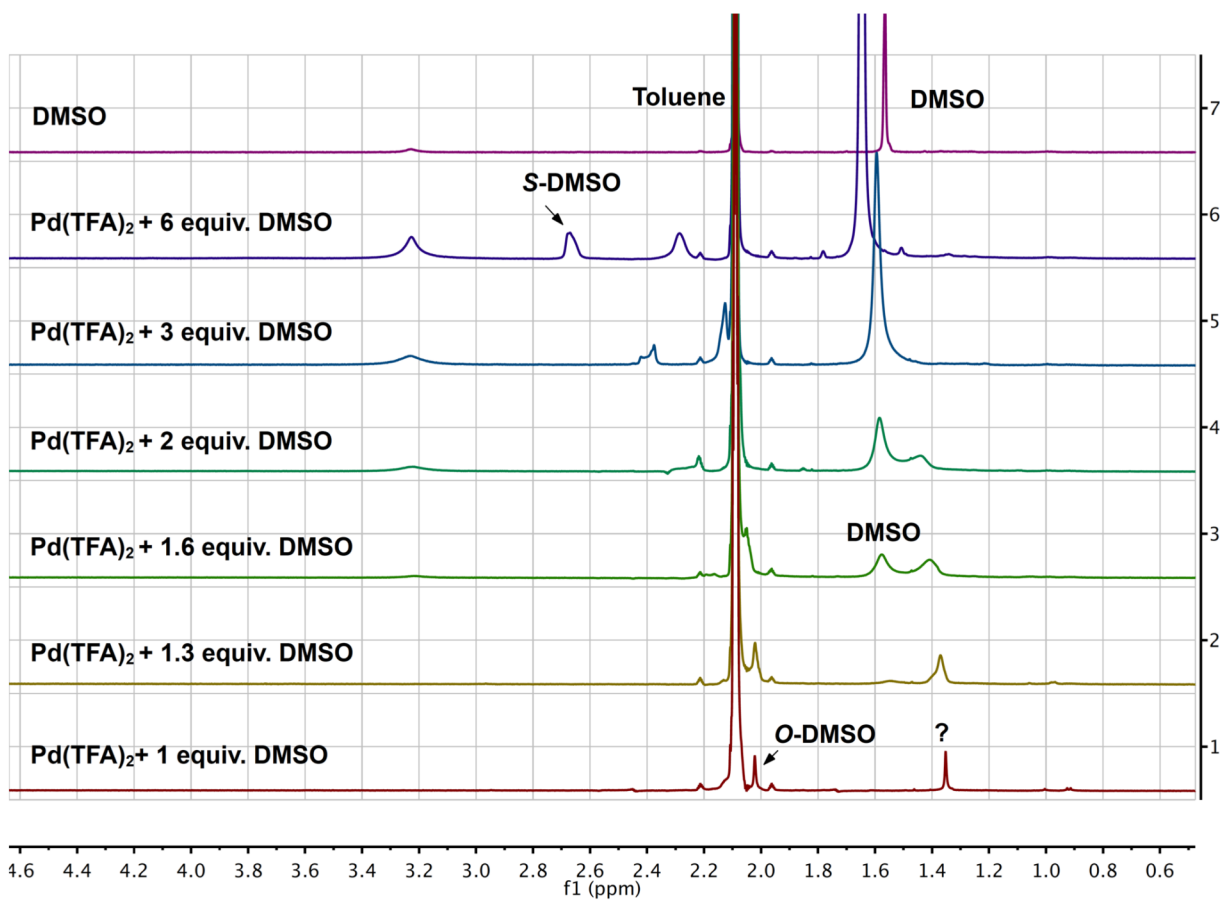


Figure A-2.9. ^1H NMR spectra of $\text{Pd}(\text{TFA})_2$ in toluene- d_8 with various quantities of DMSO at -60 $^\circ\text{C}$. Conditions: $[\text{Pd}(\text{TFA})_2] = 15$ mM (3.3 mg, 0.01 mmol), toluene- $d_8 = 0.65$ mL, -60 $^\circ\text{C}$, $[\text{DMSO}] = 15, 19.5, 24, 30, 45$ and 90 mM.

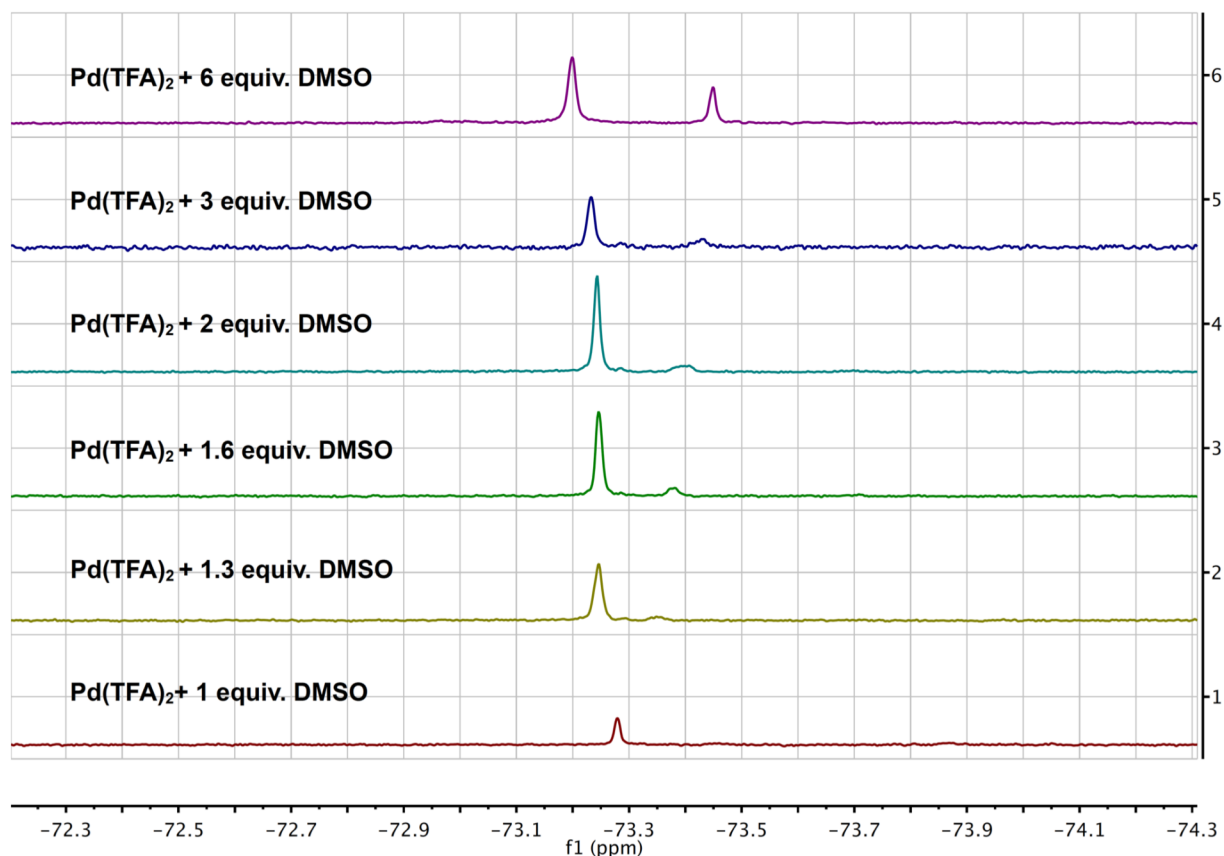


Figure A-2.10. ^{19}F NMR spectra of $\text{Pd}(\text{TFA})_2$ in $\text{toluene-}d_8$ with various quantities of DMSO at $-60\text{ }^\circ\text{C}$. Conditions: $[\text{Pd}(\text{TFA})_2] = 15\text{ mM}$ (3.3 mg, 0.01 mmol), $\text{toluene-}d_8 = 0.65\text{ mL}$, $-60\text{ }^\circ\text{C}$, $[\text{DMSO}] = 15, 19.5, 24, 30, 45$ and 90 mM .

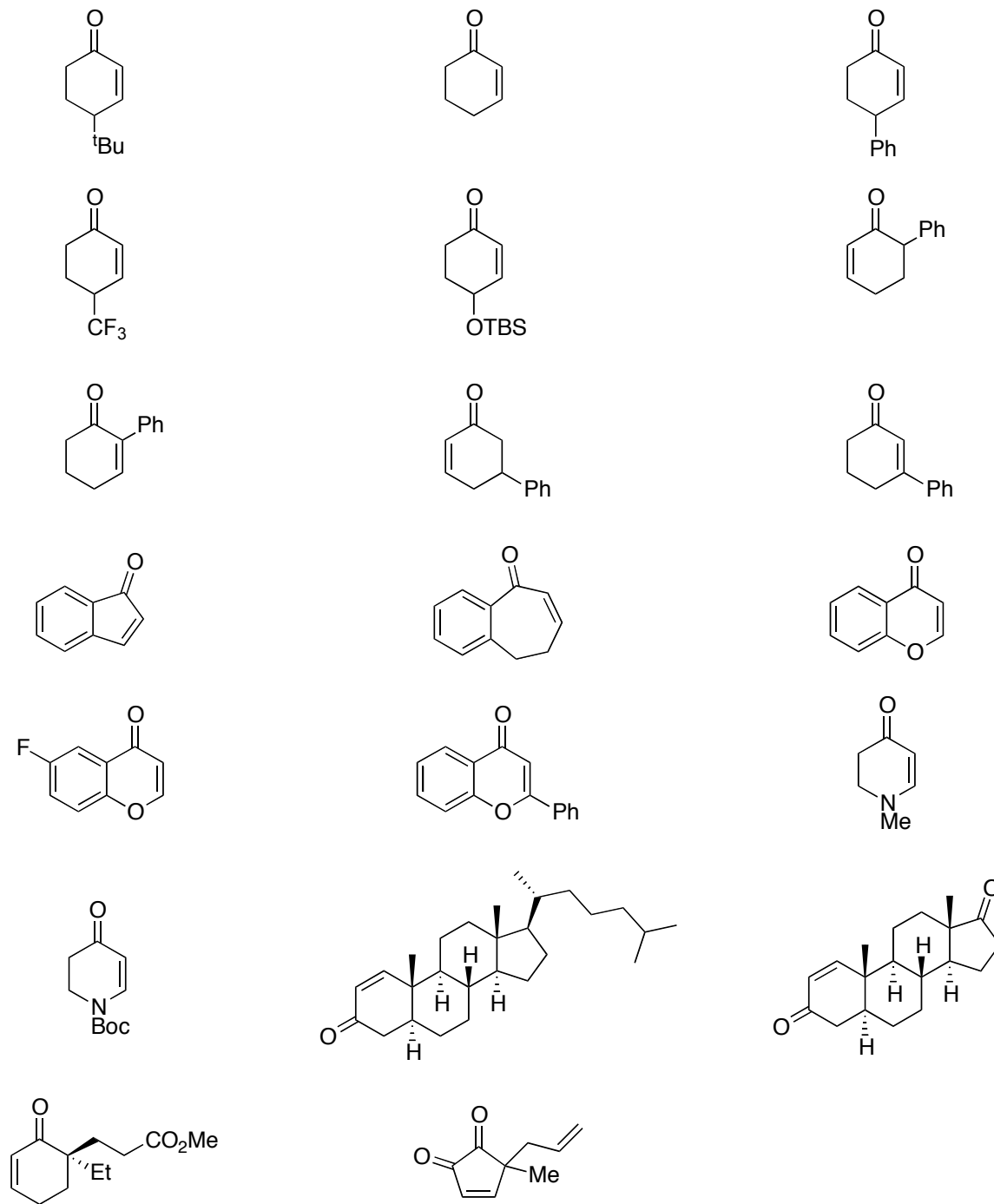
1. The use of an internal reference has been reported in several DOSY NMR experiments. For an example, see: Sliwa, A.; Marchand-Brynaert, J.; Luhmer, M. *Magn. Reson. Chem.* **2011**, *49*, 812-815.

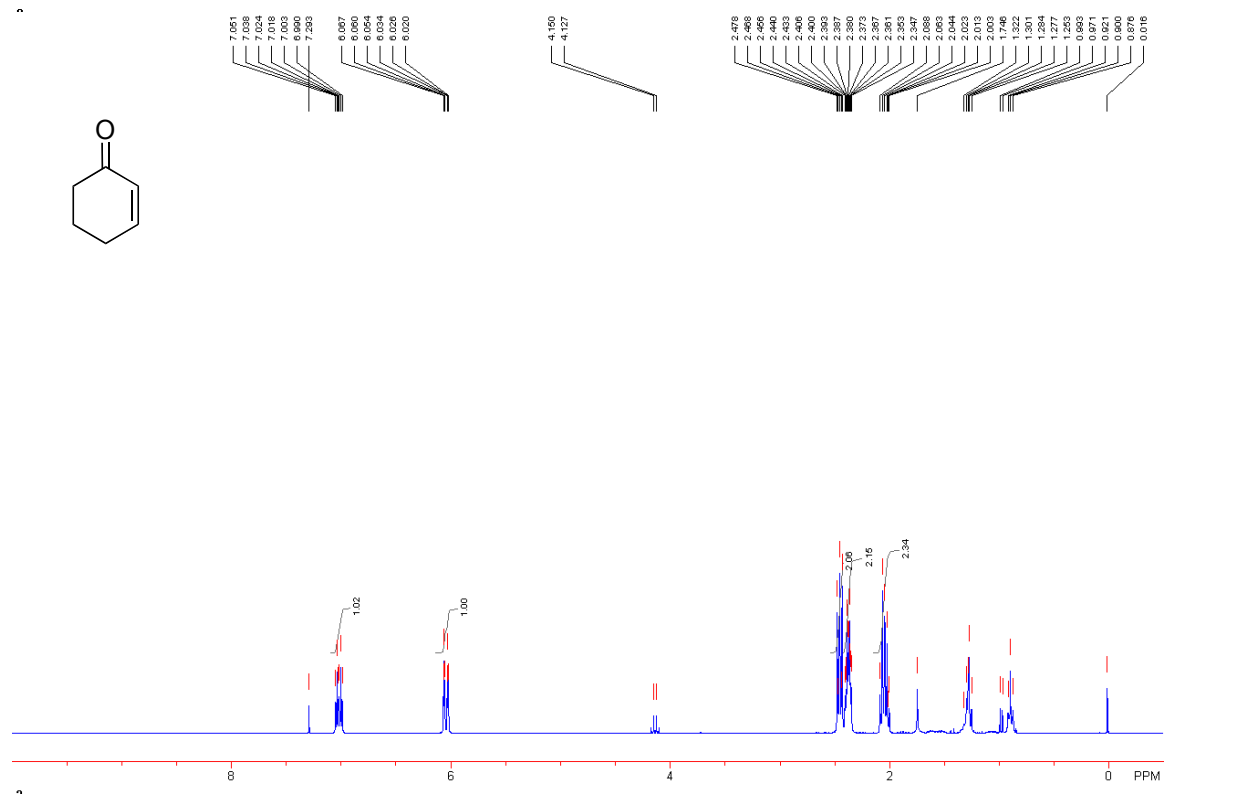
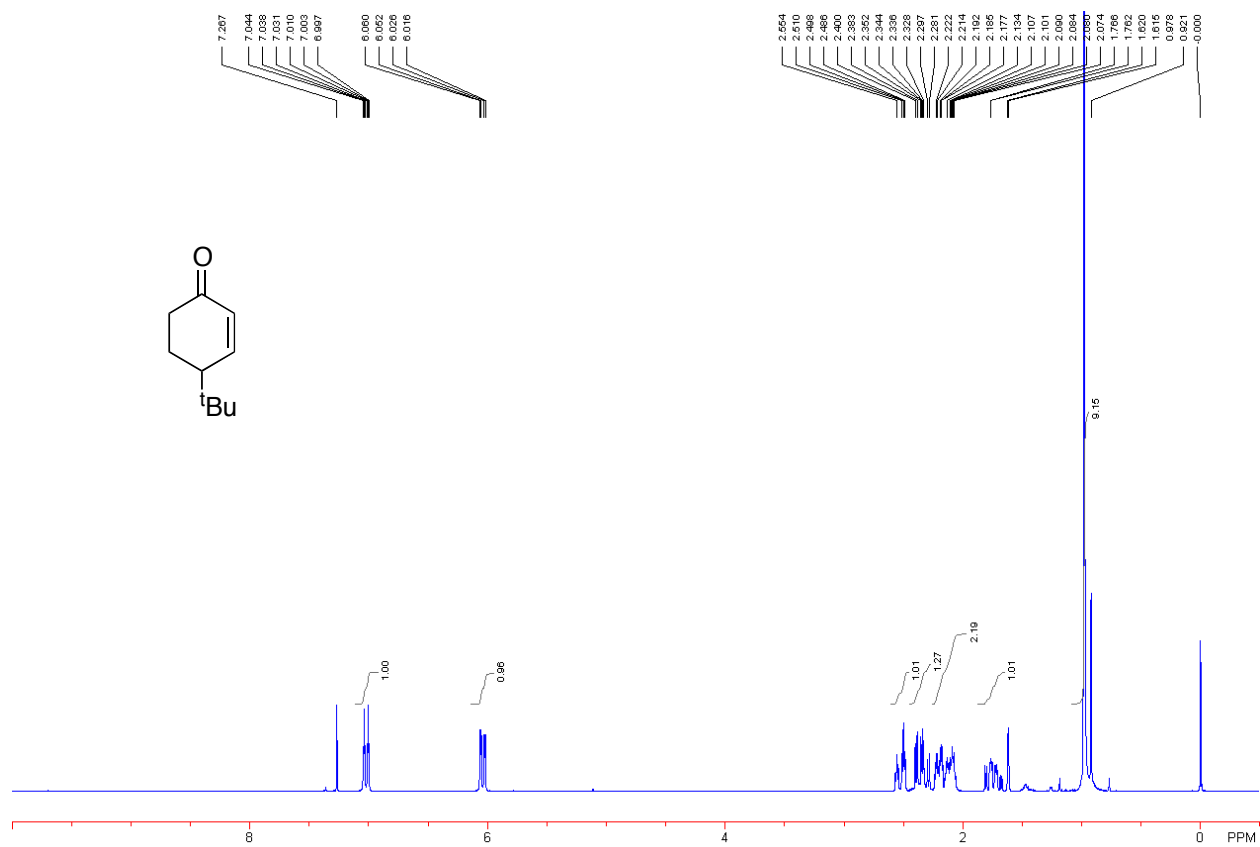
2. Stephenson, T. A.; Morehouse, S. M.; Powell, A. R.; Heffer, J. P.; Wilkinson, G. J. *Chem. Soc. (Resumed)* **1965**, 3632-3640.

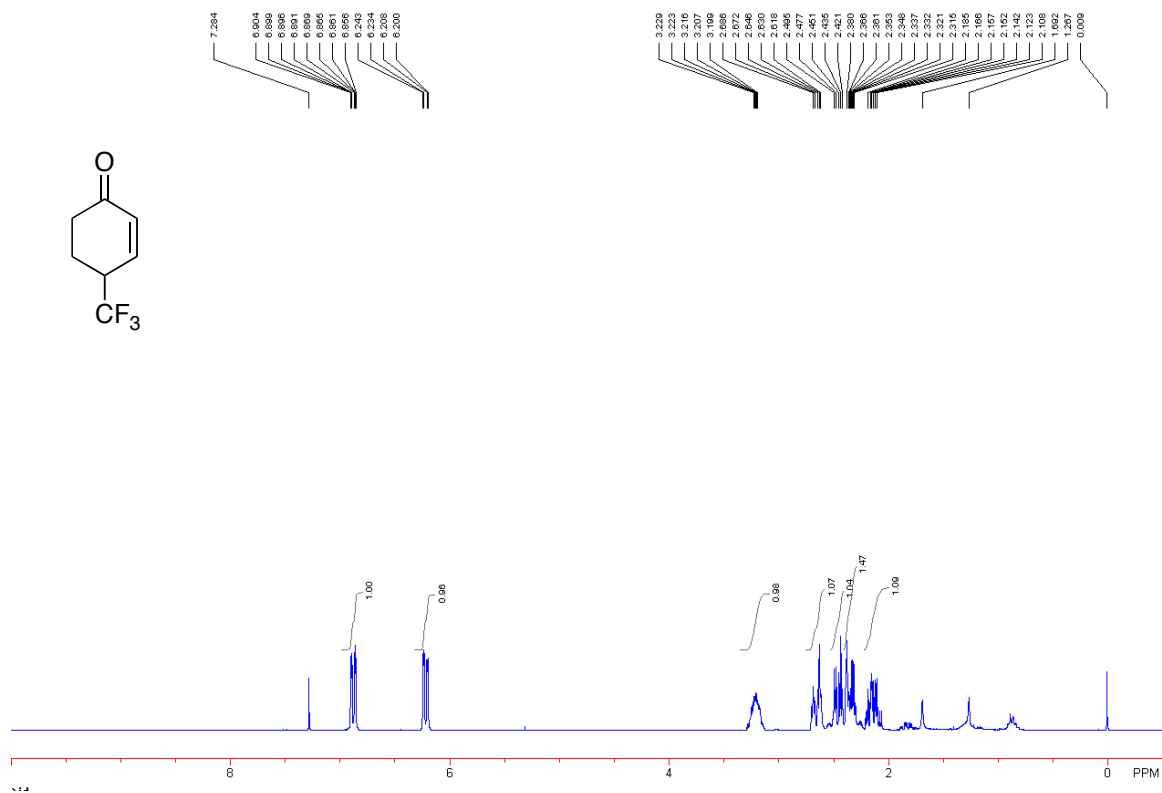
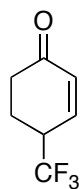
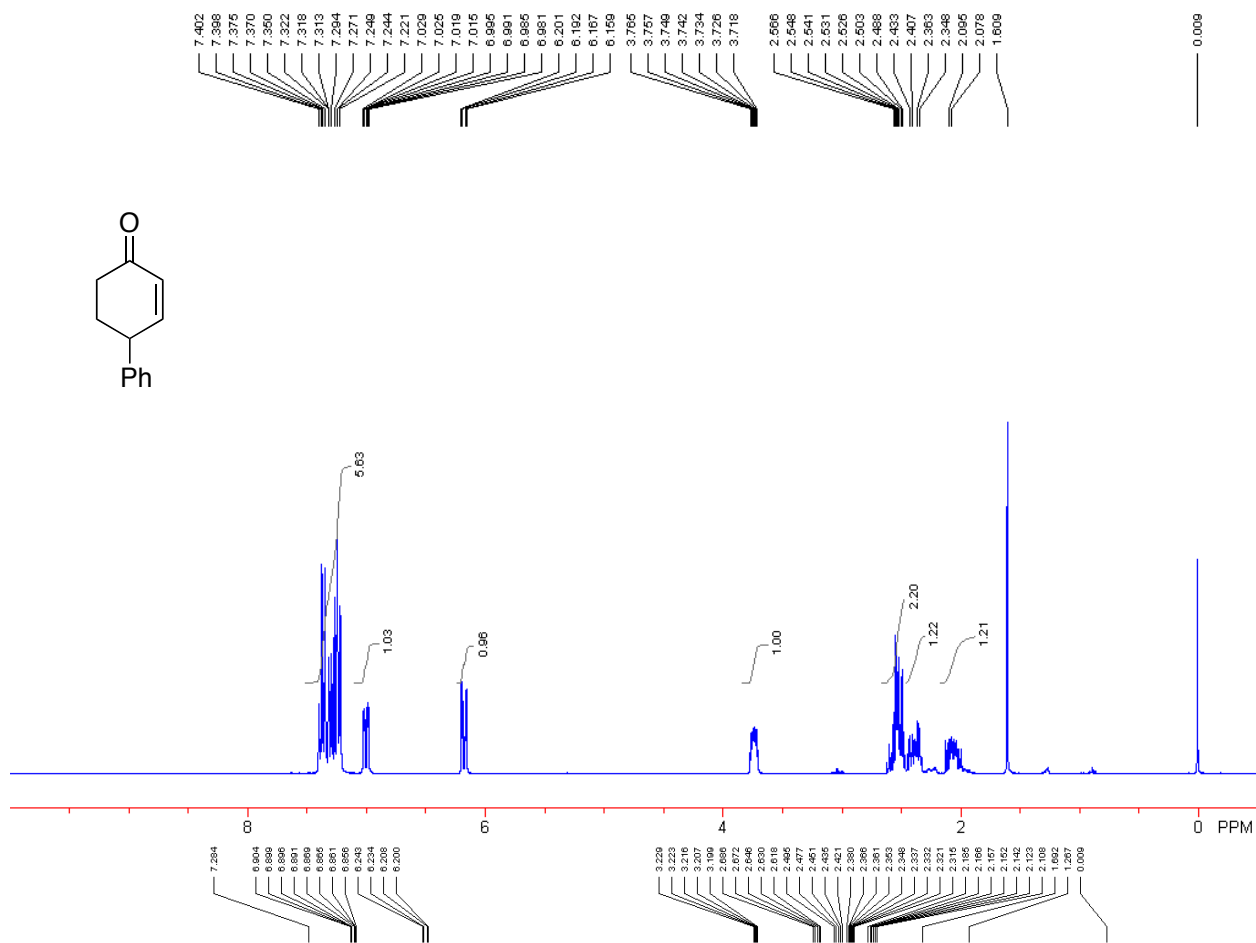
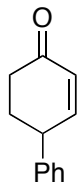
Appendix 3

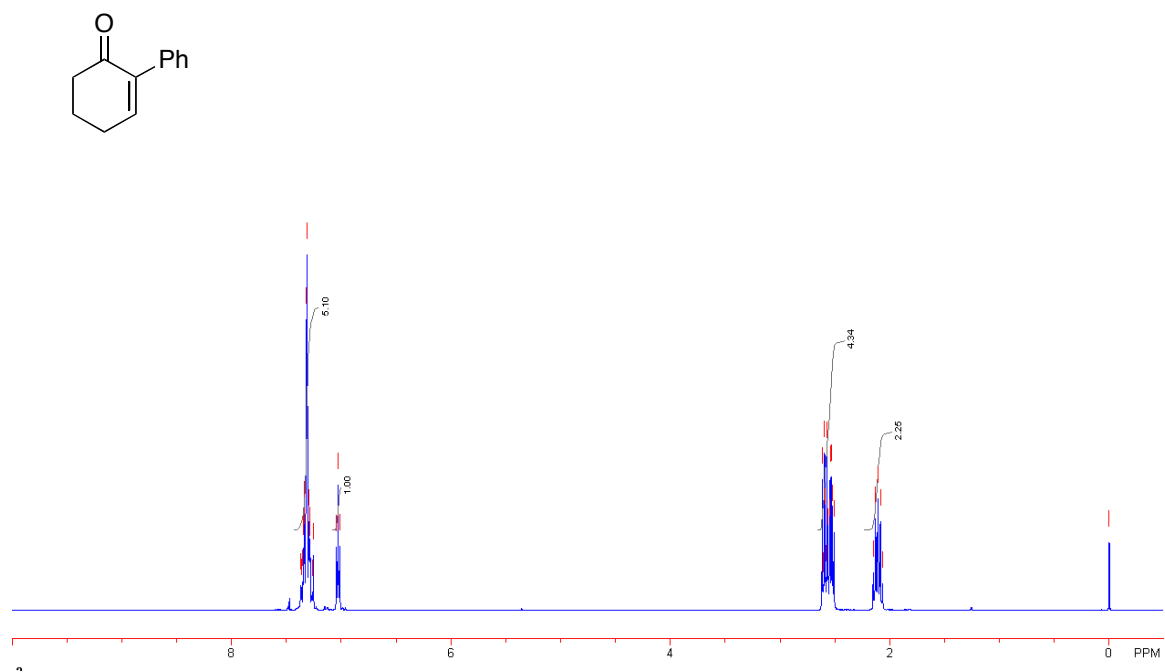
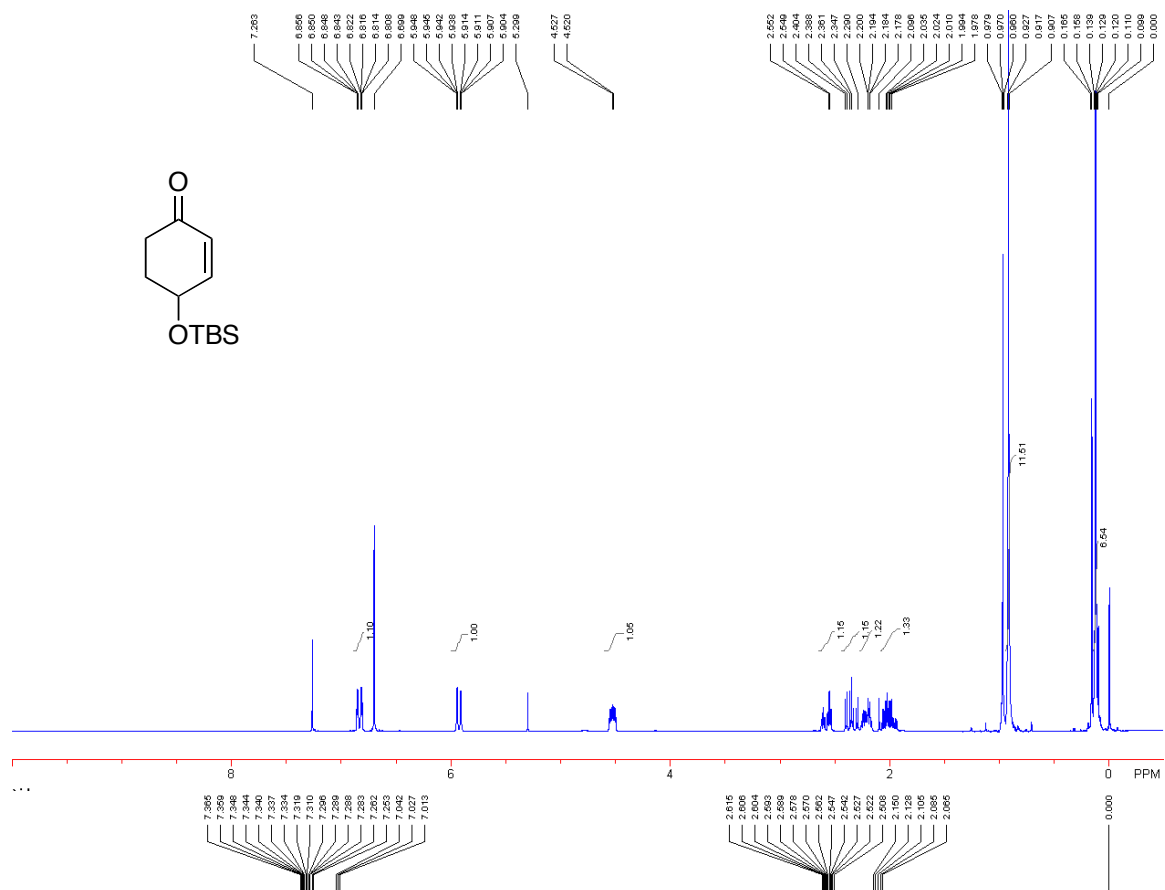
NMR Spectra of Compounds

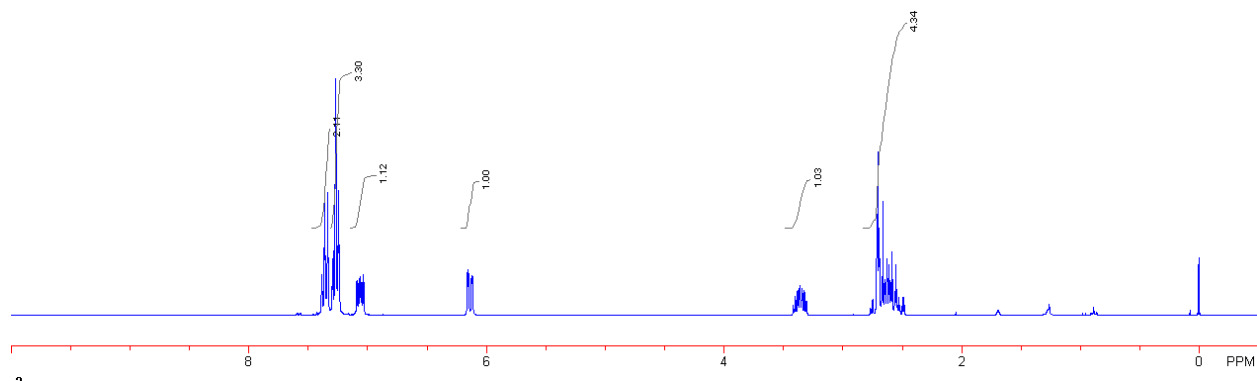
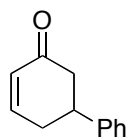
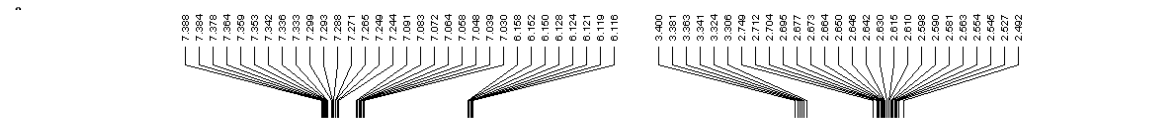
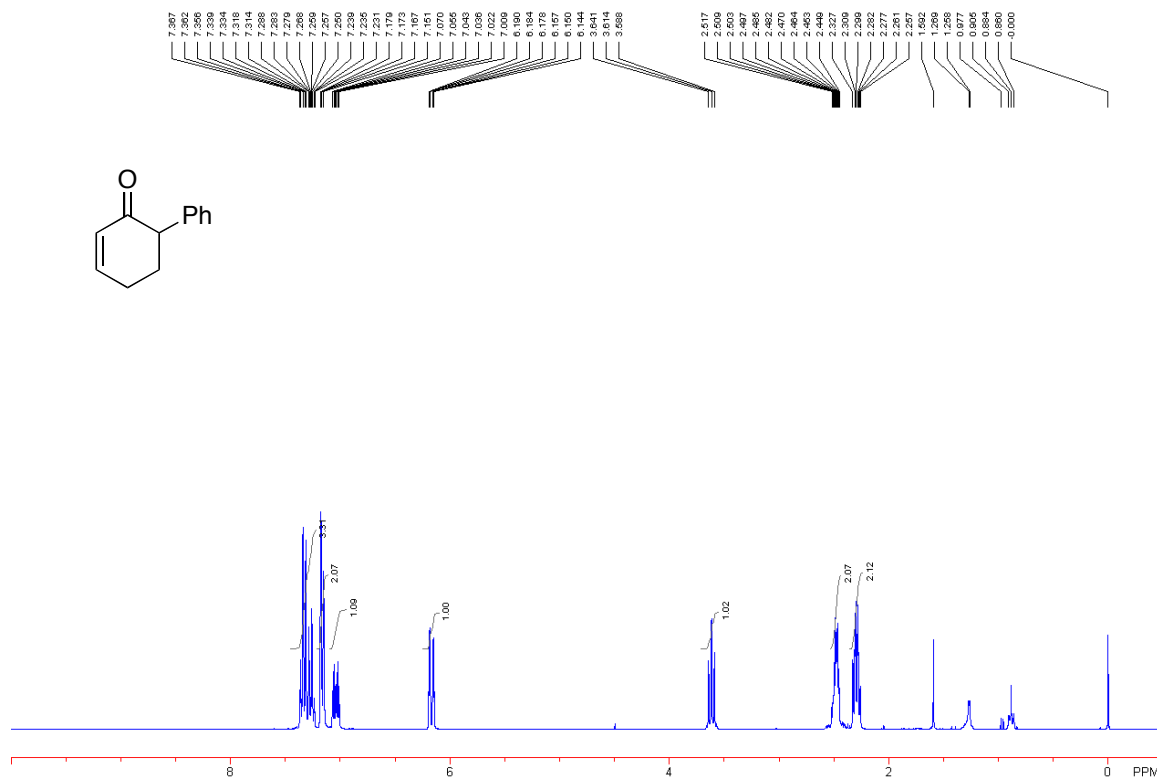
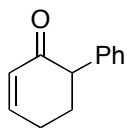
Compounds from Chapter 2

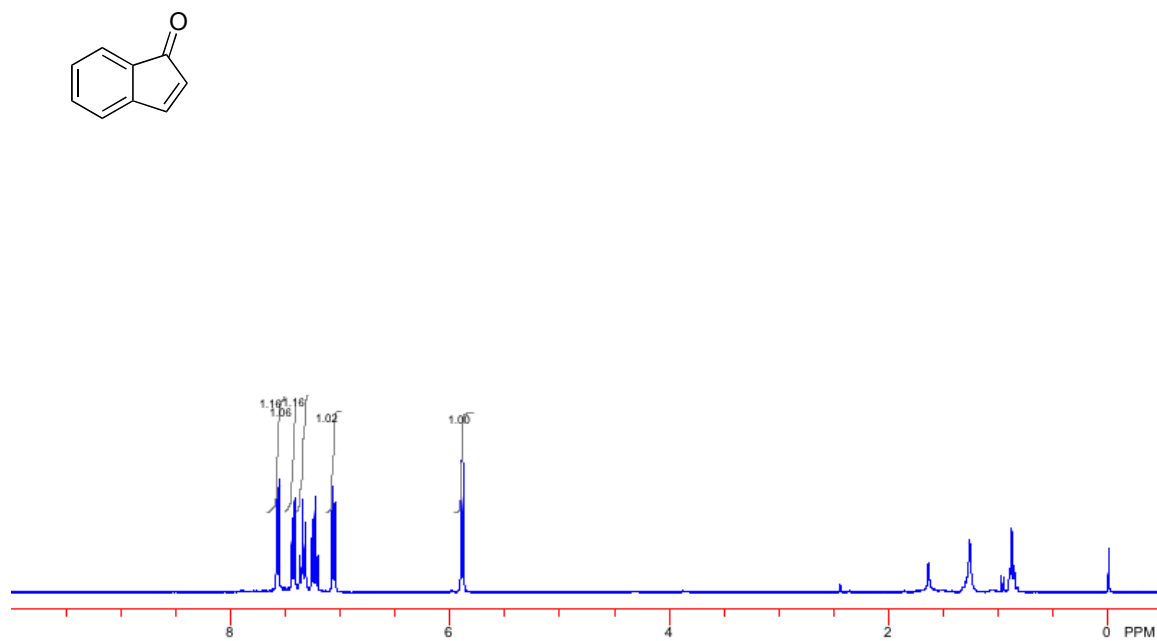
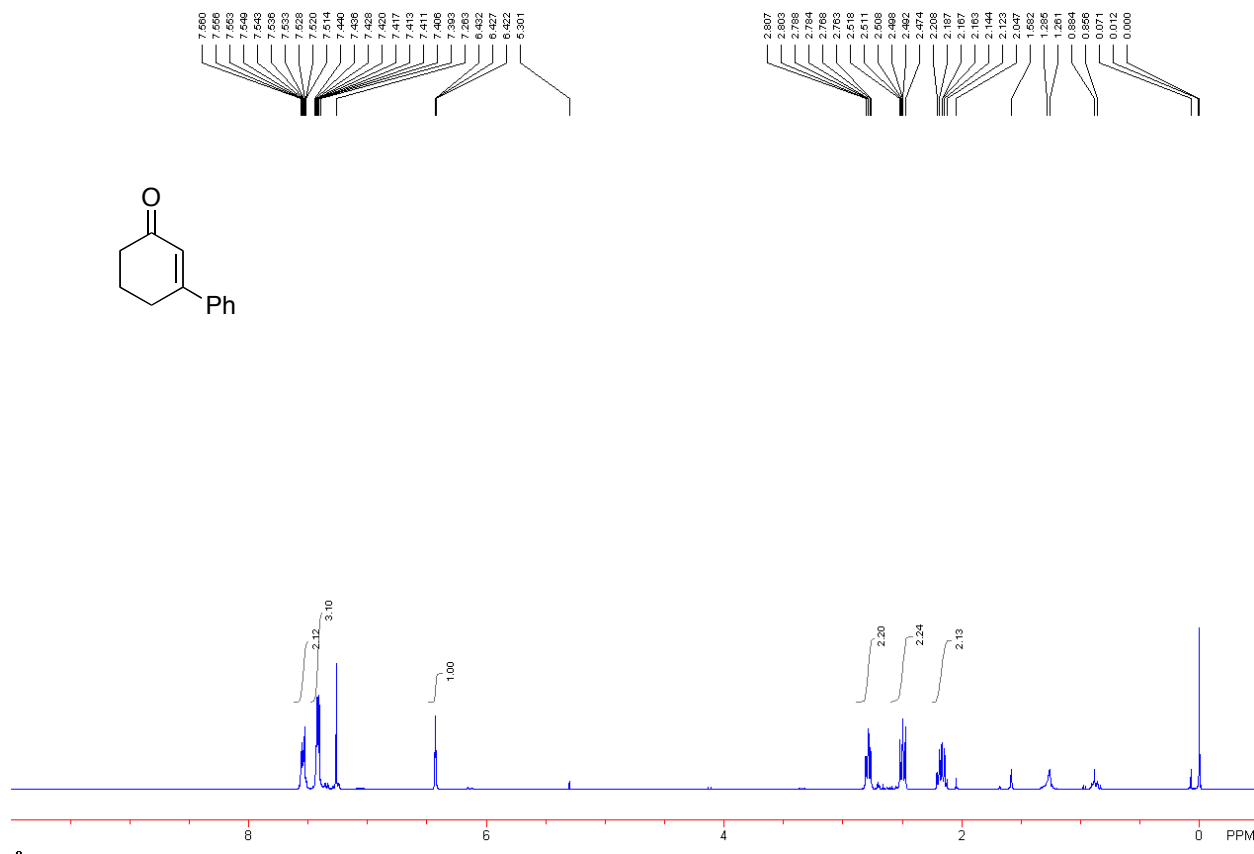


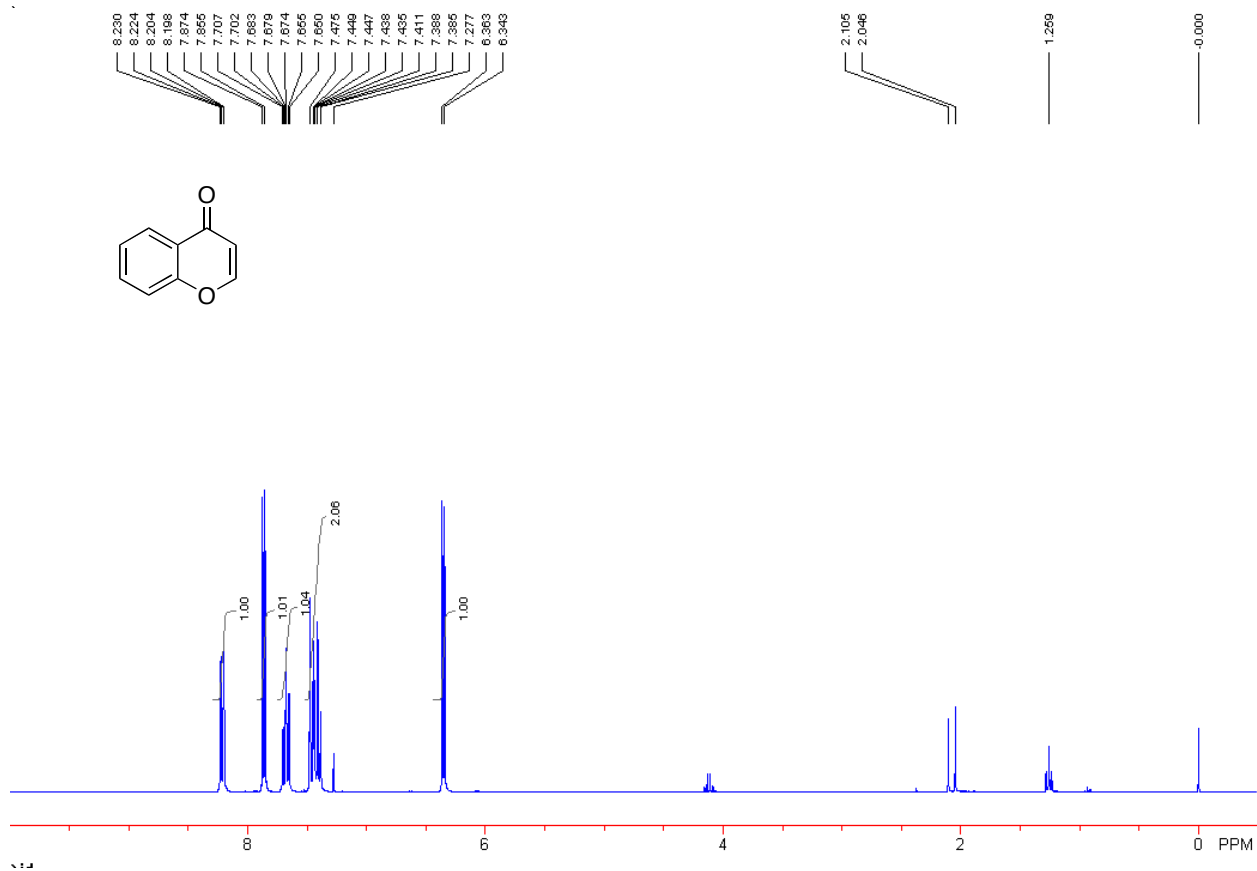
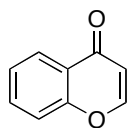
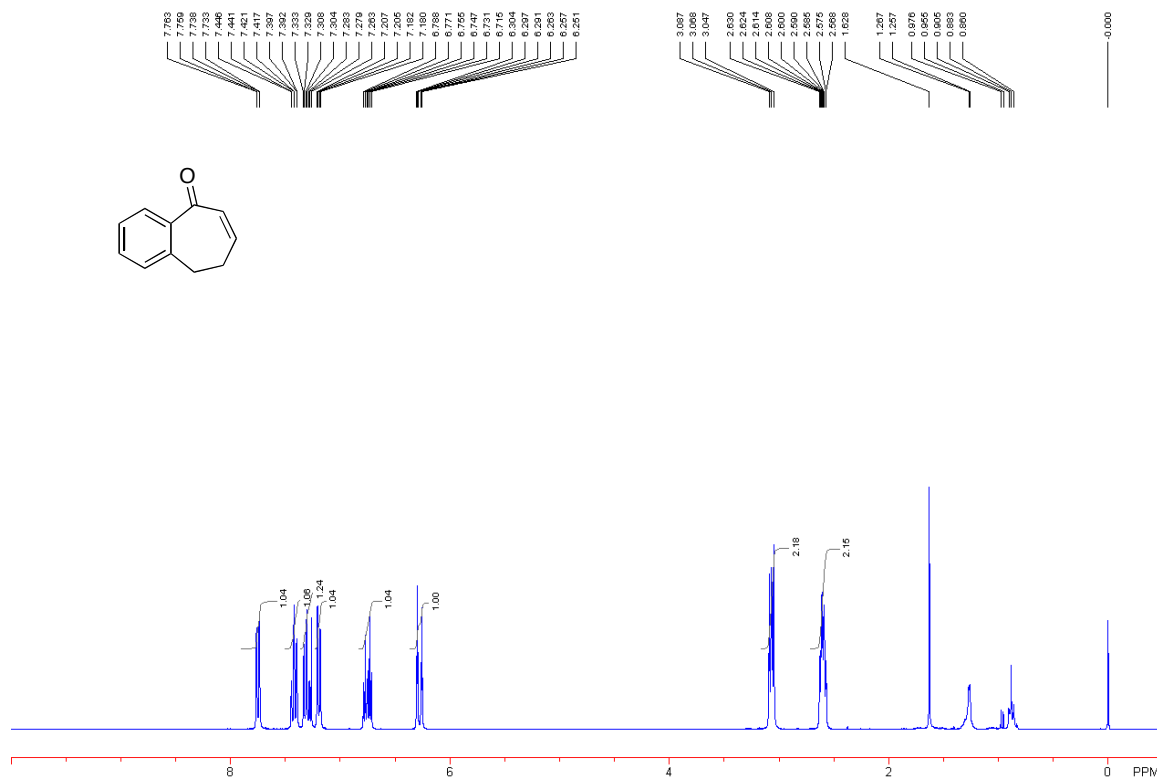
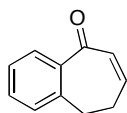


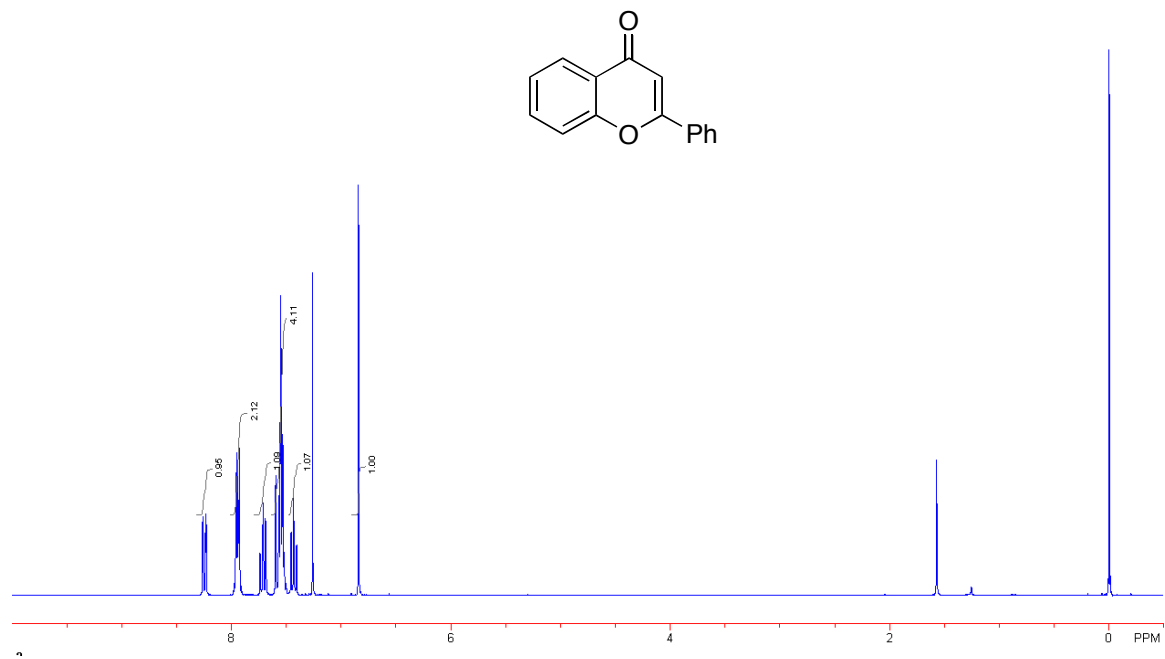
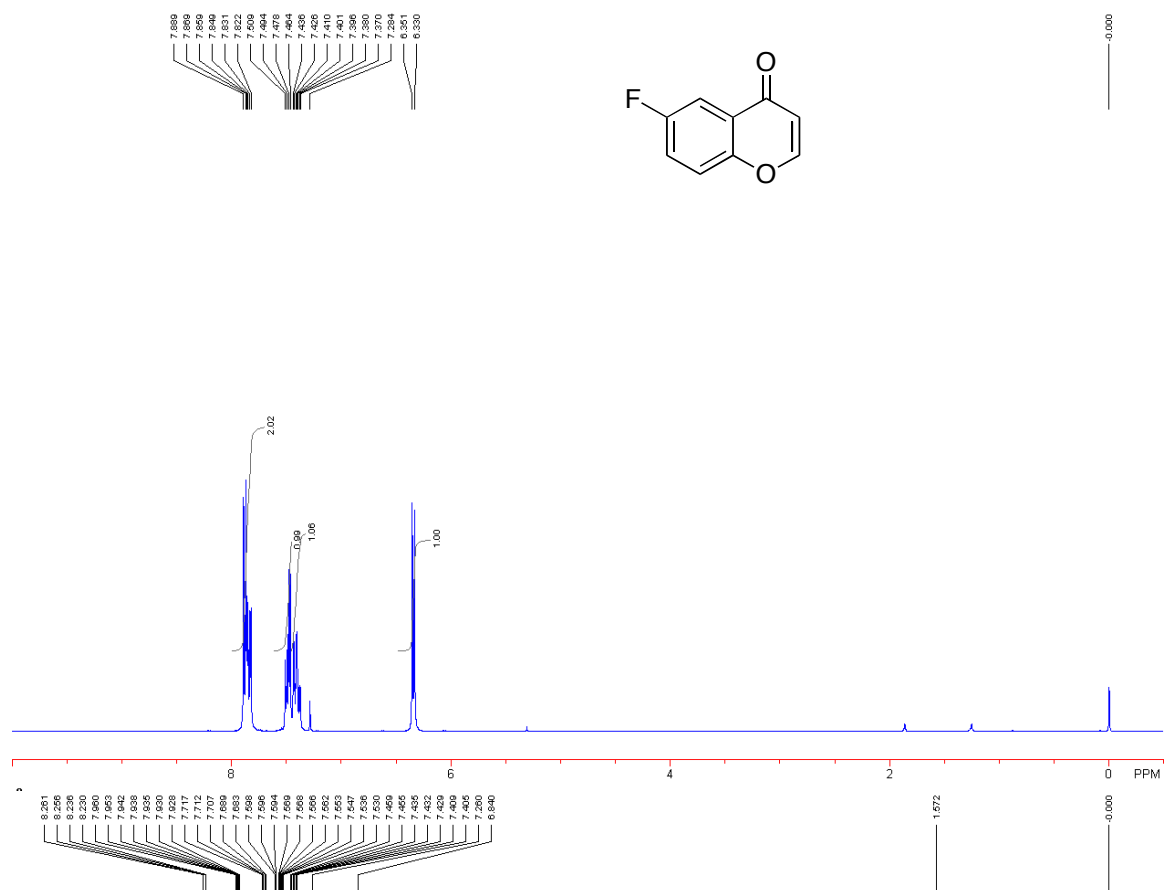


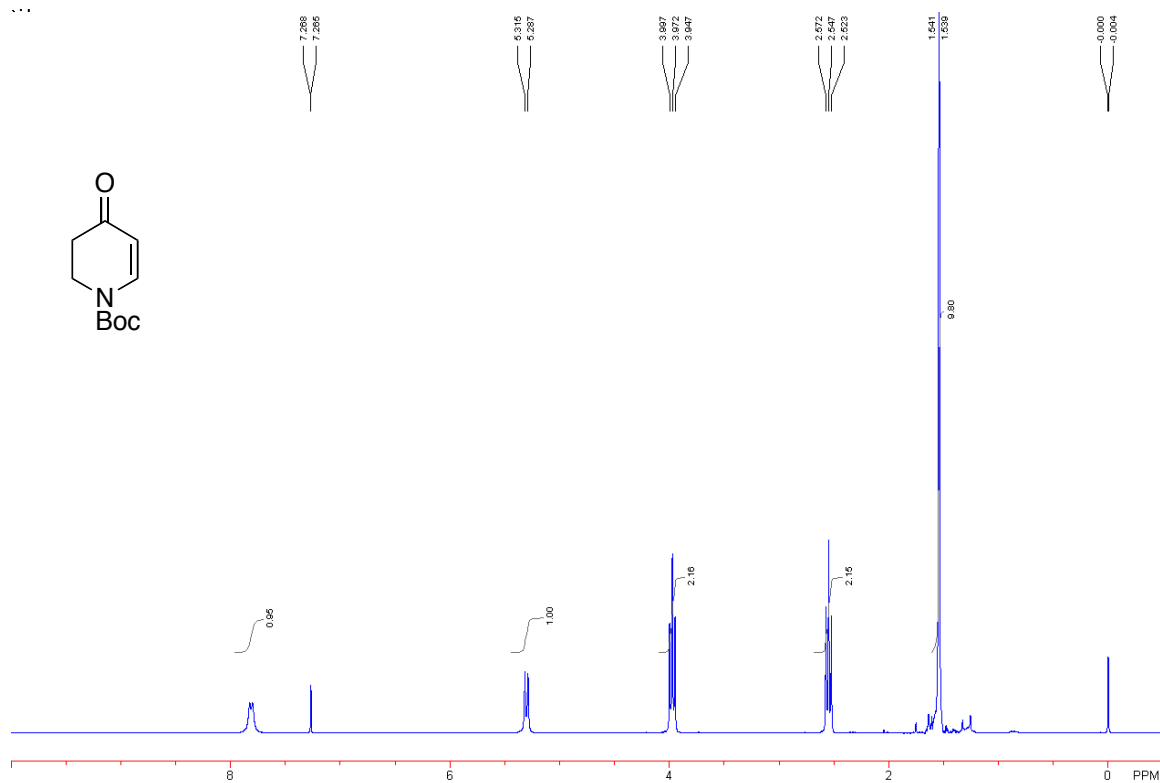
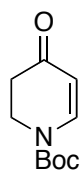
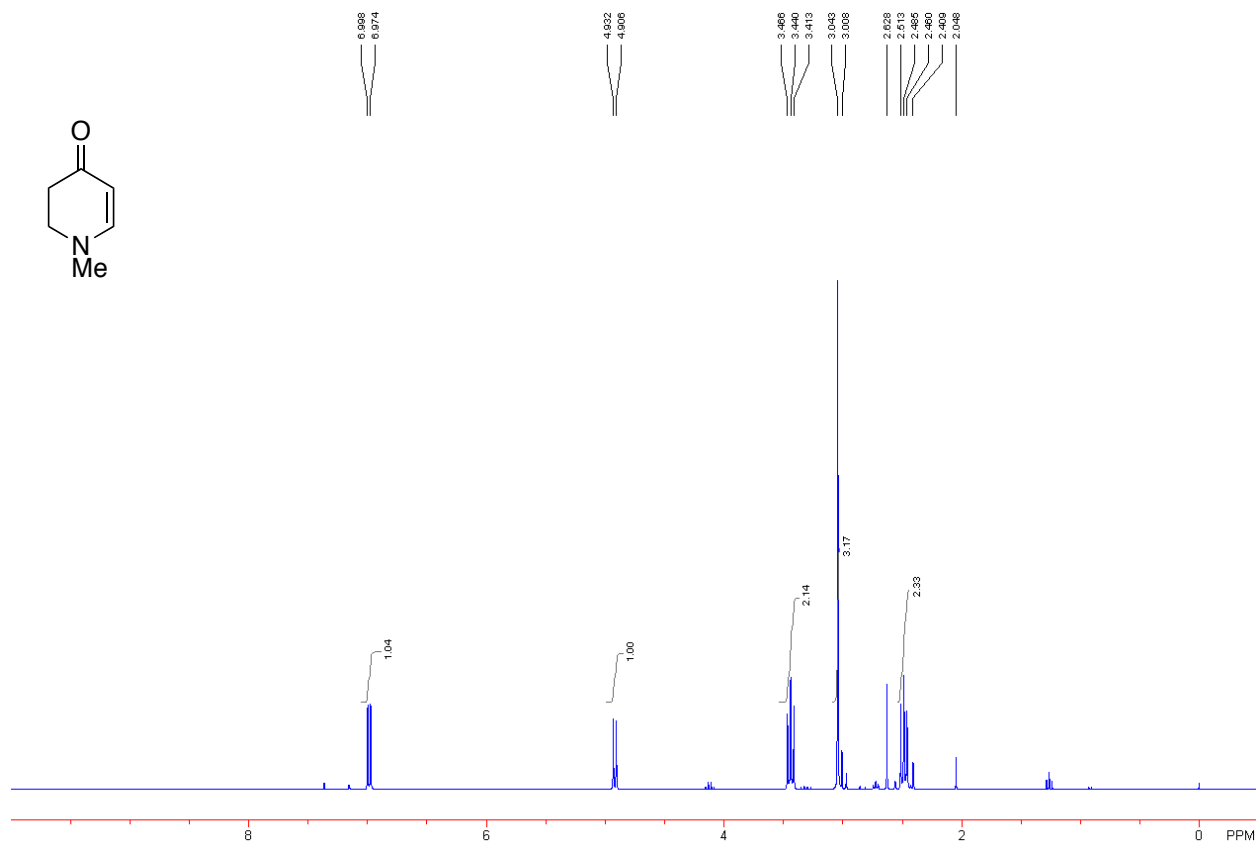
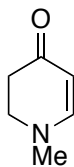


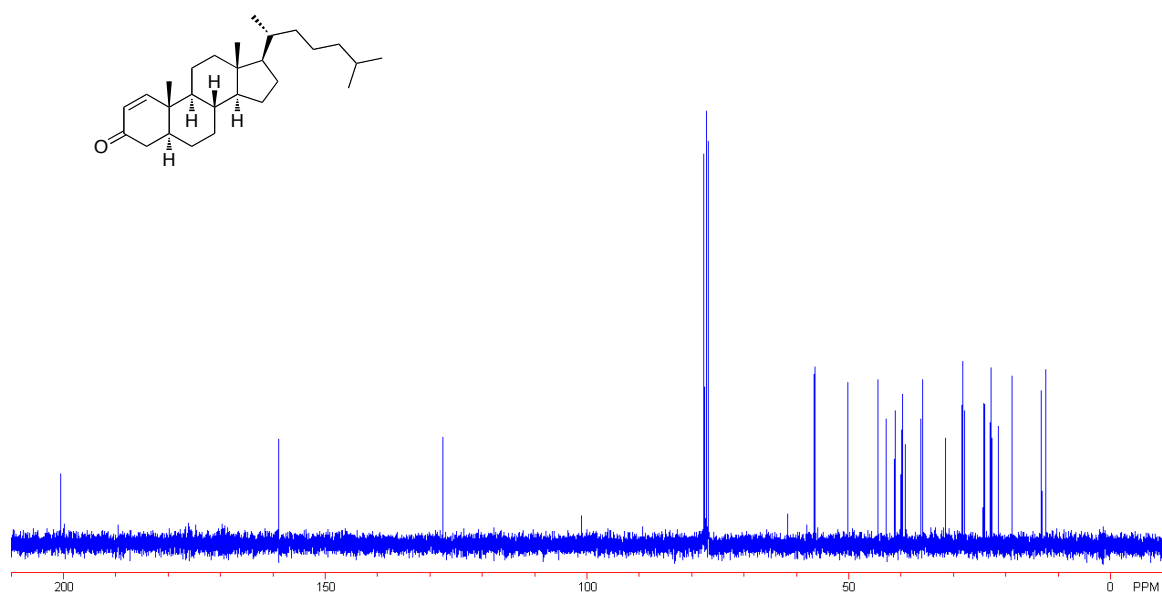
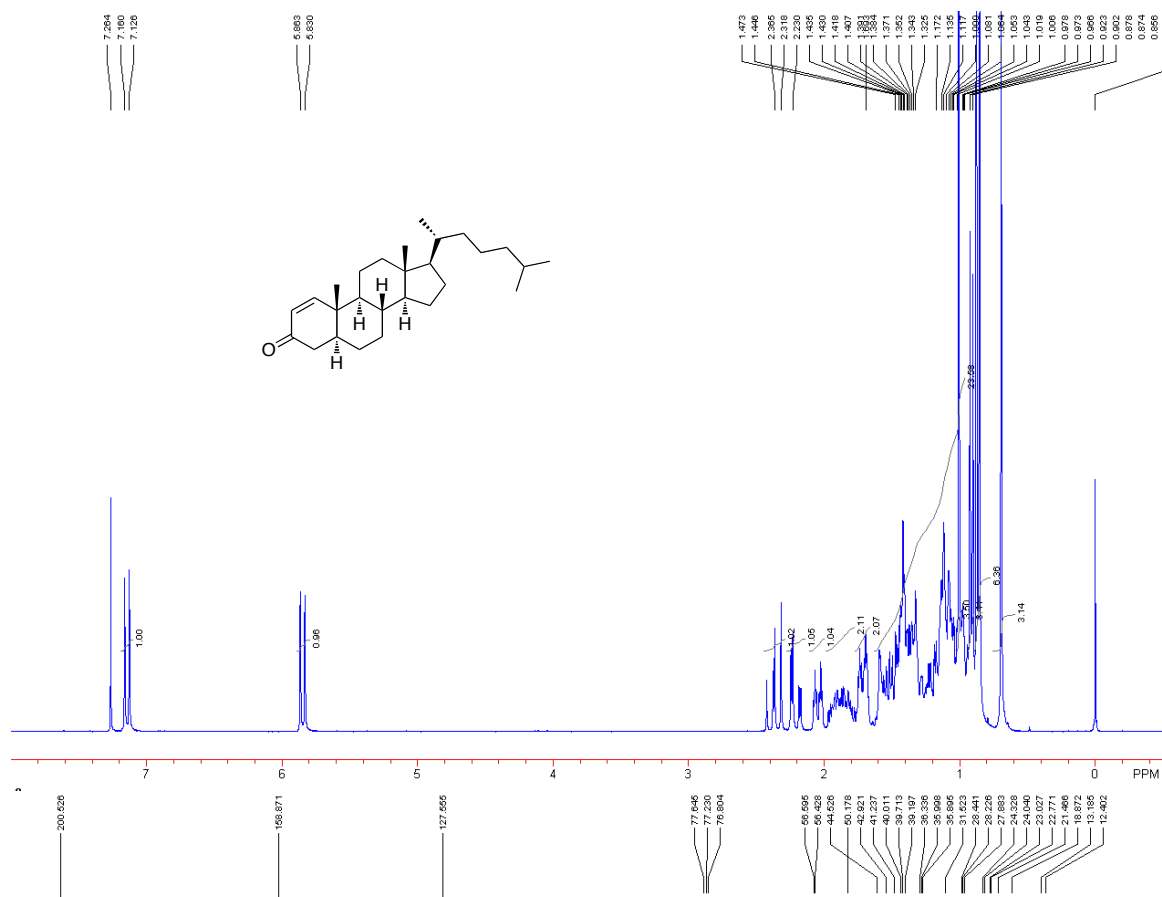


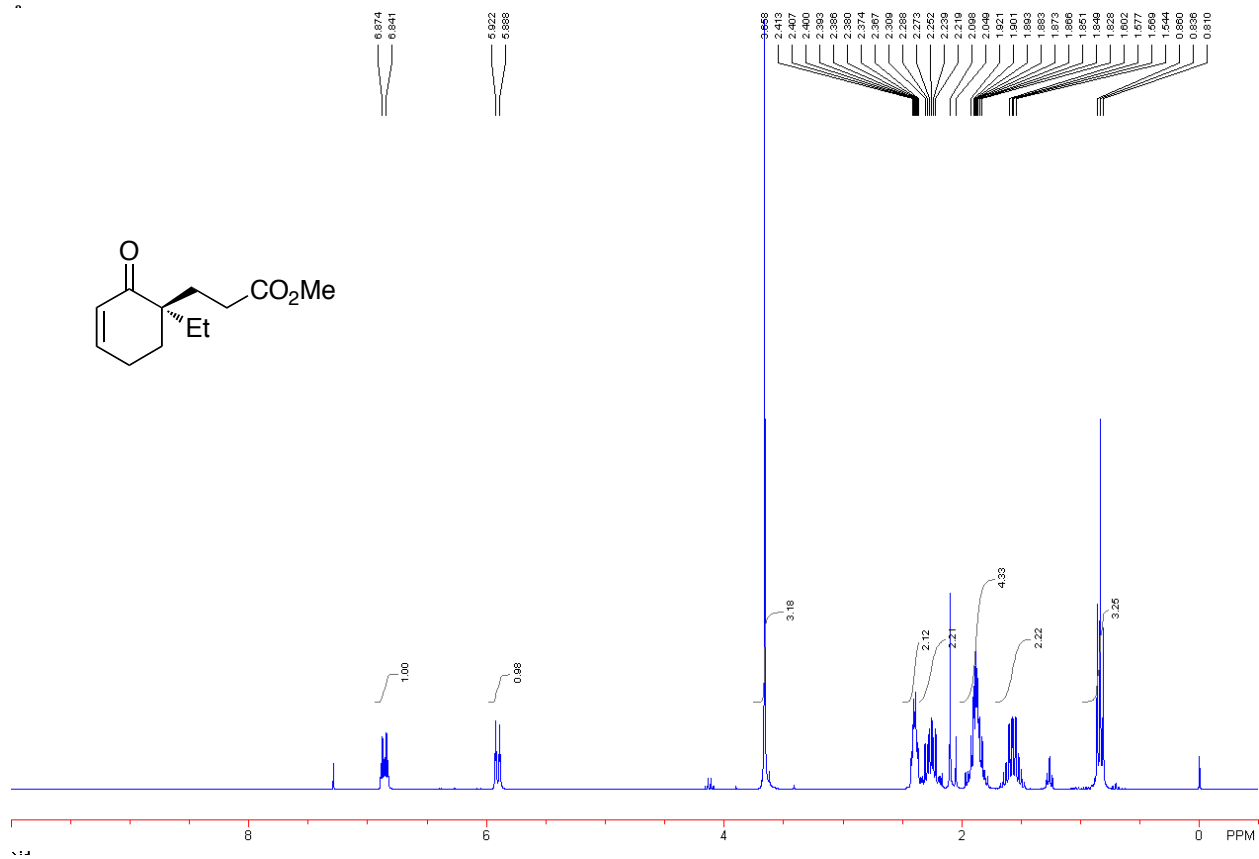
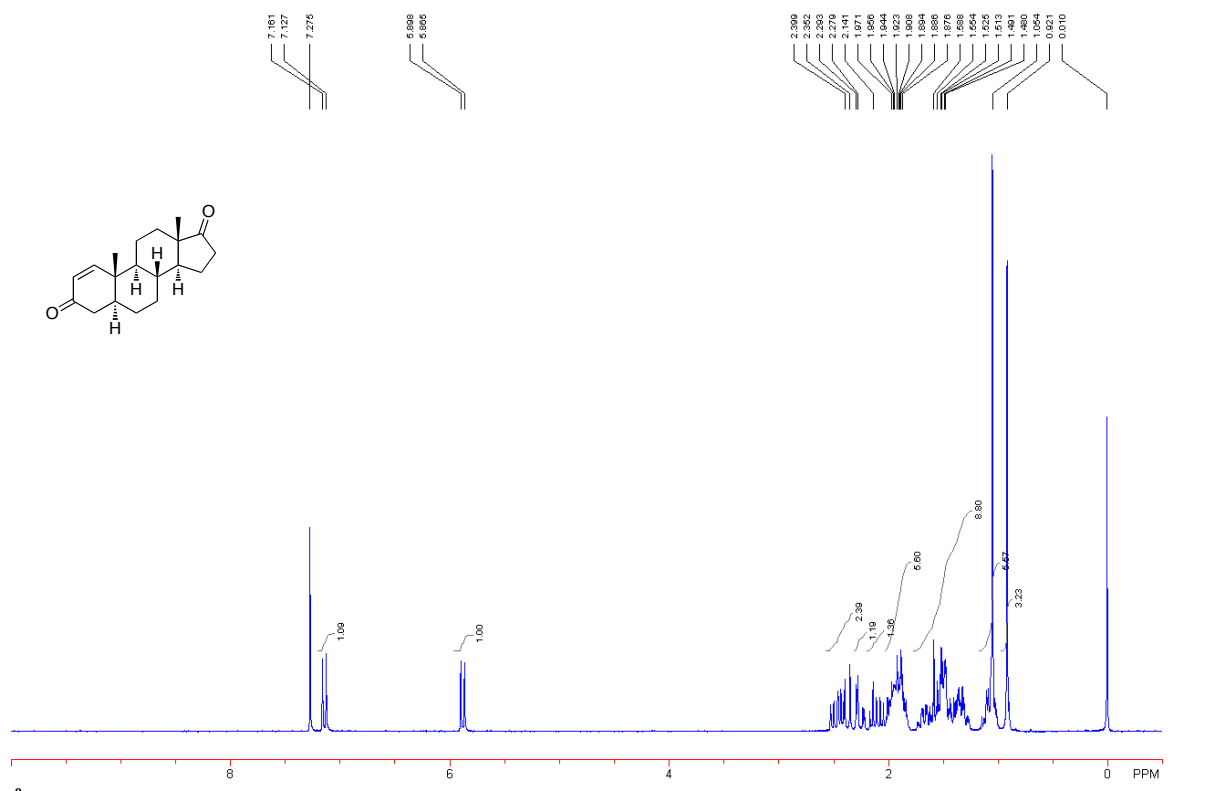


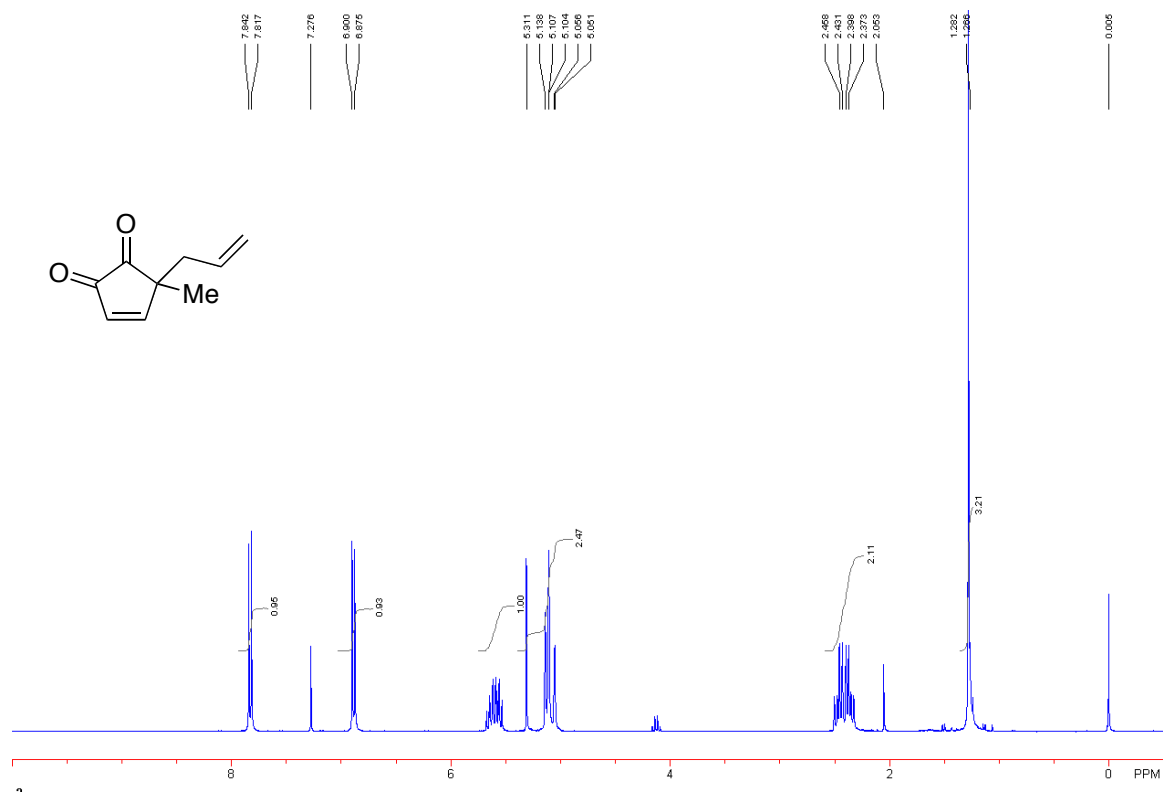




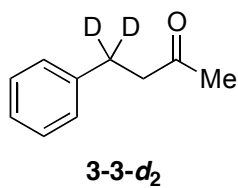
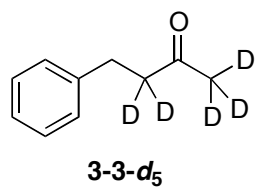
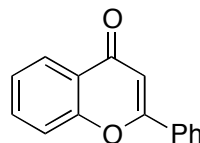
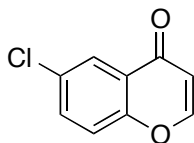
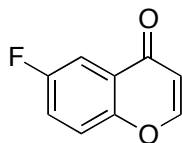
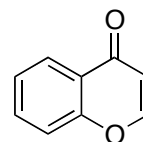
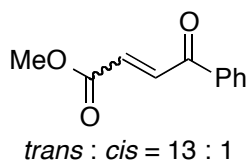
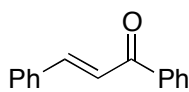
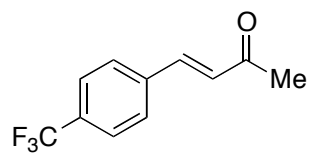
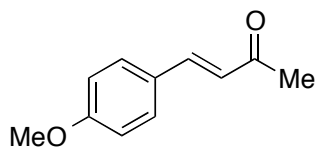
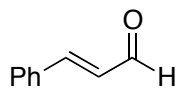
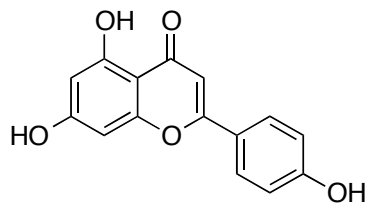
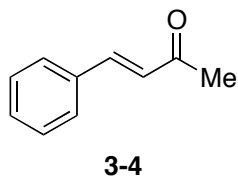
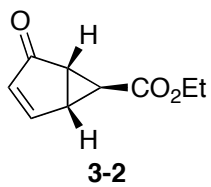


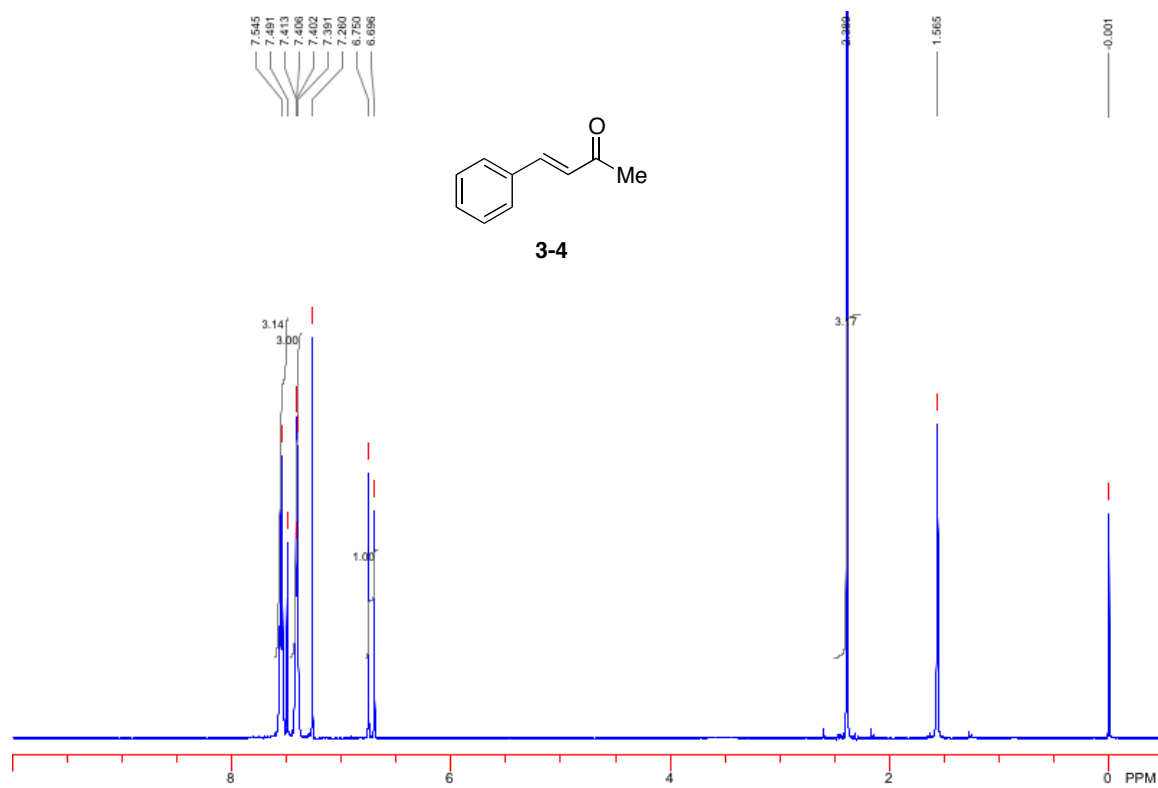
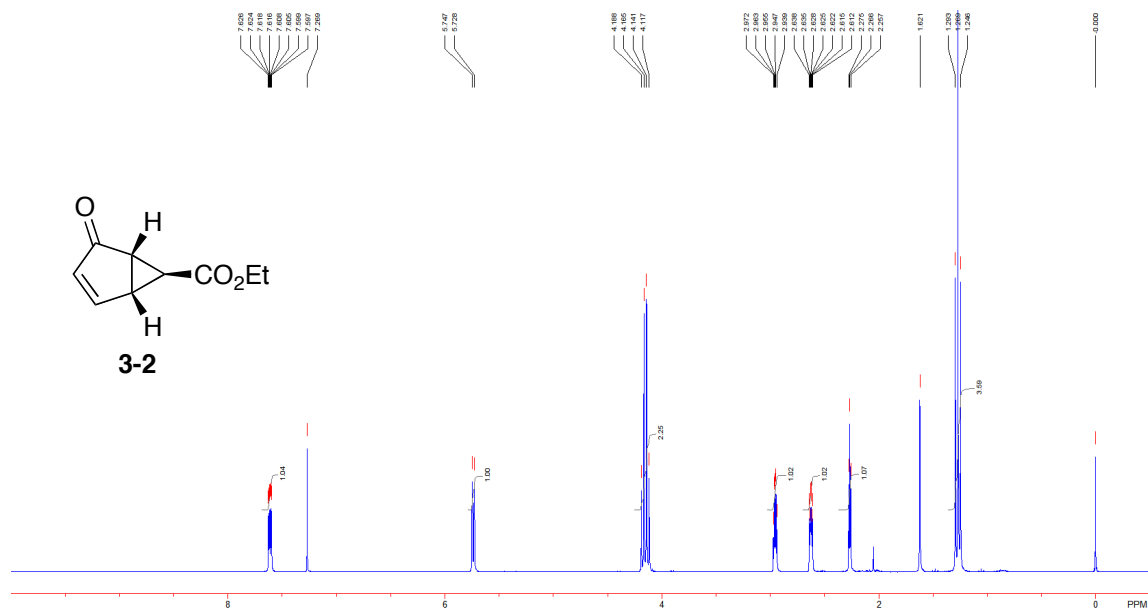


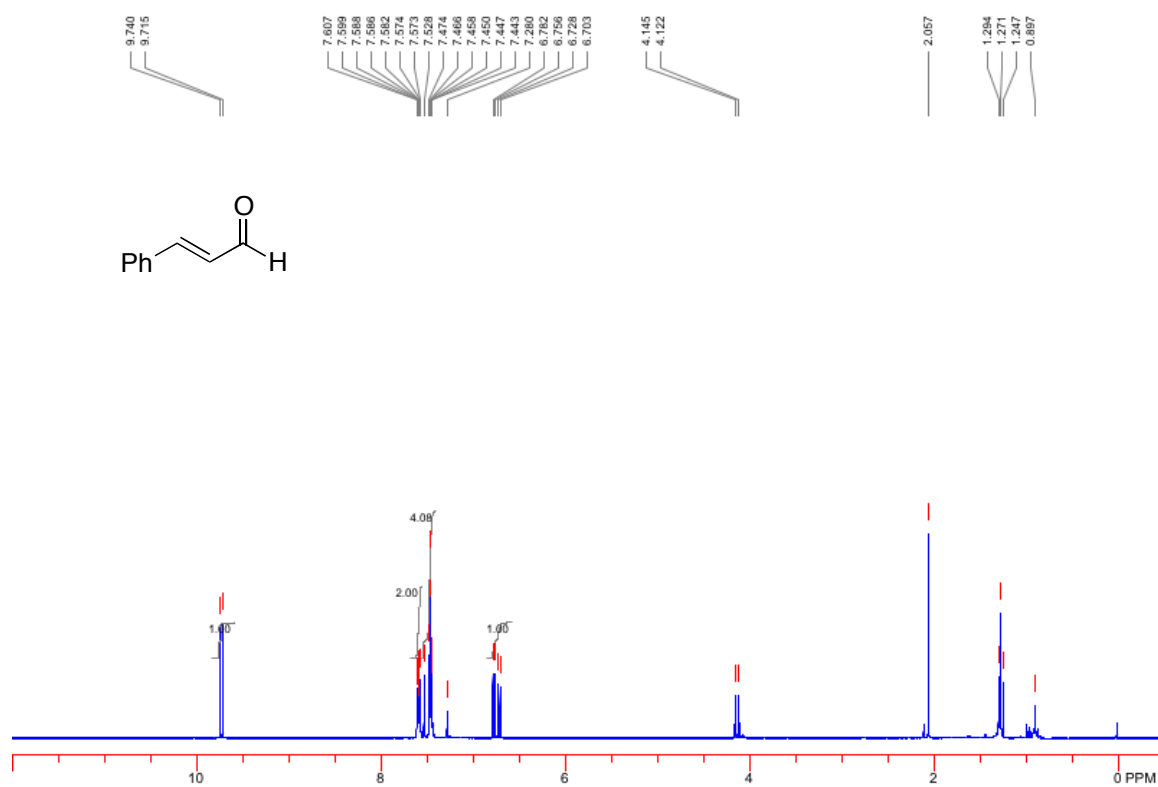
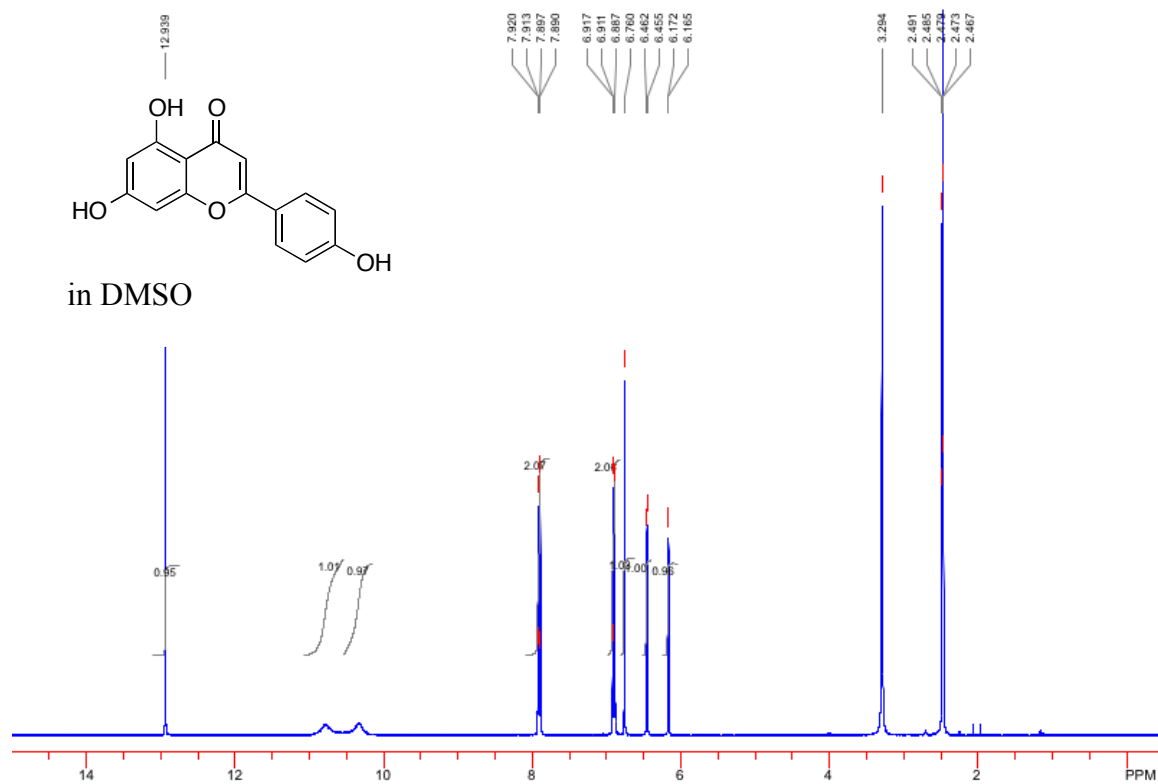


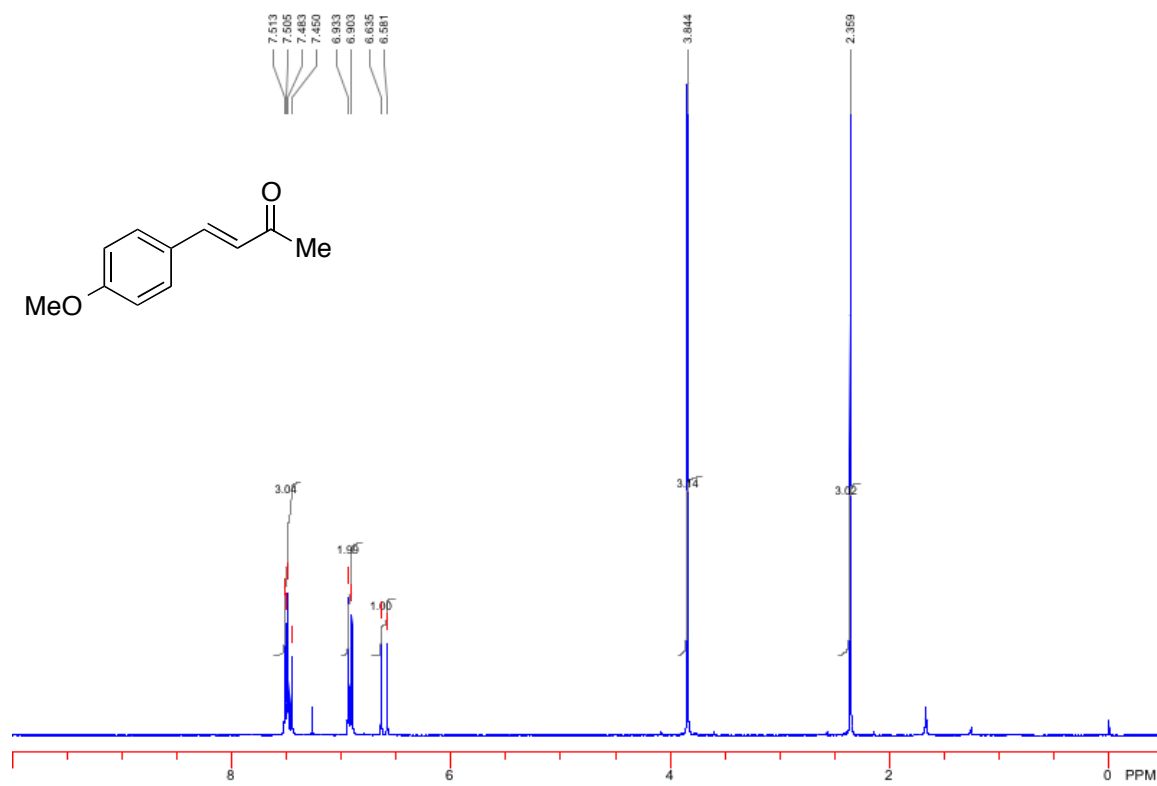
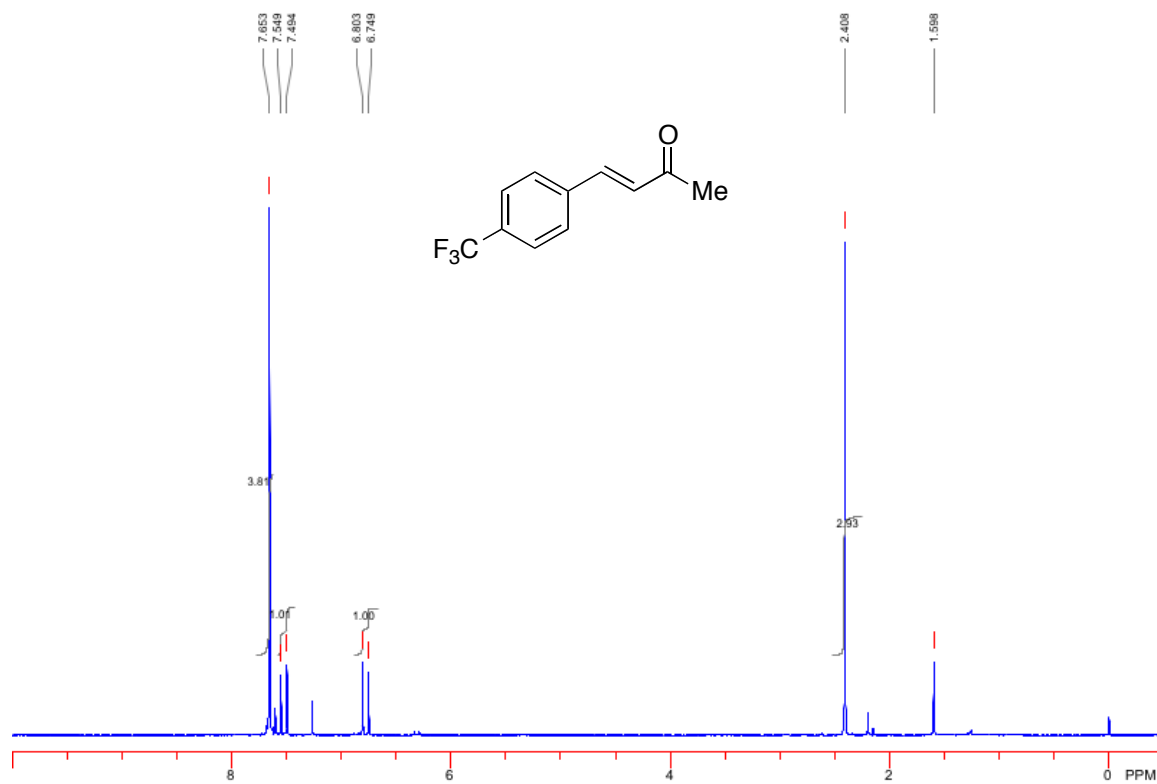


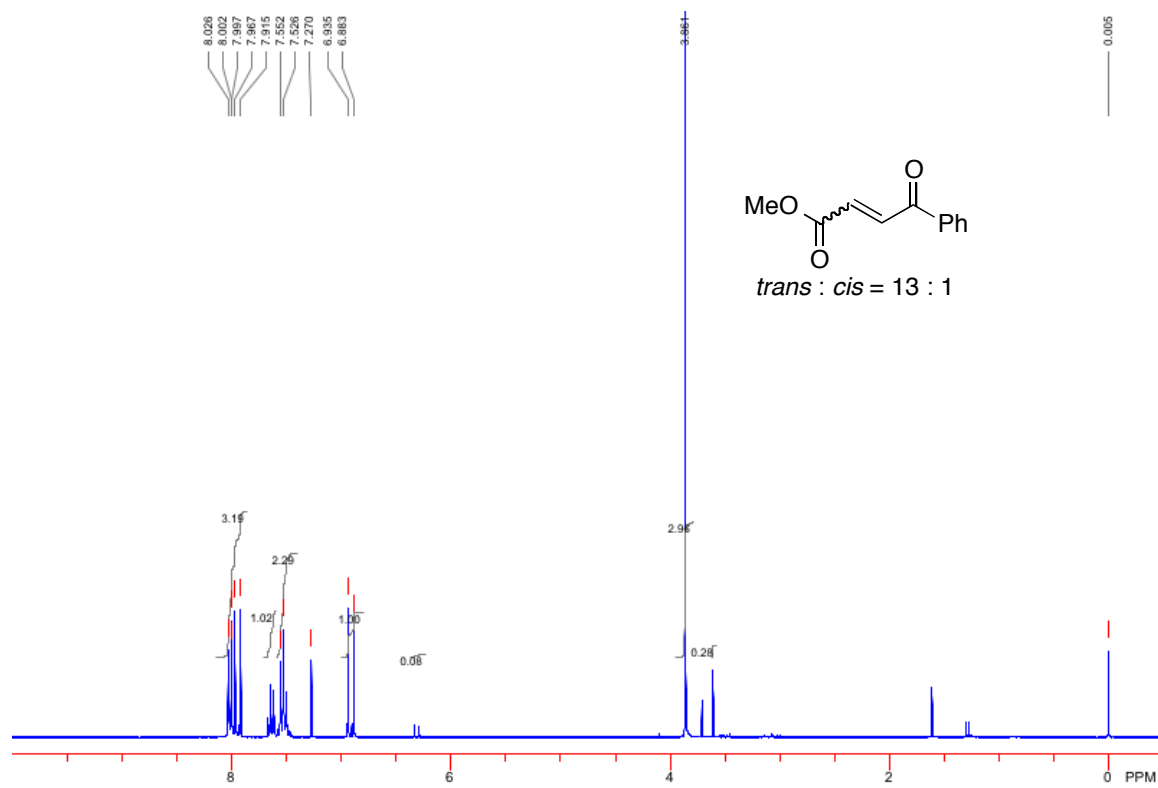
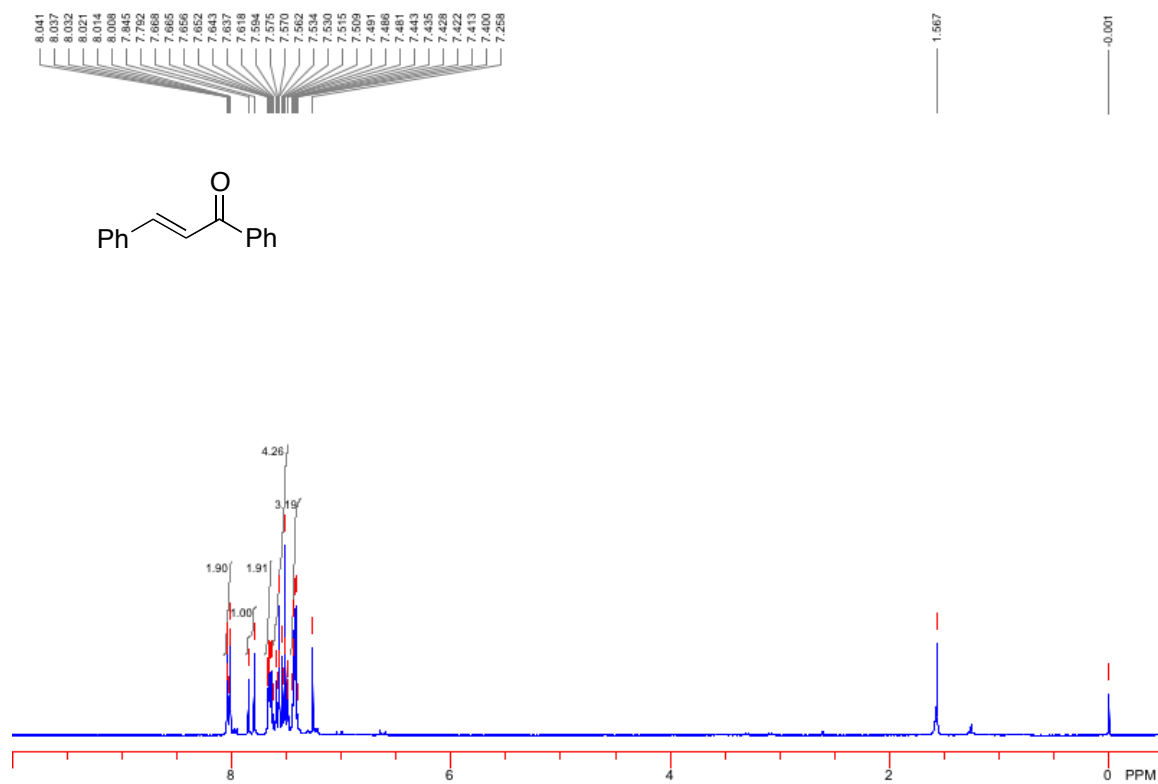
Compounds from Chapter 3

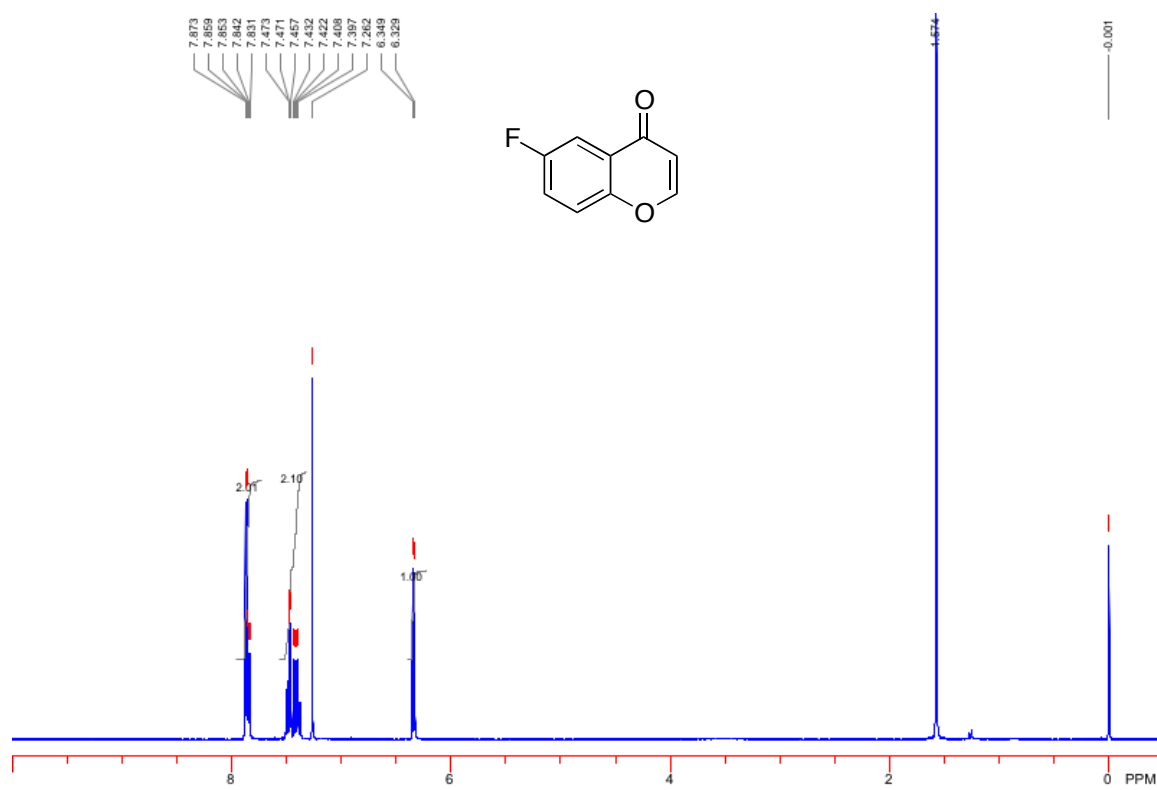
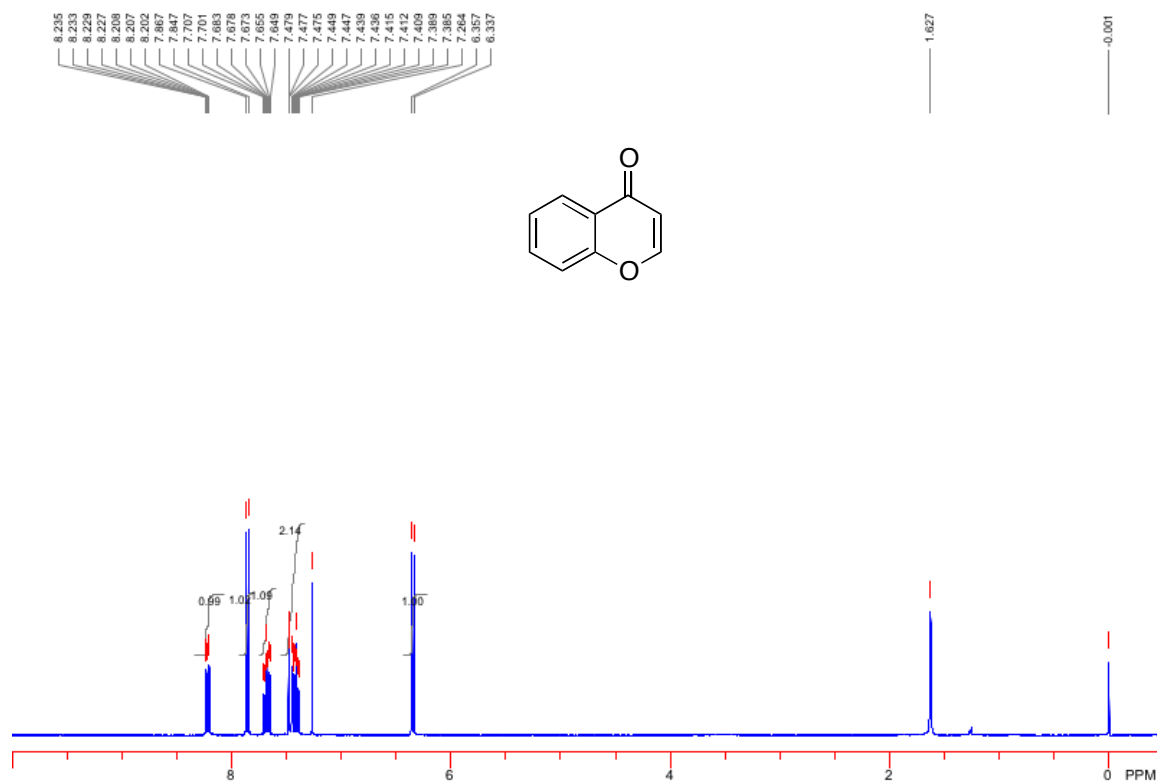


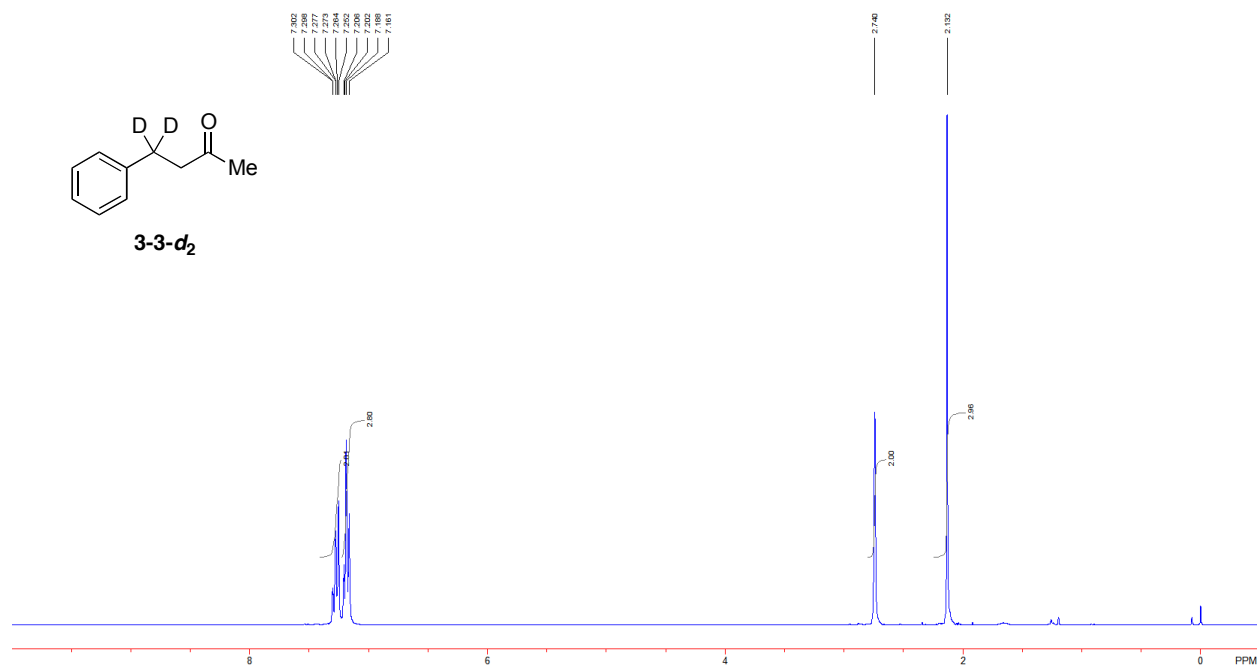
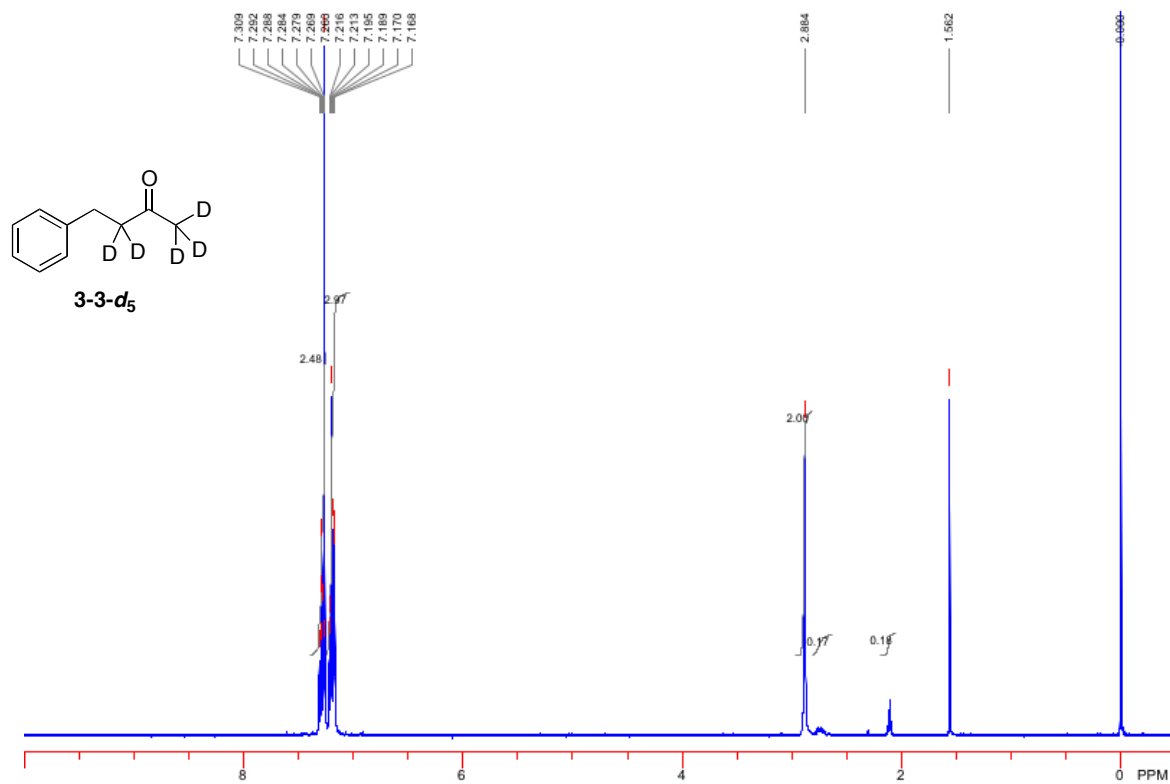


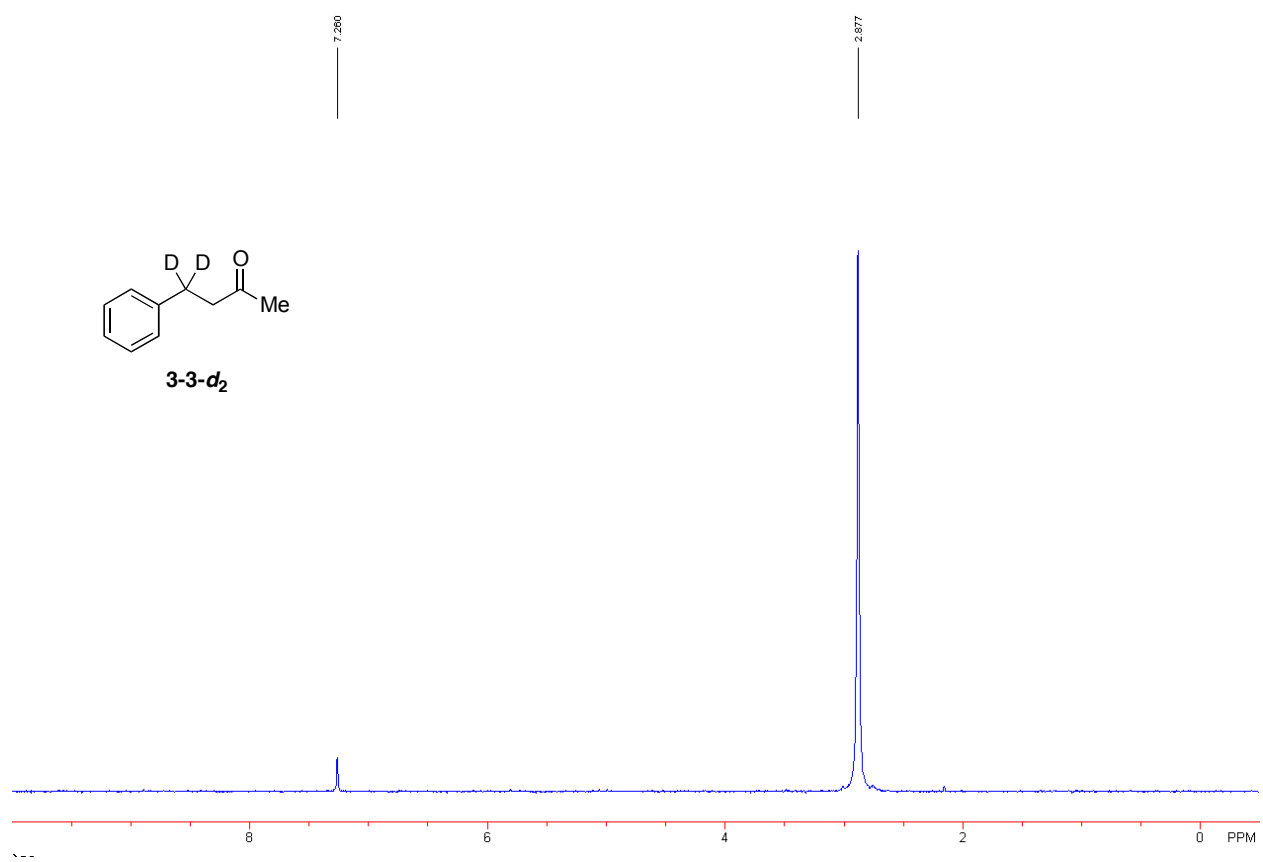
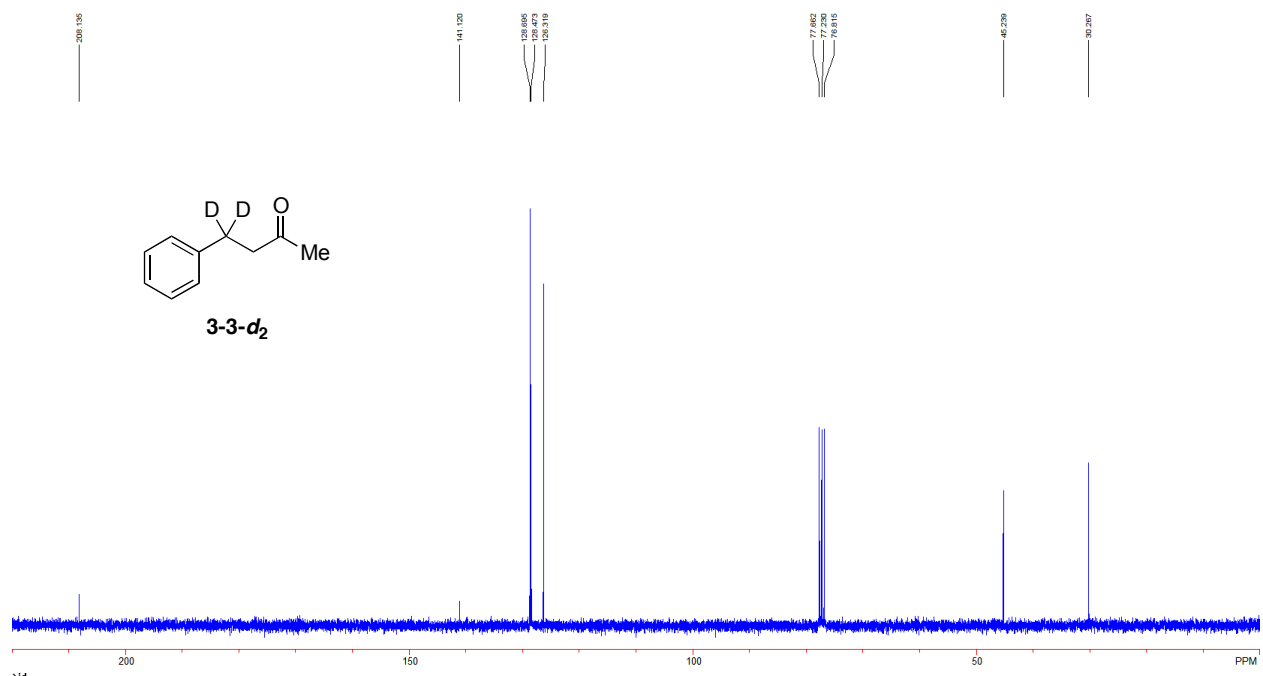


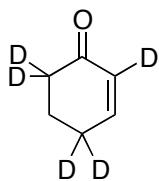
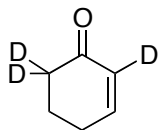


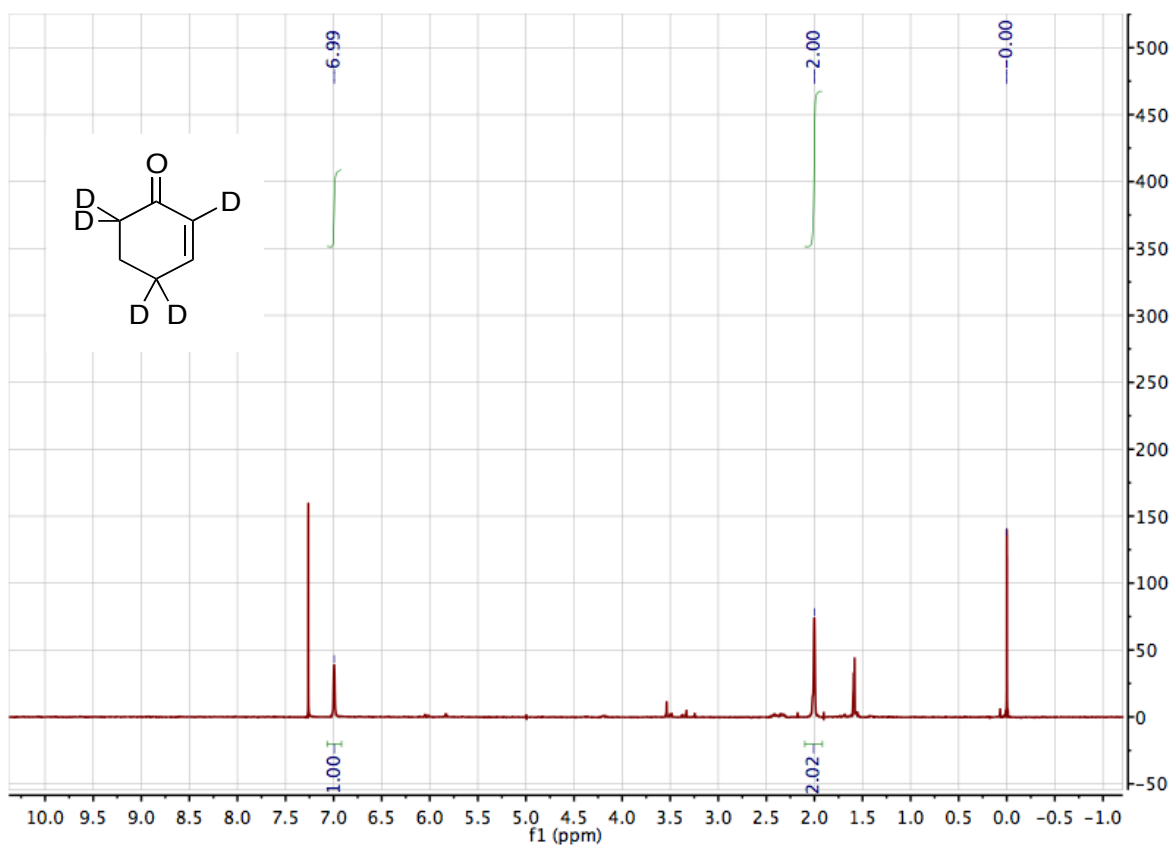
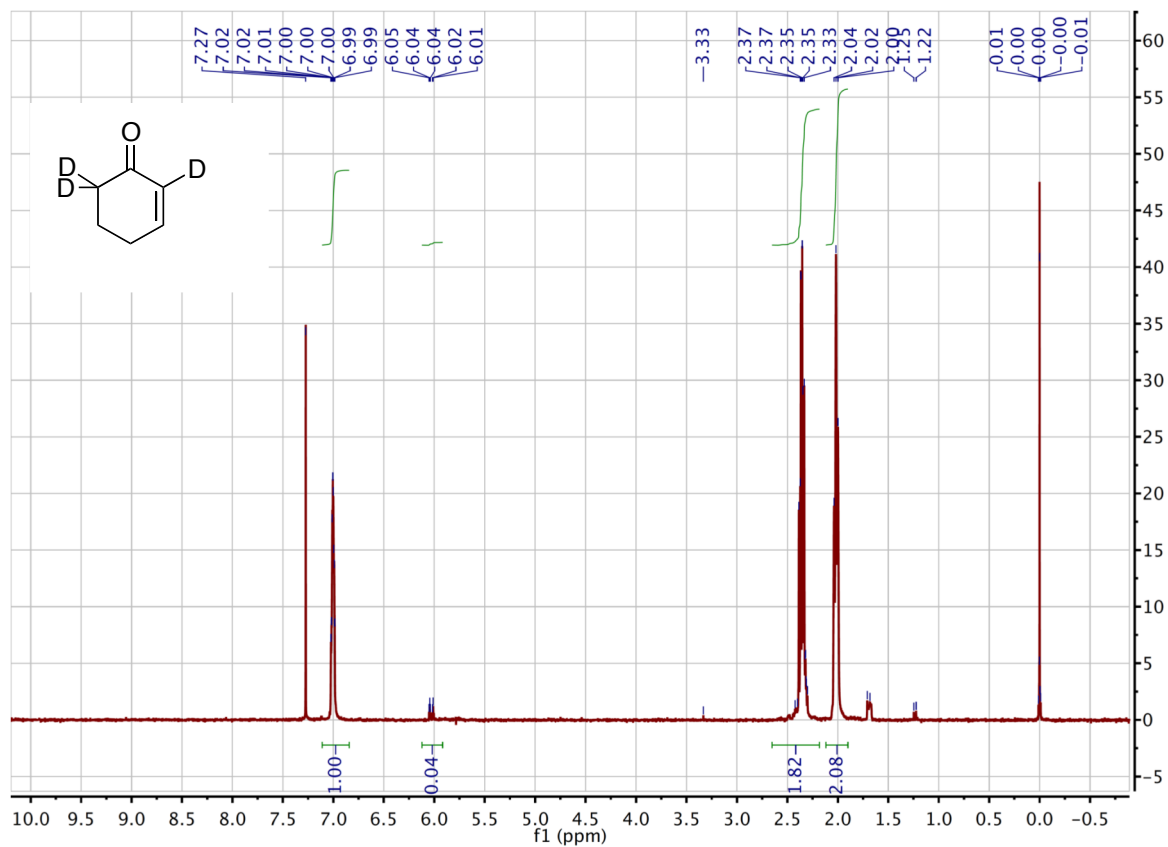








Compounds from Chapter 5 and 6



Appendix 4:

X-Ray Crystal Structure Determination

Data collection and structural solutions performed by Dr. Ilia A. Guzei and Lara C. Spencer

University of Wisconsin-Madison

Compounds Characterized by X-ray Diffraction Analysis.**Pd(DMSO)₂(TFA)₂ 4-3a****Pd(DMSO)(H₂O)(TFA)₂ 4-2a**

Pd(DMSO)₂(TFA)₂ 4-3a***Data Collection***

An orange crystal with approximate dimensions 0.38 x 0.25 x 0.14 mm³ was selected under oil under ambient conditions and attached to the tip of a MiTeGen MicroMount©. The crystal was mounted in a stream of cold nitrogen at 100(1) K and centered in the X-ray beam by using a video camera.

The crystal evaluation and data collection were performed on a Bruker SMART APEXII diffractometer with Cu K_α ($\lambda = 1.54178 \text{ \AA}$) radiation and the diffractometer to crystal distance of 4.03 cm.

The initial cell constants were obtained from three series of ω scans at different starting angles. Each series consisted of 50 frames collected at intervals of 0.5° in a 25° range about ω with the exposure time of 5 seconds per frame. The reflections were successfully indexed by an automated indexing routine built in the APEXII program. The final cell constants were calculated from a set of 9217 strong reflections from the actual data collection.

The data were collected by using the full sphere data collection routine to survey the reciprocal space to the extent of a full sphere to a resolution of 0.82 Å. A total of 23704 data were harvested by collecting 17 sets of frames with 0.6° scans in ω and ϕ with an exposure time 6/12 sec per frame. These highly redundant datasets were corrected for Lorentz and polarization effects. The absorption correction was based on fitting a function to the empirical transmission surface as sampled by multiple equivalent measurements. [1]

Structure Solution and Refinement

The systematic absences in the diffraction data were uniquely consistent for the space group $P2_1/n$ that yielded chemically reasonable and computationally stable results of refinement [2-3].

A successful solution by the direct methods provided most non-hydrogen atoms from the E -map. The remaining non-hydrogen atoms were located in an alternating series of least-squares cycles and difference Fourier maps. All non-hydrogen atoms were refined with anisotropic displacement coefficients. All hydrogen atoms were included in the structure factor calculation at idealized positions and were allowed to ride on the neighboring atoms with relative isotropic displacement coefficients.

The final least-squares refinement of 212 parameters against 3154 data resulted in residuals R (based on F^2 for $I \geq 2\sigma$) and wR (based on F^2 for all data) of 0.0218 and 0.0600, respectively.

The molecular diagram is drawn with 50% probability ellipsoids.

References

- [1] Bruker-AXS. (2007-2011) APEX2, SADABS, and SAINT Software Reference Manuals. Bruker-AXS, Madison, Wisconsin, USA.
- [2] Sheldrick, G. M. (2008) SHELXL. *Acta Cryst.* **A64**, 112-122.

- [3] Guzei, I.A. (2006-2011). Internal laboratory computer programs "G1", "ResIns", "FCF_filter", "Modicifer".
- [4] Pennington, W.T. (1999) *Diamond. J. Appl. Cryst.* **32**(5), 1028-1029.

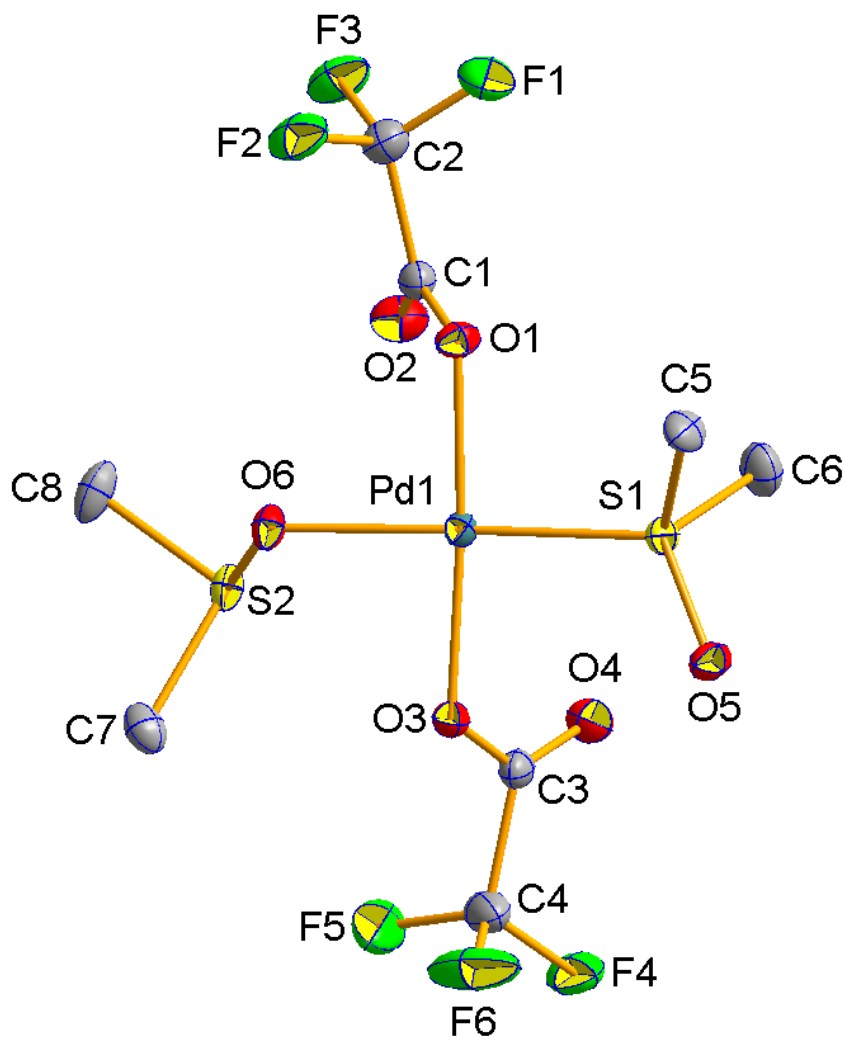


Figure A-4.1. A molecular drawing of Pd(DMSO)₂(TFA)₂ **4-3a**. All hydrogen atoms attached to carbon atoms were omitted for clarity.

Table A-4.1. Crystal data and structure refinement for Pd(DMSO)₂(TFA)₂ **4-3a**.

Identification code	stahl137	
Empirical formula	C ₈ H ₁₂ F ₆ O ₆ PdS ₂	
Formula weight	488.70	
Temperature	100(1) K	
Wavelength	1.54178 Å	
Crystal system	Monoclinic	
Space group	P2 ₁ /n	
Unit cell dimensions	a = 12.4209(7) Å	α = 90°.
	b = 7.6174(6) Å	β = 99.822(5)°.
	c = 17.6595(12) Å	γ = 90°.
Volume	1646.36(19) Å ³	
Z	4	
Density (calculated)	1.972 Mg/m ³	
Absorption coefficient	12.313 mm ⁻¹	
F(000)	960	
Crystal size	0.38 x 0.25 x 0.14 mm ³	
Theta range for data collection	4.05 to 71.75°.	
Index ranges	-15 ≤ h ≤ 15, -9 ≤ k ≤ 9, -21 ≤ l ≤ 21	
Reflections collected	23704	
Independent reflections	3154 [R(int) = 0.0200]	
Completeness to theta = 67.00°	99.8 %	
Absorption correction	Analytical with SADABS	
Max. and min. transmission	0.2794 and 0.0892	
Refinement method	Full-matrix least-squares on F ²	
Data / restraints / parameters	3154 / 0 / 212	
Goodness-of-fit on F ²	1.015	
Final R indices [I > 2σ(I)]	R1 = 0.0218, wR2 = 0.0599	
R indices (all data)	R1 = 0.0219, wR2 = 0.0600	
Largest diff. peak and hole	0.902 and -0.612 e.Å ⁻³	

Table A-4.2. Atomic coordinates ($\times 10^4$) and equivalent isotropic displacement parameters ($\text{\AA}^2 \times 10^3$) for $\text{Pd}(\text{DMSO})_2(\text{TFA})_2$ **4-3a**. $U(\text{eq})$ is defined as one third of the trace of the orthogonalized U^{ij} tensor.

	x	y	z	U(eq)
Pd(1)	8706(1)	4095(1)	1733(1)	14(1)
S(1)	8468(1)	1775(1)	2428(1)	16(1)
S(2)	8842(1)	6139(1)	276(1)	18(1)
F(1)	12224(1)	4885(2)	3278(1)	38(1)
F(2)	11566(1)	7378(2)	2856(1)	38(1)
F(3)	12741(1)	6065(2)	2296(1)	38(1)
F(4)	5968(1)	608(2)	-290(1)	37(1)
F(5)	6323(2)	3220(3)	-612(1)	67(1)
F(6)	5337(1)	2764(3)	254(1)	63(1)
O(1)	10107(1)	4703(2)	2441(1)	19(1)
O(2)	11046(2)	4486(3)	1460(1)	28(1)
O(3)	7302(1)	3653(2)	998(1)	18(1)
O(4)	7914(2)	1083(2)	604(1)	25(1)
O(5)	7370(1)	1014(2)	2275(1)	23(1)
O(6)	8825(1)	6396(2)	1145(1)	18(1)
C(1)	10939(2)	4888(3)	2109(1)	19(1)
C(2)	11884(2)	5805(3)	2645(2)	25(1)
C(3)	7254(2)	2254(3)	596(1)	19(1)
C(4)	6195(2)	2199(4)	-12(2)	31(1)
C(5)	8788(2)	2401(3)	3408(1)	23(1)
C(6)	9439(2)	98(3)	2361(2)	28(1)
C(7)	7581(2)	7043(3)	-200(1)	25(1)
C(8)	9738(2)	7848(3)	92(2)	30(1)

Table A-4.3. Bond lengths [Å] and angles [°] for Pd(DMSO)₂(TFA)₂ **4-3a**.

Pd(1)-O(1)	2.0158(15)	O(2)-C(1)	1.215(3)
Pd(1)-O(3)	2.0170(16)	O(3)-C(3)	1.276(3)
Pd(1)-O(6)	2.0554(16)	O(4)-C(3)	1.210(3)
Pd(1)-S(1)	2.1994(5)	C(1)-C(2)	1.543(3)
S(1)-O(5)	1.4633(17)	C(3)-C(4)	1.550(3)
S(1)-C(5)	1.774(2)	C(5)-H(5A)	0.9800
S(1)-C(6)	1.776(3)	C(5)-H(5B)	0.9800
S(2)-O(6)	1.5509(16)	C(5)-H(5C)	0.9800
S(2)-C(8)	1.778(2)	C(6)-H(6A)	0.9800
S(2)-C(7)	1.784(3)	C(6)-H(6B)	0.9800
F(1)-C(2)	1.327(3)	C(6)-H(6C)	0.9800
F(2)-C(2)	1.335(3)	C(7)-H(7A)	0.9800
F(3)-C(2)	1.333(3)	C(7)-H(7B)	0.9800
F(4)-C(4)	1.319(3)	C(7)-H(7C)	0.9800
F(5)-C(4)	1.345(4)	C(8)-H(8A)	0.9800
F(6)-C(4)	1.309(4)	C(8)-H(8B)	0.9800
O(1)-C(1)	1.281(3)	C(8)-H(8C)	0.9800
O(1)-Pd(1)-O(3)	176.15(6)	F(4)-C(4)-F(6)	107.5(2)
O(1)-Pd(1)-O(6)	89.30(7)	F(4)-C(4)-F(5)	106.5(2)
O(3)-Pd(1)-O(6)	86.93(7)	F(6)-C(4)-F(5)	107.7(3)
O(1)-Pd(1)-S(1)	91.30(5)	F(4)-C(4)-C(3)	112.6(2)
O(3)-Pd(1)-S(1)	92.36(5)	F(6)-C(4)-C(3)	112.9(2)
O(6)-Pd(1)-S(1)	174.19(5)	F(5)-C(4)-C(3)	109.3(2)
O(5)-S(1)-C(5)	109.46(11)	S(1)-C(5)-H(5A)	109.5
O(5)-S(1)-C(6)	108.94(12)	S(1)-C(5)-H(5B)	109.5
C(5)-S(1)-C(6)	102.49(13)	H(5A)-C(5)-H(5B)	109.5
O(5)-S(1)-Pd(1)	115.18(7)	S(1)-C(5)-H(5C)	109.5
C(5)-S(1)-Pd(1)	107.42(8)	H(5A)-C(5)-H(5C)	109.5
C(6)-S(1)-Pd(1)	112.55(9)	H(5B)-C(5)-H(5C)	109.5
O(6)-S(2)-C(8)	101.70(11)	S(1)-C(6)-H(6A)	109.5
O(6)-S(2)-C(7)	105.01(11)	S(1)-C(6)-H(6B)	109.5
C(8)-S(2)-C(7)	99.08(13)	H(6A)-C(6)-H(6B)	109.5
C(1)-O(1)-Pd(1)	114.86(14)	S(1)-C(6)-H(6C)	109.5
C(3)-O(3)-Pd(1)	116.74(14)	H(6A)-C(6)-H(6C)	109.5
S(2)-O(6)-Pd(1)	113.96(9)	H(6B)-C(6)-H(6C)	109.5
O(2)-C(1)-O(1)	129.1(2)	S(2)-C(7)-H(7A)	109.5
O(2)-C(1)-C(2)	119.9(2)	S(2)-C(7)-H(7B)	109.5
O(1)-C(1)-C(2)	111.0(2)	H(7A)-C(7)-H(7B)	109.5
F(3)-C(2)-F(1)	107.7(2)	S(2)-C(7)-H(7C)	109.5
F(3)-C(2)-F(2)	107.1(2)	H(7A)-C(7)-H(7C)	109.5
F(1)-C(2)-F(2)	107.8(2)	H(7B)-C(7)-H(7C)	109.5
F(3)-C(2)-C(1)	111.6(2)	S(2)-C(8)-H(8A)	109.5
F(1)-C(2)-C(1)	112.2(2)	S(2)-C(8)-H(8B)	109.5
F(2)-C(2)-C(1)	110.4(2)	H(8A)-C(8)-H(8B)	109.5
O(4)-C(3)-O(3)	130.0(2)	S(2)-C(8)-H(8C)	109.5
O(4)-C(3)-C(4)	118.7(2)	H(8A)-C(8)-H(8C)	109.5
O(3)-C(3)-C(4)	111.1(2)	H(8B)-C(8)-H(8C)	109.5

Symmetry transformations used to generate equivalent atoms:

Table A-4.4. Anisotropic displacement parameters ($\text{\AA}^2 \times 10^3$) for Pd(DMSO)₂(TFA)₂ **4-3a**. The anisotropic displacement factor exponent takes the form: $-2\pi^2 [h^2 a^{*2} U^{11} + \dots + 2 h k a^* b^* U^{12}]$

	U ¹¹	U ²²	U ³³	U ²³	U ¹³	U ¹²
Pd(1)	16(1)	14(1)	12(1)	0(1)	3(1)	-1(1)
S(1)	17(1)	17(1)	14(1)	3(1)	3(1)	-1(1)
S(2)	26(1)	13(1)	16(1)	0(1)	8(1)	-1(1)
F(1)	38(1)	42(1)	29(1)	2(1)	-10(1)	-5(1)
F(2)	32(1)	27(1)	52(1)	-17(1)	0(1)	-3(1)
F(3)	22(1)	44(1)	49(1)	-6(1)	10(1)	-9(1)
F(4)	33(1)	30(1)	42(1)	-12(1)	-7(1)	-5(1)
F(5)	81(2)	57(1)	46(1)	24(1)	-34(1)	-29(1)
F(6)	25(1)	63(1)	93(2)	-44(1)	-13(1)	12(1)
O(1)	19(1)	25(1)	14(1)	-2(1)	3(1)	-5(1)
O(2)	26(1)	37(1)	21(1)	-7(1)	7(1)	0(1)
O(3)	19(1)	16(1)	19(1)	0(1)	0(1)	0(1)
O(4)	26(1)	23(1)	25(1)	-5(1)	1(1)	4(1)
O(5)	21(1)	28(1)	20(1)	4(1)	2(1)	-8(1)
O(6)	27(1)	14(1)	15(1)	-1(1)	6(1)	-2(1)
C(1)	20(1)	17(1)	19(1)	1(1)	2(1)	0(1)
C(2)	23(1)	26(1)	27(1)	-2(1)	4(1)	-2(1)
C(3)	22(1)	18(1)	17(1)	3(1)	2(1)	-3(1)
C(4)	30(1)	23(1)	36(2)	-2(1)	-7(1)	-1(1)
C(5)	28(1)	27(1)	12(1)	3(1)	1(1)	-3(1)
C(6)	29(1)	22(1)	35(1)	4(1)	8(1)	7(1)
C(7)	34(1)	24(1)	17(1)	1(1)	3(1)	5(1)
C(8)	43(2)	21(1)	31(1)	-2(1)	20(1)	-9(1)

Table A-4.5. Hydrogen coordinates ($\times 10^4$) and isotropic displacement parameters ($\text{\AA}^2 \times 10^{-3}$) for $\text{Pd}(\text{DMSO})_2(\text{TFA})_2$ **4-3a**.

	x	y	z	U(eq)
H(5A)	8256	3271	3521	34
H(5B)	9523	2911	3510	34
H(5C)	8762	1367	3734	34
H(6A)	9357	-841	2726	43
H(6B)	10178	588	2482	43
H(6C)	9319	-379	1838	43
H(7A)	6972	6358	-67	38
H(7B)	7559	7003	-757	38
H(7C)	7520	8264	-37	38
H(8A)	9462	8977	244	45
H(8B)	9777	7872	-457	45
H(8C)	10468	7636	388	45

Table A-4.6. Torsion angles [°] for Pd(DMSO)₂(TFA)₂ **4-3a**.

O(1)-Pd(1)-S(1)-O(5)	165.03(10)
O(3)-Pd(1)-S(1)-O(5)	-13.80(10)
O(6)-Pd(1)-S(1)-O(5)	69.1(5)
O(1)-Pd(1)-S(1)-C(5)	42.80(10)
O(3)-Pd(1)-S(1)-C(5)	-136.03(10)
O(6)-Pd(1)-S(1)-C(5)	-53.1(5)
O(1)-Pd(1)-S(1)-C(6)	-69.27(11)
O(3)-Pd(1)-S(1)-C(6)	111.90(11)
O(6)-Pd(1)-S(1)-C(6)	-165.2(5)
O(3)-Pd(1)-O(1)-C(1)	-71.9(10)
O(6)-Pd(1)-O(1)-C(1)	-60.00(16)
S(1)-Pd(1)-O(1)-C(1)	125.78(16)
O(1)-Pd(1)-O(3)-C(3)	132.7(9)
O(6)-Pd(1)-O(3)-C(3)	120.77(16)
S(1)-Pd(1)-O(3)-C(3)	-65.00(16)
C(8)-S(2)-O(6)-Pd(1)	-145.31(12)
C(7)-S(2)-O(6)-Pd(1)	111.85(12)
O(1)-Pd(1)-O(6)-S(2)	122.58(10)
O(3)-Pd(1)-O(6)-S(2)	-58.21(10)
S(1)-Pd(1)-O(6)-S(2)	-141.4(4)
Pd(1)-O(1)-C(1)-O(2)	-12.9(3)
Pd(1)-O(1)-C(1)-C(2)	165.32(15)
O(2)-C(1)-C(2)-F(3)	0.7(3)
O(1)-C(1)-C(2)-F(3)	-177.7(2)
O(2)-C(1)-C(2)-F(1)	-120.2(3)
O(1)-C(1)-C(2)-F(1)	61.4(3)
O(2)-C(1)-C(2)-F(2)	119.6(3)
O(1)-C(1)-C(2)-F(2)	-58.8(3)
Pd(1)-O(3)-C(3)-O(4)	3.2(3)
Pd(1)-O(3)-C(3)-C(4)	-172.84(16)
O(4)-C(3)-C(4)-F(4)	20.8(3)
O(3)-C(3)-C(4)-F(4)	-162.6(2)
O(4)-C(3)-C(4)-F(6)	142.8(3)
O(3)-C(3)-C(4)-F(6)	-40.6(3)
O(4)-C(3)-C(4)-F(5)	-97.4(3)
O(3)-C(3)-C(4)-F(5)	79.2(3)

Symmetry transformations used to generate equivalent atoms:

Pd(DMSO)(H₂O)(TFA)₂ 4-2a***Data Collection***

An orange crystal with approximate dimensions 0.38 x 0.10 x 0.10 mm³ was selected under oil under ambient conditions and attached to the tip of a MiTeGen MicroMount©. The crystal was mounted in a stream of cold nitrogen at 100(1) K and centered in the X-ray beam by using a video camera.

The crystal evaluation and data collection were performed on a Bruker Quazar SMART APEXII diffractometer with Mo K_α ($\lambda = 0.71073 \text{ \AA}$) radiation and the diffractometer to crystal distance of 4.96 cm.

The initial cell constants were obtained from three series of ω scans at different starting angles. Each series consisted of 12 frames collected at intervals of 0.5° in a 6° range about ω with the exposure time of 1 second per frame. The reflections were successfully indexed by an automated indexing routine built in the APEXII program suite. The final cell constants were calculated from a set of 9985 strong reflections from the actual data collection.

The data were collected by using the full sphere data collection routine to survey the reciprocal space to the extent of a full sphere to a resolution of 0.70 Å. A total of 22130 data were harvested by collecting 4 sets of frames with 0.5° scans in ω and ϕ with exposure times of 1 sec per frame. These highly redundant datasets were corrected for Lorentz and polarization effects. The absorption correction was based on fitting a function to the empirical transmission surface as sampled by multiple equivalent measurements. [1]

Structure Solution and Refinement

The systematic absences in the diffraction data were uniquely consistent for the space group $P2_1/n$ that yielded chemically reasonable and computationally stable results of refinement [2-4].

A successful solution by the direct methods provided most non-hydrogen atoms from the E -map. The remaining non-hydrogen atoms were located in an alternating series of least-squares cycles and difference Fourier maps. All non-hydrogen atoms were refined with anisotropic displacement coefficients. All hydrogen atoms were included in the structure factor calculation at idealized positions and were allowed to ride on the neighboring atoms with relative isotropic displacement coefficients.

There is also one half molecule of solvate ethyl acetate per Pd complex in the asymmetric unit. The solvent molecule is disordered over a crystallographic inversion center.

The final least-squares refinement of 245 parameters against 4710 data resulted in residuals R (based on F^2 for $I \geq 2\sigma$) and wR (based on F^2 for all data) of 0.0204 and 0.0465, respectively. The final difference Fourier map was featureless.

The molecular diagram is drawn with 50% probability ellipsoids.

References

- [1] Bruker-AXS. (2009) APEX2, SADABS, and SAINT Software Reference Manuals. Bruker-AXS, Madison, Wisconsin, USA.
- [2] Sheldrick, G. M. (2008) SHELXL. *Acta Cryst.* **A64**, 112-122.

[3] Dolomanov, O.V.; Bourhis, L.J.; Gildea, R.J.; Howard, J.A.K.; Puschmann, H. "OLEX2: a complete structure solution, refinement and analysis program". *J. Appl. Cryst.* (2009) **42**, 339-341.

[4] Guzei, I.A. (2006-2008). Internal laboratory computer programs "Inserter", "FCF_filter", "Modicifer".

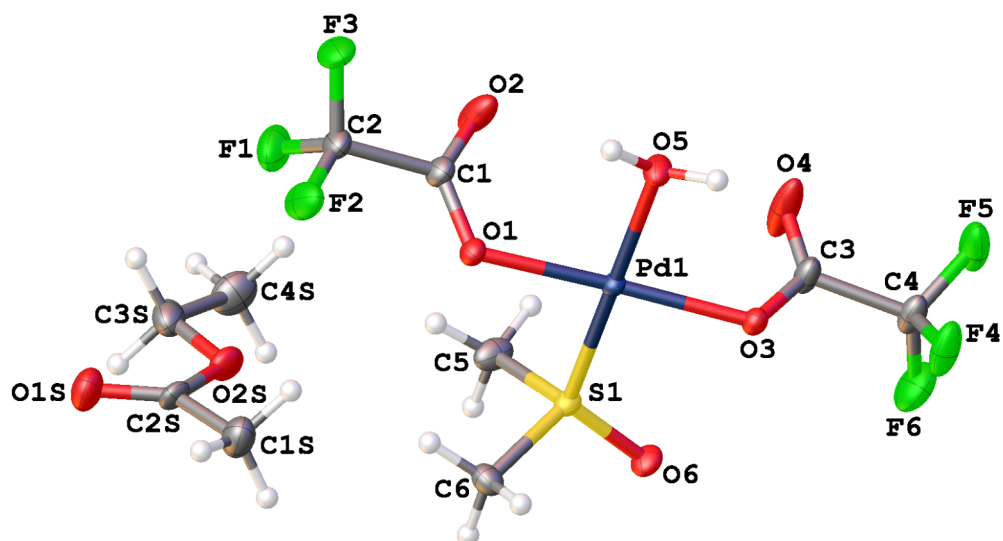


Figure A-4.2. A molecular drawing of Pd(DMSO)(H₂O)(TFA)₂ 4-2a. Note that the ethyl acetate is only 50% occupied.

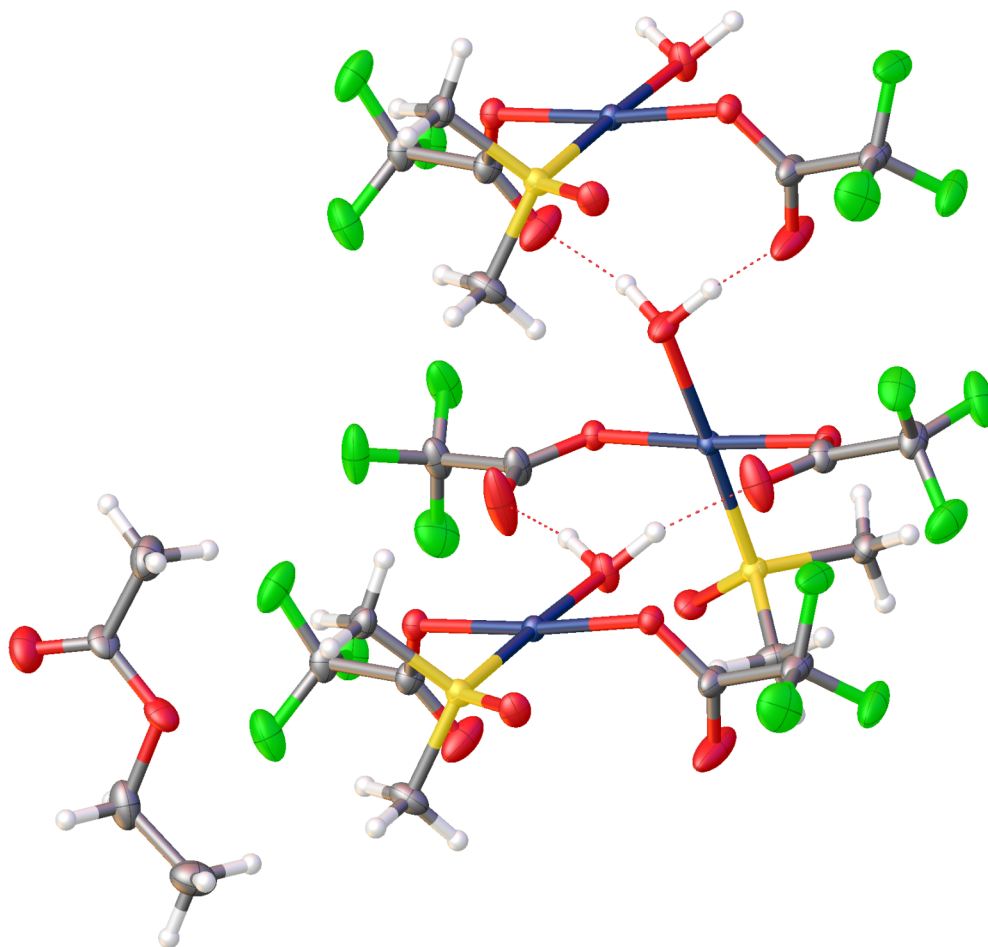


Figure A-4.3. A molecular drawing of Pd(DMSO)(H₂O)(TFA)₂ 4-2a, with the display of intermolecular hydrogen bonding interactions between H₂O and adjacent carboxylates.

Table A-4.7. Crystal data and structure refinement for Pd(DMSO)(H₂O)(TFA)₂ **4-2a**.

Identification code	stahl138	
Empirical formula	C ₆ H ₈ F ₆ O ₆ Pd S ½ C ₄ H ₈ O ₂	
Formula weight	472.64	
Temperature	100(1) K	
Wavelength	0.71073 Å	
Crystal system	Monoclinic	
Space group	P2 ₁ /n	
Unit cell dimensions	a = 8.382(4) Å	α = 90°.
	b = 7.650(3) Å	β = 98.79(3)°.
	c = 24.478(9) Å	γ = 90°.
Volume	1551.0(11) Å ³	
Z	4	
Density (calculated)	2.024 Mg/m ³	
Absorption coefficient	1.426 mm ⁻¹	
F(000)	928	
Crystal size	0.38 x 0.32 x 0.28 mm ³	
Theta range for data collection	1.68 to 30.52°.	
Index ranges	-11 ≤ h ≤ 11, -10 ≤ k ≤ 10, -34 ≤ l ≤ 34	
Reflections collected	28411	
Independent reflections	4710 [R(int) = 0.0275]	
Completeness to theta = 25.00°	99.7 %	
Absorption correction	Numerical with SADABS	
Max. and min. transmission	0.6910 and 0.6134	
Refinement method	Full-matrix least-squares on F ²	
Data / restraints / parameters	4710 / 3 /	
Goodness-of-fit on F ²	1.073	
Final R indices [I > 2σ(I)]	R1 = 0.0204, wR2 = 0.0457	
R indices (all data)	R1 = 0.0226, wR2 = 0.0465	
Largest diff. peak and hole	0.488 and -0.774 e.Å ⁻³	

Table A-4.8. Atomic coordinates ($\times 10^4$) and equivalent isotropic displacement parameters ($\text{\AA}^2 \times 10^3$) for Pd(DMSO)(H₂O)(TFA)₂ **4-2a**. U(eq) is defined as one third of the trace of the orthogonalized U^{ij} tensor.

	x	y	z	U(eq)
Pd(1)	9578(1)	2894(1)	7313(1)	13(1)
S(1)	11444(1)	4763(1)	7154(1)	16(1)
F(1)	6509(2)	4707(2)	5463(1)	42(1)
F(2)	7383(1)	2061(2)	5484(1)	40(1)
F(3)	5052(1)	2630(2)	5703(1)	34(1)
F(4)	11466(2)	1829(2)	9163(1)	40(1)
F(5)	9919(2)	3744(2)	9441(1)	45(1)
F(6)	12081(2)	4554(2)	9146(1)	46(1)
O(1)	8674(1)	2838(2)	6499(1)	18(1)
O(2)	6468(2)	4375(2)	6618(1)	40(1)
O(3)	10545(1)	2739(2)	8118(1)	17(1)
O(4)	8811(2)	4652(3)	8404(1)	55(1)
O(5)	7784(1)	1218(2)	7471(1)	23(1)
O(6)	12605(1)	5273(2)	7639(1)	22(1)
C(1)	7295(2)	3503(2)	6350(1)	21(1)
C(2)	6562(2)	3197(3)	5739(1)	24(1)
C(3)	9948(2)	3644(2)	8471(1)	24(1)
C(4)	10859(2)	3426(3)	9066(1)	27(1)
C(5)	10501(2)	6661(2)	6837(1)	26(1)
C(6)	12465(2)	3862(2)	6640(1)	22(1)
O(1S)	9959(4)	4436(4)	4367(1)	38(1)
O(2S)	9924(10)	5401(10)	5224(3)	27(1)
C(1S)	11089(17)	2710(20)	5139(4)	37(2)
C(2S)	10279(13)	4213(13)	4858(4)	23(2)
C(3S)	9069(15)	7000(18)	4986(4)	35(2)
C(4S)	8864(6)	8216(6)	5432(2)	38(1)

Table A-4.9. Bond lengths [Å] and angles [°] for Pd(DMSO)(H₂O)(TFA)₂ **4-2a**.

Pd(1)-O(3)	2.0171(13)	C(3)-C(4)	1.547(2)
Pd(1)-O(1)	2.0205(13)	C(5)-H(5C)	0.9800
Pd(1)-O(5)	2.0564(13)	C(5)-H(5D)	0.9800
Pd(1)-S(1)	2.1979(8)	C(5)-H(5E)	0.9800
S(1)-O(6)	1.4677(13)	C(6)-H(6A)	0.9800
S(1)-C(6)	1.7666(17)	C(6)-H(6B)	0.9800
S(1)-C(5)	1.7737(18)	C(6)-H(6C)	0.9800
F(1)-C(2)	1.336(2)	O(1S)-C(2S)	1.203(10)
F(2)-C(2)	1.323(2)	O(2S)-C(2S)	1.342(5)
F(3)-C(2)	1.328(2)	O(2S)-C(3S)	1.491(13)
F(4)-C(4)	1.330(2)	C(1S)-C(2S)	1.451(14)
F(5)-C(4)	1.321(2)	C(1S)-H(1SA)	0.9800
F(6)-C(4)	1.331(2)	C(1S)-H(1SB)	0.9800
O(1)-C(1)	1.265(2)	C(1S)-H(1SC)	0.9800
O(2)-C(1)	1.222(2)	C(3S)-C(4S)	1.464(15)
O(3)-C(3)	1.2673(19)	C(3S)-H(3SA)	0.9900
O(4)-C(3)	1.217(2)	C(3S)-H(3SB)	0.9900
O(5)-H(5A)	0.9580(11)	C(4S)-H(4SA)	0.9800
O(5)-H(5B)	0.9580(11)	C(4S)-H(4SB)	0.9800
C(1)-C(2)	1.547(2)	C(4S)-H(4SC)	0.9800
O(3)-Pd(1)-O(1)	175.12(5)	F(5)-C(4)-F(4)	107.34(16)
O(3)-Pd(1)-O(5)	88.62(5)	F(5)-C(4)-F(6)	107.85(16)
O(1)-Pd(1)-O(5)	89.87(5)	F(4)-C(4)-F(6)	107.74(15)
O(3)-Pd(1)-S(1)	91.18(4)	F(5)-C(4)-C(3)	111.91(14)
O(1)-Pd(1)-S(1)	90.50(4)	F(4)-C(4)-C(3)	112.77(14)
O(5)-Pd(1)-S(1)	177.93(4)	F(6)-C(4)-C(3)	109.04(16)
O(6)-S(1)-C(6)	110.26(8)	S(1)-C(5)-H(5C)	109.5
O(6)-S(1)-C(5)	109.42(8)	S(1)-C(5)-H(5D)	109.5
C(6)-S(1)-C(5)	103.87(9)	H(5C)-C(5)-H(5D)	109.5
O(6)-S(1)-Pd(1)	115.56(5)	S(1)-C(5)-H(5E)	109.5
C(6)-S(1)-Pd(1)	107.91(6)	H(5C)-C(5)-H(5E)	109.5
C(5)-S(1)-Pd(1)	109.17(7)	H(5D)-C(5)-H(5E)	109.5
C(1)-O(1)-Pd(1)	117.62(10)	S(1)-C(6)-H(6A)	109.5
C(3)-O(3)-Pd(1)	119.45(10)	S(1)-C(6)-H(6B)	109.5
Pd(1)-O(5)-H(5A)	115.8(12)	H(6A)-C(6)-H(6B)	109.5
Pd(1)-O(5)-H(5B)	115.5(12)	S(1)-C(6)-H(6C)	109.5
H(5A)-O(5)-H(5B)	104.51(16)	H(6A)-C(6)-H(6C)	109.5
O(2)-C(1)-O(1)	129.32(15)	H(6B)-C(6)-H(6C)	109.5
O(2)-C(1)-C(2)	115.33(15)	C(2S)-O(2S)-C(3S)	115.9(6)
O(1)-C(1)-C(2)	115.34(14)	O(1S)-C(2S)-O(2S)	122.2(6)
F(2)-C(2)-F(3)	108.27(15)	O(1S)-C(2S)-C(1S)	127.1(11)
F(2)-C(2)-F(1)	108.04(15)	O(2S)-C(2S)-C(1S)	110.7(8)
F(3)-C(2)-F(1)	106.97(15)	C(4S)-C(3S)-O(2S)	109.5(6)
F(2)-C(2)-C(1)	113.45(14)	C(4S)-C(3S)-H(3SA)	109.8
F(3)-C(2)-C(1)	110.24(14)	O(2S)-C(3S)-H(3SA)	109.8
F(1)-C(2)-C(1)	109.65(15)	C(4S)-C(3S)-H(3SB)	109.8
O(4)-C(3)-O(3)	129.56(15)	O(2S)-C(3S)-H(3SB)	109.8
O(4)-C(3)-C(4)	117.30(15)	H(3SA)-C(3S)-H(3SB)	108.2
O(3)-C(3)-C(4)	113.12(14)		

Symmetry transformations used to generate equivalent atoms:

Table A-4.10. Anisotropic displacement parameters ($\text{\AA}^2 \times 10^3$) for Pd(DMSO)(H₂O)(TFA)₂ **4-2a**. The anisotropic displacement factor exponent takes the form: $-2\pi^2 [h^2 a^* U^{11} + \dots + 2 h k a^* b^* U^{12}]$

	U ¹¹	U ²²	U ³³	U ²³	U ¹³	U ¹²
Pd(1)	11(1)	15(1)	13(1)	-1(1)	1(1)	-2(1)
S(1)	14(1)	16(1)	16(1)	1(1)	0(1)	-3(1)
F(1)	42(1)	53(1)	29(1)	17(1)	-2(1)	-9(1)
F(2)	29(1)	68(1)	23(1)	-19(1)	0(1)	3(1)
F(3)	19(1)	52(1)	28(1)	-5(1)	-3(1)	-12(1)
F(4)	57(1)	37(1)	21(1)	-1(1)	-8(1)	25(1)
F(5)	50(1)	67(1)	18(1)	0(1)	5(1)	31(1)
F(6)	44(1)	54(1)	34(1)	-6(1)	-14(1)	-5(1)
O(1)	16(1)	22(1)	14(1)	-1(1)	0(1)	-2(1)
O(2)	27(1)	63(1)	26(1)	-16(1)	-6(1)	19(1)
O(3)	15(1)	20(1)	14(1)	0(1)	0(1)	1(1)
O(4)	64(1)	75(1)	21(1)	-11(1)	-10(1)	53(1)
O(5)	21(1)	30(1)	18(1)	3(1)	-1(1)	-11(1)
O(6)	19(1)	24(1)	20(1)	-2(1)	-3(1)	-7(1)
C(1)	18(1)	27(1)	17(1)	-3(1)	-1(1)	-2(1)
C(2)	18(1)	37(1)	17(1)	0(1)	-1(1)	-5(1)
C(3)	26(1)	29(1)	15(1)	-2(1)	-3(1)	10(1)
C(4)	29(1)	31(1)	18(1)	-4(1)	-3(1)	14(1)
C(5)	22(1)	20(1)	36(1)	9(1)	-1(1)	-2(1)
C(6)	23(1)	25(1)	21(1)	-1(1)	8(1)	-3(1)
O(1S)	36(2)	53(2)	23(1)	8(1)	-2(1)	9(1)
O(2S)	22(3)	29(3)	28(2)	11(2)	-1(2)	7(2)
C(1S)	34(3)	52(5)	23(4)	2(3)	1(3)	9(3)
C(2S)	15(3)	29(4)	22(3)	7(3)	-3(2)	7(3)
C(3S)	29(4)	51(5)	24(4)	8(3)	3(3)	-10(4)
C(4S)	38(2)	30(2)	45(2)	3(2)	-2(2)	6(2)

Table A-4.11. Hydrogen coordinates ($\times 10^4$) and isotropic displacement parameters ($\text{\AA}^2 \times 10^{-3}$) for Pd(DMSO)(H₂O)(TFA)₂ **4-2a**.

	x	y	z	U(eq)
H(5A)	8080(20)	407(17)	7768(5)	35
H(5B)	7320(20)	508(18)	7166(5)	35
H(5C)	9838	6340	6486	40
H(5D)	11329	7502	6767	40
H(5E)	9815	7189	7083	40
H(6A)	12922	2725	6765	33
H(6B)	13335	4651	6572	33
H(6C)	11703	3709	6297	33
H(1SA)	11196	1792	4869	55
H(1SB)	10454	2276	5415	55
H(1SC)	12163	3063	5323	55
H(3SA)	9703	7567	4725	41
H(3SB)	8000	6678	4780	41
H(4SA)	8310	9271	5275	58
H(4SB)	9925	8533	5634	58
H(4SC)	8221	7657	5685	58

Table A-4.12. Torsion angles [°] for Pd(DMSO)(H₂O)(TFA)₂ **4-2a**.

O(3)-Pd(1)-S(1)-O(6)	-2.14(7)
O(1)-Pd(1)-S(1)-O(6)	-177.55(7)
O(5)-Pd(1)-S(1)-O(6)	82.3(9)
O(3)-Pd(1)-S(1)-C(6)	121.78(7)
O(1)-Pd(1)-S(1)-C(6)	-53.63(7)
O(5)-Pd(1)-S(1)-C(6)	-153.8(9)
O(3)-Pd(1)-S(1)-C(5)	-125.94(8)
O(1)-Pd(1)-S(1)-C(5)	58.64(8)
O(5)-Pd(1)-S(1)-C(5)	-41.5(9)
O(3)-Pd(1)-O(1)-C(1)	138.3(5)
O(5)-Pd(1)-O(1)-C(1)	66.31(13)
S(1)-Pd(1)-O(1)-C(1)	-111.65(12)
O(1)-Pd(1)-O(3)-C(3)	-151.9(5)
O(5)-Pd(1)-O(3)-C(3)	-79.95(14)
S(1)-Pd(1)-O(3)-C(3)	97.99(13)
Pd(1)-O(1)-C(1)-O(2)	9.3(3)
Pd(1)-O(1)-C(1)-C(2)	-171.81(11)
O(2)-C(1)-C(2)-F(2)	-171.36(17)
O(1)-C(1)-C(2)-F(2)	9.6(2)
O(2)-C(1)-C(2)-F(3)	-49.8(2)
O(1)-C(1)-C(2)-F(3)	131.24(17)
O(2)-C(1)-C(2)-F(1)	67.8(2)
O(1)-C(1)-C(2)-F(1)	-111.25(17)
Pd(1)-O(3)-C(3)-O(4)	0.4(3)
Pd(1)-O(3)-C(3)-C(4)	-178.06(12)
O(4)-C(3)-C(4)-F(5)	27.3(3)
O(3)-C(3)-C(4)-F(5)	-154.05(17)
O(4)-C(3)-C(4)-F(4)	148.4(2)
O(3)-C(3)-C(4)-F(4)	-32.9(2)
O(4)-C(3)-C(4)-F(6)	-91.9(2)
O(3)-C(3)-C(4)-F(6)	86.72(19)
C(3S)-O(2S)-C(2S)-O(1S)	1.5(8)
C(3S)-O(2S)-C(2S)-C(1S)	-179.4(13)
C(2S)-O(2S)-C(3S)-C(4S)	-176.2(5)

Symmetry transformations used to generate equivalent atoms:

Table A-4.13. Hydrogen bonds for Pd(DMSO)(H₂O)(TFA)₂ **4-2a** [Å and °].

D-H...A	d(D-H)	d(H...A)	d(D...A)	<(DHA)
O(5)-H(5A)...O(2)#1	0.9580(11)	1.689(4)	2.6312(19)	166.9(17)
O(5)-H(5B)...O(4)#1	0.9580(11)	1.692(5)	2.634(2)	166.6(18)

Symmetry transformations used to generate equivalent atoms:

#1 -x+3/2,y-1/2,-z+3/2